Transition Metal Complexes with Ring Incorporated Thiosemicarbazones: Syntheses, Structures and Spectral Properties

Thesis submitted to

Cochin University of Science and Technology

in partial fulfilment of the requirements for

the award of the degree of

Doctor of Philosophy

in

Chemistry

by

LALY K.

Department of Applied Chemistry
Cochin University of Science and Technology
Kochi - 682 022

July 2011

Transition Metal Complexes with Ring Incorporated Thiosemicarbazones: Syntheses, Structures and Spectral Properties

Ph. D. Thesis under the Faculty of Science

Author:

LALY K.
Research Fellow, Department of Applied Chemistry
Cochin University of Science and Technology
Kochi, India 682 022
E mail: kmlaly1@gmail.com

Research Advisor:

Dr. M. R. Prathapachandra Kurup
Professor
Department of Applied Chemistry
Cochin University of Science and Technology
Kochi, India 682 022
Email: mrp@cusat.ac.in

Department of Applied Chemistry
Cochin University of Science and Technology
Kochi, India 682 022

July 2011

Front cover: One dimensional polymeric arrangement of [Cu(mts)] along *a* axis, EPR Spectrum of [Mn(bmts)].

Back cover: Floral patterns formed by packing arrangement of $[Zn_2(bpts)_2]$ along *c* axis.

.... to my Chachan and Ammachy


हिरण्मयेन पात्रेण सत्यस्चापिहितं मुखम्।
तत्वं पूषन् अपावृणु सत्यधर्माय दृष्टये।।
(ईशावस्य उपानिष्त् 15)

DEPARTMENT OF APPLIED CHEMISTRY
COCHIN UNIVERSITY OF SCIENCE AND TECHNOLOGY
KOCHI - 682 022, INDIA

Dr. M.R. Prathapachandra Kurup
Professor

Phone Off. : 0484-2862423
Phone Res. : 0484-2576904
Telex : 885-5019 CUIN
Fax : 0484-2575804
Email : mrp@cusat.ac.in
mrp_k@yahoo.com

Certificate

This is to certify that the thesis entitled "**Transition Metal Complexes with Ring Incorporated Thiosemicarbazones: Syntheses, Structures and Spectral Properties**" submitted by Ms. Laly.K., in partial fulfillment of the requirements for the degree of Doctor of Philosophy, to the Cochin University of Science and Technology, Kochi-22, is an authentic record of the original research work carried out by her under my guidance and supervision. The results embodied in this thesis, in full or in part, have not been submitted for the award of any other degree.

M. R. Prathapachandra Kurup
(Supervisor)

DECLARATION

I hereby declare that the work presented in this thesis entitled "**Transition Metal Complexes with Ring Incorporated Thiosemicarbazones: Syntheses, Structures and Spectral Properties**" is based on the original work carried out by me under the guidance of Dr. M.R. Prathapachandra Kurup, Professor, Department of Applied Chemistry, Cochin University of Science & Technology and has not been included in any other thesis submitted previously for the award of any degree.

Kochi -22
25th July 2011

Laly K.

Acknowledgement

The materialization of this thesis had been a truly enriching and ennobling experience though the paths had not always been strewn with roses. I have many a faces to thank, those who have stood by me in thick and thin.

My obeisance to the God Almighty, who has always made me aware that He knows better than me what is best for me. I have always been privileged to receive His grace in the various phases of my personal and academic life. One of the greatest boons that He has bestowed on me in my academic pursuits is my supervising guide Prof. M.R. Prathapachandra Kurup who rendered on me scholarly guidance, imperative suggestions and personal attention at all stages of this research work. His dedication and enthusiasm to work have been a constant source of inspiration and encouragement for me. I owe my profound respect to him.

I express my sincere thanks to Prof. K.K. Mohammed Yusuff for his encouragement, timely suggestions and support as my doctoral committee member. I am very much thankful to Prof. K. Sreekumar, Head, Department of Applied Chemistry, CUSAT for the support and co-operation during the period of this work. I extend my heartfelt thanks to Prof. K. Girish Kumar, Former Head, for providing the necessary help and valuable suggestions. I am thankful for the support received from all the teaching and non-teaching staff of the Department of Applied Chemistry, CUSAT.

I deeply acknowledge the heads of the institutions of SAIF Kochi, IISc Bangalore, IIT Chennai and IIT Bombay for the services rendered in sample analyses. I place my special acknowledgement to Dr. E. Suresh CSMCRI, Bhavnagar and Prof M.V. Rajasekharan, School of Chemistry, Hyderabad for single crystal XRD studies of the compounds and Prof. V.P.N Namboothiri, International School of Photonics for fluorescence studies.

I am grateful to my senior researchers Dr. Rohith. P. John, Dr. Sreekanth, Dr. Seena E.B., Dr. P.F. Rapheal, Dr. Sreesha Sasi, Dr. U.L. Kala, Dr. Manoj E., Dr. Leji Latheef, Dr. Suja Krishnan and Dr. Neema Ani Mangalam for their help and cooperation.

I fondly remember my lab mates M/s Jessy Emmanuel, M/s Annie C.E, Mr. K. Jayakumar, Mr. Asokan K.P. and Mr. Sithambaresan who still carry the fire in minds like

me along with the academic life. Energising moments were given by Renjusha, Nancy, Reena, Dhanya, Sarika, Roji, Shimi, Jinsa, Bibitha, Anju, Nisha and Reshma in the lab. I profusely thank all of them for creating a cordial environment in the lab. I express my best wishes with gratitude to M/s. Renjini Joseph of Analytical Lab and M/s. Tintu R of ISP for breaking time barriers to help me.

I am deeply grateful to Dr. Shibu, Saji and all the staff of SAIF, Kochi for their kind help and support extended to me throughout the course of the work.

Dr. P. Karthikeyan, former HOD, Maharajas College Ernakulam encouraged me with his esteemed words and was always a constant source of inspiration throughout this endeavour. I am grateful to all my colleagues and friends of Maharajas College, Ernakulam. I wish to place on record my gratitude to the great teachers, mentors and my intimate friends who have inspired and influenced me at different stages of my education.

I remember with gratitude and courtesy, Mr. V. A. Shamsudeen, Principal, GPTC, Kalmassery for being supportive, and considerate whenever I needed them. I remember the help and cooperation extended to me by all my colleagues. I acknowledge with love Dr. Gopikrishna M and Dr. Dhanya Ravindran and my sister Jaya for their technical support in constructively editing this thesis. I extend my sincere thanks to Mr. Binoop Kumar of Indu Photos for the help provided in the documentation of the thesis.

My parents deserve special mention for their invaluable support and prayers. I dedicate this thesis before the fond memories of my father who may be watching me through the stars. I express my extreme gratitude to my uncles, aunts, brothers, sisters, cousins and in-laws for the love and support extended to me.

Especially, I keep in mind, my husband and bosom crony, V.S Thankappan for his encouragement and understanding. Thank you for being a persistent source of support. It is only with a heart brimming with love that I can remember Sreeju and Sruthy who sacrificed even their yearning moments with their amma for realising her dreams.

Finally, I would like to thank everybody who in their own way contributed to the successful realization of the thesis. I also express my apology for not being able to name each and every one in these pages.

Laly K.

Preface

Werner's Chemistry now enjoys a prominent place in the wide spectrum of natural as well as applied sciences as it is incessantly involved in the quest of exploring and unveiling newer and newer frontiers. The driving force of this development is the recognition of the interdisciplinary nature of the subject as in bioinorganic chemistry, biomimetic chemistry and so on. This thesis stems from the growing interest to understand the versatility in the coordination properties of transition metals with different ligand environments. The diversity in structures and extended delocalization exhibited by the transition metal complexes of heterodentate ligands have resulted in unravelling the modes of action of metalloenzymes, development of metallocycles, tuning of variable valency of the metal via ligand control of reduction potentials etc. Custom design of complexes with organic chelating ligand systems and comprehension of their structures have contributed much to newly emerging areas.

The work embodied in the thesis was carried out by the author in the Department of Applied Chemistry during the period 2005-2011. The work presented in this thesis describes the synthesis, structural and spectral characterization of ring incorporated thiosemicarbazones of 2,6-diacetylpyridine and their transition metal complexes. Chapter 1 offers a conceptual framework of thiosemicarbazones and their transition metal complexes with an extensive literature survey relating the history, stereochemistry, applications and recent developments. Various instrumental techniques like CHN analysis, infrared, electronic spectra and X-ray diffraction studies used in the study are discussed in this chapter. Chapter 2 deals with the design, syntheses and characterization of the ligand systems. 2,6-Diacetylpyridine bis(thiosemicarbazone) and its ring incorporated derivatives at both arms were the ligand systems. A morpholine ring incorporated monothiosemicarbazone was also included in the study.

First row transition metal complexes were mainly included in this study, though some cadmium complexes also were studied. Chapter 3 describes the syntheses and characterization of manganese(II) complexes. Chapter 4 comprises of the syntheses and characterization of iron(III) complexes. Chapter 5 deals with the syntheses and characterization of nickel(II) complexes. Chapter 6 explains the syntheses, structure and characterization of copper(II) complexes. Chapter 7 delineates the syntheses, structures and characterization of zinc(II) complexes. Chapter 8 portrays syntheses and characterization of cadmium(II) complexes. Studies on fluorescence activity of one of the cadmium complexes are included in this chapter. The thesis ends with a concluding chapter which sums up the important revelations of the previous chapters.

…..ഇ൹ര…..

CONTENTS

Chapter 3

Synthesis and Characterization of Mn(II) Complexes.....53 - 74

Chapter **7**

Synthesis, Structures and Spectral Characterization of Zinc(II) Complexes .....135 - 164

…..ꕥ…..

Curriculum Vitae

LALY K
Associate Professor in Chemistry
Government Polytechnic College
Kalamassery P.O. Pin. 673102
Ernakulam Dt. Kerala State
E-mail: kmlaly@cusat.ac.in, kmlaly1@gmail.com

ACADEMIC PROFILE

Pursuing Ph.D (Inorganic Chemistry)
(2005 – present)
Topic of work: Transition Metal Complexes with Ring Incorporated Thiosemicarbazones: Syntheses, Structures and Spectral properties
Supervising Guide : Dr. M.R. Prathapachandra Kurup, Professor, Dept. Of Applied Chemistry, CUSAT, Kochi

MCA
64% (2003)
KIHRD Centre No: 1425, Ernakulam
Indira Gandhi National Open University
New Delhi, Pin 110068

M Phil
Inorganic Chemistry
65.6% (2000)
Dept. of Applied Chemistry
Cochin University of Science & Technology
Kochi -22, Kerala

M Sc Applied Chemistry
Sp: Pharmaceutical Chemistry
64.4% (1980)
Maharajas College, Ernakulam
Kerala University, Kerala

B Sc Chemistry
74.2% (1978)
Union Christian College, Aluva, Ernakulam
Kerala University, Kerala

Pre Degree
60% (1975)
Union Christian College, Aluva, Ernakulam
Kerala University, Kerala

SSLC

68.7% (1973)
St. John's HSS, Kavalangad
Nellimattom P O Ernakulam(Dt)

ACHIEVEMENTS

- Completed M Phil Inorganic Chemistry under FIP in 2000.
- Financial assistance from UGC in 2004 for a minor research project entitled Investigations of Structural, Spectral and Biological Properties of Some Transition Metal Complexes of Some Multidentate Ligands.
- Presented a science programme "Sasthradeepthi" in Akasavani, FM, Kochi for years.
- Member of Art of Living Family.

RESEARCH EXPERIENCE

- Six years research experience in the field of coordination complexes.

TEACHING EXPERIENCE

- More than twenty nine years of teaching experience in various govt. colleges in Kerala.

COMPUTING SKILLS

- Expertise in MS-Office, Adobe Phtoshop
- ISIS Draw, Chemsketch, Chemdraw, Origin 6.0 etc.
- Familiar with crystallographic softwares like Shellxtl, Diamond, Wingx etc.
- Expertise in EPR simulation packages like Easyspin.
- Experienced in using instruments like UV-VIS spectrophotometer, IR spectrometer, Gouy balance etc.

PERSONAL PROFILE

Father's name	A Kunjuraman
Husband's name	V S Thankappan
Date of Birth	18-05-1958
Gender	Female
Family Status	Married & have two children.
Nationality	Indian
Languages Known	English, Hindi, Malayalam
Permanent address	Govt. Qtrs. No. IVA/2/8 Thrikkakara P O Ernakulam 682 021, Kerala Ph.No. 9447326906

…..ഇ൹…..

Papers/Conferences

1. Synthesis and spectral investigations of Mn(II) complexes of pentadentate bis(thiosemicarbazones), Suja Krishnan, K. Laly, M.R.P. Kurup, Spectrochim. Acta A, 75 (2010) 585.

2. Transition metal complexes of 2-(2-methoxyphenylmethylene) hydrazinecarbothioamide – synthesis, characterization and biological activity studies, K. Laly, M.R.P. Kurup, National Conference on Materials for the New Millenium (Matcon-2001), Dept of Applied Chemistry, Cochin University of Science and Technology, Cochin-22, 1-3 March 2001.

3. Chelating properties of a monothiosemicarbzone, K. Laly, M.R.P. Kurup, ICCOC- 2009, Dept. of Chemistry, Bharathiar University, Coimbatore, March 19-20 2009.

4. Versatility in the coordination of N_3S_2 donor ligands of a heterocyclic diketone , K. Laly, M.R.P. Kurup, MTIC-XIII, IISc Bangalore, Dec 7-9, 2009.

5. EPR Characterization of a copper(II) complex with S,N,N,N,S-pentadentate N^4-heterocyclicthiosemicarbazone, K. Laly, M.R.P. Kurup, Matcon-2010, Dept of Applied Chemistry, Cochin University of Science and Technology, Cochin-22, 1-3 March 2010.

Abbreviations

H_2bts	2,6-diacetylpyridine bis(thiosemicarbazone)
H_2bmts	2,6-diacetylpyridine bis(3-morpholinothiosemicarbazone
H_2bpts	2,6-diacetylpyridine bis(3-pyrrolidinothiosemicarbazone)
H_2mts	2,6-diacetylpyridine mono(3-morpholinothiosemicarbazone)
Complex 1	$[Mn(Hbts)(OAc)]\cdot CH_3OH\cdot H_2O$
Complex 2	$[Mn(bmts)]\cdot CH_3OH$
Complex 3	$[Mn(bpts)]\cdot 0.5H_2O$
Complex 4	$[Mn(Hmts)_2]$
Complex 5	$[Fe(H_2bpts)Cl_2]Cl\cdot CH_3OH$
Complex 6	$[Fe(Hmts)Cl_2]$
Complex 7	Ni(bts)]·0.5DMF
Complex 8	$[Ni(Hbmts)Cl]Cl\cdot CH_3CN$
Complex 9	$[Cu(bts)]\cdot H_2O$
Complex 10	$[Cu_3(bmts)_2(OAc)_2]$
Complex 11	$[Cu(H_2bmts)]Cl_2\cdot 2CH_3OH$
Complex 12	[Cu(bpts)]
Complex 13	[Cu(mts)]
Complex 14	$[Zn_2(bts)_2]\cdot DMF\cdot CH_3OH$
Complex 15	$[Zn(bmts)]\cdot H_2O$
Complex 16	$[Zn_2(bpts)_2]$
Complex 17	$[Zn(bpts)]\cdot H_2O$
Complex 18	$[Zn(Hmts)_2]\cdot H_2O$
Complex 19	[Cd(bts)]
Complex 20	$[Cd(H_2bmts)Br_2]$
Complex 21	$[Cd(bmts)]\cdot H_2O$
Complex 22	$[Cd(H_2bpts)\ Br_2]\cdot 2.5\ H_2O$
Complex 23	[Cd(bpts)]
Complex 24	$[Cd(Hmts)Br]\cdot 2H_2O$
DMF	Dimethylformamide
N_{azo}	Azomethine nitrogen
N_{py}	Pyridine nitrogen

Chapter 1

Thiosemicarbazones – A Conceptual Framework

Contents

1.1 Introduction

During the 20th century inorganic chemistry has been greatly enriched by the continuing development of coordination chemistry and the entry of new thinking from an organic perspective. The two important aspects of life, the ability to capture solar energy and the ability for controlled release of that energy have been contributing much for the development of this perspective. The catalysts controlling such activities are enzymes which control the synthesis and degradation of biologically important molecules. Most of the enzymes depend on a metal ion for their activity. There has been a remarkable growth in the understanding of biological systems containing transition metal ions [1]. Custom design of complexes with organic chelating ligand systems will require newer diversified donor systems. The new coordination compounds [2] with redox-

tunable properties point to the need of including more electronegative nitrogen, oxygen and sulfur atoms in the ligand structure. Determination of structure of many metalloproteins has further emphasized the importance of ONS donors. The development of advanced spectral characterization techniques for calculating spectroscopic parameters, accurately predicting structures and understanding chemical reactivity blessed this situation.

1.2 Thiosemicarbazones

In this context coordination complexes of heterodentate ligands [3-5] has been a subject of interest to many researchers and thiosemicarbazones are a class of heterodentate ligands with NS donor groups. They are obtained by the condensation of the appropriate thiosemicarbazide with an aldehyde or ketone. The structural features include an azomethine group and a thioamide group as shown in the structure below.

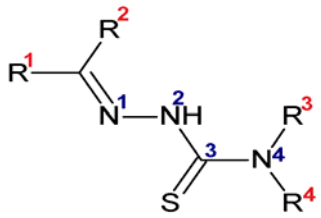

R^1, R^2: H, alkyl, aryl or heterocyclic
R^3, R^4: H, alkyl, aryl, heterocyclic or part of a cyclic system

When R^2 is heterocyclic like pyridine an additional functionality also is included to give NNS donors. When R^3 and R^4 of the thioamide group are part of a cyclic system a ring incorporated thiosemicarbazone is formed. Such pendant arm containing thiosemicarbazones are found to have interesting structural and biological properties.

The acid character of N^2H is another feature of thiosemicarbazone which allows the donor site to be either neutral or anionic. When coordinated as anionic ligands the conjugation is extended throughout the skeleton. It has

been proposed that extended conjugation enhances biological activity [6]. The structure-activity correlation studies of heterocyclic thiosemicarbazones [7] by Wilson et al found that the activity is affected by changing the S of the thiocarbonyl group, parent aldehyde or ketone, N^4 substituent and the position of attachment of aldehyde or ketone. The molecular features essential for such activities is ascertained by designing synthetic routes to modify, replace or substitute the derived thiosemicarbazone ligand.

1.3 Thiosemicarbazones of dialdehydes and diketones

Thiosemicarbazones of dialdehydes and diketones have been area of interest since a new kind of proligands highly polydentate in nature is obtained. Ketoaldehydes, dialdehydes or diketones when condensed with appropriate thiosemicarbazide in 1:2 ratio will give bis(thiosemicarbazones). If R^2 group is alkyl, they can be tetradentate and if heterocyclic, they can be pentadentate due to an additional functionality. Bis(thiosemicarbazones) (Fig. 1.1) was first synthesized by Bahr fiftysix years ago [8]. It has been found that synthesis of aryl substituted bis(thiosemicarbazone) proligands if not carefully controlled may lead to the formation of cyclised products [9].

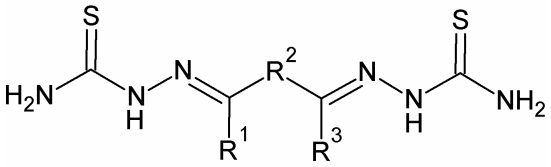

R^1, R^3: alkyl or aryl
R^2: alkyl or heterocyclic

Fig. 1.1 General structure of a bis(thiosemicarbazone).

The parent carbonyl compound and the thiosemicarbazide if taken in 1:1 ratio monothiosemicarbazones as shown in Fig. 1.2 (a) are formed. Monothiosemicarbazones can give rise to SNNO or SNN donor sites depending on the conditions of complexation. Complexes of monothiosemicarbazones [10]

were first isolated along with the synthesis of Cd(II) complexes of bis (thiosemicarbazones).

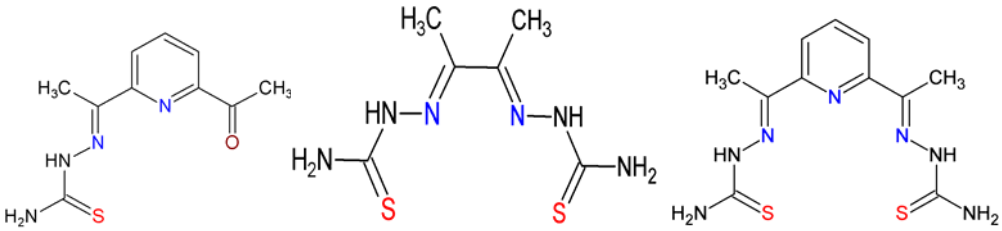

(a) (b) (c)

Fig. 1.2 (a) 2,6-diacetylpyridine mono(thiosemicarbazone). (b)Diacetylbis(thiosemicarbazone) (c) 2,6-diacetylpyridine bis(thiosemicarbazone)

Diacetylbis(thiosemicarbazone), 2,6-diacetylpyridine bis(thiosemicarbazone) and 2,6-diacetylpyridine mono(thiosemicarbazone) (Fig. 1.2) are some examples for these type of compounds. In the case of heterocyclic bis(thiosemicarbazones) the ligand can be dianionic which results in a highly delocalized system on extended conjugation as shown in Fig. 1.3. Some of the compounds are found to be showing fluorescence.

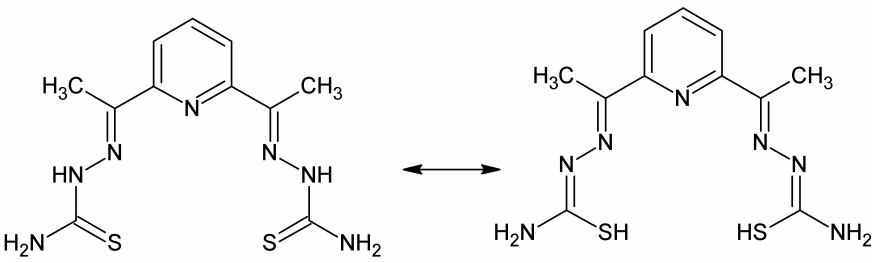

Fig. 1.3 The extended conjugation of 2,6-diacetylpyridine bis(thiosemicarbazone) on enolization.

1.4 Ring incorporated thiosemicarbazones

Biological activity of thiosemicarbazones is found to be related to the substituent at ^{4}N position. Studies of these compounds have been done by incorporating different rings. NMR studies show that they exist in chloroform

solution as mixture of isomers. However few crystal structures have been solved for those compounds. Structural studies and coordinating properties of hexamethyleneiminyl, pentamethyleneiminyl, tetramethyleneiminyl and morpholino group substituted thiosemicarbazones have been done. Though they have not found to change the number of donor groups, the activity of the compound is affected with ring incorporation. The studies made by de Souza et al. [11] show that 2,6-diacetylpyridine bis(3-hexamethyleneiminylthiosemicarbazone) show that the structure is almost planar except for the hexamethyleneimine rings which are tilted in opposite directions from the plane of the molecule. It is found to possess a bifurcated *E′* structure similar to 2-acetylpyridine-3-hexamethyleneiminylthiosemicarbazone.

1.5 Isomerism of thiosemicarbazones

Heterocyclic ^{4}N-substituted or ring incorporated thiosemicarbazones have been characterized in three isomeric types *Z*, *E* and *E′*. With respect to the azomethine bond it is the *Z*-isomer of 2-acetylpyridine-^{4}N-methylthiosemicarbazone (Fig.1.4a) which makes it possible to be involved in H-bonding and a six membered ring is formed by pyridyl nitrogen N1, N2 and N3 [12]. 2-Acetylpyridine-^{4}N-ethylthiosemicarbazone (Fig. 1.4b) is the *E* form with respect to azomethine bond.

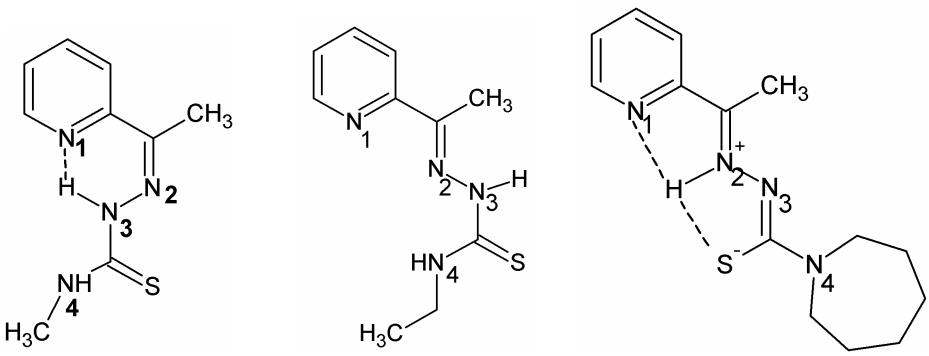

(a) (b) (c)

Fig. 1.4 *Z*, *E* and *E′* forms of 2-acetylpyridine-^{4}N-substituted thiosemicarbazones.

In the *E′* form, 2-acetylpyridine-3-hexamethyleneiminylthiosemicarbazone (Fig. 1.4c) the N_3 hydrogen has moved to N_2, bonded to both N_1 and thione sulfur giving a bifurcated H-bonding. This has been supported by single crystal X-ray studies in which the bond lengths are found to be 1.21 Å for N_2–H, 2.61 Å for N_1–H and 1.82 Å for S–H [11].

In case of 2,6-diacetylpyridine bis(3-hexamethyleneiminylthiosemicarbazone) [11] as noted above the crystal structure reported is *E′* bifurcated structure. Whereas in case of 2,6-diacetylpyridine bis(^{4}N-ethylthiosemicarbazone), a symmetric structure with the two arms disposed on either side of the pyridine ring [13] and a solvated form [14] are reported.

The stereochemistry adopted by thiosemicarbazones while interacting with transition metal ions depend on the denticity and the charge on the ligand. This in turn depends on the thione ↔ thiol equilibrium. As a result depending on the preparing condition, a neutral, dianionic or monoanionic complex can be formed. The steric effects of various substituents on the thiosemicarbazone backbone, additional interactions such as intramolecular hydrogen bonding also plays a role in stereochemistry.

1.6 Versatile chelating modes and geometry

Usually pentadentate ligands can form square pyramidal or trigonal bipyramid geometry in complexes. Many of the compounds which appear to be five coordinate on close examination are found to be tetrahedral or octahedral geometry. If electrostatic forces alone are the forces operating in bonding five coordinate complexes are found to disproportionate into four and six coordinate species. As far as the stability is concerned mostly the compounds are considered as distorted SP, distorted TBP or highly distorted structures i.e., something between SP and TBP. Proligands of 2,6-diacetylpyridine initially synthesized were hydrazones [15-19] and semicarbazones [20,21]. A number of transition

metal complexes [5] synthesized were found to be heptacoordinate adopting a pentagonal- bipyramid geometry along with anions or water molecules as coligands resulting in the formation of a neutral complex [22-25]. Mn(II) [26], Fe(II) [27], In(III) [28], Sn(IV) [29], and mononuclear Zn(II) [30] were found to be heptacoordinate. It was convinced that the equatorial positions were occupied by pentadentate ligand system and the axial positions by coligands. In case of deprotonated zinc complex of 2,6-diacetylpyridine bis(2′-pyridylhydrazone) the two arms of same molecule was coordinating to two zinc centers with bridging by the central pyridine ring [15]. Binuclear Zn(II) complexes of bis(thiosemicarbazones) were found to show {6+6}, {6+4}, {4+4} and {5+5} coordination geometries [31-34]. Binuclear Zn complex synthesized from a dialdehyde with {5+5} coordination was found to adopt a trigonal bipyramid geometry [35]. Ni(II) complex of 2,6-diformylpyridine bis(^{4}N-dimethylthiosemicarbazone) prefer a square planar geometry by excluding azomethine N and thiolato S of one of the arm and including hydrazinic N [23]. Planar Pd(II) and Ni(II) complexes of 1-phenylglyoxal bis(^{4}N-diethylthiosemicarbazone) [36] have been reported to have coordinated in the same way. Bis(thiosemicarbazonato) Cd(II) complex reported is a sulfur bridged box dimer [14] in which each Cd(II) center is distorted pentagonal bipyramidal.

Copper complexes of bis(thiosemicarbazones) are found to be having versatile geometries in which a very interesting trinuclear complex is also reported [37]. Schematic representation of the coordination modes of different thiosemicarbazones (Fig. 1.5) shows versatile possibilities. The structures of some of the complexes (Fig. 1.6 – 1.9) show chelating rings in all of them. The stability of them can be accounted by the five membered fused chelating rings formed in all of them. Schematic representation of some zinc complexes are also shown in Fig. 1.10 and Fig. 1.11.

Diorganothallium(III) complexes of 2,6-diacetylpyridine monothiosemicarbazone were prepared to study the coordinating behaviour of monothiosemicarbazone and found to be tetracoordinating [38]. Ru(II) complex of a monothiosemicarbazone was found to be tridentate coordination through NNS donor sites occupying a meridional plane [24]. The Cd(II) complex [10] of 2,6-diacetylpyridine monothiosemicarbazone is also reported in which a pentagonal bipyramid geometry is found. Such geometry is evolved along with coligands.

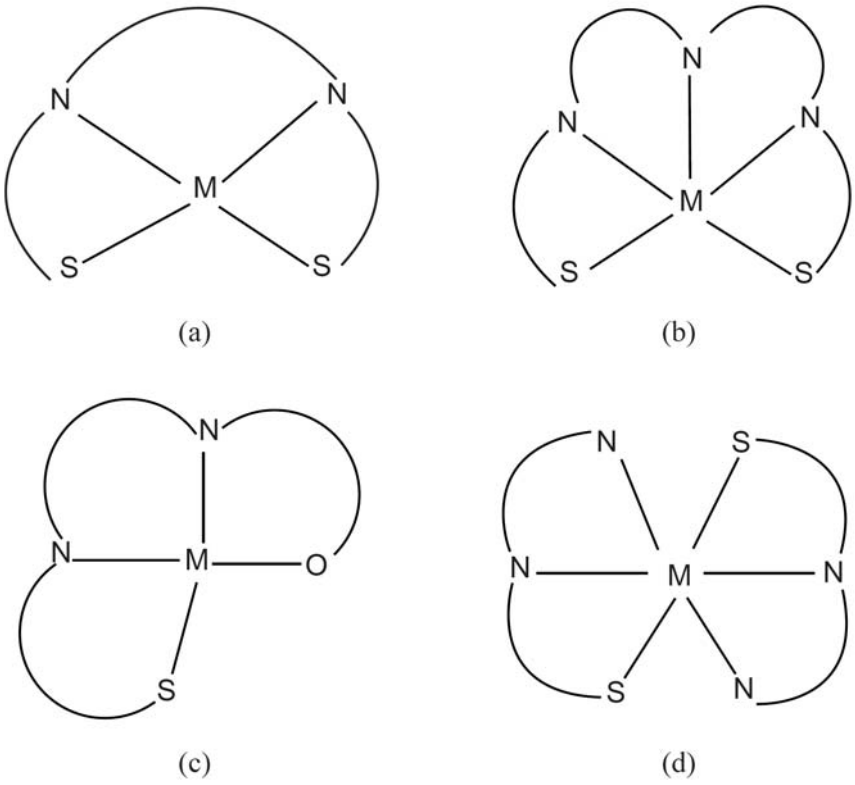

Fig. 1.5 Schematic representation of coordination modes of (a) alkyl bis(thiosemicarbazone) (b) heterocyclic bis(thiosemicarbazone) (c) Tetradentate heterocyclic monothiosemicarbazone (d) meridional tridentate heterocyclic monothiosemicarbazone.

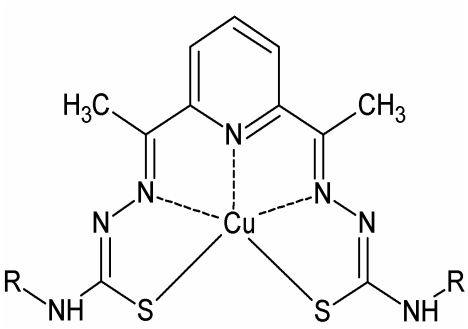

Fig.1.6 Mononuclear pentadentate Cu(II) complex.

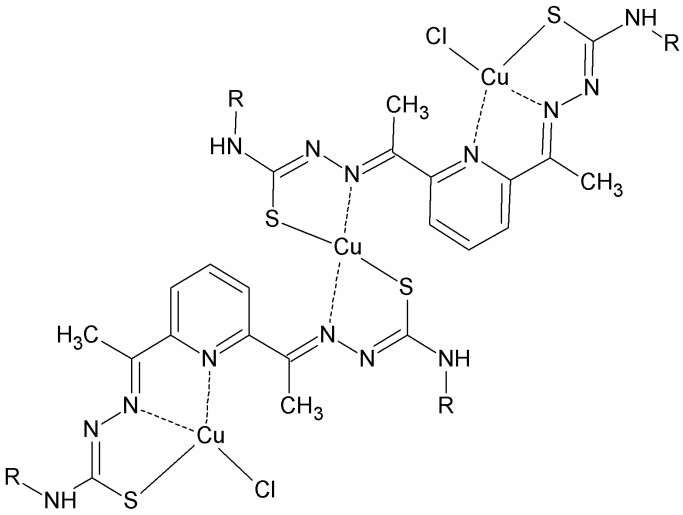

Fig.1.7 A trinuclear Cu(II) complex with a pentadentate ligand.

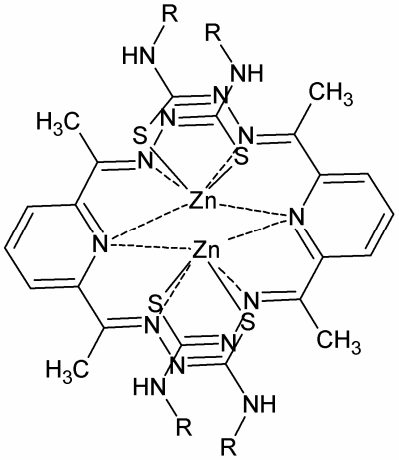

Fig. 1.8 A dinuclear Zn(II) complex with bridging pyridine rings.

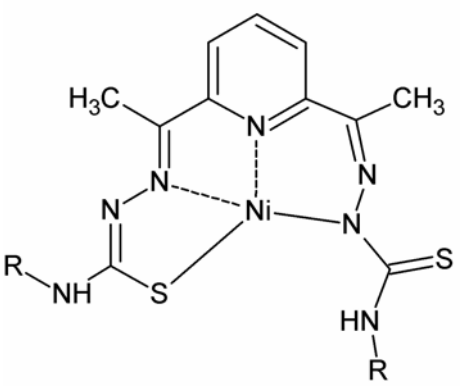

Fig. 1.9 A square planar Ni(II) complex in which hydrazinic N is coordinated.

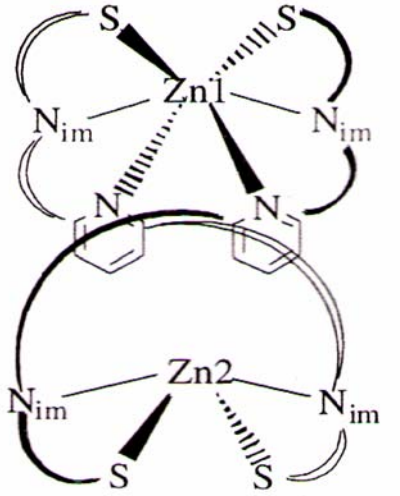

Fig. 1.10 Schematic stereo representation of [6+4] zinc(II) complex.

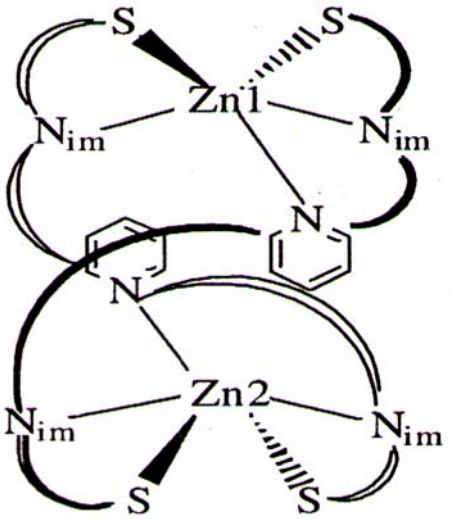

Fig. 1.11 Schematic stereo representation of [5+5] zinc(II) complex.

1.7 Applications

Thiosemicarbazones and their complexes have been studied for a considerable period of time for their versatile properties like redox nature, biological activity etc. Traces of interest date back to the beginning of the 20th century but the first reports on their medical applications began to appear in the fifties as drugs against tuberculosis and leprosy. In Open Crystallography Journal Pelosi has made a review on structure activity study on thiosemicarbazones and complexes [39-43].

1.7.1 Biological activity

Heterocyclic thiosemicarbazones, a class of compounds possessing a wide spectrum of medicinal properties have been studied for activity against bacterial and viral infections, tuberculosis, leprosy, coccidiosis and malaria [44-48]. They have been investigated for superoxide dismutase-like radical scavengers [49]. Commercialization of methisazone, an antiviral agent resulted in Maboran. Recently Triapine (3-aminopyridine-2-carboxaldehyde thiosemicarbazone) has been developed as an anticancer drug and reached clinical phase II [39].

1.7.2 Analytical applications

The analytical applications of these compounds extend in the microestimation of steroid ketones [50], di-2-pyridylketone thiosemicarbazone for estimation of Fe, 2-acetylpyridine thiosemicarbazone for Au(III) and several metals like copper, tin, zinc etc. In most of the cases the estimation is done spectrophotometrically [51].

1.7.3 Enzyme modelling

Transition metal complexes of ligands containing N/S donor centers are found to constitute the active centers of several metalloenzymes such as

hydrogenases, xanthine oxidase and nitrogenase [52]. Hence bis (thiosemicarbazones) are used for synthesizing model complexes for the active sites of metalloenzymes with mixed N/S donor centers such as nitrile hydratase since they also are having an N_3S_2 donor set [53]. The active sites of carbon monoxide hydrogenase, acetyl coenzyme synthase A etc also have been recent area of interest.

1.7.4 Radiolabelling and image sensing

There is a wide interest in designing novel imaging probes for biological targets, which can be employed *in vivo* with a range of molecular imaging techniques to attain research and clinical objectives. Non-invasive techniques such as PET (positron emission tomography) and SPECT (single photon emission computerised tomography), can be used to follow the *in vivo* distribution of radiolabelled metal complexes of interest in terms of therapeutic and imaging applications. Fluorescence microscopy has been recently used to follow the uptake of such molecules in living cells. The uptake of zinc bis(thiosemicarbazone) complexes in human cancer cells has been studied by fluorescence microscopy and the cellular distribution established, including the degree of uptake in the nucleus [54]. Bis(thiosemicarbonato)copper complexes [55] being fluorescent are found to be useful in radiolabelling. They are hence useful for diagnostic imaging of Alzheimer's disease by binding to amyloid-β-plaques, the compounds supposed to be associated with the disease [56]. Cu-ATSM has been found to be particularly selective in hypoxia and multidrug resistance. The hypoxic selectivity of Cu(II) bis(thiosemicarbazones) have been found to be dependent on the redox potential of complexes which in turn depends on the back bone substituents of the thiosemicarbazone skeleton [57].

1.7.5 Construction of novel materials and devices

Recently bis(thiosemicarbazones) have been found to be suitable for the construction of discrete multimetallohelicates since they have two long arms

containing two soft sulfur donor atoms [58]. The controlled self assembly of the building blocks resulted in double-stranded dinuclear zinc(II) and tetranuclear Cu(I) helicates. Helicates are used for the construction of novel materials, devices and machines with programmed properties and functions such as luminescence, DNA binding or anion binding.

1.8 Scope and objectives of the present work

As a continuation of the foregoing discussion bis(thiosemicarbazones) has been found to be proligands which are having very versatile donor possibilities to produce different geometries of complexes. Designing of ligand with redox tunable properties can be attained by using highly delocalized systems. It can be inferred that many areas of ring incorporated heterocyclic bis(thiosemicarbazones) are still to be explored. Similarly the behaviour of ring incorporated monothiosemicarbazone and its complexes seem to be an interesting area. Hence it has been decided to select 2,6-diacetylpyridine as the diketone and two tailored ring incorporated thiosemicarbazides containing a heterocyclic unit like morpholine or pyrrolidine as the starting materials for the ligands. Since the compound contains two thiosemicarbazone moieties it can be neutral, dianionic or monoanionic in complex formation. Along with, a free unsubstituted bis(thiosemicarbazone) and a monothiosemicarbazone also are synthesized. Some first row divalent transition metals like Mn(II), Ni(II), Cu(II) and Zn(II) are the selected as metal centers. However a trivalent Fe(III) and a second row divalent Cd(II) also are included in the list.

The objectives of the present work are

a) To design and synthesize some ring incorporated thiosemicarbazones by taking 2,6-diacetylpyridine and the thiosemicarbazide in appropriate ratios.

b) Characterization of the thiosemicarbazones using IR, UV, NMR, CV etc.

c) Study the coordination behavior of these ligands.

d) To synthesize transition metal complexes of transition metals.

e) To study the composition and spectral properties using IR, UV, EPR, NMR, CV etc.

f) To study the structure of the complexes by single crystal X-ray diffraction methods.

g) To analyse any application oriented properties of these complexes.

1.9 Characterization techniques

In order to achieve the above objectives the characterization techniques used are enlisted as follows.

1.9.1 Estimation of carbon, hydrogen, nitrogen and sulfur

Elemental analyses of C, H, N and S present in all the compounds were done on a Vario EL III CHNS elemental analyzer at the SAIF, Cochin University of Science and Technology, Kochi-22, Kerala, India. Based on the elemental composition possible structures were drawn using the ACD/Chemsketch Freeware software.

1.9.2 Conductivity measurements

The molar conductivities of the complexes in DMF solutions (10^{-3} M) at room temperature were measured using a direct reading conductivity meter at the Department of Applied Chemistry, CUSAT, Kochi, India.

1.9.3 Magnetic susceptibility measurements

Magnetic susceptibility measurements of the complexes were carried out on a Vibrating Sample Magnetometer using $Hg[Co(SCN)_4]$ as a calibrant at the SAIF, Indian Institute of Technology, Madras and Gouy Balance at the Department of Applied Chemistry, CUSAT, Kochi, India.

1.9.4 IR spectral studies

Infrared spectra of some of the complexes were recorded on a JASCO FT-IR-5300 Spectrometer in the range 4000-400 cm^{-1} using KBr pellets at the Department of Applied Chemistry, CUSAT, Kochi, India. IR spectra were also recorded on a Thermo Nicolet AVATAR 370 DTGS model FT-IR Spectrophotometer with KBr pellets at the SAIF, Kochi, India.

1.9.5 Electronic spectral studies

Electronic spectra in the range 200-500 nm were recorded on a Cary 5000 version 1.09 UV-VIS-NIR Spectrophotometer using solutions in acetonitrile /DMF at the SAIF, Kochi, India. The spectra in the range 200-900 nm were recorded on a UV-vis Double Beam UVD-3500 spectrometer at the Department of Applied Chemistry, CUSAT, Kochi, India.

1.9.6 NMR spectral studies

The ^{1}H, ^{13}C NMR spectra, D_2O exchange and DEPT experiments were recorded using Bruker AMX 400 Spectrometer, with $CDCl_3$ as solvent and TMS as standard at the Sophisticated Instruments Facility, Indian Institute of Science, Bangalore, India and using Bruker 400 Spectrometer with DMSO as solvent at the SAIF, Kochi.

1.9.7 EPR spectroscopy

EPR spectra were recorded in a Varian E-112 X-band EPR Spectrometer using TCNE as a standard at SAIF, IIT, Bombay, India. The *g* factors were quoted relative to the standard marker TCNE ($g = 2.00277$).

1.9.8 X-ray crystallography

Crystallography is the experimental science of determining the arrangement of atoms in crystals. For an object to be visible, its size needs to be at least half the wavelength of the light being used to see it. Since visible

light has a wavelength much longer than the distance between atoms, molecules are not seen in it. In order to see molecules it is necessary to use a form of electromagnetic radiation with a wavelength of the order of bond lengths, such as X-rays. When X-rays are beamed at the crystal, electrons diffract the X-rays, which cause a diffraction pattern. Using Fourier transformation, these patterns can be converted into electron density maps. These maps show contour lines of electron density. Since electrons more or less surround atoms uniformly, it is possible to determine where atoms are located. Unfortunately since hydrogen has only one electron, it is difficult to map hydrogen. A three dimensional picture is obtained by rotating the crystal at different angles. A computerized detector produces two dimensional electron density maps for each angle of rotation. The third dimension comes from comparing the rotation of the crystal with the series of images. Computer programs use this method to come up with three dimensional spatial coordinates.

Single crystal X-ray crystallographic analysis of one of the zinc compound was carried out using Siemens SMART CCD area–detector diffractometer at the Analytical Science Division, Bhavnagar, Gujarat, India. The structures were solved by direct methods with the program SHELXS-97 and refined by least-square on F_o^2 using the SHELXL software package [59].

X-ray diffraction measurements of other complexes were carried out on a CrysAlis CCD diffractometer with graphite-monochromated Mo Kα (λ = 0.71073 Å) radiation at National Single Crystal X-ray Facility, IIT Bombay, Mumbai, India and University of Hyderabad, Hyderabad, India. The program CrysAlis RED was used for data reduction and cell refinement [60]. The structures were solved by direct methods using SHELXS and refined by full-matrix least-squares refinement on F^2 using SHELXL. The graphical tools used were Diamond version 3.1f [61] and Mercury [62].

1.9.9 Cyclic voltammetry

Cyclic voltammetric measurements were done on a PC interfaced electrochemical analyzer (BAS Epsilon Bioanalytical system USA) with a three electrode compartment system consisting of a glassy carbon working electrode, platinum wire counter electrode and Ag/Ag^+ reference electrode, at the Department of Applied Chemistry, CUSAT, Kochi, India. The solutions of complexes in DMSO (10^{-3}M) after degassing (N_2 bubbling for 15 mts) containing 0.1M TBAC (tetrabutylammonium chloride) as the supporting electrolyte have been used to study the electrochemical properties. The voltammogram is run between the potentials of –200 and +200 mV at a scan speed of 100 mV/s.

1.9.10 Fluorescence spectrophotometry

Fluorescence spectroscopy is an important investigational tool in many areas of analytical science, due to its extremely high sensitivity and selectivity which is used across a broad range of chemical, biochemical and medical research. It is an essential investigational technique allowing detailed, real-time observation of the structure and dynamics of intact biological systems with extremely high resolution. In the pharmaceutical industry it has almost completely replaced radiochemical labeling.

Fluorescence studies are conducted with a Cary Eclipse fluorescence spectrophotometer with scan software 1.1(132) at the International School of Photonics, Cochin University of Science and Technology, Kerala.

1.10 Conclusion

This chapter deals with a brief historical outline on the studies of thiosemicarbazones, bonding and geometrical aspects, applications, scope and various characterization techniques. The ligands decided to be synthesized are thiosemicarbazones of 2,6-diacetylpyridine.

References

[1] J.E. Huheey, E.A. Keiter, R.L. Keiter, O.K. Medhi, Inorganic Chemistry: Principles of Structure and Reactivity, 4th ed. Pearson Education.

[2] U. Siemeling, Z. Anorg. Allg. Chem. 631 (2005) 2957.

[3] B.S. Garg, M.R.P. Kurup, S.K. Jain, Y.K. Bhoon, Trans. Met. Chem. 13 (1988) 309.

[4] M.J.M. Campbell, Coord. Chem. Rev. 15 (1975) 279.

[5] T.S. Lobana, R. Sharma, G. Bawa, S. Khanna, Coord. Chem. Rev. 253 (2009) 977.

[6] L. Latheef, E.B. Seena, M.R.P. Kurup, Inorg. Chim. Acta 362 (2009) 2515.

[7] B.A. Wilson, R. Venkataraman, C. Whitaker, Q. Tillison, Int. J. Environ. Res. Public Health 2 (2005) 170.

[8] G. Bahr, G. Schleizer, Z. Anorg. Chem. 280 (1955) 161.

[9] L. Alsop, A.R. Cowley, J.R. Dilworth, P.S. Donnelly, J.M. Peach, J.T. Rider, Inorg. Chim. Acta 358 (2005) 2770.

[10] J.S. Casas, E.E. Castellano, M.S. Garcia-Tasende, A. Sanchez, J. Sordo, J. Sukerman-Schepector, Z. Anorg. Allg. Chem. 623 (1997) 825.

[11] G.F. deSouza, D.X. West, C.A. Brown, J.K. Swearingen, J. Valdes-Matrinez, R.A. Toscano, S.H. Ortega, M. Horner, A.J. Bortoluzzi, Polyhedron 19 (2000) 841.

[12] D.X. West, G.A. Bain, R.J. Butcher, J.P. Jasinski, Y. Li, R.P. Pozdniakiv, J. Valdes-Matrinez, R.A. Toscano, S.H. Ortega, Polyhedron 15 (1996) 665.

[13] M. Vázquez, M.R. Bermejo, A.M. González-Noya, R. Pedrido, M.J. Romero, Angew. Chem. Int. Ed. 44 (2005) 4182.

[14] R. Pedrido, A.M. González-Noya, M.J. Romero, M. Martínez-Calvo, M.V. López, E. Gómez-Fórneas, G. Zaragoza, M.R. Bermejo, Dalton Trans. (2008) 6776.

[15] D. Wester, G.J. Palenik, Inorg. Chem. 15 (1976) 755.

[16] C. Lorenzini, C. Pelizzi, G. Pelizzi, G. Predieri, J. Chem. Soc., Dalton Trans. (1983) 721.

[17] C. Carini, G. Pelizzi, P. Tarasconi, *C*. Pelizzi, K.C. Molloy, P.C. Waterfield, J. Chem. Soc., Dalton Trans. (1989) 289.

[18] L.P. Battaglia, A.B. Corradi, C. Pelizzi, G. Pelosi, P. Tarasconi, J. Chem. Soc., Dalton Trans. (1990) 3857.

[19] S. Naskar, D. Mishra,. S.K. Chattopadhyay, M. Corbella, A.J. Blake, Dalton Trans. (2005) 2428.

[20] D. Wester, G.J. Palenik, J. Am. Chem. Soc. 95 (1973) 6505.

[21] G.J. Palenik, D.W. Wester, Inorg. Chem. 17 (1978) 865.

[22] J.S. Casas, M.S. Garcia-Tasende, J. Sordo, Coord. Chem. Rev. 209 (2000) 197.

[23] C.A. Brown, W. Kaminsky, K.A. Claborn, K.I. Goldberg. D.X. West, J. Braz. Chem. Soc. 13 (2002) 10.

[24] M. Maji, S. Ghosh, S.K. Chattopadhyay, T.C.W. Mak, Inorg. Chem. 36 (1997) 2938.

[25] M.A. Ali, A.H. Mirza, J.D. Chartres, P.V. Bernhardt, Polyhedron 30 (2011) 299.

[26] R. Pedrido, M.R. Bermejo, M.J. Romero, M. Vázquez, López, A.M. González-Noya, M. Maneiro, M.J. Rodriguez, M.I. Fernandez, Dalton Trans. (2005) 572.

[27] G. Dessy, V. Fares. Cryst. Struct. Commun. 10 (1981) 1025.

[28] S. Abram, C. Maichle-Mossmer, U. Abram, Polyhedron 17 (1998) 131.

[29] J.S. Casas, A. Castiñeiras, A. Sanchez, J. Sordo, A. Vazquez-Lopez, M.C. Rodriguez-Argüelles, U. Russo. Inorg. Chim. Acta 221 (1994) 61.

[30] A. Bino, N. Cohen, Inorg. Chim. Acta 210 (1993) 11.

[31] R. Pedrido, M.R. Bermejo, M.J. Romero, A.M. González-Noya, M. Manerio, M.I. Fernández, Inorg. Chem. Commun. 8 (2005) 1036.

[32] M.A. Ali, A.H. Mirza, R.J. Butcher, M.T.H. Tarafder, M.A. Ali, Inorg. Chim. Acta 320 (2001) 1.

[33] M.A. Ali, A.H. Mirza, C.W. Voo, A.L. Tan, P.V. Bernhardt, Polyhedron 22 (2003) 3433.

[34] M.A. Ali, A.H. Mirza, R.J. Butcher, M.T.H. Tarafder, M.A. Ali, Polyhedron 25 (2006) 3337.

[35] M.L. Duran, A. Sousa, J. Romero, A. Castiñeiras, E. Bermejo, D.X. West, Inorg. Chim. Acta 294 (1999) 79.

[36] Castiñeiras, E. Bermejo, D.X. West, A.K. El-Sawaf, J.K. Swearingen, Polyhedron 17 (1998) 2751.

[37] C.A. Brown, D.X. West, Trans. Met. Chem. 28 (2003) 154.

[38] J.S. Casas, E.E. Castellano, M.S. Garcia-Tasende, A. Sanchez, J. Sordo, M.J. Vidarte, Polyhedron 17 (1998) 2249.

[39] G. Pelosi, Open Crystallography Journal 3 (2010) 16.

[40] M.J.M. Campbell, Coord. Chem. Rev. 15 (1975) 279.

[41] S.B. Padhye, G.B. Kauffman, Coord. Chem. Rev. 63 (1985) 127.

[42] D.X. West, A.E. Liberta, S.B. Padhye, R.C. Chikate, P.B. Sonawane, A.S. Kumbhar, R.G. Yerande, Coord. Chem. Rev. 123 (1993) 49.

[43] E.L. Chang, C. Simmers, D.A. Knight, Pharmaceuticals 3 (2010) 1711.

[44] J.P. Scovill, D.L. Klayman, C.F. Franchino, J. Med. Chem. 25 (1982) 1261.

[45] D.L. Klayman, J.P. Scovill, J.F. Bartosevich, C.J. Mason, J. Med. Chem. 22 (1979) 1367.

[46] D.L. Klayman, J.F. Bartosevich, T.S. Griffin, C.J. Mason, J.P. Scovill, J. Med. Chem. 22 (1979) 855.

[47] I.H. Hall, K.G. Rajendran, D.X. West, A.E. Liberta, Anticancer Drugs 4 (1993) 251.

[48] P. Genova, T. Varadinova, A.I. Matesanz, D. Marinova, P. Souza, Toxicol. Appl. Pharmacol. 197 (2004) 107.

[49] K. Vada, Y. Fujibayashi, A. Yokoyama, Arch. Biochem. Biophys. 310 (1994) 1.

[50] W.H. Pearlman, E. Cerceo, J. Biol. Chem. 203 (1953) 127.

[51] R.B. Singh, B.S. Garg, R.P. Singh, Talanta 25 (1978) 619.

[52] S. Pal, A.K. Barik, P. Aich, S.-M. Peng, G.-H. Lee, S.K. Kar, Struct. Chem. 18 (2007) 149.

[53] A. Panja, C. Campana, C. Leavitt, M.J. Van Stipdonk, D.M. Eichhorn, Inorg. Chim. Acta 362 (2009) 1348.

[54] A.R. Cowley, J. Davis, J.R. Dilworth, P.S. Donnelly, R. Dobson, A. Nightingale, J.M. Peach, B. Shore, D. Kerr, L. Seymour, Chem. Commun. (2005) 845.

[55] S. Lim, K.A. Price, S.-F. Chong, B.M. Paterson, A. Caragounis, K.J. Barnham, P.J. Crouch, J.M. Peach, J.R. Dilworth, A.R. White, P.S. Donnelly, J. Biol. Inorg. Chem. 15 (2010) 225.

[56] S. Lim, B.M. Paterson, M.T. Fodero-Tavoletti, G.J. O'Keefe, R. Cappai, K.J. Barnham, V.L. Villemagne, P.S. Donnelly, Chem. Commun. 46 (2010) 5437.

[57] A.R. Cowley, J.R. Dilworth, P.S. Donelly, E. Labisbal, A. Sousa, J. Am. Chem. Soc. 124 (2002) 5270.

[58] M.R. Bermejo, A.M. González-Noya, R.M. Pedrido, M.J. Romero, M. Vázquez, Angew. Chem. Int. Ed. 44 (2005) 4182.

[59] G.M. Sheldrick, Acta Cryst. A64 (2008) 112.

[60] CrysAlis CCD and CrysAlis RED Versions 1.171.29.2 (CrysAlis 171. NET), Oxford Diffraction Ltd., Abingdon, Oxfordshire, England, 2006.

[61] K. Brandenburg, Diamond Version 3.1f, Crystal Impact GbR, Bonn, Germany, 2008.

[62] C.F. Macrae, P.R. Edgington, P. McCabe, E. Pidcock, G.P. Shields, R. Taylor, M. Towler, J. van de Streek, J. Appl. Cryst. 39 (2006) 453.

…..ൠ…..

Chapter 2

Synthesis and Spectral Characterization of Proligands

Contents

2.1 Introduction

Thiosemicarbazones constitute an important class of N, S-donor ligands which show heterodentate chelation in complex formation [1-6]. The most attraction of these chelating compounds is the formation of five or six membered fused chelating rings including the metal center having some aromatic character [7-11]. They can be synthesized by designing tailored synthetic routes to modify, replace or substitute different groups. Proligands with additional functionalities thus obtained can be used for synthesizing model systems which mimic several metalloenzyme systems. Starting with a heterocyclic aldehyde or ketone can provide an additional donor group whereas a heterocyclic ketoaldehyde or diketone provide almost double donor groups like in a bis(thiosemicarbazone). They have been proven to be potentially beneficial biologically active compounds. They have been receiving considerable attention due to their broad therapeutic activity like antimalarial, antibacterial, antifungal, antiHIV etc [12-14]. They have been found to exist in various isomeric forms like *E*, *Z* and *E′* forms [15].

Bis(thiosemicarbazones), synthesized by Bahr [16] about fiftysix years ago belong to the class of tetradentate or pentadentate ligands depending on the availability of donor sites. They are excellent chelating agents when compared with thiosemicarbazones of monoaldehydes or ketones which form comparatively less stable compounds with metal ions. They have been studied to mimic superoxide dismutase like activity [17]. The planarity of many complexes suggests a possible intercalating behaviour towards DNA. Certain complexes of bis(thiosemicarbazones) are found to have promising properties in hypoxia and multidrug resistance which attract enormous interest in development of inhibitors of multidrug resistance proteins.

Studies on heterocyclic thiosemicarbazones capable of tridentate coordination have been done extensively [18]. But heterocyclic bis(thiosemicarbazones) capable of pentadentate coordination due to their bileptic nature show very interesting versatile coordinating possibilities. These compounds though with lot of application possibilities, still lack attention or an extensive study. Structural and spectral studies of bis(ring incorporated thiosemicarbazones) are still uncovered areas. Unsubstituted and substituted bis(thiosemicarbazones) are found to show variations in structure, isomerism and stereochemistry. Hence it was decided to synthesize some bis(N^4-ring incorporated thiosemicarbazone) of 2,6-diacetylpyridine and study their coordination modes. A monothiosemicarbazone of 2,6-diacetylpyridine was also included in this work.

For the synthesis 2,6-diacetylpyridine, selected as the diketone was condensed with thiosemicarbazide, 3-morpholinothiosemicarbazide and 3-pyrrolidinothiosemicarbazide. The latter two were synthesized by a four stage process which involved the synthesis of N^4-methyl N^4-phenylthiosemicarbazide followed by transamination.

Three bis(thiosemicarbazones) and one monothiosemicarbazone have been synthesized. Usually the numbering of these compounds are done after considering thiosemicarbazide as the main skeleton which is as shown in Fig. 2.1.

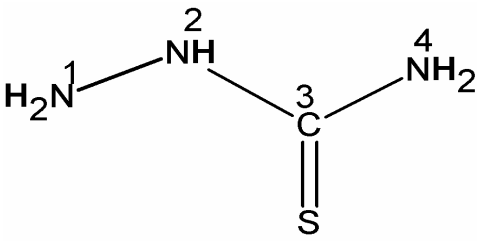

Fig. 2.1 Thiosemicarbazide skeleton with numbering.

Though the skeleton is numbered like this, the numbering scheme of the proligands used in this thesis is as given in Fig. 2.2. An element based numbering is followed. The ligands synthesized are presented below. Since they are expected to be diprotic with two enolizable protons the following acronyms are used.

a) 2,6-diacetylpyridine bis(thiosemicarbazone) (H_2bts)

b) 2,6-diacetylpyridine bis(3-morpholinothiosemicarbazone) (H_2bmts)

c) 2,6-diacetylpyridine bis(3-pyrrolidinothiosemicarbazone) (H_2bpts)

d) 2,6-diacetylpyridine mono(3-morpholinothiosemicarbazone) (H_2mts)

This chapter contains the synthesis and spectral characterization of the proligands. For the synthesis of H_2bts a general procedure by Mohan et al. [19] and for the others an adaptation of Scovill's procedure [20] are used.

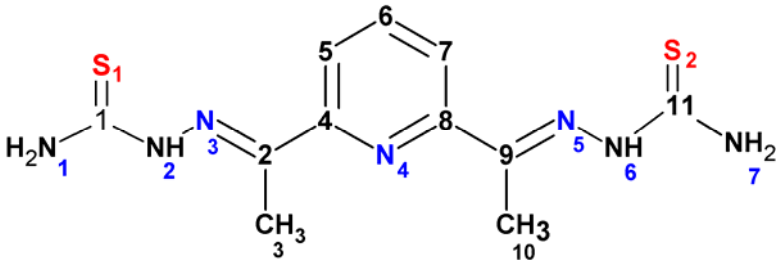

H_2bts

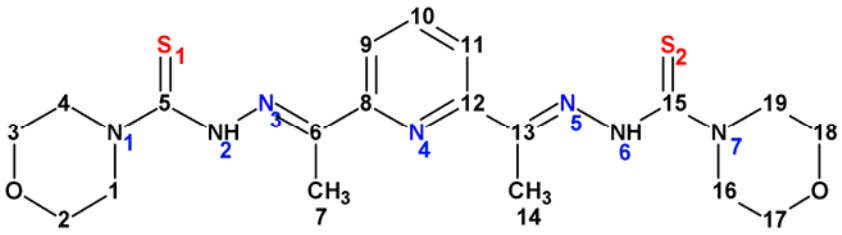

H_2bmts

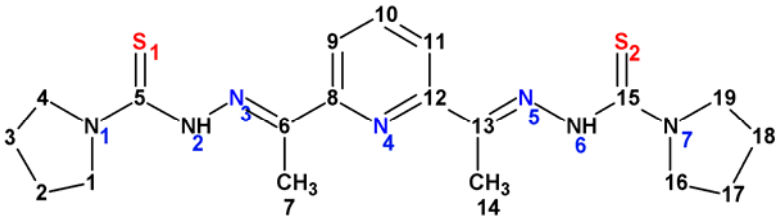

H_2bpts

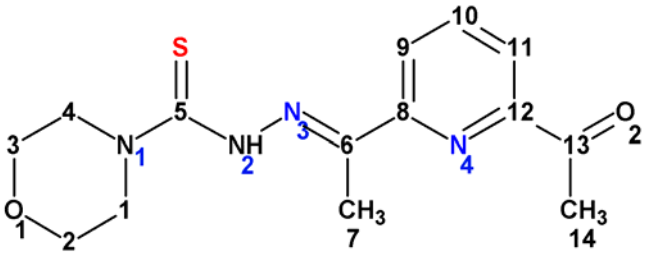

H_2mts

Fig. 2.2 Proposed structures and numbering schemes for ligand systems.

2.2 Experimental

2.2.1 Materials

2,6-Diacetylpyridine (Aldrich), hydrazine hydrate, sodium chloroacetate (Merck), carbon disulphide (Glaxo), N-methylaniline, pyrrolidine and morpholine were used as supplied for the preparation of the ligands. Ethanol and acetonitrile were the solvents used.

2.2.2 Synthesis of precursors

2.2.2.1 *Synthesis of carboxymethyl N-methyl, N-phenyldithiocarbamate*

A mixture of 12.0 ml (5.2 g, 0.2 mol) of carbon disulfide and 21.6 ml (21.2 g, 0.2 mol) of N-methylaniline was treated with aqueous solution of 8.4 g (0.21 mol) of NaOH in 250 ml. On stirring at room temperature for 4 h the organic layer disappeared completely. The straw colored solution was treated with 23.2 g (0.2 mol) of sodium chloroacetate and allowed to stand overnight (17 h).

After acidifying the solution with 25 ml of conc. HCl the solid which separated was collected and dried (Scheme 2.1). Yield of the buff colored product is 81% (39.5 g) mp 198 °C.

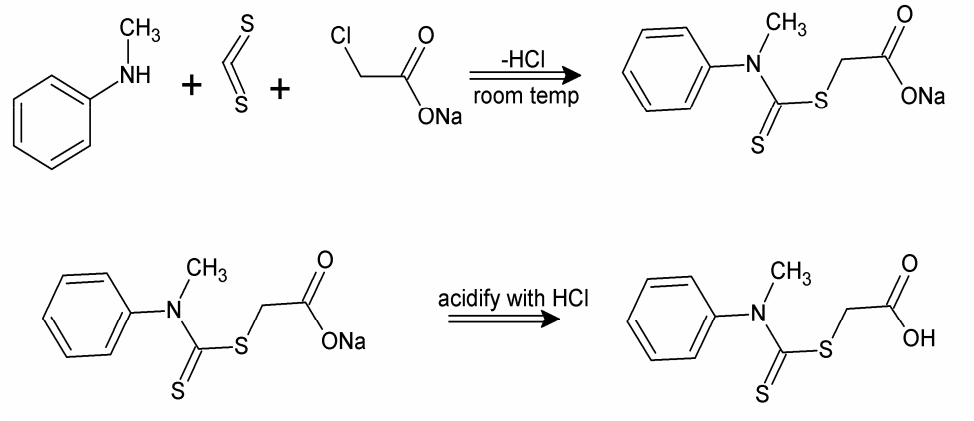

Scheme 2.1 Synthesis of carboxymethyl N-methyl, N-phenyldithiocarbamate

2.2.2.2 *Synthesis of N^4-methyl-N^4-phenylthiosemicarbazide*

A mixture of 17.7 g (0.0733 mol) of carboxymethyl-N-methyl-N-phenyl dithiocarbamate in 20 ml of 98% hydrazine hydrate and 10 ml of water was heated in the rings of a steam bath at 85 °C. After 3 minutes crystals began to separate. Heating was continued for an additional 22 minutes. The crystals were collected by filtration, washed well with water and dried. The crude product was recrystallised from a mixture of 50 ml ethanol and 25 ml water. This yielded about 10.8 g (81%) of stout crystals of N^4-methyl-N^4-phenyl 3-thiosemicarbazide (Scheme 2.2).

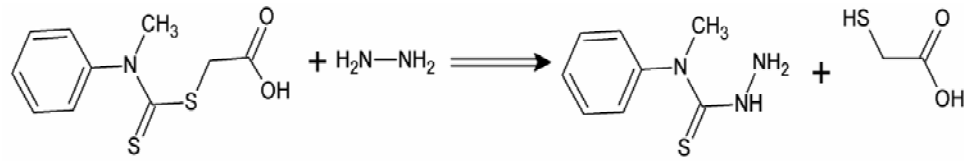

Scheme 2.2 Synthesis of N^4-methyl N^4-phenyl-3-thiosemicarbazide.

2.2.2.3 *Preparation of pyrolidine-1-carbothiohydrazide*

A solution of 1 g of N^4-methyl-N^4-phenyl-3-thiosemicarbazide (5.52 mmol) in 5 ml acetonitrile was treated with 395 mg (5.52 mmol) of pyrrolidine and the resulting solution was heated under reflux for 15 minutes. The solution was chilled and the separated were collected and washed well with acetonitrile. This afforded 570 mg (71%) of colorless needles of pyrollidine-1-thiosemicarbazide (Scheme 2.3). (m.p. 172-174 °C).

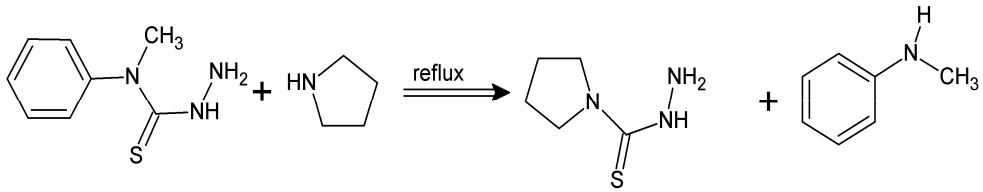

Scheme 2.3 Synthesis of pyrrolidine-1-carbothiohydrazide.

2.2.2.4 *Preparation of morpholine-4-carbothiohydrazide*

A solution of 1 g of N^4-methyl-N^4-phenyl-3-thiosemicarbazide (5.52 mmol) in 5 ml acetonitrile was treated with 0.174 g (5.52 mmol) of morpholine and the resulting solution was heated under reflux for 15 minutes. The solution was chilled and the separated were collected and washed well with acetonitrile. This afforded 0.6 g (67%) of colorless needles of morpholine-4-carbothiohydrazide (Scheme 2.4).

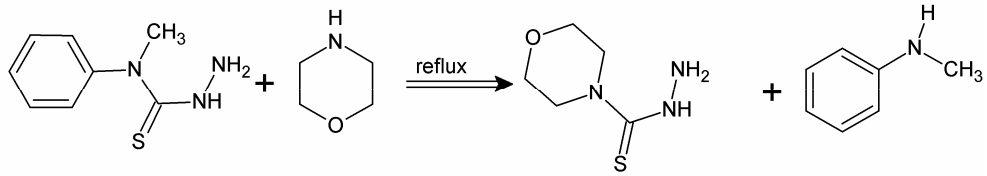

Scheme 2.4 Synthesis of morpholine-4-carbothiohydrazide.

2.2.3 Synthesis of proligands

2.2.3.1 *Synthesis of 2,6-diacetylpyridine bis(thiosemicarbazone) (H_2bts)*

A solution of 1 mmol (0.163 g) of 2,6-diacetylpyridine in 5 ml ethanol was mixed with 2 mmol (0.182 g) thiosemicarbazide 5 ml ethanol (Scheme 2.5) and refluxed over a steam bath. One drop of glacial acetic acid was added to the refluxing mixture and refluxing continued for half an hour. The pale yellow colored product started to form in the reaction medium was completed by keeping overnight. The product was filtered and washed with 1:1 methanol-water mixture and dried over P_4O_{10} *in vacuo*. The compound was recrystallised from methanol.

Yield, 65%; m.p, 241 °C; Elem. Anal. Found (calcd)%: C, 42.52 (42.21); H, 5.71 (5.61); N, 28.51 (28.71); S, 18.11 (18.78).

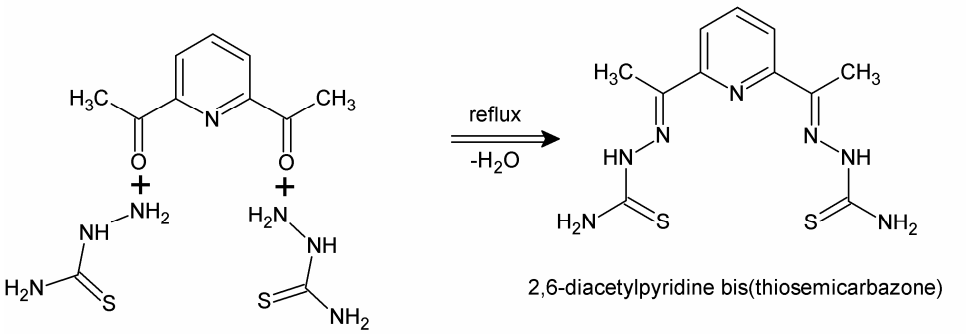

Scheme 2.5

2.2.3.2 *Synthesis of 2,6-diacetylpyridine bis(3-morpholinothiosemicarbazone) (H_2bmts)*

A solution of 1 mmol (0.163 g) of 2,6-diacetylpyridine in 5 ml ethanol was mixed with 2 mmol (0.322 g) morpholine-4-carbothiohydrazide in 5 ml ethanol and refluxed. One drop of glacial acetic acid was added to the refluxing mixture and refluxing continued for half an hour. Formation of yellow colored product in the reaction medium was completed by keeping overnight. The product was filtered and washed with ethanol and dried over P_4O_{10} (Scheme 2.6) *in vacuo*. The compound was recrystallised from methanol.

Yield, 55%; m.p, 151 °C; Elem. Anal. Found (calcd)%: C, 48.51 (48.80); H, 5.82 (6.25); N, 20.73 (20.97); S, 12.46 (13.71).

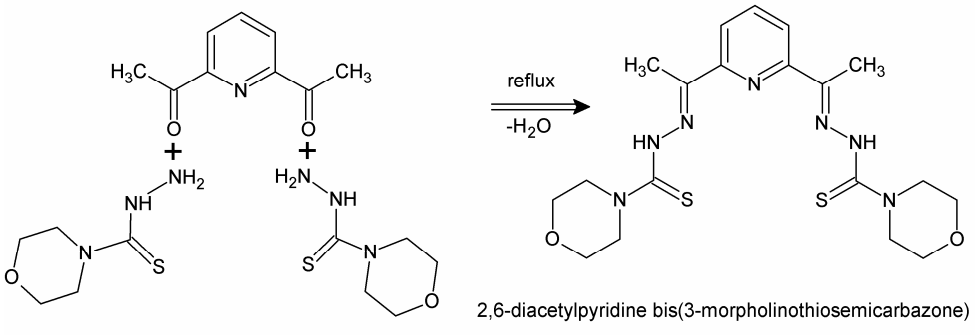

Scheme 2.6

2.2.3.3 *Synthesis of 2,6-diacetylpyridine bis(3-pyrroldinothiosemicarbazone) (H_2bpts)*

A solution of 1 mmol (0.163 g) of 2,6-diacetylpyridine in 5 ml ethanol was mixed with 2 mmol (0.290 g) pyrrolidine-1-carbothiohydrazide in 5 ml ethanol and refluxed. After the addition of one drop of glacial acetic acid to the refluxing mixture, refluxing was continued for half an hour. Formation of the bright yellow colored product in the reaction medium was completed by keeping overnight. The product was filtered and washed with ethanol and dried over P_4O_{10} (Scheme 2.7) *in vacuo*. The compound was recrystallised from methanol.

Yield, 67%; m.p 221 °C, Elem. Anal. Found (calcd)%: C, 52.98 (52.39); H, 6.56 (6.71); N, 22.94 (22.51).

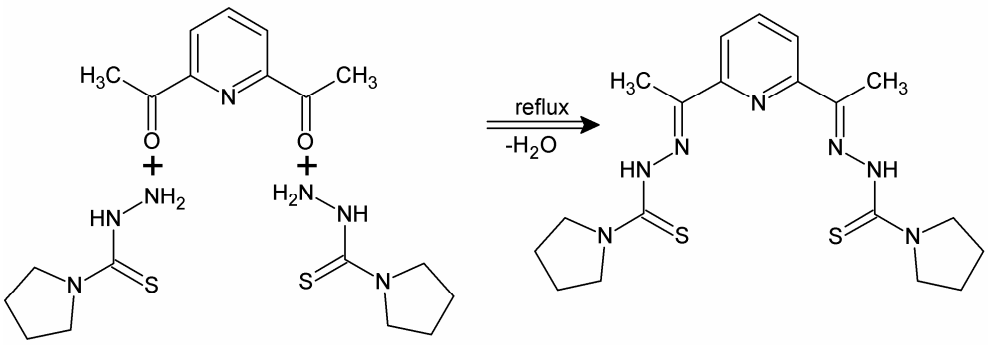

Scheme 2.7

2.2.3.4 *Synthesis of 2,6-diacetylpyridine mono(3-morpholinothiosemicarbazone) (H_2mts)*

To a solution of 1 mmol (0.163 g) of 2,6-diacetylpyridine in 5 ml ethanol, a solution of 1 mmol (0.161 g) morpholine-4-carbothiohydrazide in 5 ml ethanol was added slowly with stirring and then refluxed. To the refluxing mixture one drop of glacial acetic acid was added and refluxing continued for half an hour. Formation of the yellow product was completed in the reaction medium after keping overnight. The product filtered was washed with ethanol and dried

over P_4O_{10} (Scheme 2.8) *in vacuo*. The compound was recrystallised from methanol.

Yield, 45%; m.p., 169 °C; Elem. Anal. Found (calcd)%: C, 54.22 (54.88); H, 5.60 (5.92); N, 18.30 (18.29); S, 10.73 (10.47).

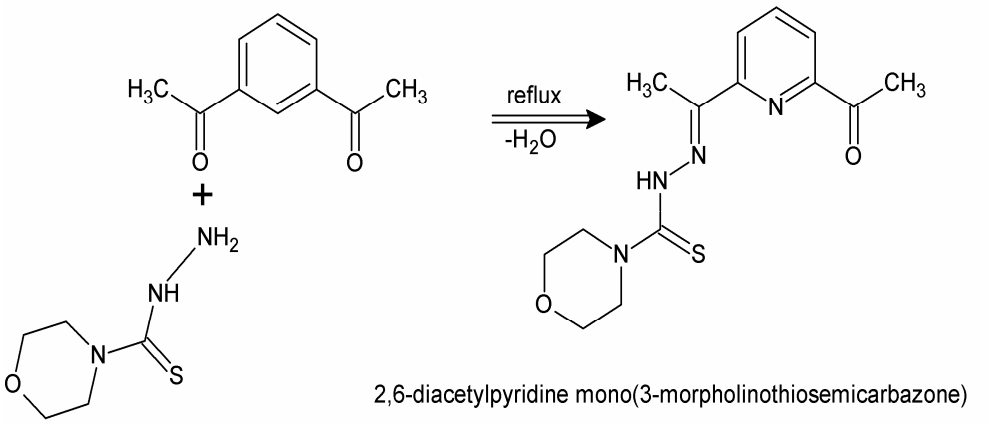

Scheme 2.8

2.3 Results and discussion

The precursors synthesized are pyrrolidine-1-carbothiohydrazide and morpholine-4-carbothiohydrazide. For the synthesis a facile method adopted by Scovill [19] was used. Carboxymethyl N-methyl-N-phenyldithiocarbamate was synthesized by a modification of the method of Holmberg and Psilanderheilm [21]. It is an addition reaction involving the addition of N-methylaniline and sodium chloroacetate to carbon disulfide. During the second stage N^4-methyl-N^4-phenylthiosemicarbazide was synthesized which is an improved method of Stanovnik and Tisler [22]. The dithiocarbamate group is replaced by hydrazine leading to the formation of the thiosemicarbazide. During the third stage the required thiosemicarbazides were synthesized. This was done by a transamination reaction for which the mechanism may be depicted as follows (Scheme 2.9). A secondary amine like N-methylaniline serves as a better leaving group for a more nucleophilic amine like pyrrolidine

or morpholine. The transamination proceeds by the standard addition elimination mechanism. Nucleophilic addition of an amine to the thicarbonyl group produces a tetrahedral intermediate. Elimination of N-methylaniline from this intermediate reforms the thiocarbonyl group resulting in a new N^4-substituted thiosemicarbazide.

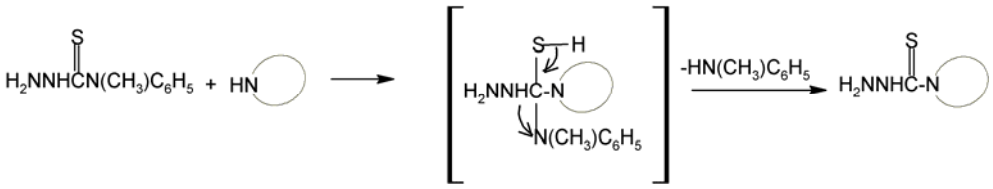

Scheme 2.9

The ligands were synthesized by adapting a modified Scovill's procedure. The N^4-methyl-N^4-phenylthiosemicarbazide synthesized was made to undergo transamination with morpholine/pyrrolidine in acetonitrile. The thiosemicarbazides were condensed with 2,6-diacetylpyridine in 1:2 ratio for bis(thiosemicarbazones) and 1:1 ratio for monothiosemicarbazone. The stoichiometries, color and elemental analyses data are given along with the synthesis. The elemental analyses results show that the experimental data are in accordance to the calculated values within the limits of experimental error. All the ligands are found to be stable at room temperature and are fairly soluble in DMF, DMSO and chloroform whereas almost soluble in ethanol or methanol and insoluble in water. They are oxidized by conc. HNO_3.

2.3.1 IR spectral studies

The interpretation of infrared spectra involves the correlation of absorption bands in the spectrum of an unknown compound with the known absorption frequencies for type of bonds. The characteristic bands for the ligands recorded as KBr discs are listed in Table 2.1. IR spectral analysis

supports the presence of characteristic groups in the ligands. All the ligands are having pyridine and thioamide groups in common. Pyridine ring vibrations that have been considered mainly are ring breathing vibrations and in-plane deformations since they are affected on coordination. Of the four thioamide bands I, II, III and IV, the IV band, which has a substantive contribution due to the thiocarbonyl stretching and bending vibration has been studied for all compounds. Hence the presence of characteristic bands in the spectrum indicates the presence of these groups in the molecule. The upward or downward shift or disappearance of the band can be correlated to coordination that has occurred.

Table 2.1 IR spectral data (cm^{-1}) of thiosemicarbazones.

Compound	$\nu(N^4–H)$/ $\nu(N^2–H)$	ν(C=O)	ν(C=N)	ν/δ(C–S)	ν(N–N)	Band III pyridine ring	py(ip)
H_2bts	3422/3160	--	1603	1360, 809	1103	1441	715
H_2bmts	3164	--	1613	1361, 792	1103	1463	741
H_2bpts	3370	--	1605	1360, 818	1130	1450	658
H2mts	3094	1691	1613	1365, 814	1110	1463	734

H_2bts: The spectrum (Fig. 2.3) of H_2bts bands at 3422 and 3160 cm^{-1} are assigned to $\nu(N^4–H)$ and $\nu(N^2–H)$ respectively. The azomethine stretching vibration ν(C=N) which is characteristic of a Schiff base is observed at 1603 cm^{-1}. The IVth band, which has a substantive contribution due to the thiocarbonyl bending vibration in the free bis(thiosemicarbazones) is found at 809 cm^{-1}. The medium peak observed at 1103 cm^{-1} is found to be due to ν(N–N). The thiocarbonyl group show stretching vibrations at 1360 cm^{-1}, while additional bands in the broad region of 1500-700 cm^{-1} are due to vibrations involving interactions between C=S stretching and C–N stretching of the C=S groups attached to a nitrogen atom [23]. Lack of a band at *ca* 2750 cm^{-1} indicates the

absence of –SH stretching absorptions in the molecule and hence the thione form is present in the solid state. The band III pyridine ring vibrations are at 1441 cm^{-1} whereas the in-plane-deformation at 715 cm^{-1}.

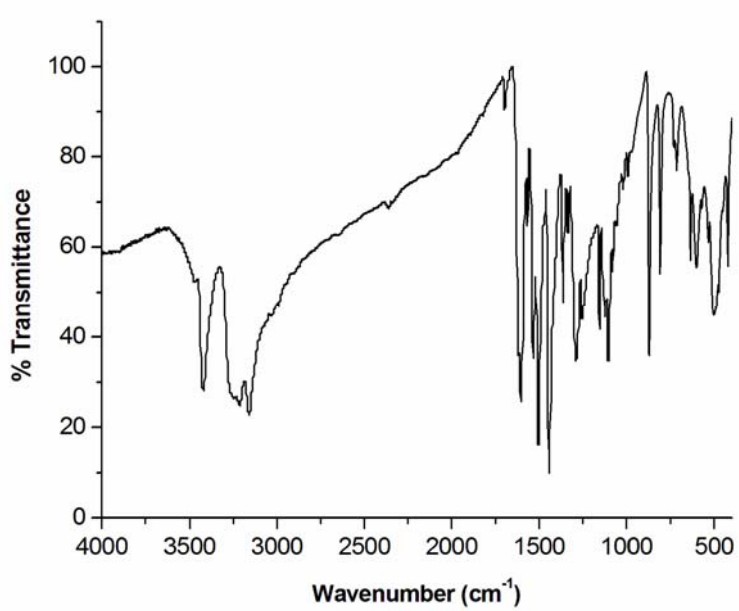

Fig. 2.3 IR spectrum of H_2bts.

H_2bmts: In the IR spectrum (Fig. 2.4) of H_2bmts the band at 3164 cm^{-1} is assigned to $\nu(N^2–H)$ and absence of a band at higher wavenumber indicates the tertiary nature of N^4. The azomethine stretching vibration ν(C=N) is at 1613 cm^{-1} which absorbs at a slightly higher energy in the morpholine ring incorporated H_2bmts. The medium peak observed at 1103 cm^{-1} is found to be due to ν(N–N) hydrazinic bond. The thiocarbonyl groups show stretching and bending vibrations at 1361 and 792 cm^{-1}. The band III pyridine ring vibrations are at 1463 cm^{-1} whereas the in-plane ring deformation is at 741 cm^{-1}. The CH stretching vibrations of morpholine ring system is observed at 2968 and 2867 cm^{-1}. Hence the incorporation of morpholine ring system by transamination is confirmed.

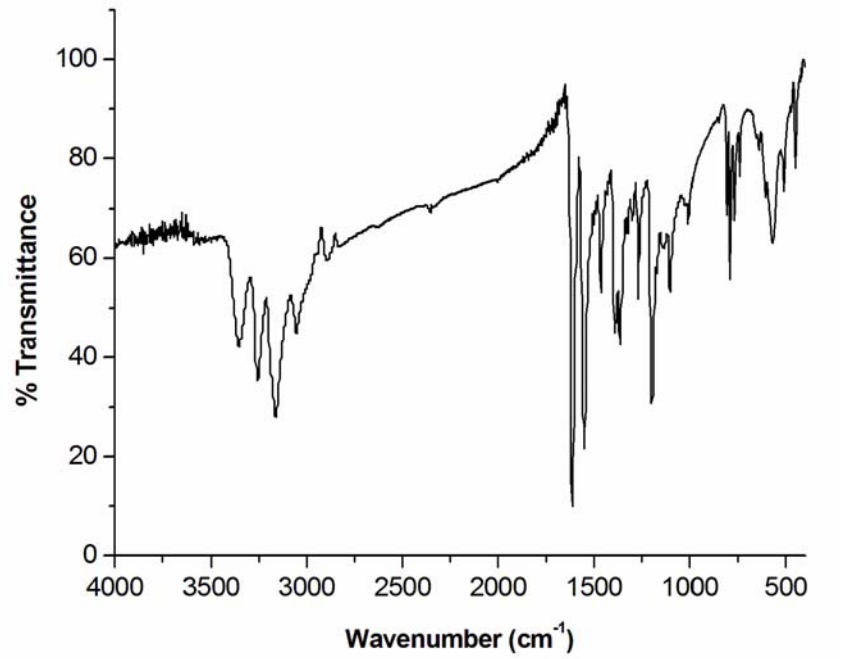

Fig. 2.4 IR spectrum of H_2bmts.

H_2bpts: The IR spectrum (Fig. 2.5) of H_2bpts exhibits a medium band at 3370 cm^{-1} which is assigned to $\nu(N^2–H)$ vibration. The stretching vibrations due to ν(C=N) characteristic of a Schiff base is observed at 1605 cm^{-1}. The band at 1130 cm^{-1} is due to ν(N–N) hydrazinic bond. The stretching and bending vibration bands due to the thiocarbonyl band are observed at 1360 and 818 cm^{-1}. The in plane ring deformation is found at 658 cm^{-1} [23]. The CH stretching vibrations of pyrrolidine ring system are observed at 2968 and 2867 cm^{-1}. Hence the substitution of pyrrolidine system by transamination is confirmed.

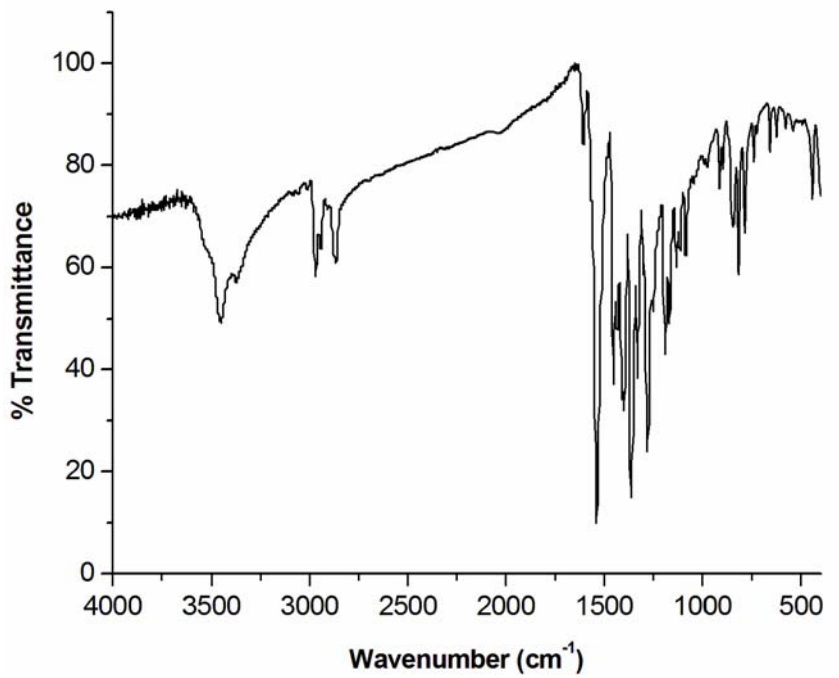

Fig. 2.5 IR spectrum of H_2bpts.

H_2mts : The vibrational bands of the monosubstituted compound (Fig. 2.6) are found to be almost the same as that of the bis(thiosemicarbazone), H_2bmts. The band at 3094 cm^{-1} is assigned to $\nu(N^2–H)$. An additional strong band observed at 1691 cm^{-1} corresponding to >C=O gives evidence for an uncondensed acetyl group in the compound. The azomethine stretching vibration ν(C=N) is observed at 1613 cm^{-1}. The medium peak observed at 1110 cm^{-1} is found to be due to ν(N–N). The stretching and bending vibration bands due to the thiocarbonyl band is observed at 1365 and 814 cm^{-1}. The band III pyridine ring vibrations are at 1463 cm^{-1} whereas the in-plane ring deformation at 734 cm^{-1}.

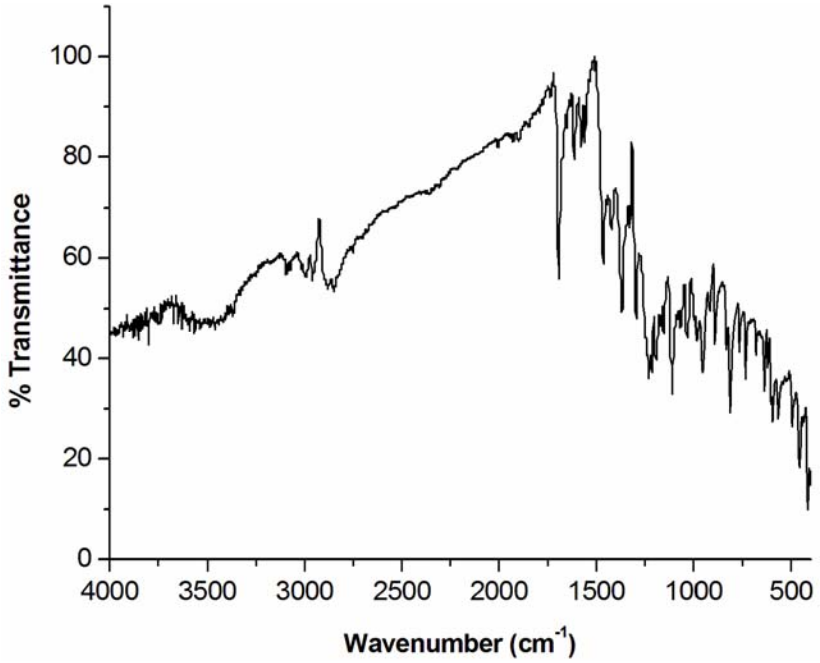

Fig. 2.6 IR spectrum of H_2mts.

2.3.2 Electronic spectral studies

The electronic spectra of organic molecules containing chromophores are usually complex because the superposition of vibrational transitions on the electronic transition results in broad bands of absorption that often appears to be continuous. The complex nature of the spectra makes detailed theoretical analysis difficult or impossible. Besides the conjugation of chromophores has a profound effect on spectral properties resulting in the absorption maxima shifting to longer wavelengths.

The energies required for transitions involving *n* or π electrons to π^* excited state bring the absorption peaks into an experimentally convenient region [24]. The intraligand absorption maxima obtained for2,6-diacetylpyridine bis(^{4}N-dimethylthiosemicarbazone) are found to be around 38,000 cm^{-1} for $\pi \rightarrow \pi^*$ and around 30,000 cm^{-1}. A shoulder at around 24000 cm^{-1} is due to the $n \rightarrow \pi^*$ transition of the thioamide function. The band obtained

for the bright yellow compound is due to bifurcated hydrogen bonding leading to the conjugation for one of the thiosemicarbazone moieties [18]. For H_2bmts, H_2bpts and H_2mts absorption maxima are obtained around 24000 cm^{-1} which supports the bifurcated hydrogen bonding in one of the arms. It can be also interpreted that the $n \rightarrow \pi^*$ transition of the thioamide function undergo a bathochromic shift when thiosemicarbazone moieties have a ring incorporated at N^4 position [25].

The intraligand absorption maxima observed for the ligands are shown in Table 2.2.

Table 2.2 Electronic spectral assignments of ligands.

Compound	UV-vis absorption bands (cm^{-1})
H_2bts	32130, 30540
H_2bmts	37640, 32250, 29810, 24390
H_2bpts	43820, 33680, 31000, 24450
H_2mts	43680, 37840, 29500, 24750

H_2bts: The electronic spectrum (Fig. 2.7) of the ligand in acetonitrile shows the absorption maxima at 30540 cm^{-1}. This has been assigned as the $n \rightarrow \pi^*$ transition. A shoulder observed at 32130 cm^{-1} is assigned as the $\pi \rightarrow \pi^*$ transition.

H_2bmts: The electronic spectrum (Fig. 2.8) of H_2bmts in acetonitrile shows a shoulder at 32250 cm^{-1} due to $\pi \rightarrow \pi^*$ transition. The sharp peak obtained at 29810 cm^{-1} is due to $n \rightarrow \pi^*$ transition. A weak absorbance peak is also obtained at 24390 cm^{-1} as $n \rightarrow \pi^*$ transition due to the thioamide function [25].

H_2bpts: (Fig. 2.9) The $\pi \rightarrow \pi^*$ transition is observed at 43820 and 33680 cm^{-1} whereas the $n \rightarrow \pi^*$ transition is observed at 31000 cm^{-1}. Here also a less intense band due to $n \rightarrow \pi^*$ transition is observed at 24450 cm^{-1}.

H_2mts: The $\pi \rightarrow \pi^*$ transition (Fig. 2.10) is observed at 43680 cm^{-1} as a sharp peak. The $n \rightarrow \pi^*$ transition is less intense and observed at 29500 cm^{-1}. A weak absorbance found at 24750 cm^{-1} assigned as due to the thioamide function.

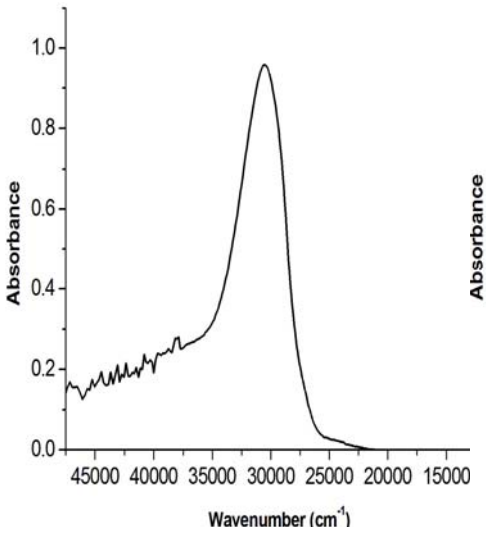

Fig. 2.7 Electronic spectrum of H_2bts.

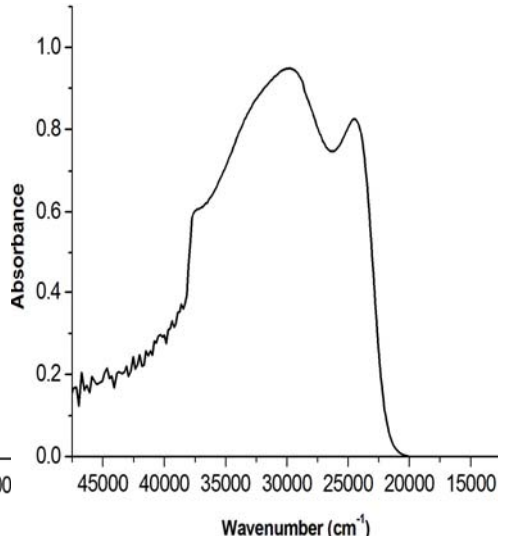

Fig. 2.8 Electronic spectrum of H_2bmts.

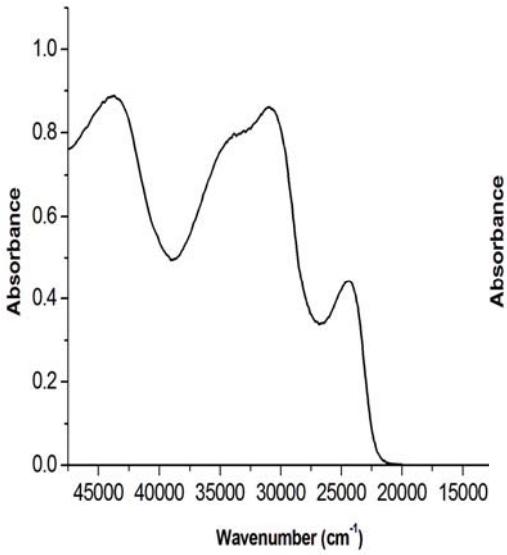

Fig. 2.9 Electronic spectrum of H_2bpts.

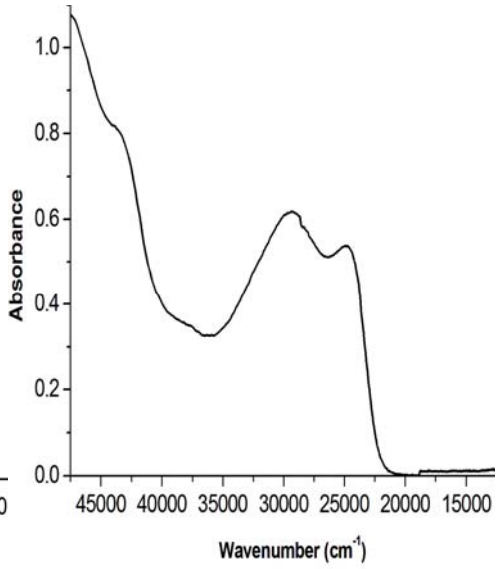

Fig. 2.10 Electronic spectrum of H_2mts.

2.3.3 NMR spectral studies

The ^{1}H and ^{13}C NMR spectra of all the compounds were recorded. The D_2O exchange, DEPT are also done. Data assignments were done by comparing the values with already reported results and the standard values given in literature [26-29]. The values are assigned along with tentative structures since single crystal X-ray studies were not possible. ^{13}C NMR spectrum of H_2bmts was not taken since already reported values in literature support the ^{1}H NMR.

H_2bts: The ^{1}H NMR spectrum of H_2bts along with spectral assignments are given in Fig. 2.11.

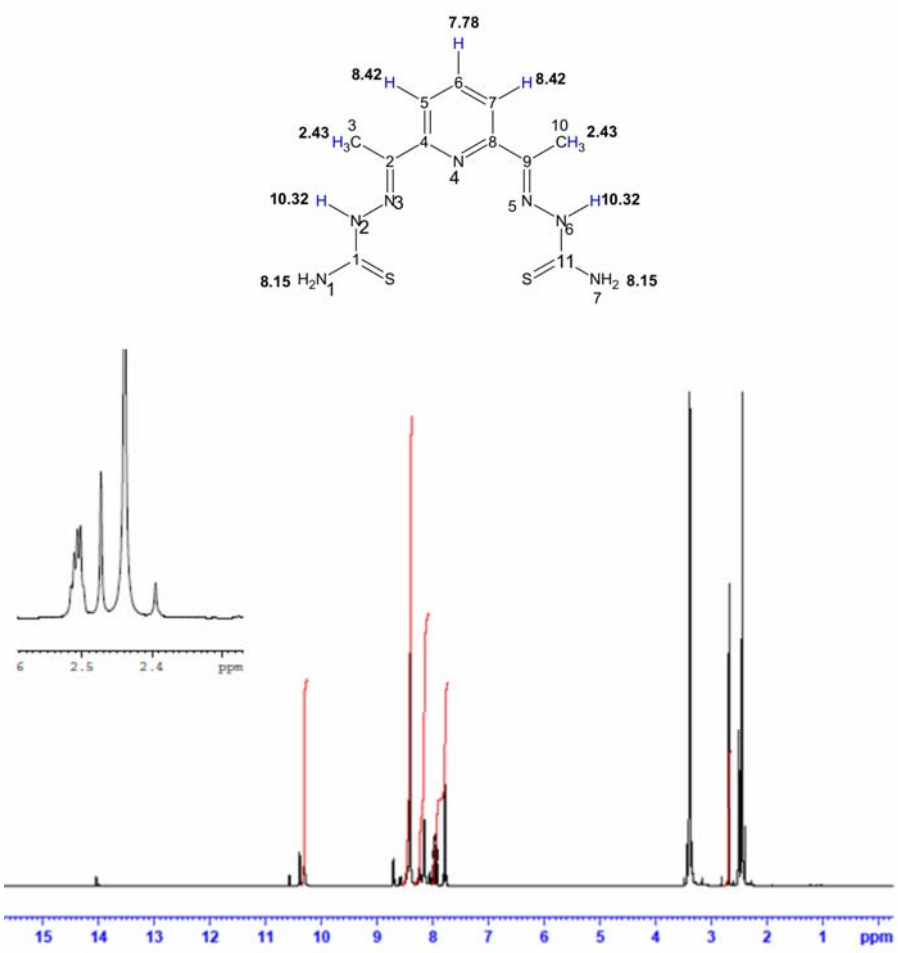

Fig. 2.11 ^{1}H NMR spectrum of H_2bts along with peak assignment.

The two arms of the bileptic compound being unsubstituted are found to be almost equivalent magnetically. The N2/6 protons appearing at 10.32 ppm are shifted downfield and found to be exchangeable with D_2O. This may be due to the fact that they are attached to a heteroatom and so are easily subjected to hydrogen bonding. The terminal N1/7 H_2 gave a singlet at 8.15 ppm. A sharp singlet, which integrates as six hydrogens at δ = 2.43 ppm is assigned as the methyl protons. Pyridine ring protons are assigned as a triplet at 7.78 ppm due to the para proton and a doublet 8.42 ppm due to the protons at the meta positions [28].

The ^{13}C NMR spectrum of the compound (Fig. 2.12) shows carbon signals supporting the ^{1}H NMR assignments. If proton decoupled ^{13}C method is used, it provides direct information about the carbon skeleton of the molecule alone. C1/11 signal (δ = 179.04 ppm) and C2/9 signal (δ = 148.06 ppm) are found to be farther downfield. In the pyridine skeleton the ortho carbons are deshielded to 153.49 ppm when compared with 149.8 ppm of free pyridine whereas the meta carbons are at 120.84 ppm and the para carbon 136.63 ppm. In the DEPT spectrum the signals due to C1, C2, C4, C8, C9 and C11 disappear whereas C3, C5, C6, C7 and C10 are retained positive. This shows that C3, C5, C6, C7 and C10 have odd number of hydrogens whereas the other carbons are without protons. These assigned values of ^{1}H and ^{13}C NMR spectra give evidence for the structure assigned.

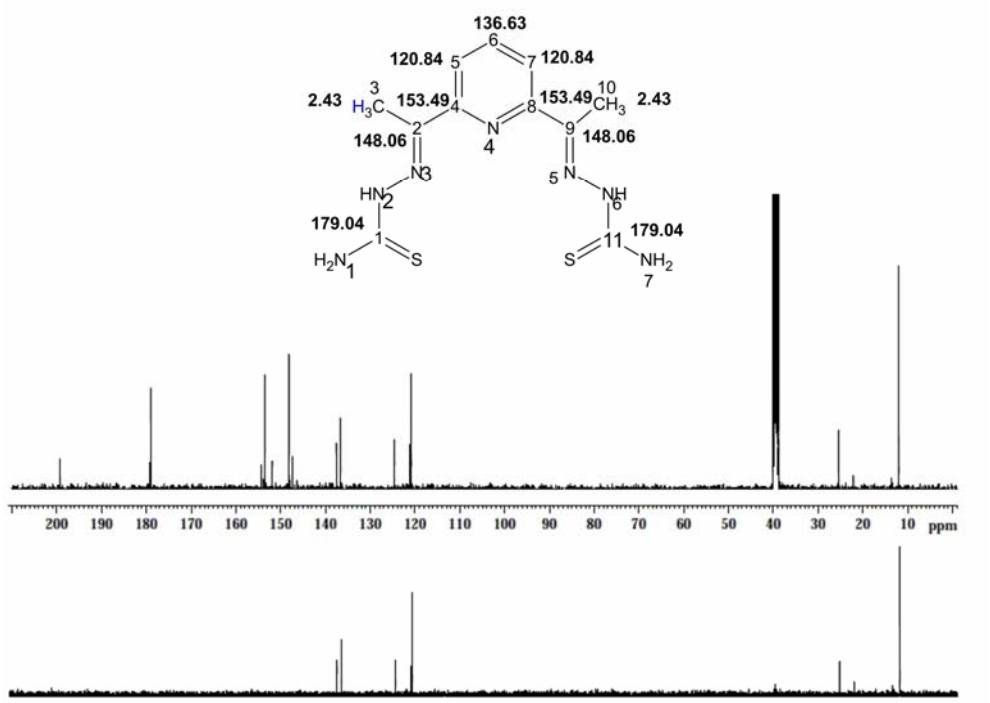

Fig. 2.12 ^{13}C NMR spectrum of H_2bts with DEPT along with peak assignment.

H_2bmts : The ^{1}H NMR spectrum of H_2bmts along with the values assigned are represented in Fig. 2.13. It appears to be a complex spectrum and implies the magnetically non-equivalent nature of the bileptic molecule. The values are assigned by comparing with reported spectrum [30] in which the proton resonances for NH groups are reported as 8.58 ppm for the *E*-form and 15.4 ppm which is farthest downfield for the *E′*-form being the bifurcated H-bonding form. The resonating peaks obtained at 8.58 and 15.4 ppm were assigned to the N2H and N6H respectively. These values indicate that one of the arm is with *E* configuration and the other *E′* configuration with a bifurcated H-bond [17]. A triplet obtained at 7.81 ppm and two doublets at 7.96 and 7.62 ppm are assigned for the pyridyl protons. The protons of the two methyl groups found as two singlets imply their magnetically nonequivalent nature. The assignment of morpholine ring protons are done by considering the triplets obtained in the spectrum. The protons nearer to the nitrogen are more

deshielded than the protons nearer to oxygen due to the influence of the thione sulfur. The multiplets obtained are shown in the inset of Fig. 2.13.

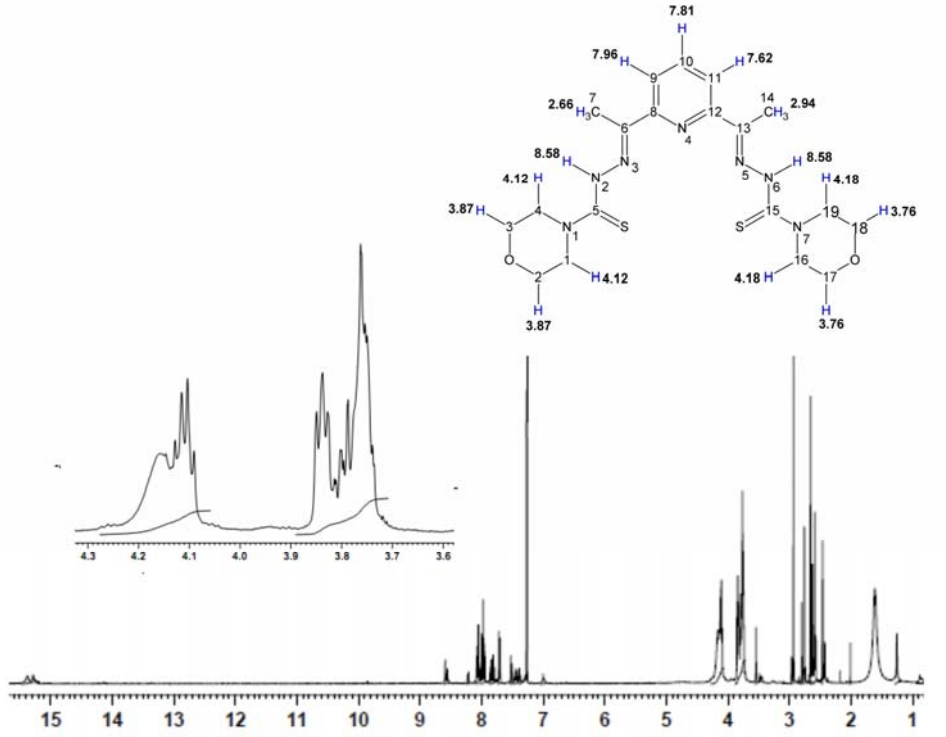

Fig. 2.13 ^{1}H NMR spectrum of H_2bmts along with peak assignment.

H_2bpts: The ^{1}H spectrum of H_2bpts was recorded in $CDCl_3$ as solvent. The tentative structure, numbering and the spectral assignments are given in Fig. 2.14. In the ^{1}H NMR spectrum the proton resonances for NH groups were found at 8.68 ppm. On addition of D_2O, the signal disappears which confirm the exchangeable nature of NH protons. This indicates that these nitrogens can be easily deprotonated. A low intense peak obtained at 15.4 ppm suggests a possibility for the existence of some bifurcated *E′* form in solution. This is found to be in agreement with the morpholine analogue of the bis(thiosemicarbazone) [30]. The sharp singlets observed at 2.4 and 2.5 ppm are assigned to the methyl protons attached to C7 and C14. The aromatic protons appear as a multiplet from 7.45 to 7.96 ppm. The triplet at 1.98 ppm is

assigned as the pyrrolidine ring protons away from the electronegative N and this shows protons at C2 and C3 are magnetically equivalent. The triplet at 3.95 ppm assigned as the ring protons nearer to electronegative N resonates at a downfield signal showing that C1 and C4 are magnetically equivalent. The protons of the other pyrrolidine ring show two broad peaks almost at the same region. These protons are found to be more deshielded when compared with free pyrrolidine.

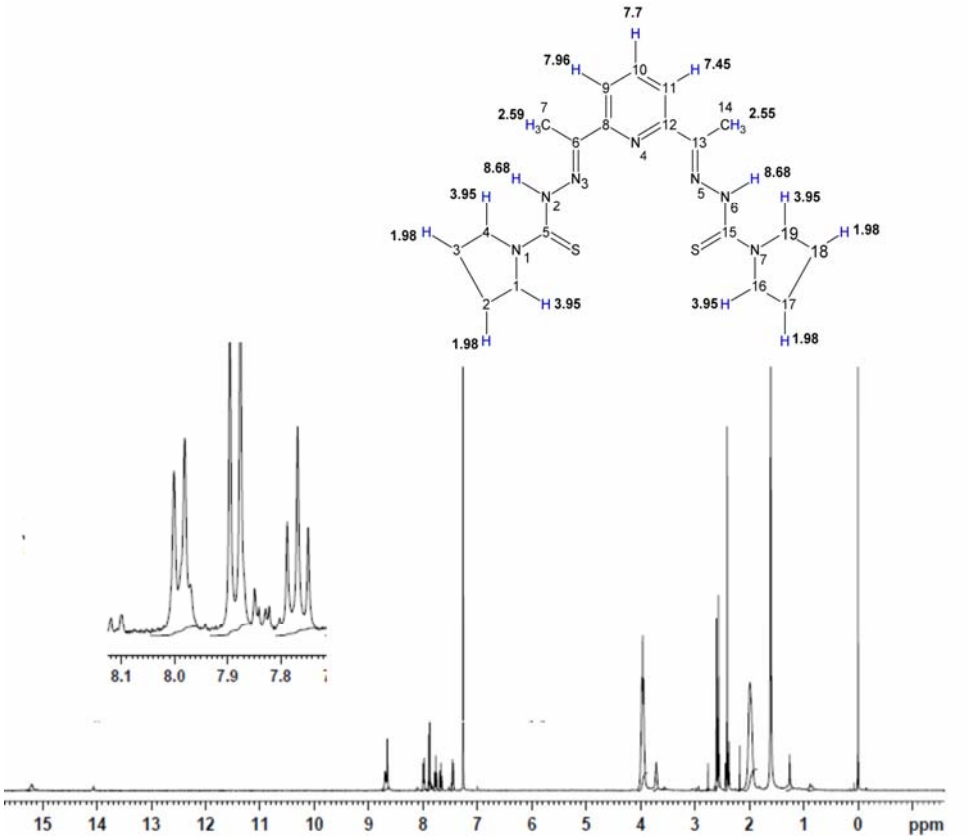

Fig. 2.14 ^{1}H NMR spectrum of H_2bpts along with peak assignment.

The ^{13}C NMR spectral studies support the carbon skeleton structure obtained by proton NMR spectrum. The proton decoupled ^{13}C spectrum (Fig. 2.15) of H_2bpts contains peaks corresponding to eight magnetically unique carbon atoms [9]. The pyrrolidine ring carbons C2/3 appear at a δ value of

19.28 and C1/4 at 46.24 ppm respectively. The thiocarbonyl carbons C5/15 resonate farthest downfield at 172.18 ppm. These two carbons are the most deshielded because of extensive electron delocalization along the conjugated framework of carbon skeleton, which reduces the electron density around the carbon atom.

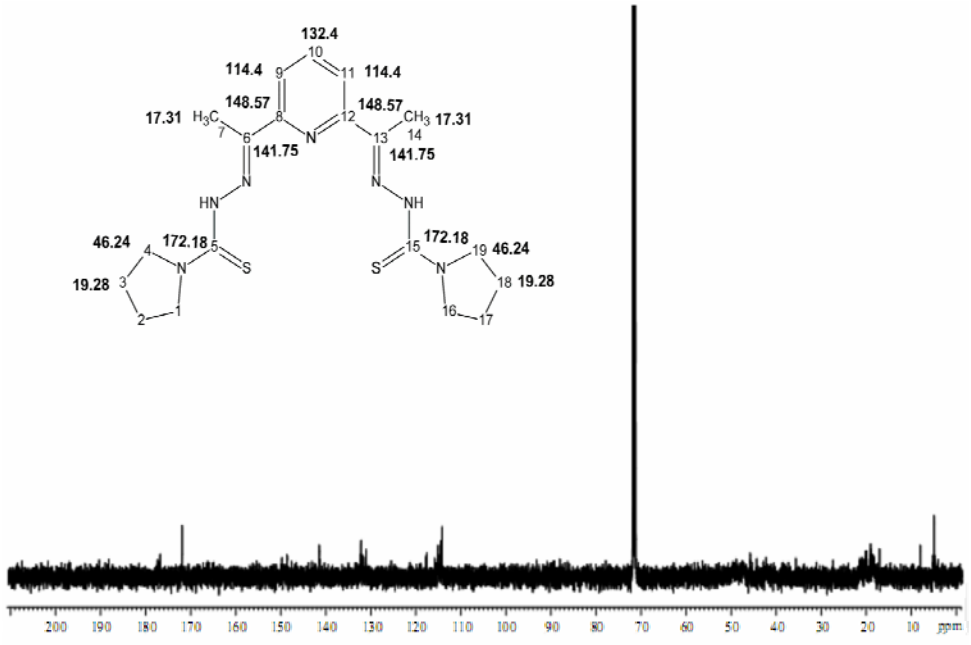

Fig. 2.15 ^{13}C NMR spectrum of H_2bpts along with peak assignment.

C6/13 of the azomethine group resonates at 141.75 ppm. In the pyridyl ring the ortho C8/12 adjacent to pyridyl N are found to resonate at 148.57 ppm. The resonating peaks for meta carbon atoms and the para carbon atom are found to be at 114.4 and 132.4 ppm respectively. C7/14 peaks of the methyl groups are found at 17.31 ppm. The DEPT spectrum provides evidence for the assignment.

H_2mts: In the ^1H NMR spectrum (Fig. 2.16) of H_2mts the N2H proton due to hydrogen bonding is shifted downfield to resonate at 15.2 ppm [17]. This assignment was confirmed since the peak was found to be exchangeable with

D_2O. The assignment of chemical shifts is based on reported studies of similar thiosemicarbazones [31]. The pyridyl protons were found to resonate at different downfield values resulting in a multiplet. The C14 methyl protons shift downfield to 2.93 ppm due to the nearby keto group whereas the C7 methyl protons found as a singlet at 2.65 ppm. The morpholine protons C2/3 near the oxygen resonate to give a broad peak at 3.7- 3.9 ppm whereas C1/4 protons near the nitrogen gives a triplet at 4.1 - 4.2 ppm. This downfield shift when compared with unsubstituted morpholine indicates the deshielding of protons. The characteristic peaks obtained for morpholine protons are placed in the inset in Fig. 2.16.

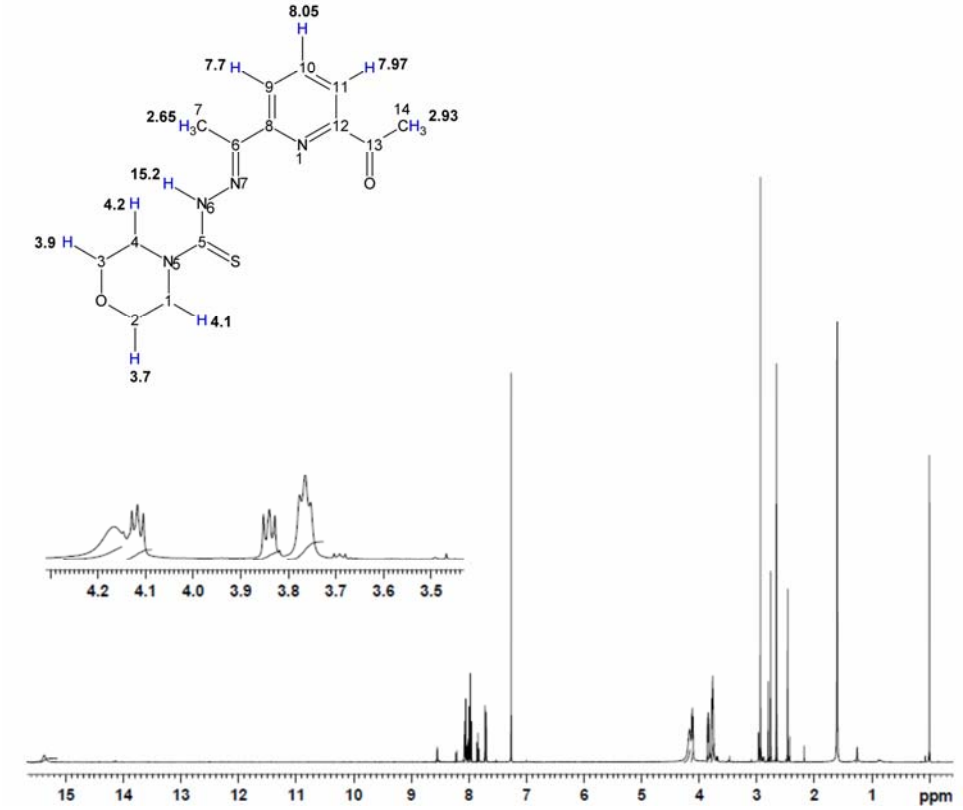

Fig. 2.16 ^{1}H NMR spectrum of H_2mts along with peak assignment.

The proton decoupled ^{13}C spectrum of H_2mts contains twelve peaks corresponding to twelve magnetically unique carbon atoms [9]. The morpholine ring carbons C2/3 appear at a δ value of 66.71 and C1/4 at 52.34

ppm. The thiocarbonyl carbon C5 resonates farthest downfield at 199.49 ppm followed by the carbonyl carbon C13 at 185.84 ppm. These two carbons are the most deshielded because of extensive electron delocalization along the conjugated framework of carbon skeleton, which reduces the electron density around the carbon atom. The C6 of the azomethine group resonate at 153.23 ppm. In the pyridyl ring the ortho C8 and C12 adjacent to pyridyl N are found to resonate downfield 147 and 148 ppm. The resonating peaks for meta carbon atoms and the para carbon atom are almost same as the values for free pyridine. C7 and C14 differ by almost double the δ value. The down field shift of the C14 may be due to the nearby keto group. The DEPT spectrum shows the resonances for the protonated carbon atoms.

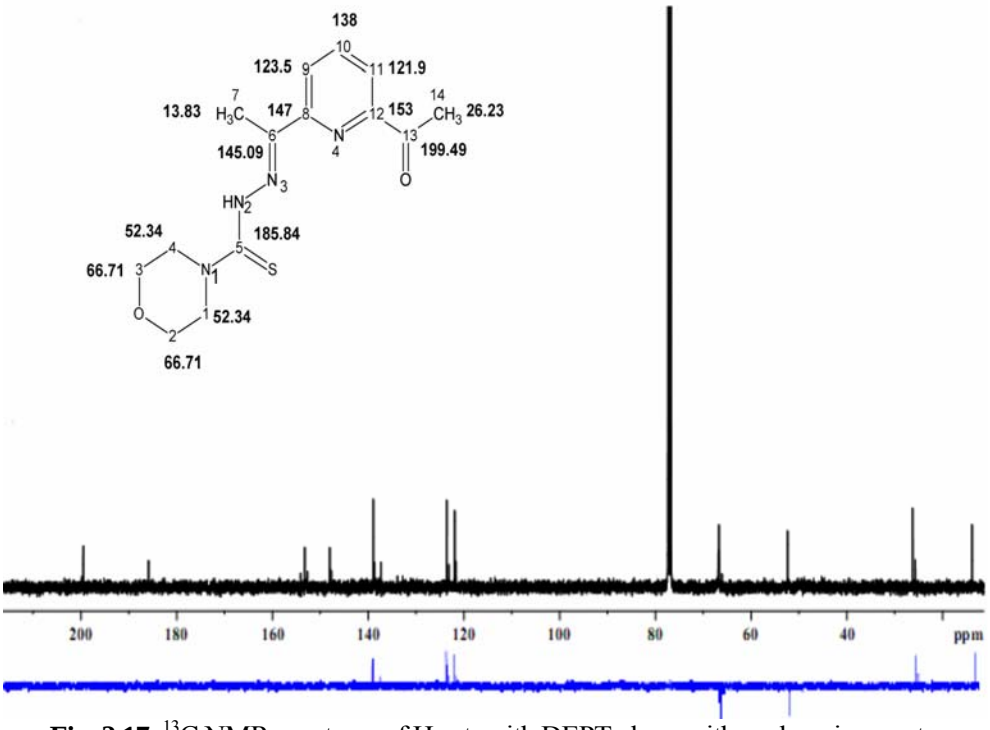

Fig. 2.17 ^{13}C NMR spectrum of H_2mts with DEPT along with peak assignment.

The disappearance of signals at 199.49, 185.84, 153.23, 147 and 148 ppm confirm the assignments already made being nonprotonated. The two negative signals can

be clearly distinguished as due to the methylene groups of the morpholine ring. The remaining five positive signals are due to C9, C10, C11, C7 and C14.

These data together with the data derived from the elemental analysis, IR and electronic spectra confirmed the proposed structures given to these ligands.

2.3.4 Cyclic voltammetric study of H_2mts

For studying the redox behaviour of ligand systems cyclic voltammetric studies are found to be useful. Usually depending on the redox nature of the complex a reversible, quasireversible or irreversible cyclic voltammograms are obtained [32,33]. The redox behaviour has been investigated using the DMSO solutions of H_2mts and 0.1 M TBAC as the supporting electrolyte. The experimental data and the cyclic voltammogram recorded for H_2mts are given in Fig. 2.18. Examination of the graph gives an irreversible oxidation peak under the experimental condition giving an oxidation peak at E_{pa} = 0.120 V. The oxidation peak may be due to the oxidation of thione group.

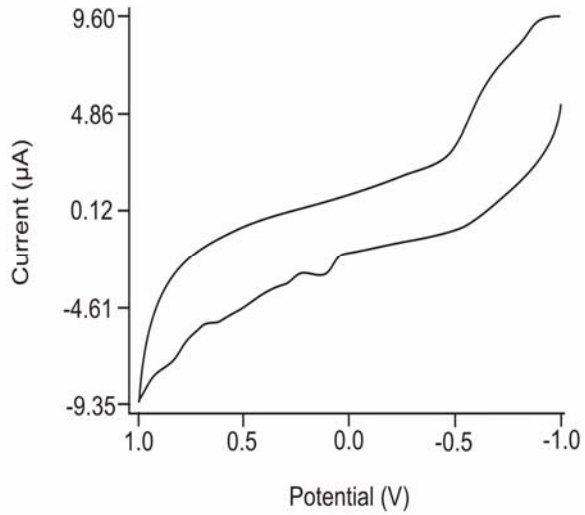

Fig. 2.18 Cyclic voltammetric responses relative to a 10^{-3} M [H_2mts], 0.1 M TBAC, glassy carbon working electrode, Scan rate 100 mV s^{-1}.

References

[1] T.S. Lobana, R. Sharma, G. Bawa, S. Khanna, Coord. Chem. Rev. 253 (2009) 977.

[2] B.S. Garg, M.R.P. Kurup, S.K. Jain, Y.K. Bhoon, Trans. Met. Chem. 13 (1988) 92.

[3] R.P. John, A. Sreekanth, M.R.P. Kurup, S.M. Mobin, Polyhedron 21 (2002) 2515.

[4] E.B. Seena, B.N. Bessy Raj, M.R.P. Kurup, E. Suresh, J. Chem. Cryst. 36 (2006) 189.

[5] V. Philip, V. Suni, M.R.P. Kurup, M. Nethaji, Polyhedron 23 (2004) 1225.

[6] A.I. Matesanz, J.M. Perez, P. Navarro, J.M. Moreno, E. Colacio, P. Souza, J. Inorg. Biochem. 76 (1999) 29.

[7] J.S. Casas, M.S. Garcia-Tasende, J. Sordo, Coord. Chem. Rev. 209 (2000) 197.

[8] S.B. Padhye, P.B. Sonawane, D.X. West, Struct. Bond. 1 (1991) 76.

[9] M. Joseph, A. Sreekanth, V. Suni, M.R.P. Kurup, Spectrochim. Acta A 64 (2005) 637.

[10] L. Latheef, E.B. Seena, M.R.P. Kurup, Inorg. Chim. Acta 362 (2009) 2515.

[11] A. Sreekanth, H.-K, Fun, M.R.P. Kurup, Inorg. Chem. Commun. 7 (2004) 1250.

[12] R. Pedrido, M.R. Bermejo, M.J. Romero, M. Vazquez, A.M. Gonzalez-Noya, M. Maneiro, M.J. Rodriguez, M.I. Fernandez, Dalton Trans. (2005) 572.

[13] A.E. Liberta, S.B. Padhye, R.C. Chikate, P.B. Sonawane, A.S. Kumbhar, R.G.Yerande, Coord. Chem. Rev. 123 (1993) 49.

[14] B.A. Wilson, R. Venkatraman, C. Whitaker, Q. Tillison, Int. J. Environ. Res. Public Health 2 (2005) 170.

[15] D.X. West, G.A. Bain, R.J. Butcher, J.P. Jasinski, Y. Li, R.P. Pozdniakiv, J. Valdes-Matrinez, R.A. Toscano, S.H. Ortega, Polyhedron 15 (1996) 665.

[16] G. Bahr, G. Schleizer, Z. Anorg. Chem. 280 (1955) 161.

[17] J.P. Holland, F.I. Aigbrihio, H.M. Betts, P.D. Bonnitcha, P. Burke, M. Christlieb, G.C. Churchil, A.R. Cowley, J.R. Dilworth, P.S. Donelly, J.C. Green, J.M. Peach, S.R. Vasudevan, J.E. Warren, Inorg. Chem. 46 (2007) 465.

[18] C.A. Brown, D.X. West, Trans. Met. Chem. 28 (2003) 154.

[19] M. Mohan, P. Sharma, P. Kumar, N.K. Jha, Inorg. Chim. Acta 125 (1986) 9.

[20] J.P. Scovill, Phosphorus Sulfur Silicon 60 (1991) 15.

[21] B. Holmberg, B. Psilanderhielm, J. Prakt. Chem. 82 (1910) 2234.

[22] B. Stanovik, M. Tisler, J. Org. Chem. 25 (1960) 2234.

[23] D.X. West, I.S. Billeh, J.P. Jasinski, J.M. Jasinski, R.J. Butcher, Trans. Met. Chem. 23 (1998) 209.

[24] D.A. Skoog, F.J. Holler, T.A. Niemann, Principles of Instrumental Analysis, 5th Ed. Thomson Learning Inc 1998.

[25] V. Philip, Ph.D. thesis, Cochin University of Science and Technology, 2004.

[26] J.S. Casas, A. Castineiras, A. Sanchez, J. Sordo, A. Vasquez-Lopez, Inorg. Chim. Acta 221 (1994) 61.

[27] J.S. Casas, E.E. Castellano, M.S. Garcia-Tasende, A. Sanchez, J. Sordo, J. Sukerman-Schepector, Z. Anorg. Allg. Chem. 623 (1997) 825.

[28] M.C. Rodrìguez-Arguelles, M.B. Ferrari, F. Bisceglie, C. Pelizzi, G. Pelosi, S. Pinelli, M. Sassi, J. Inorg. Biochem. 98 (2004) 313.

[29] R. Pedrido, A. M. Gonalez-Noya, M.J. Romero, M.M. Calvo, M.V. Lopez, E. Gomez-Forneas, G. Zaragoza, M.R. Bermejo, Dalton Trans. (2008) 6776.

[30] K. Nomiya, K. Sekino, M. Ishikawa, A. Honda, M. Yokoyama, N.C. Kasuga, H.Yokoyama, S.Nakano, K.Onodera, J. Inorg. Biochem. 98 (2004) 601.

[31] J.S. Casas, E.E. Castellano, M.S. Garcia-Tasende, A. Sanchez, J. Sordo, M.J. Vidarte, Polyhedron 17 (1998) 2249.

[32] A. Abu-Hussen, W. Linert, Spectrochim. Acta Part A 74 (2009) 214.

[33] R. Joseph, K.G. Kumar, Anal. Letters 42 (2009) 2309.

Chapter 3

Synthesis and Characterization of Mn(II) Complexes

Contents

3.1 Introduction

Manganese is a pinkish gray, hard and brittle metal. It is an essential element for all living species. Traces of manganese are found in many plants and bacteria, and a healthy human adult has about 10-20 mg of manganese in his body. It is an essential component to steel production.

Manganese, being the middle member in the first row of transition elements shows maximum number of oxidation states (-3 to +7). Mn^{2+}, the most stable oxidation state also as inferred from the Latimer diagram, in most of the complexes are found to be in high spin since exchange energy favors high spin [1]. Two functional values can be assigned for manganese; as a lewis acid in +2 oxidation state and as an oxidative catalyst in higher oxidation states [2-4].

Manganese is an essential element in many biological processes like oxygen evolving complex photosystem II, superoxide dismutase etc. Enzymes like oxygen evolving complex (OEC), containing manganese, catalyses the cleavage of water by photo oxidation [5]. In redox enzymes of manganese it exists as Mn^{2+} in ribonucleotide reductase [6] and thiosulfate oxidase [7] whereas as Mn^{3+} in SOD [8]. It catalyses the dismutation of superoxide

radicals to oxygen and hydrogen peroxide. Numerous manganese complexes have been prepared with the aim of modeling these enzymes. By designing more effective functional models of manganese containing active sites we can control the metal based redox potential of these complexes [9].

Very few reports on the manganese complexes of 2,6-diacetylpyridine bis (thiosemicarbazones) are there in the literature. However such pentadentate systems are reported to exist as pentagonal-bipyramidal complexes along with anions or water molecules [10-13]. Manganese complexes of monothiosemicarbazones are not at all reported.

3.2 Experimental

3.2.1 Materials

The syntheses of the proligands are discussed in Chapter 2. Solvents being pure were used as supplied. Manganese acetate used was Analar grade and used as supplied for the preparation of the complexes. Solvents used were methanol and dimethylformamide.

3.2.2 Synthesis of complexes

3.2.2.1 *Synthesis of [Mn(Hbts)(OAc)]·CH_3OH·H_2O (**1**)*

H_2bts (0.155 g, 0.5 mmol) was dissolved in 2 ml of DMF and diluted with 15 ml methanol. This was slowly added to a hot solution of $Mn(OAc)_2·4H_2O$ (0.123 g, 0.5 mmol) in 15 ml methanol. The mixture was refluxed for 3 hours and allowed to cool. The yellow complex formed was filtered, washed in methanol followed by ether and dried *in vacuo* over P_4O_{10}.

Yield 75%, Elem. Anal. found (calcd)% for $C_{14}H_{23}MnN_7O_4S_2$: C, 35.81 (35.59); H, 4.61 (4.91); N, 20.78 (20.75); S, 13.71 (13.57); μ (B.M.), 5.69.

3.2.2.2 *Synthesis of [Mn(bmts)]·CH_3OH (**2**)*

$Mn(OAc)_2·4H_2O$ (0.123 g, 0.5 mmol) was dissolved in 15 ml methanol and heated. H_2bmts (0.225 g, 0.5 mmol) was dissolved in 2 ml of DMF and

diluted with 15 ml methanol and this mixture was slowly added to the above solution. The mixture was refluxed for 3 hours and allowed to cool. The dull yellow complex formed was filtered, washed in methanol followed by ether and dried over P_4O_{10} *in vacuo*.

Yield 78%, Elem. Anal. found (calcd)% for $C_{20}H_{29}MnN_7O_3S_2$: C, 44.95 (44.94); H, 5.05 (5.47); N, 18.37 (18.34); S, 12.25 (12.00); μ (B.M.), 6.18.

3.2.2.3 *Synthesis of [Mn(bpts)]·0.5H_2O* ***(3)***

H_2bpts (0.209 g, 0.5 mmol) was dissolved in 2 ml of DMF and diluted with 15 ml methanol. This was slowly added to a hot solution of $Mn(OAc)_2{\cdot}4H_2O$ (0.123 g, 0.5 mmol) in 15 ml methanol. The mixture was refluxed for 3 hours and allowed to cool. The dull yellow crystalline complex formed was filtered, washed in methanol followed by ether and dried over P_4O_{10} *in vacuo*.

Yield 75%, Elem. Anal. found (calcd)% for $C_{19}H_{26}MnN_7OS_2$: C, 47.80 (47.59); H, 5.47 (5.47); N, 20.92 (20.45); S, 13.18 (13.37); μ (B.M.), 5.72.

3.2.2.4 *Synthesis of [Mn(Hmts)$_2$]* ***(4)***

H_2mts (0.153 g, 0.5 mmol) was dissolved in 2 ml of DMF and diluted with 15 ml ethanol. This was slowly added to a hot solution of $Mn(OAc)_2{\cdot}4H_2O$ (0.123 g, 0.5 mmol) in 15 ml ethanol. The mixture was refluxed for 3 hours and allowed to cool. The dark yellow complex formed was filtered, washed in methanol followed by ether and dried over P_4O_{10} *in vacuo*.

Yield 73%, color: brown, Elem. Anal. found (calcd)% for $C_{28}H_{34}MnN_8O_4S_2$: C, 50.78 (50.52); H, 5.52 (5.15); N, 16.74 (16.83); S, 9.53 (9.63); μ (B.M.), 6.03.

3.2.3 Physical measurements

Various physical measurements used are discussed in Chapter 1. CHNS analyses were carried out using Vario EL III CHNS analyzer at the SAIF,

Kochi, India. IR spectra were recorded on a Thermo Nicolet AVATAR 370 DTGS model FT-IR Spectrophotometer with KBr pellets at the SAIF, Kochi, India. Electronic spectra in 200-900 nm range were recorded on a Cary 5000 version 1.09 UV-VIS-NIR Spectrophotometer using solutions in DMF/DMSO at the SAIF, Kochi, India. EPR spectra were recorded in a Varian E-112 X-band EPR Spectrometer using TCNE as a standard at SAIF, IIT, Bombay, India. The *g* factors were quoted relative to the standard marker TCNE (g = 2.00277). Cyclic voltammetric measurements were done on a PC interfaced electrochemical analyzer (BAS Epsilon Bioanalytical system USA) with a three electrode compartment system consisting of a glassy carbon working electrode, platinum wire counter electrode and Ag/Ag^{+} reference electrode, at the Department of Applied Chemistry, CUSAT, Kochi, India.

3.3 Results and discussion

Equimolar ratios of the ligands and the metal acetate yielded the yellow or dull yellow colored metal complexes. Colors, elemental analyses data and magnetic susceptibility values of the complexes are presented in the synthesis. The elemental analyses data show that all the compounds except **1** are coordinated in the doubly deprotonated form. In compound **1,** one of the arms of thiosemicarbazone moiety is in thiolate form whereas the other is in the thione form. Similar examples of thiosemicarbazone complexes in which both the thione and thiolate forms of the ligand co-exist have been reported [14]. The yellow or bright yellow color of the ligand deepens on complexation. The ligand is quickly converted to the thiolato form and gets deprotonated.

3.3.1 Magnetic susceptibility

Because of the additional stability due to the half filled *d* orbital, Mn(II) generally forms high spin complexes with an orbitally degenerate ^{6}S ground state term. A spin only magnetic moment of 5.92 B.M., independent of

temperature and stereochemistry is expected [15]. The magnetic moments obtained for all complexes are found to be around this value indicating the presence of five unpaired electrons and hence they are high spin complexes.

3.3.2 IR spectra

IR spectral bands which are considered for the study of complexes are the $\nu(N^2–H)$, ν(C=N), ν(N–N), ν/δ(C=S), band III pyridine ring vibrations and in plane ring deformation bands. The ν(C=N) band of all complexes are found to be shifted to lower wavenumber in the spectrum indicating the coordination of the azomethine nitrogen to the metal. Disappearance of $\nu(N^2–H)$ band is an indication of deprotonation of the ligand upon coordination. This is also supported by the shift in ν(N–N) band to higher frequencies. This indicates greater bond strength due to increase in double bond character. Involvement of the pyridine nitrogen in coordination is indicated by the variations observed in the ring breathing vibrations of pyridine ring and the in-plane ring deformation band of pyridine. The variations in the stretching and bending vibrations of the thioamide band are considered for the coordination of the >C=S group. The significant bands obtained in the vibrational spectra of the four ligands and their Mn(II) complexes along with their tentative assignments are given in Table 3.1.

Table 3.1 IR spectral assignments of Mn(II) complexes along with the ligands.

Compound	$\nu(N^4–H)$/ $\nu(N^2–H)$	ν(C=O)	ν(C=N)	ν/δ(C–S)	ν(N–N)	Band III pyridine ring	py(ip)
H_2bts·CH_3OH	3214/ 3160	--	1603	1360, 872	1103	1441	715
[Mn(Hbts)(OAc)]· $CH_3OH·H_2O$ (**1**)	3292/ 3172	-	1588	1338, 786	1021	1406	753
H_2bmts	3164	--	1613	1361, 792	1103	1463	741
[Mn(bmts)]·CH_3OH **(2)**	--	--	1586	1314, 798	1111	1469	650
H_2bpts·H_2O	3370	--	1605	1360, 818	1130	1450	658
[Mn(bpts)]·0.5H_2O (**3**)	--	--	1588	1296, 798	1149	1399	625
H_2mts	3094	1691	1613	1365, 814	1110	1463	734
[Mn(Hmts)$_2$] (**4**)	--	1690	1584	1399, 887	1111	1447	714

In the spectrum of complex **1** (Fig. 3.1), the bands corresponding to $\nu(N^2–H)$ and $\nu(N^4–H)$ present in H_2bts are found to shift to higher wavenumbers indicating strengthening of the bond. The ν(C=N) band of compound **1** is found to be shifted from 1603 to 1588 cm^{-1} in the spectrum. This is also supported by the shift in ν(N–N) to higher frequencies. The ring breathing vibrations and the in-plane ring deformation band of pyridine ring shift from 1441 to 1406 cm^{-1} and from 715 to 753 cm^{-1} respectively. This confirms the involvement of the pyridine nitrogen in coordination. The stretching and bending vibrations of the thioamide band observed at 1360 and 872 cm^{-1} shift to 1338 and 786 cm^{-1} respectively. The bands at 1630 and 1545 cm^{-1} correspond to the symmetric and asymmetric stretching vibrations of the acetate group, consistent with the presence of a monodentate acetate group in the complex [16].

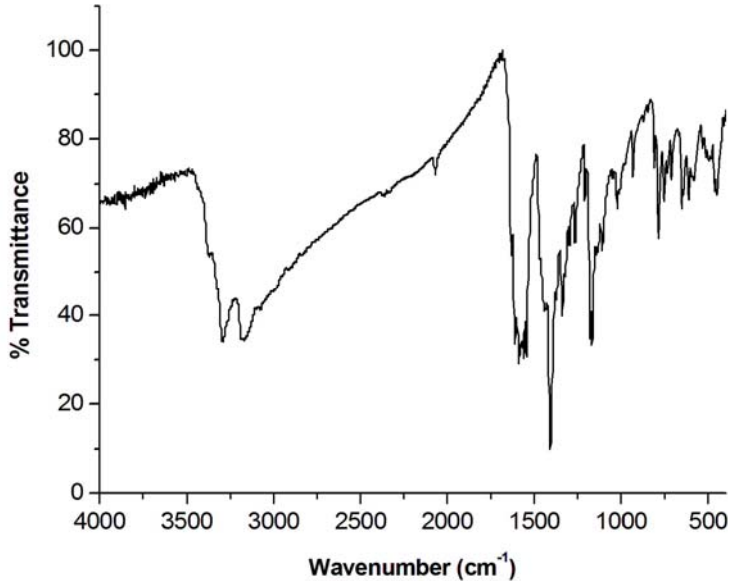

Fig. 3.1 IR spectrum of $[Mn(Hbts)(OAc)]\cdot CH_3OH\cdot H_2O$ (**1**).

The spectrum of the complex **2** (Fig. 3.2) reveals a broad band with low intensity around 3446 cm^{-1}. This can be due to the presence of methanolic OH group. The $\nu(N^2–H)$ vibration band observed in the ligand at around 3160 cm^{-1}

is found to disappear in all complexes except **1**. The azomethine band found at 1613 cm^{-1} for the uncomplexed ligand is shifted to 1586 cm^{-1} upon coordination. The band at 1621 cm^{-1} is assigned to the –C=N–N=C– moiety, newly formed as a result of deprotonation of the ligand on coordination [17,18]. Coordination via the thiolato sulfur is indicated by a decrease in the frequency to 1314 cm^{-1} of the stretching vibration of the thioamide band which was observed at 1361 cm^{-1} for the uncomplexed ligand. Variations are observed for the ring breathing vibrations and in-plane ring deformation band of pyridine ring indicating coordination of pyridine nitrogen. The vibrations due to the methylene groups of the morpholine ring are observed at 2965 and 2840 cm^{-1}.

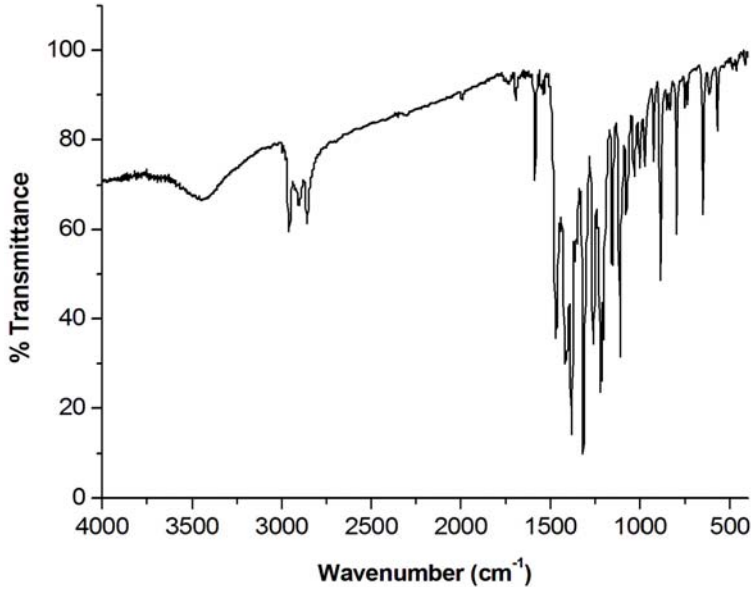

Fig. 3.2 IR spectrum of [Mn(bmts)]·CH_3OH (**2**).

In the spectrum of complex **3** (Fig. 3.3), the azomethine band found at 1605 cm^{-1} for the uncomplexed ligand is shifted to 1588 cm^{-1} which confirms the coordination of azomethine nitrogen to the metal center. The vibrations due to the methylene groups of the pyrrolidine ring are observed at 2966 and 2865 cm^{-1}. The ν(N–N) band shifts to 1149 cm^{-1} on coordination which is a measure of the

bond strength. Coordination via the thiolato sulfur is confirmed by a decrease in the frequency to 1296 and 798 cm^{-1} of the thioamide band which was observed at 1360 and 818 cm^{-1} for the uncomplexed ligand. Coordination of the pyridine nitrogen is confirmed by the ring breathing vibrations and the in-plane ring deformation band at 1399 and 625 cm^{-1}.

The spectrum of complex **4** (Fig. 3.4) reveals a deprotonated anionic structure for the ligand. The keto group of the compound absorbs almost at the same frequency as that of the free ligand. This makes the coordination of the keto group ambiguous. The azomethine band shifts to 1584 cm^{-1} on coordination from 1613 cm^{-1} in the uncomplexed ligand. The stretching and bending vibrations due to the thioketo group lowers when compared with the free ligand indicating strong coordination with enolization followed by deprotonation. Coordination of the pyridine nitrogen is confirmed by the in-plane ring deformation band at 714 cm^{-1}.

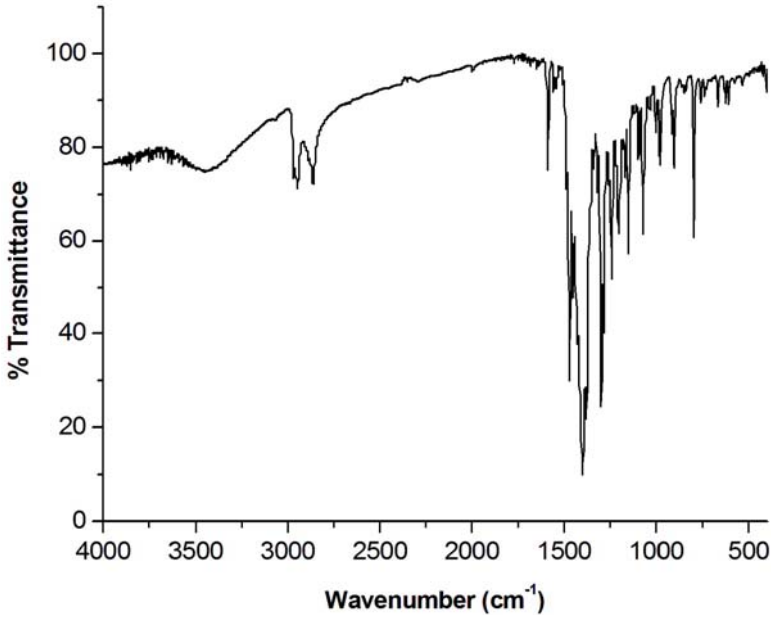

Fig. 3.3 IR spectrum of $[Mn(bpts)]\cdot 0.5H_2O$ (**3**).

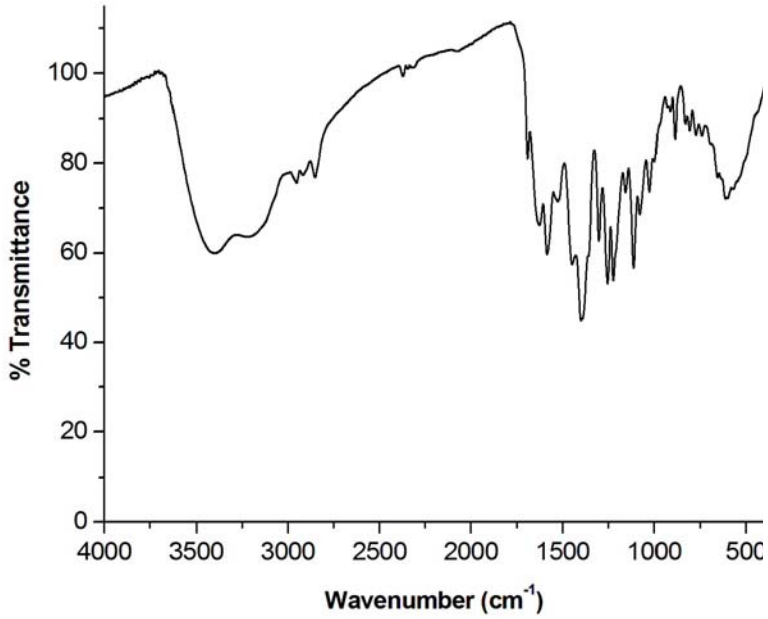

Fig. 3.4 IR spectrum of $[Mn(Hmts)_2]$ (**4**).

IR assignments support the fact that in all the complexes except **1** enolization followed by deprotonation has occurred resulting in anionic forms of the ligands.

3.3.3 Electronic spectra

The electronic spectra of the complexes were taken in acetonitrile. The spectral assignments are given in Table 3.2. A variety of colors shown by the transition metal complexes arise from electronic transitions that arise between levels whose spacings correspond to the wavelengths available in visible light. This spacing depends on factors such as the geometry of the complex, the nature of the ligands present and the oxidation state of the central metal atom. Hence the electronic spectra of complexes can provide valuable information related to bonding and structure. Interpretation of the electronic spectra however seems to be complex since in addition to these, several factors like interelectron repulsion also will affect the transitions [1].

Three types of transitions that are studied in electronic spectra are intraligand, charge transfer and *d-d* transitions. Charge transfer transitions are transitions in which an electron is transferred from one atom or a group in the molecule to another atom or group. Such transitions are usually of high intensity, usually occurring at the violet end of visible spectrum. Since a charge transfer transition originate from the redox nature of the metal ion and the ligand two types of transitions can occur namely, ligand to metal or metal to ligand. The *d-d* transitions usually originate from the electron transfer within the *d-d* orbitals of the metal. Based on the selection rules this transfer can give rise to spin allowed and forbidden transitions.

Table 3.2 Electronic spectral assignments Mn(II) complexes along with ligands.

Compound	UV-vis absorption bands (cm^{-1})
H_2bts	32130, 30540
[Mn(Hbts)(OAc)]·CH_3OH·H_2O (**1**)	31840, 27200, 22660
H_2bmts	37640, 32250, 29810, 24390
[Mn(bmts)]·CH_3OH (**2**)	32350, 29950, 25070
H_2bpts	43820, 33680, 31000, 24450
[Mn(bpts)]·0.5H_2O (**3**)	29880, 26870, 21740
H_2mts	43680, 37840, 29500, 24750
[Mn(Hmts)$_2$] (**4**)	37000, 30280, 25750

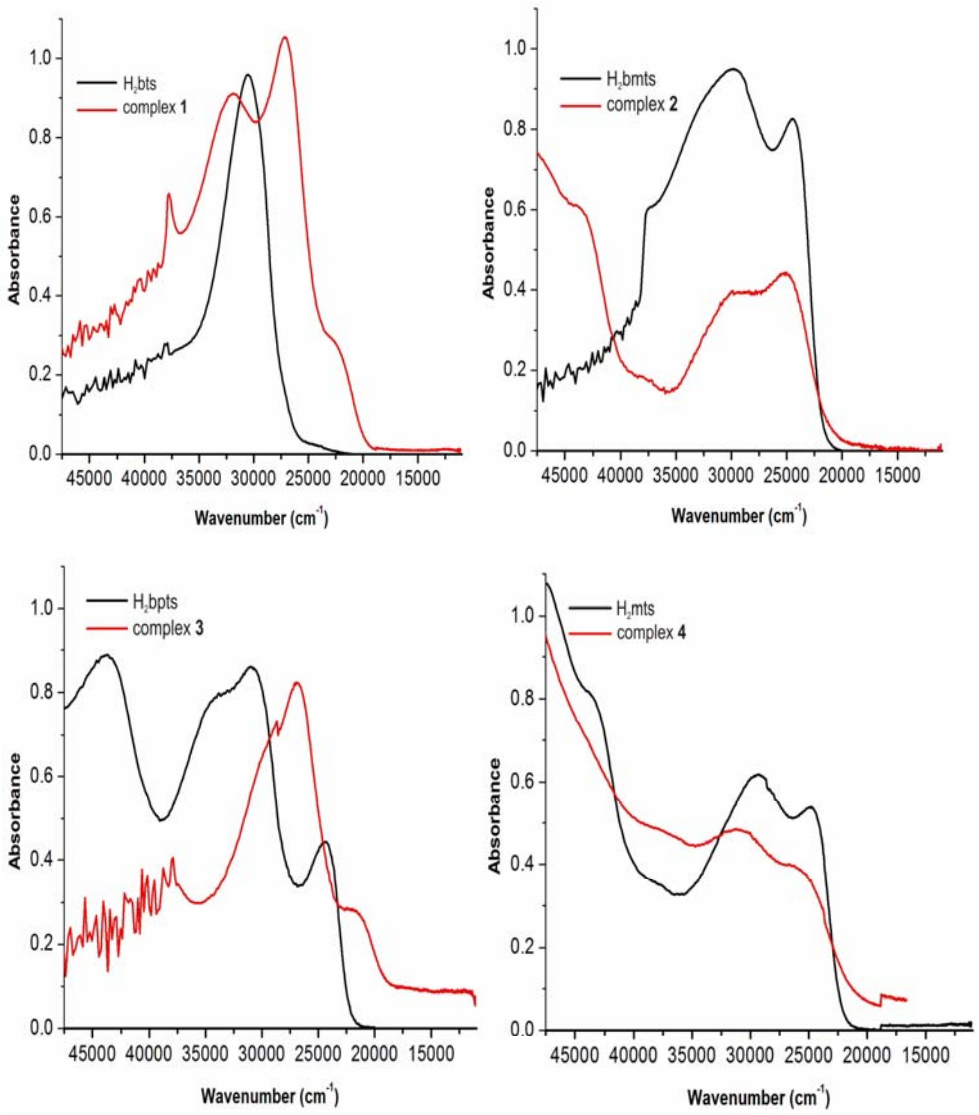

Fig. 3.5 Electronic spectra of complexes compared with ligands.

The ground state of the high spin octahedral Mn^{2+} ion is $^6A_{1g}$. Since there are no other terms of sextet spin multiplicity, all the *d-d* transitions in high spin d^5 complexes are not only Laporte forbidden but also spin forbidden [1]. Absorptions due to doubly forbidden transitions are extremely weak, even weaker than those for singly forbidden transitions. In addition very weak absorption bands to spin quartets *viz*. ^4G, ^4F, ^4D and ^4P are also

possible. Hence the four transitions possible are $^6A_{1g} \rightarrow {}^4T_{1g}(G)$, $^6A_{1g} \rightarrow {}^4T_{2g}(D)$ and $^6A_{1g} \rightarrow {}^4E_g(G)$, $^4A_{1g}(F)$. In the case of all the complexes intraligand transitions are found to have a bathochromic shift. None of the complexes show any *d-d* transition bands or they are obscured by the intense charge transfer bands. The electronic spectra of the complexes are presented as comparative spectra with the corresponding ligands in Fig. 3.5. The thioamide band for ring incorporated systems found around 24500 cm^{-1} for all ligands except H_2bts is either weakened or obscured by the charge transfer transitions.

3.3.4 EPR spectra

The EPR spectra of polycrystalline sample at 298 K and solution at 77 K were recorded in the X band using 100 kHz field modulation. The *g* factors were quoted relative to the standard marker TCNE (g = 2.00277). The EPR parameters are represented in Table 3.3. The polycrystalline state EPR spectra of all the complexes are found to be isotropic in nature with a *g* value almost equal to the spin only value.

Since Mn^{2+} ions are with five unpaired electrons, S = 5/2. Zero field splitting produces three doubly degenerate spin states, $M_s = \pm 5/2, \pm 3/2, \pm 1/2$ known as Kramer's degeneracy and no $M_s = 0$ state, leads to a special case of zero field splitting. On the application of a magnetic field, each of the doubly degenerate sets will further split producing six levels. As a result five transitions are produced, which will appear as a series of lines in the spectrum. Since the manganese nucleus has a nuclear spin I = 5/2, each spectral lines due to a particular M_s level undergoes hyperfine splitting into six fine lines [19].

A wide variety of bonding geometries are shown by manganese complexes. EPR spectroscopy has been shown to be a powerful tool to study them [20,21]. The spin Hamiltonian for Mn(II) may be described as

$$\hat{H} = g\beta BS + D[S_z^2 - S(S+1)/3] + E(S_x^2 - S_y^2)$$

where *B* is the magnetic field vector, *g* is the spectroscopic splitting factor, *D* is the axial zero field splitting term, *E* is the rhombic zero field splitting parameter and *S* is the electron spin vector. If *D* and *E* are very small, compared with *gβBS,* five EPR transitions corresponding to $\Delta m_s = \pm 1$ are expected. However, when *D* or *E* is very large, the lowest doublet has effective *g* values of $g_{\parallel} = 2$, $g_{\perp} = 6$ for $D \neq 0$ and $E = 0$. But for $D = 0$ and $E \neq 0$, the middle Kramer's doublet has a g_{iso} value of 4.29 [22,23].

The EPR spectrum (Fig. 3.6) of the compound **1** in polycrystalline state at 298 K exhibited an isotropic signal centered on *g* (2.024) which may be due to dipolar interactions and enhanced spin lattice relaxation [22].

Table 3.3 EPR spectral assignments of Mn(II) complexes.

Compound	*g* (polycrystalline state at 298 K)	*g* (DMF at 77 K)
$[Mn(Hbts)(OAc)]\cdot CH_3OH\cdot H_2O$ (**1**)	2.024	1.978, 2.333, 2.748, 3.6, 4.361
$[Mn(bmts)]\cdot CH_3OH$ (**2**)	1.990	2.012, 2.742, 3.367, 4.576, 6.189
$[Mn(bpts)]\cdot 0.5H_2O$ (**3**)	2.024	3.785
$[Mn(Hmts)_2]$ (**4**)	2.011	1.831, 7.400

For compound **1** the spectrum (Fig. 3.7) obtained in DMF at 77 K contain altogether thirty splittings with five *g* values of 4.36, 3.60, 2.75, 2.33 and 1.98. This is due to the five transitions produced, followed by the hyperfine splitting. Hence the spectrum we get is five sets of lines corresponding to five transitions with different energy, appearing at different field positions, each with six hyperfine splittings.

Compound **2** gave an isotropic signal in the spectrum (Fig. 3.8) in polycrystalline state at 298 K. This compound also gave five *g* values of 6.189, 4.576, 3.367, 2.742 and 2.012 when the spectrum (Fig. 3.9) was taken in DMF at 77 K. From the spectrum it can be seen that the intensity is greatest for the central

lines and smallest for the outermost lines. This indicates fine splitting of the absorption band because of non-degeneracy arising from zero field splitting [24].

In case of compound **3** an isotropic spectrum (Fig. 3.10) was obtained in polycrystalline state at 298 K and a more broadened isotropic spectrum (Fig. 3.11) at 77 K. The broadening of the spectra can be due to the spin-lattice relaxation and spin-spin interactions.

The EPR spectra of the compound $[Mn(Hmts)_2]$ was simulated using EasySpin [25] and the *g* values were gathered. The spectrum (Fig. 3.12) obtained in polycrystalline state at 298 K is found to be isotropic with a *g* value of 2.011. In the spectrum of the compound (Fig. 3.13) in DMF solution at 77 K two transitions were observed for which a *g* value of 7.4 at low field and 1.831 at high field were obtained.

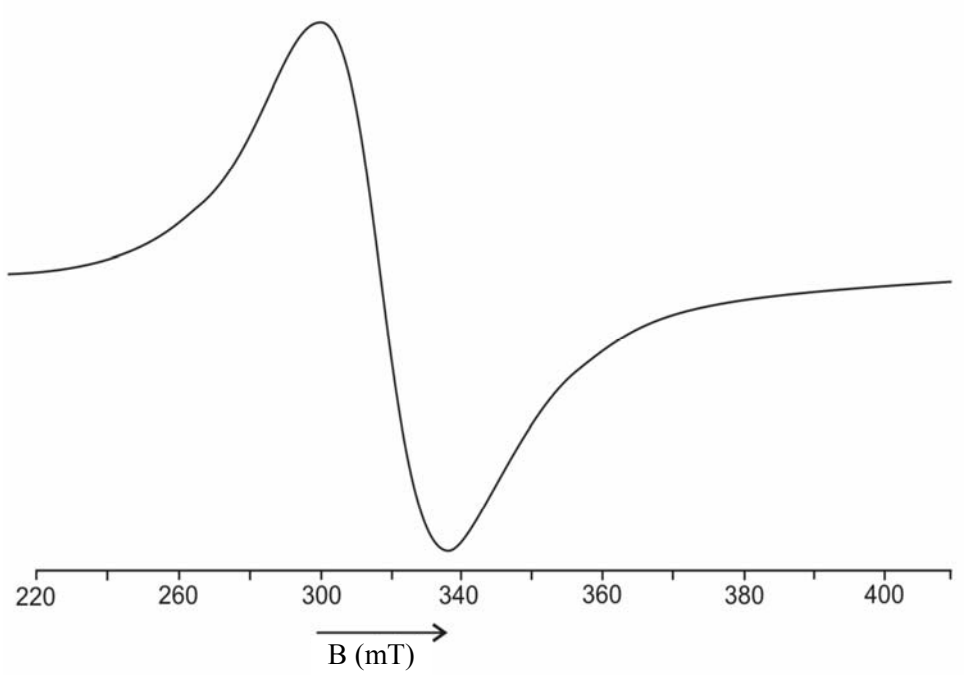

Fig. 3.6 X band EPR spectrum of $[Mn(Hbts)(OAc)]\cdot CH_3OH\cdot H_2O$ (**1**) in DMF at 298 K.

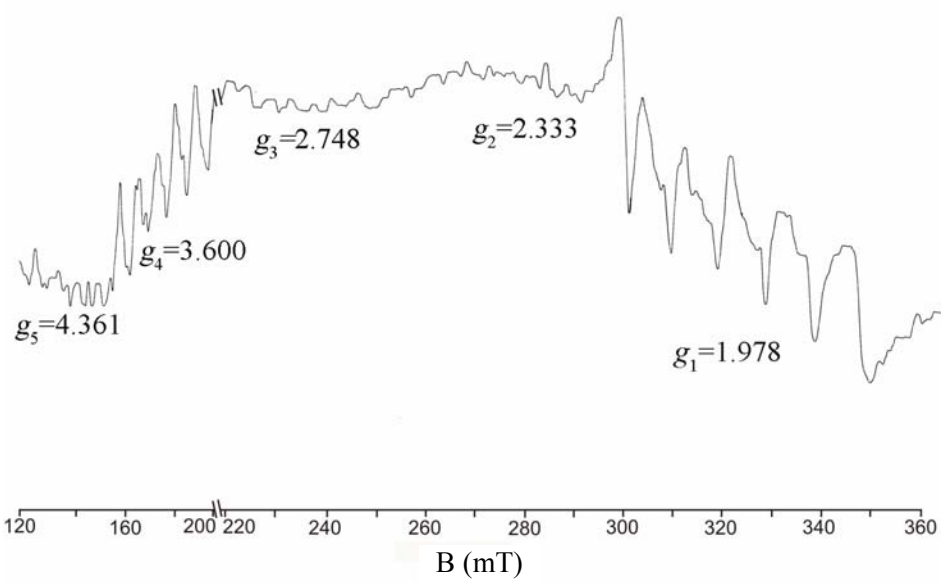

Fig. 3.7 X band EPR spectrum of [Mn(Hbts)(OAc)]·CH_3OH·H_2O (**1**) in DMF at 77 K.

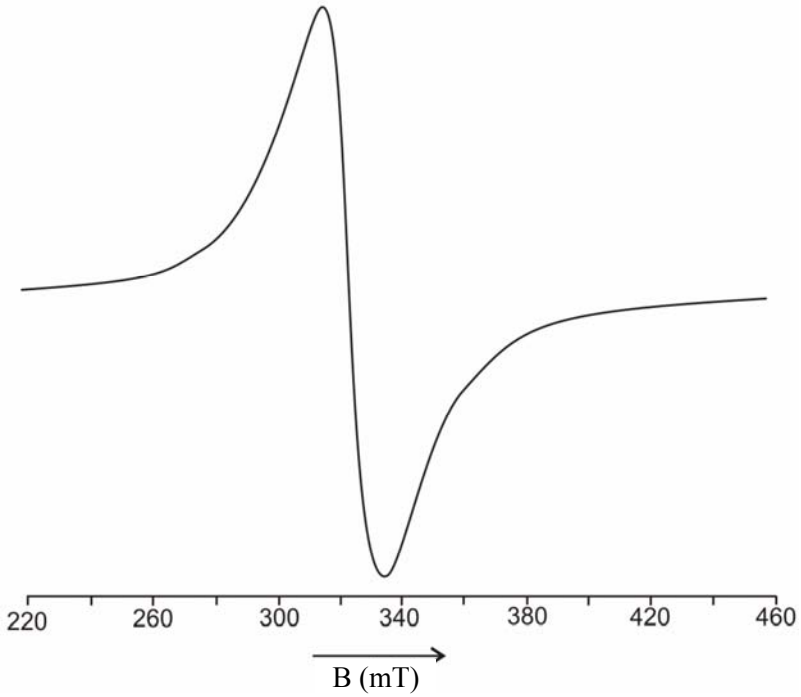

Fig. 3.8 X band EPR spectrum of [Mn(bmts)]·CH_3OH (**2**) in polycrystalline state at 298 K.

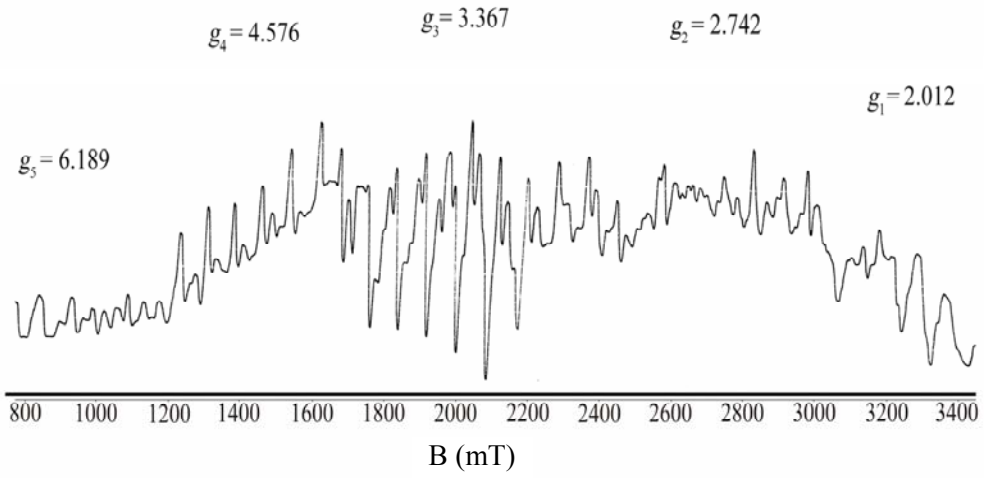

Fig. 3.9 X band EPR spectrum of [Mn(bmts)]·CH_3OH (**2**) in DMF at 77 K.

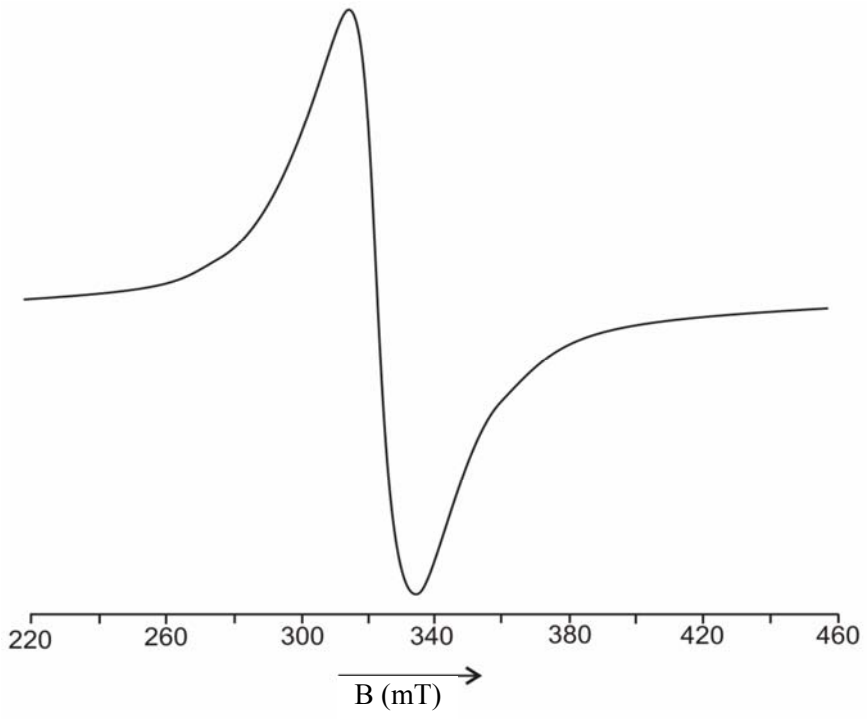

Fig. 3.10 X band EPR spectrum of [Mn(bpts)]·0.5H_2O (**3**) in polycrystalline state at 298 K.

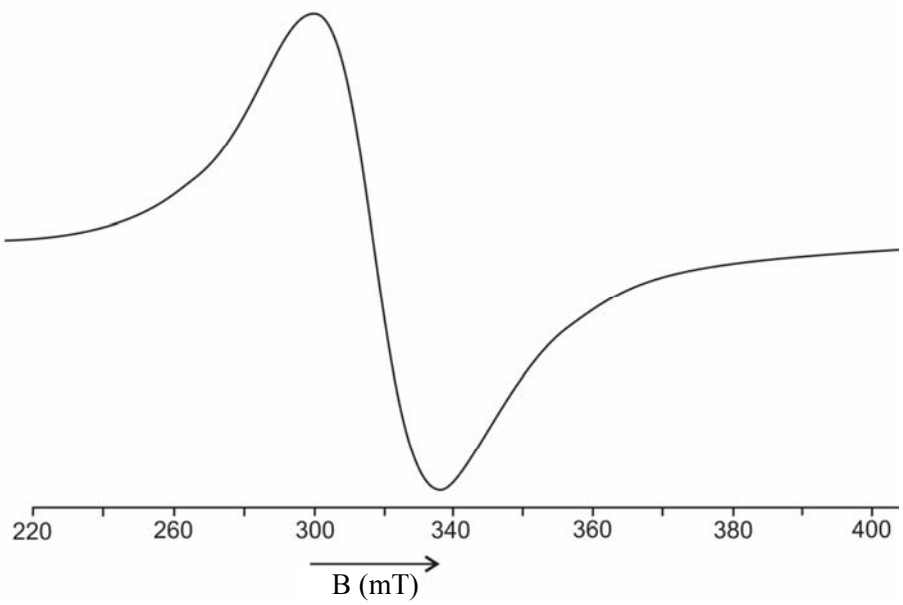

Fig. 3.11 X band EPR spectrum of [Mn(bpts)]·0.5H_2O (**3**) in DMF at 77 K.

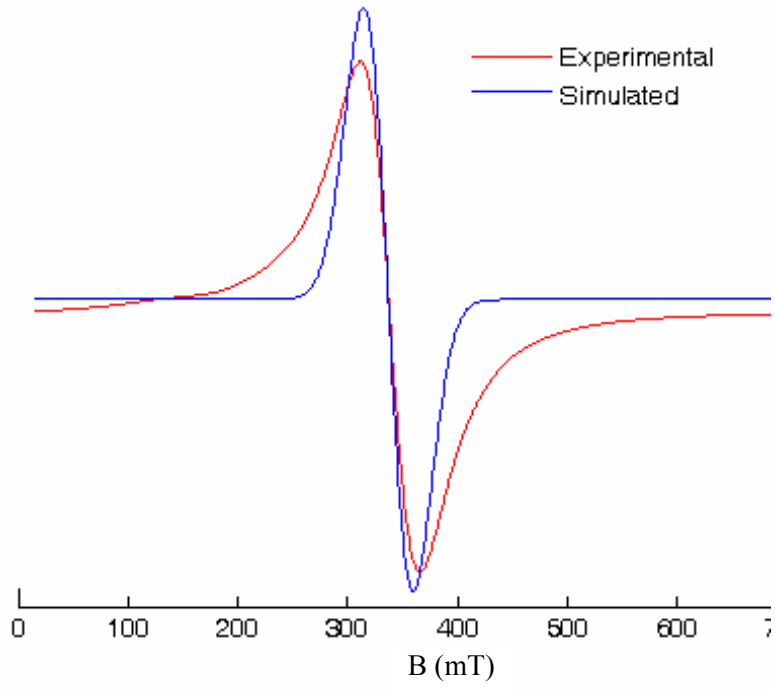

Fig. 3.12 X band EPR spectrum of [$Mn(Hmts)_2$] (**4**) in polycrystalline state at 298 K.

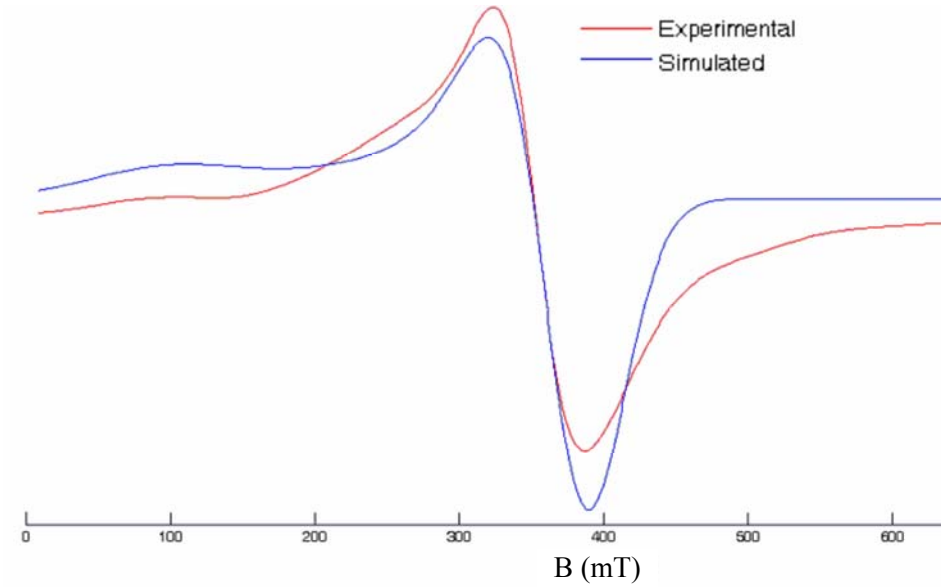

Fig. 3.13 EPR spectrum of $[Mn(Hmts)_2]$ (**4**) in DMF at 77 K.

3.3.5 Cyclic voltammetric studies

The electrochemical properties of metal complexes with sulfur donor atoms have been studied with great interest in order to monitor spectral and structural changes accompanying electron transfer [26]. Ligands which can produce π-electron delocalization along the ligand and the metal centre on complexation are found to stabilize first row transition metals in unusual oxidation states [27,28].

The redox behaviour has been investigated using the DMSO solutions of the complexes and 0.1 M TBAC as the supporting electrolyte. Here the electrochemical properties of two Mn(II) complexes are studied. The experimental data and the cyclic voltammogram recorded for [Mn(bpts)] are given in Fig. 3.14d. Examination of the graph shows that the reduction of manganese is irreversible under the experimental condition giving a reduction peak at 200 mV. This indicates the influence of the ligand system by extended conjugation on the metal centre.

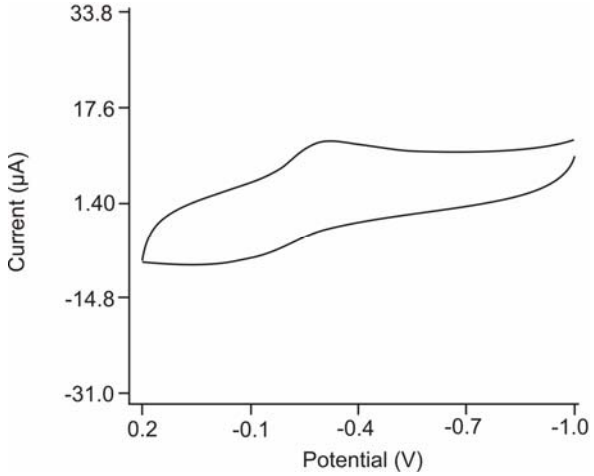

Fig. 3.14 Cyclic voltammetric responses relative to a 10^{-3} M [Mn(bpts)], 0.1 M TBAC, glassy carbon working electrode, scan rate 100 mVs^{-1}.

The experimental data and cyclic voltammogram of $[Mn(Hmts)_2]$ as given in Fig. 3.15 also gave an irreversible reduction peak at -651 mV. The oxidation peak obtained for H_2mts disappeared in the complex. Hence it can be inferred that the thione group in H_2mts which was available for oxidation. Hence the coordination of the thiolato sulfur can be confirmed from this. π-electron delocalization of the ligand with metal centre provides the unusual stability for the manganese complex.

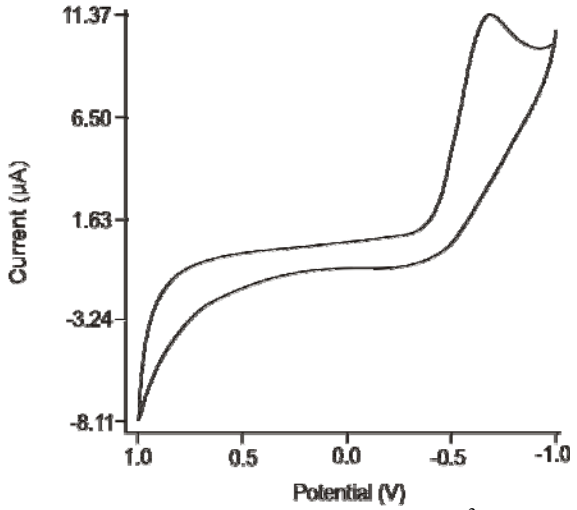

Fig. 3.15 Cyclic voltammetric responses relative to a 10^{-3} M $[Mn(Hmts)_2]$, 0.1 M TBAC, glassy carbon working electrode, scan rate 100 mV s^{-1}.

3.4 Conclusion

Four manganese complexes with four pentachelating rings were synthesized. All the compounds except **1** were found to coordinate in the deprotonated dianionic form. Though the ligands are expected to be pentadentate, the structural assignment was difficult since single crystals suitable for XRD studies are not obtained. $[Mn(Hmts)_2]$ is supposed to be octahedral since IR studies show no considerable shift to the C=O band. Manganese was found to be in the high spin state according to the magnetic susceptibility measurements and EPR spectroscopy. CV studies infer a π-electron delocalized system for the complex to give an irreversible reduction peak.

References

[1] J.E. Huheey, E.A. Keiter, R.L. Keiter, O.K. Medhi, Inorganic Chemistry: Principles of Structure and Reactivity, 4th ed., Pearson Education.

[2] V.L. Pecoraro (Ed), Manganese Redox Enzymes, VCH, New York, 1992.

[3] J. Stube, J. Biol. Chem. 265 (1990) 5329.

[4] A. Berkessel, M. Frauenkron, T. Schwenkreis, A. Steinmetz, G. Baum, D. Fenske, J. Mol. Catal. A: Chem. 113 (1996) 321.

[5] R. Cammack, A. Chapman, L. Wei- Ping, A. Katagouni, D.P. Kelley, FEBS Lett. 253 (1989) 239.

[6] M.L. Ludwig, A.L. Metzger, K.A. Pattridge, W.C. Stallings, J. Mol. Biol. 219 (1991) 335.

[7] D. P. Kessissoglou, Coord. Chem. Rev. 185 (1990) 837.

[8] D.P. Kessissoglou, Bioinorganic Chemistry: An Inorganic Perspective of Life, NATO, Scientific Affairs Division.

[9] E.A. Lewis, J.R. Lindsay, P.H. Walton, S.J. Archibald, S.P. Foxon, G.M.P. Giblin, J. Chem. Soc., Dalton Trans. (2001) 1159.

[10] T.S. Lobana, R. Sharma, G. Bawa, S. Khanna, Coord. Chem. Rev. 253 (2009) 977.

[11] G.J. Palenik, D.W. Wester, Inorg. Chem. 17 (1978) 864.

[12] S. Nakar, D. Mishra, S.K. Chattopadhyay, M. Corbella, A.J. Blake, Dalton Trans. (2005) 2428.

[13] R. Pedrido, A.M. Gonzalez-Noya, M.J. Romero, M. Martinez-Calvo, M.V. Lopez, E. Gomez-Forneas, G. Zaragoza, M.R. Bermejo, Dalton Trans. (2008) 6776.

[14] P. Souza, A.I. Matesanz, V. Fernandez, J. Chem. Soc., Dalton Trans. (1996) 3011.

[15] B.N. Figgis, Introduction to Ligand Fields, Wiley Eastern Limited, New Delhi, 1976.

[16] B.S. Garg, M.R.P. Kurup, S.K. Jain, Y.K. Bhoon, Trans. Met. Chem. 13 (1988) 309.

[17] M.J.M. Campbell, Coord. Chem. Rev. 17 (1975) 279.

[18] L.J. Ackerman, J.W. Webb, D.X. West, Trans. Met. Chem. 24 (1999) 562.

[19] S. Krishnan, K. Laly, M.R.P. Kurup, Spectrochim. Acta A 75 (2010) 585.

[20] M. Goodgame, I. Hussain, Inorg. Chim. Acta 174 (1990) 245.

[21] S. Chandra, L. K. Gupta, Spectrochim. Acta Part A 61(2005) 2549.

[22] B.S. Garg, M.R.P. Kurup, S.K. Jain, Y.K. Bhoon, Trans. Met. Chem. 13 (1988) 309.

[23] K.B. Pandey, R. Singh, P.K. Mathur, R.P. Singh, Trans. Met. Chem. 11 (1986) 347.

[24] R.S. Drago, Physical Methods in Inorganic Chemistry, Reinhold Publishing Corporation, New York.

[25] St. Stoll, Spectral Simulations in solid-state EPR, Ph.D. Thesis, ETH Zurich, 2003.

[26] A.M. Bond, R.L. Martin, Coord. Chem. Rev. 54 (1984) 23.

[27] A. Cinquantini, R. Cini, R. Seeber, P. Zanello, J. Electroanal. Chem. 121 (1981) 301.

[28] D.C. Olson, V.P. Mayweg, J.N. Schrauzer, J. Am. Chem. Soc. 88 (1966) 4876.

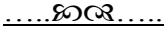

Chapter 4

Synthesis and Characterization of Fe(III) Complexes

Contents

"*The sea of chemicals from which life began contained abundant ferrous iron, while the atmosphere contained no oxygen. Once blue-green algae began synthesis of chlorophyll to capture the energy of the sun, dioxygen appeared in the atmosphere and ferrous iron became oxidized to its ferric form. Although the ferrous state of iron is quite water soluble, the ferric state of iron is very insoluble in water at neutral pH. Thus, most living organisms had to develop mechanisms to solubilize and acquire this element*."

Sigel and Sigel

4.1 Introduction

Iron is the most common element in the whole planet earth, produced in abundance as a result of fusion in high mass stars. It is a metal placed in the first transition series with symbol Fe derived from *ferrum*. It serves more biological roles than any other metal being vital to both plants and animals. Iron providing a means for transport and storage of oxygen plays a crucial role in circulatory system. It is present in several enzymes and proteins which

catalyze many redox reactions [1],[2]. The biological evolution of iron has been narrated by Sigel and Sigel [3].

Iron is found to occur in +2 (d^6) and +3 (d^5) oxidation states in compounds. Most of the Fe(II) complexes are found to be octahedral, tetrahedral, square planar or trigonal bipyramidal geometry though dodecahedral complexes are also known to exist. First transition metal complex of a heterocyclic bis(thiosemicarbazone) reported was a pentagonal bipyramidal Fe(II) complex [4].

Iron(III) complexes may be low spin or high spin with an octahedral geometry being the most common. There have been several reports on iron(III) complexes of 2-acetylpyridine thiosemicarbazone [5], 2-dipyridyl ketone thiosemicarbazone [6], 2-formylpyridine thiosemicarbazone [7], and substituted 2-acetylpyridine thiosemicarbazone [8].

Model complexes for the active sites of metalloenzymes with mixed N/S coordination sphere such as nitrile hydratase, acetyl coenzyme A synthase have been synthesized recently [9]. Novel orally active iron chelators with high iron mobilization efficacy and low toxicity suitable for the treatment of iron overload disease are designed and synthesized [10]. Transition metal complexes of 2,6-diacetylpyridine bis(thiosemicarbazone) have a versatile geometry resulting in mono, di and trinuclear compounds. Iron complexes are found to be seven coordinate pentagonal bipyramidal, octahedral or mixed valent tetranuclear cluster [11].

4.2 Experimental

4.2.1 Materials

The synthesis of the proligands is discussed in Chapter 2. Solvents being pure were used as supplied. Anhydrous ferric chloride (Merck) was used as supplied for the preparation of the complexes. Solvents used were methanol and dichloromethane.

4.2.2 Synthesis of complexes

4.2.2.1 *Synthesis of [Fe(H_2bpts)Cl_2]Cl·CH_3OH (**5**)*

H_2bpts (0.209 g, 0.5 mmol) was dissolved in 15 ml dichloromethane. This was slowly added to a hot solution of $FeCl_3$ (0.163 g, 0.5 mmol) in 15 ml methanol. The mixture was refluxed for 3 hours and allowed to cool. The dark brown crystalline complex formed was filtered, washed in methanol followed by ether and dried over P_4O_{10} *in vacuo*.

Yield 60%; Elem. Anal. found (calcd.)% for $C_{19}H_{29}Cl_3FeN_7OS_2$: C, 39.52 (39.26); H, 5.67 (5.11); N, 15.70 (16.02); S, 9.43 (10.40); μ (B.M.), 5.44; Λ_M, 51 $ohm^{-1}\,cm^2\,mol^{-1}$.

4.2.2.2 *Synthesis of [Fe(Hmts)Cl_2] (**6**)*

H_2mts (0.153 g, 0.5 mmol) was dissolved in 15 ml dichloromethane. This was slowly added to a hot solution of $FeCl_3$ (0.163 g, 0.5 mmol) in 15 ml methanol. The mixture was refluxed for 3 hours and allowed to cool. The dark brown complex formed was filtered, washed in methanol followed by ether and dried over P_4O_{10} *in vacuo*.

Yield 75%; Elem. Anal. found (calcd.)% for $C_{14}H_{17}Cl_2FeN_4O_2S$: C, 38.29 (38.91); H, 4.23 (3.97); N, 13.75 (12.97); S, 8.30 (7.42); μ (B.M.), 5.18; Λ_M, 40 $ohm^{-1}\,cm^2\,mol^{-1}$.

4.2.3 Physical measurements

Various physical measurements used are discussed in Chapter 1. CHNS analyses were carried out using Vario EL III CHNS analyzer at the SAIF, Kochi, India. IR spectra were recorded on a Thermo Nicolet AVATAR 370 DTGS model FT-IR Spectrophotometer with KBr pellets at the SAIF, Kochi, India. The far-IR spectra were recorded using polyethylene pellets in the 500 -100 cm^{-1} region on a nicolet Magna 550 FTIR instrument at the SAIF, Indian Institute of Technology, Mumbai. Electronic spectra in the range 200-900 nm were

recorded on a Cary 5000 version 1.09 UV-VIS-NIR Spectrophotometer using solutions in DMF/DMSO at the SAIF, Kochi, India. EPR spectra were recorded in a Varian E-112 X-band EPR Spectrometer using TCNE as a standard at SAIF, IIT, Bombay, India. The *g* factors were quoted relative to the standard marker TCNE (g = 2.00277). Cyclic voltammetric measurements were done on a PC interfaced electrochemical analyzer (BAS Epsilon Bioanalytical system USA) with a three electrode compartment system consisting of a glassy carbon working electrode, platinum wire counter electrode and Ag/Ag^{+} reference electrode, at the Department of Applied Chemistry, CUSAT, Kochi, India.

4.3 Results and discussion

Equimolar ratios of the ligands and the metal chloride yielded the dark brown colored metal complexes. Colors, elemental analyses data and magnetic susceptibility values of the complexes are represented along with synthesis. The yellow or bright yellow color of the ligand deepens on complexation. The elemental analyses data show in compound **5** the ligand is in neutral form whereas in compound **6** it is found to be in the deprotonated form. The molar conductivity of compound **5** reveals 1:1 electrolytic nature. Hence the compounds **5** and **6** can be represented as $[Fe(H_2bpts)Cl_2]Cl{\cdot}CH_3OH$ and $[Fe(Hmts)Cl_2]$ respectively.

Fe(III) ion being d^5 is the half filled state of *d* orbital affording additional stability. High spin Fe(III) complexes in general, have magnetic moments at room temperature very close to the spin only value of 5.9 B.M. Fe(III) complexes with a low spin-high spin equilibrium are found to be having a sub-normal magnetic moment [12]. Such complexes are said to be having an ion pair geometry. The magnetic susceptibility measurements of compounds **5** and **6** gave values 5.44 and 5.14 B.M. respectively and support the high spin state of Fe(III) ion in the complexes.

4.3.1 IR spectra

The significant bands obtained in the vibrational spectra of the H_2bpts and the Fe(III) complex along with their tentative assignments are given in Table 4.1. The *ν*(C=N) bands of both H_2bpts and H_2mts are found to be shifted to lower wavenumber in the spectra indicating the coordination of the azomethine nitrogen to the metal. Involvement of the pyridine nitrogen in coordination is indicated by the variations observed in the ring breathing vibrations of pyridine ring and the in-plane ring deformation band of pyridine as in the case of manganese complexes.

In the spectrum of complex **5** (Fig. 4.1), the *ν*(N^2–H) peak though weakened is observed at 3303 cm^{-1}. This indicates the compound to be in neutral form. The azomethine band found at 1605 cm^{-1} for the uncomplexed ligand is shifted to 1592 cm^{-1} upon coordination. The vibrations due to the methylene groups of the pyrrolidine ring are observed at 2906 and 2840 cm^{-1}. The *ν*(N–N) band shifts to 1149 cm^{-1} on coordination which is a measure of the increase in bond strength. Coordination via the thiolato sulfur is indicated by a decrease in the frequency to 1300 and 806 cm^{-1} of the thioamide band which was observed at 1360 and 818 cm^{-1} for the uncomplexed ligand. Coordination of the pyridine nitrogen is confirmed by the ring breathing vibrations and the in-plane ring deformation band at 1435 and 668 cm^{-1}.

Terminal M–Cl stretching bands are usually observed in the range of 200 - 400 cm^{-1} with a value of 384 cm^{-1} for *ν*(Fe–Cl) [12]. The coordination of the chloro group to the metal centre can be inferred by the broad band found at 401 cm^{-1} in the far-IR spectrum. The *ν*(Fe–N) band is observed for both complexes at *ca* 280 cm^{-1} which confirm the coordination of pyridine nitrogen to iron.

Table 4.1 IR spectral assignments of H_2bpts and complex (**5**).

Compound	$\nu(N^2–H)$	ν(C=N)	ν/δ(C–S)	ν(N–N)	Band III pyridine ring	py(ip)
H_2bpts·H_2O	3370	1605	1360, 818	1130	1450	658
[Fe(H_2bpts)Cl_2]Cl·CH_3OH (**5**)	3303	1592	1300, 806	1149	1435	668

The IR spectral assignments of H_2mts and the Fe(III) complex are given in Table 4.2. The spectrum of complex **6** (Fig. 4.2) reveals a deprotonated anionic structure for the ligand. The band observed at 1691 cm^{-1} due to ν(C=O) group for the ligand is found to have a blue shift to 1713 cm^{-1} for compound **6**. This confirms the coordination of the keto group to the metal centre. The azomethine band shifts to 1584 cm^{-1} on coordination from 1613 cm^{-1} in the uncomplexed ligand. The stretching and bending vibrations due to the thioketo group lowers when compared with the free ligand indicating strong coordination with enolization followed by deprotonation. Coordination of the pyridine nitrogen is confirmed by the in-plane ring deformation band at 714 cm^{-1}. The band found at 384 cm^{-1} in the far-IR spectrum of compound **6** is indicative of the usual ν(Fe–Cl) band [5,13].

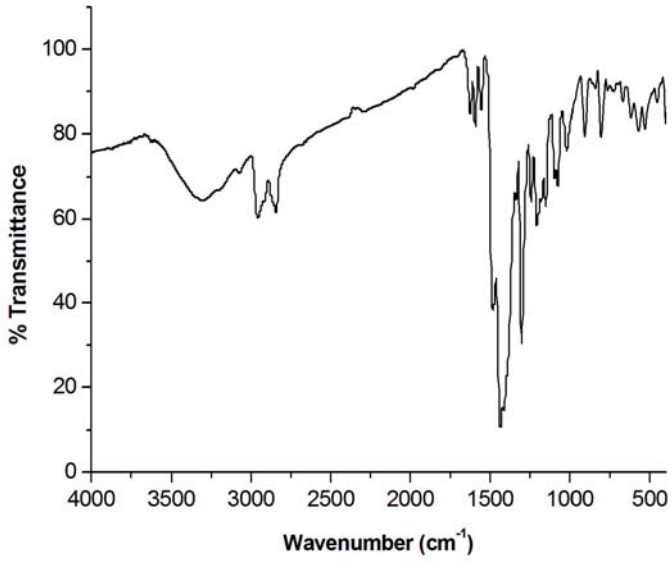

Fig. 4.1 IR spectrum of [Fe(H_2bpts)Cl_2]Cl·CH_3OH (**5**).

Table 4.2 IR spectral assignments of H_2mts and complex (**6**).

Compound	$\nu(N^2–H)$	ν(C=O)	ν(C=N)	ν/δ(C–S)	ν(N–N)	Band III pyridine ring	py(ip)
Hmts	3094	1691	1613	1365, 814	1110	1463	734
[Fe(mts)Cl_2] (**6**)	--	1713	1593	1341, 804	1116	1492	745

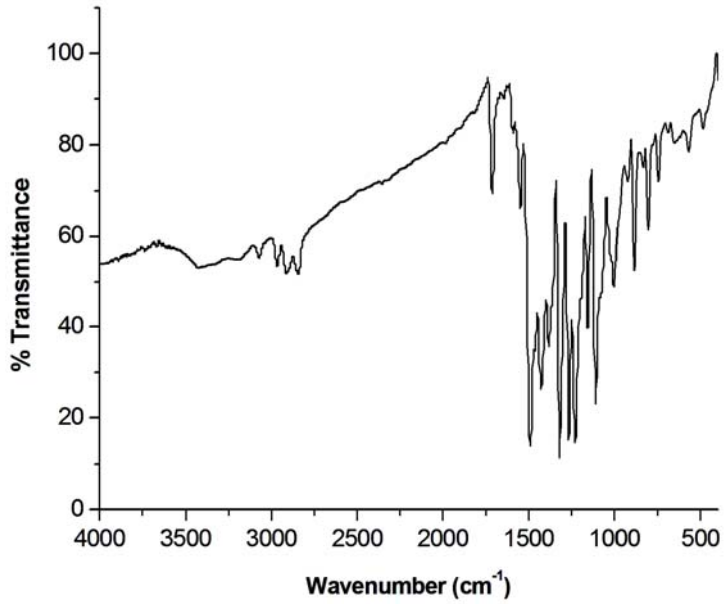

Fig. 4.2 IR spectrum of [Fe(Hmts)Cl_2] (**6**).

4.3.2 Electronic spectra

Since for d^5 complexes, the low energy term for the free ion is ^6S, it splits in a weak octahedral field to give $^6A_{1g}$, as the ground state. Significant spectral assignments for various intra-ligand and charge transfer transitions for Fe(III) complexes are listed in Table 4.3.

Table 4.3 Electronic spectral assignment Fe(III) complexes.

Compound	UV-vis absorption bands (cm^{-1})
H_2bpts	43820, 33680, 31000, 24450
[Fe(H_2bpts)Cl_2]Cl·CH_3OH (**5**)	35230, 29260, 21150, 12780
H_2mts	43680, 37840, 29500, 24750
[Fe(Hmts)Cl_2] (**6**)	31110, 27910, 15840, 11680

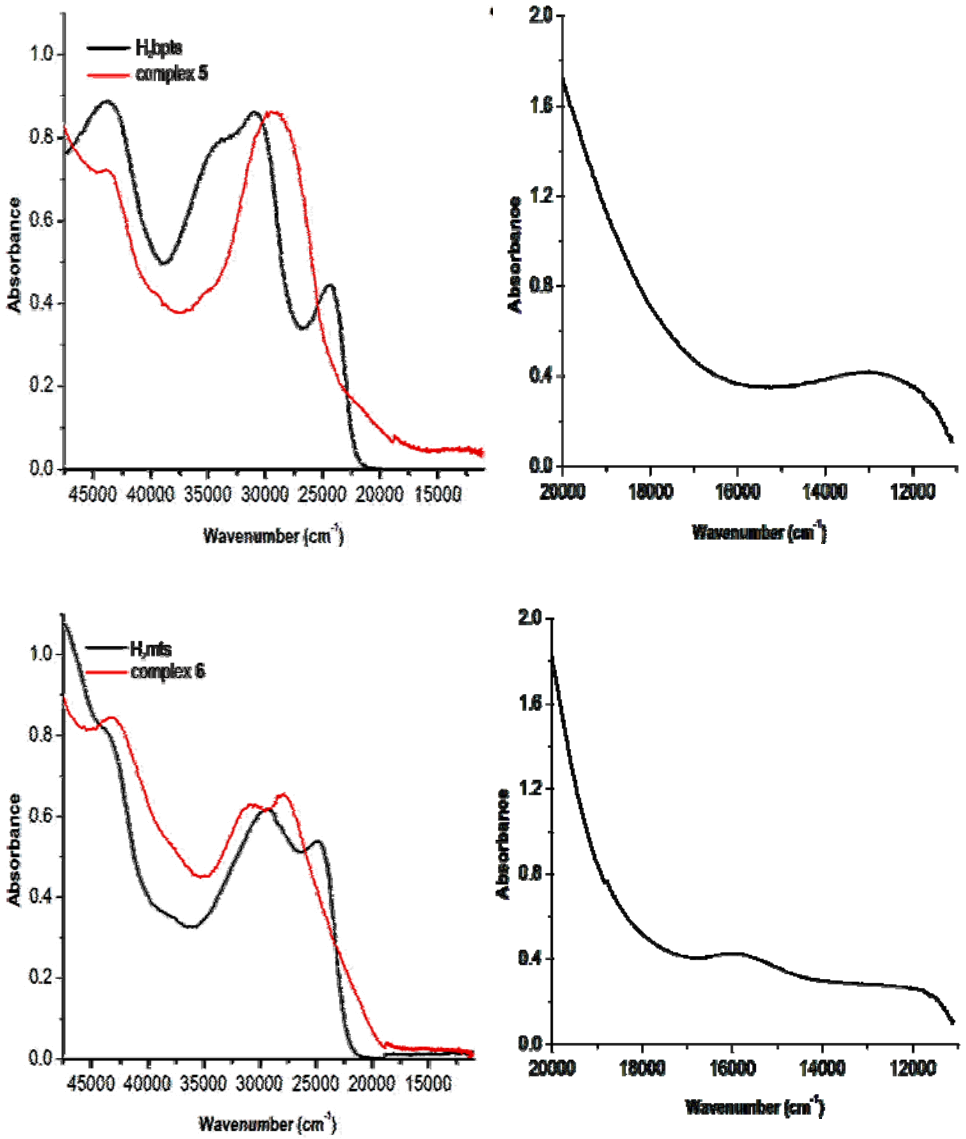

Fig. 4.3 Electronic spectra of Fe(III) complexes with 20000 -12000 cm^{-1} region of the respective complex on the right.

The intraligand transitions have undergone a bathochromic shift due to the donation of a lone pair of electrons to the metal indicating the coordination of azomethine nitrogen. It can be also due to the >C=S bond being weakened and the conjugation system getting enhanced on complexation [14]4,15]. Not only the *d-d* transitions but also the charge transfer bands are also found to be

very weak for these complexes. The band found at *ca* 24000 cm^{-1} due to the ring incorporated thioamide band of the ligand disappears in the complex. The weak band found at *ca* 16000 cm^{-1} may be assigned as $^4T_{1g}$ (^4G) ← $^6A_{1g}$ transition. Electronic spectra of both complexes along with *d-d* transitions are given in Fig. 4.3.

4.3.3 EPR spectral studies

EPR spectroscopy has been used as a powerful tool for the structural interpretation of several biologically important compounds. The EPR spectra of the iron(III) complexes in the polycrystalline state at 298 K and solution at 77 K were recorded in the X band using 100 kHz field modulation. The *g* factors were quoted relative to the standard marker TCNE (g = 2.00277). The EPR parameters are represented in Table 4.4. The spin Hamiltonian used for fitting the EPR spectrum originally proposed by Bleaney and Stevens is

$$\hat{H} = g\beta BS + D[S_z^2 - S(S+1)/3] + E(S_x^2 - S_y^2) \quad \text{.....(a)}$$

where B is the magnetic field vector, g is the spectroscopic splitting factor, D is the axial zero field splitting term, E is the rhombic zero field splitting parameter and S is the electron spin vector [16].

If D and E are zero an isotropic absorption line with a g value slightly greater than 2 is observed. If D and E are finite but small, five EPR transitions are observed. If D or E are large compared to $g\beta B$ the eigen values and vectors of (a) in zero magnetic field are easily found to be three Kramer's doublets. When $D \neq 0$, $E = 0$, the lowest doublet has the effective g values as $g = 2$, $g = 6$. When $D = 0$, $E \neq 0$, the middle doublet has an isotropic g value of 4.29 [17-19]. It has been found that the ratio of $E/D = \lambda$ is in the range of 0 – 1/3, $\lambda = 0$ implying axial symmetry [20].

For complex **5** the spectrum (Fig. 4.4) obtained in polycrystalline state at 298 K is found to be isotropic and a *g* value close to 2 is obtained whereas in DMF at 77 K (Fig. 4.5) shows two transitions at $g = 4.40$ and 2.04.

In the case of complex **6** (Fig. 4.6) the spectrum obtained in polycrystalline state at 298 K gave a broad signal at $g \approx 6$ and another signal at $g \approx 2$ indicating the dominance of the rhombic zero field splitting term *E*. In frozen DMF at 77 K, (Fig. 4.7) the anisotropic transition shifts to a high field end at $g \approx 4.4$ for complex **6** and a better transition is observed. The spectral assignments are presented in Table 4.4.

Table 4. 4 EPR spectral assignments for Fe(III) complexes.

Compound	*g* in DMF at 77K	*g* polycrystalline state at 298 K
$[Fe(H_2bpts)Cl_2]Cl{\cdot}CH_3OH$ (**5**)	4.40, 2.04	1.989
$[Fe(Hmts)Cl_2]$ (**6**)	4.30, 1.88	6.149, 2.009

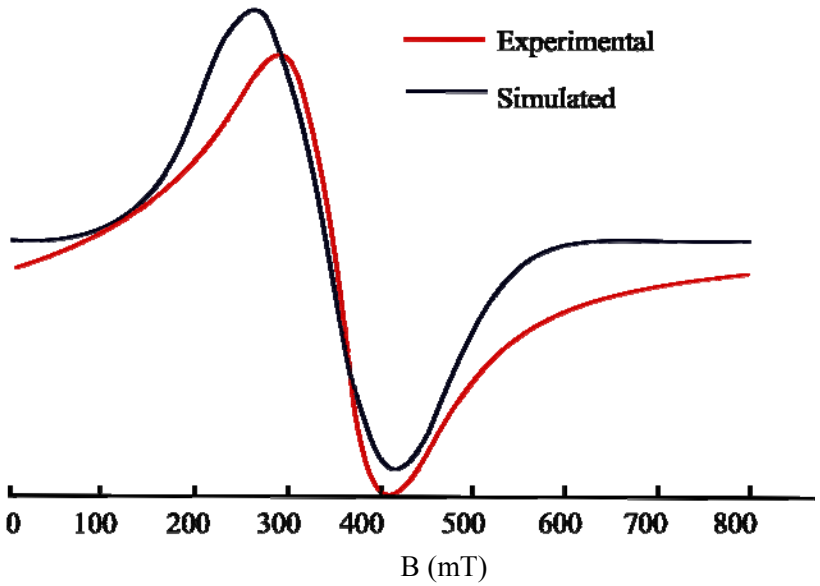

Fig 4.4 X band EPR spectrum (simulated) of $[Fe(H_2bpts)Cl_2]Cl{\cdot}CH_3OH$ (**5**) in polycrystalline state at 298 K.

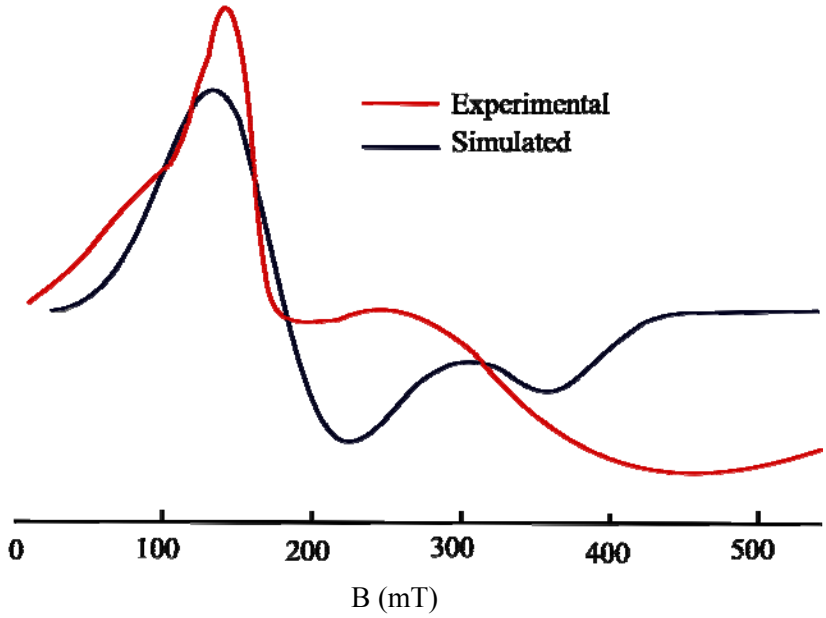

Fig 4.5 X band EPR spectrum (simulated) of [Fe(H_2bpts)Cl_2] Cl·CH_3OH (**5**) in DMF at 77 K.

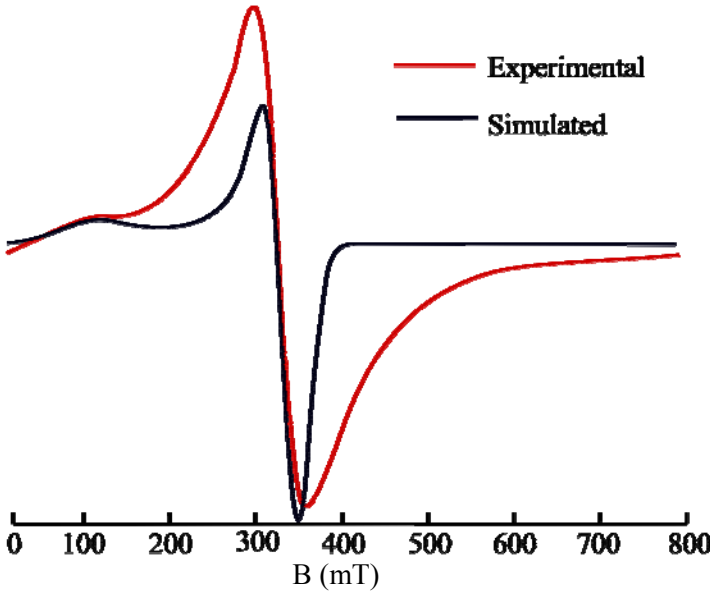

Fig 4.6 X band EPR spectrum of [Fe(Hmts)Cl_2] (**6**) in polycrystalline state at 298 K.

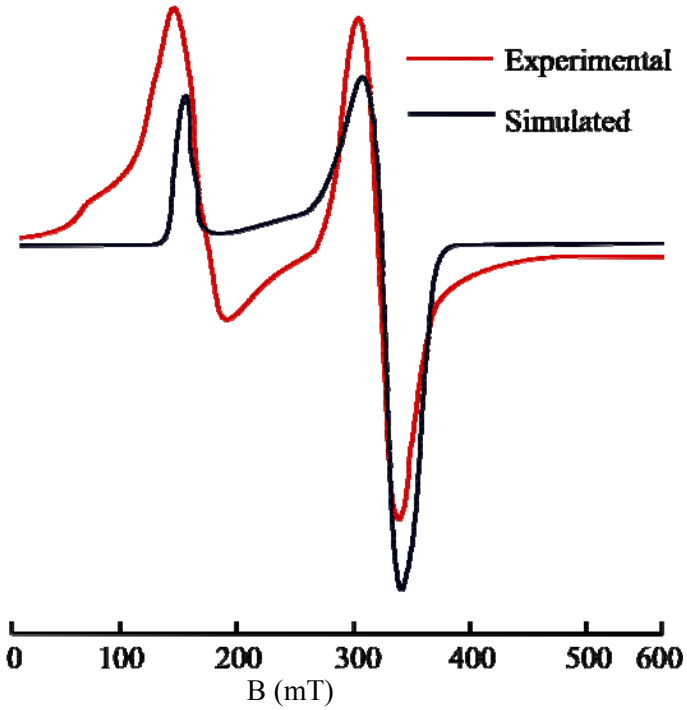

Fig 4.7 X band EPR spectrum of [Fe(Hmts)Cl_2] (**6**) in DMF at 77 K.

4.3.4 Cyclic voltammetric studies

The structural changes accompanying electron transfer can be studied in this method. The redox behaviour has been investigated using the DMSO solutions of the complexes and 0.1 M TBAC as the supporting electrolyte. Usually depending on the redox nature of the complex a reversible, quasireversible or irreversible cyclic voltammograms are obtained [21]. No CV was obtained for compound **5** whereas CV obtained for compound **6** (Fig. 4.10) was found to be irreversible in nature. On comparing with that of the ligand (Fig. 2.18) the oxidation peak obtained for the ligand disappeared in the CV of compound **6**. Absence of this peak indicate the nonavailability of thione sulfur for oxidation and hence confirms the coordination of sulfur to Fe(III). Formation of an irreversible CV indicates the redox tunability offered by the monothiosemicarbazone system which otherwise give a reversible CV for Fe(II)/ Fe(III) systems.

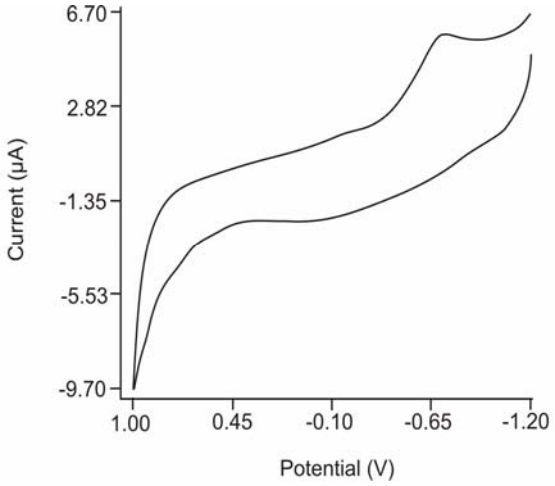

Fig. 4.8 Cyclic voltammetric responses relative to a 10^{-3} M [Fe(Hmts)Cl_2] (**6**), 0.1 M TBAC, glassy carbon working electrode, scan rate 100 mV/s.

4.4 Conclusion

Two iron complexes have been synthesized and spectral and structural studies have been done. Compound **5** is found to be a 1:1 electrolyte with the ligand in the neutral form. Compound **6** contains anionic ligand and is non-electrolyte. Hence [Fe(H_2bpts)Cl_2]Cl·CH_3OH and [Fe(Hmts)Cl_2] are the molecular formula assigned. Spectral studies show them to be high spin complexes and geometry proposed as pentagonal bipyramid and octahedral respectively. An irreversible voltammogram obtained from CV studies of compound **6** indicate redox tunable nature of monothiosemicarbazone system.

References

[1] www. Webelements.com/iron.

[2] H.B. Dunford, D. Dolphin, K.N. Raymond, L. Sieker, The biological role of iron- a look at the metabolism of iron and its subsequent uses in living organisms, D. Reidel Publishing Company, Dodrecht, Holland.

[3] A. Sigel, H. Sigel, Metal Ions in Biological Systems. Vol. 35: Iron Transport and Storage in Microorganisms, Plants and Animals, Marcel Dekker, Inc. New York, 1998.

[4] G. Dessy, V. Fares, Cryst. Struct. Commun. 10 (1981) 1025.

[5] B.S. Garg, M.R.P. Kurup, S.K. Jain, Y.K. Bhoon, Synth. React. Inorg. Met.-Org. Chem. 28 (1998) 1415.

[6] A. Sreekanth, M.R.P. Kurup, Polyhedron 23 (2004) 969.

[7] R. Raina, T.S. Srivastava, Inorg. Chim. Acta 91 (1984) 137.

[8] R. Raina, T.S. Srivastava, Indian. J. Chem. 22A (1983) 701.

[9] A. Panja, C. Campana, C. Leavitt, M.J. Van Stipdonk, D.M. Eichhorn, Inorg. Chim. Acta 362 (2009) 1348.

[10] D.S. Kalinowski, P.C. Sharpe, P.V. Bernhardt, D.R. Richardson, J. Med. Chem. 51 (2008) 331.

[11] T.S. Lobana, R. Sharma, G. Bawa, S. Khanna, Coord. Chem. Rev. 253 (2009) 977.

[12] B.S. Garg, M.R.P. Kurup, S.K. Jain, Y.K. Bhoon, Synth. React. Inorg. Met.-Org. Chem. 28 (1998) 1415.

[13] K. Nakamoto, Infrared and Raman spectra of Inorganic and Coordination compounds, 5th ed., Wiley, New York, 1997.

[14] V. Philip, V. Suni, M. Nethaji, M.R.P. Kurup, Polyhedron 25 (2006) 1931.

[15] I.-X. Li, H.-.Tang, Yi-Zhi Li, M. Wang, L.-F. Wang, C.-G. Xia, J. Inorg. Biochem. 78 (2000) 167.

[16] B. Bleaney, M.C.M. Obrein, Proc. Phy. Soc. London Sect. B 69 (1956) 1216.

[17] J.S. Griffith, The Theory of Transition Metal Ions, Cambridge University Press, London, 1961.

[18] R.D. Dowsing, J.F. Gibson, J. Chem. Phy. 50 (1969) 294.

[19] S.A. Cotton, Coord. Chem. Rev. 8 (1972) 185.

[20] S.A. Cotton, Chem. Phy. Lett. 41 (1976) 606.

[21] A. Abu-Hussen, W. Linert, Spectrochim. Acta Part A 74 (2009) 214.

Chapter 5

Synthesis and Characterization of Ni(II) Complexes

Contents

5.1 Introduction

Nickel is a silvery white metal which has been mistaken for copper and silver during earlier times. In several minerals it combines with sulfur. Nickel occupies 22nd position in the earth's crust. It is an ultra trace element both essential and toxic to human as well as animal beings [1]. Nickel being, a ferromagnetic element with d^8 electronic configuration and +2 as the most common oxidation state occupy a mid position in the periodic table. Exposure limit to nickel metal and soluble compounds has been fixed to 0.05 mg/cm^3. Nickel sulfide fumes and dust are believed to be carcinogenic. Sensitized individuals may show an allergy to nickel affecting their skin. Nickel carbonyl is an extremely toxic gas [2].

Recently coordination chemistry of nickel(II) complexes with sulfur donors have received considerable attention due to the identification of active sites of biological nickel centers with sulfur donor sites. As far as the known coordination chemistry of nickel many aspects of these biological nickel ions are unusual and unpredictable. Several hydrogenases and coenzymes are reported to contain this interesting metal. Redox nickel centers that can cycle between +3, +2 and +1 oxidation states, are found in thiolate rich and

tetrapyrrole ligand environments [3-7]. Nickel(II) is used as a spectroscopic probe in metal replacement studies of other metalloenzyme systems [8-11].

Coordination polymers presently play an important role in current science due to their potential for various functional materials. The self assembly of multimetallic complexes held together by intermolecular forces plays a key role in the development of supramolecular architecture. Hydrogen bonding interactions play vital roles for molecular recognition in several biological systems.

Thiosemicarbazone containing a heterocyclic ring give rise to NNS tridentate systems, which have been extensively investigated [12-14]. Kasuga et al in his nickel paper studied the antimicrobial activity of nickel complexes and correlated the activity and molecular structure. There are reports on nickel(II) complexes of butane-2,3-dione [15], glyoxaldehyde [16] bis{N(3)-substitutedthiosemicarbazones}. Pentadentate ligands of 2,6-diacetylpyridine S-benzyldithiocarbazate [17], 2,6-diacetylyridine bis{1-phthalazinylhydrazone} [18] and 2,6-diformylpyridinebis{N^4-dimethylthiosemicarbazone} [19] have also been found to give nickel(II) complexes of versatile geometries.

5.2 Experimental

5.2.1 Materials

Details regarding the synthesis of H_2bts and H_2bmts are described in Chapter 2. Nickel acetate tetrahydrate (CDH) and nickel chloride hexahydrate (Merck) were used as supplied for the preparation of the complexes. dimethylformamide, acetonitrile and methanol were the solvents used.

5.2.2 Synthesis of complexes

5.2.2.1 *Synthesis of [Ni(bts)]·0.5DMF (**7**)*

Nickel acetate was used for preparing the complex. H_2bts (0.155 g, 0.5 mmol) was dissolved in 2 ml of DMF and diluted with 15 ml methanol.

This was slowly added to a hot solution of $Ni(OAc)_2 \cdot 4H_2O$ (0.124 g, 0.5 mmol) in 15 ml methanol. The mixture was refluxed for 3 hours and allowed to cool. The dark brown complex formed was filtered, washed in methanol followed by ether and dried *in vacuo* over P_4O_{10}.

Yield, 55%; Elem. Anal. Found (calcd)% for $C_{25}H_{33}N_{15}Ni_2OS_4$: C, 37.89 (37.29); H, 3.68 (4.13); N, 26.67 (26.09); μ (B.M.): 0.877.

5.2.2.2 *Synthesis of [Ni(Hbmts)Cl]Cl·CH₃CN* ***(8)***

H_2bmts (0.225 g, 0.5 mmol) was dissolved in 15 ml of acetonitrile. This was slowly added to a hot solution of $NiCl_2 \cdot 6H_2O$ (0.119 g, 0.5 mmol) in 15 ml methanol. The mixture was refluxed for 4 hours and allowed to cool. The dark brown complex formed was filtered, washed in methanol followed by ether and dried over P_4O_{10} *in vacuo*.

Yield, 50%; Elem. Anal. Found (calcd)% for $C_{21}H_{30}Cl_2N_8NiO_2S_2$: C, 40.04 (40.67); H, 5.19 (4.88); N, 18.45 (18.07); S, 10.65 (10.34); μ (B.M.): 2.93; Λ_M, 53 $ohm^{-1}cm^2mol^{-1}$

5.2.3 Physical measurements

Various physical measurements used are discussed in Chapter 1. CHN analyses were carried out using Vario EL III CHNS analyzer at the SAIF, Kochi, India. IR spectra were also recorded on a Thermo Nicolet AVATAR 370 DTGS model FT-IR Spectrophotometer with KBr pellets at the SAIF, Kochi, India. The far-IR spectra were recorded using polyethylene pellets in the 500 -100 cm^{-1} region on a nicolet Magna 550 FTIR instrument at the SAIF, Indian Institute of Technology, Mumbai. Electronic spectra in the range 200-900 nm were recorded on a Cary 5000 version 1.09 UV-VIS-NIR Spectrophotometer using solutions in acetonitrile at the Dept. of Applied Chemistry, CUSAT, Kochi, India.

5.3 Results and discussion

Colors, elemental analyses, magnetic susceptibilities and molar conductivity for complexes are listed along with synthesis. Equimolar ratios of H_2bts and H_2bmts and the metal salts yielded brown colored metal complexes. From elemental analysis data two molecules of compound **7** along with one molecule of DMF are present and hence the molecular formula [Ni(bts)]·0.5H_2O. Compound **7** is formed by coordinating with doubly deprotonated form of H_2bts whereas **8** in the monodeprotonated form. Magnetic susceptibility value shows complex **7** to be weakly paramagnetic. Though square planar Ni(II) complexes are diamagnetic, weakly paramagnetic systems with low spin also have been reported [20]. This phenomenon can be due to the equilibrium between spin free and spin paired configurations. Brown and West had mentioned that such sub-normal magnetic moments are suggestive of considerable planarity for the nickel centers in such pentadentate complexes [21].

Reports of single crystal structure studies [17-19] point out the unusual coordination that occur in Ni(II) complexes of pentadentate ligands. Heterocyclic bis(thiosemicarbazones) potentially pentadentate, are reported to form four coordinate nickel complexes with a coordinated pyridine nitrogen, one thiosemicarbazone arm in the usual manner and the counterpart through hydrazinic nitrogen alone [19]. Binuclear nickel complexes with bridging pyridine nitrogens are reported to have variation in magnetic moment value depending on Ni-Ni separation as an indication of interaction between metal centres [17]. It can be concluded from conductivity measurements that compound **8** shows a 1:1 electrolytic nature. The magnetic susceptibility value for this compound was found to be quite normal for an octahedral nickel complex.

5.3.1 IR spectra

The significant bands obtained in the vibrational spectra of H_2bts and H_2bmts and their Ni(II) complexes along with their tentative assignments are

given in Table 5.1. The azomethine band of thiosemicarbazones is found to be shifted to lower wavenumbers in the spectra of complexes indicating the coordination of the azomethine nitrogen to the metal. This is also supported by the shift in ν(N–N) to higher frequencies. Involvement of the pyridine nitrogen in coordination is indicated by the variations observed in the ring breathing vibrations of pyridine ring and the in-plane ring deformation band of pyridine. Comparison of nickel(II) complexes with their copper(II) analogues suggest stronger coordination of nickel complexes [21]. Hence ν(Ni–N) absorptions are at higher energy than related bands in the analogous copper(II) complexes.

In the spectrum of complex **7** (Fig. 5.1), $\nu(N^4–H)$ vibrations are observed at 3155 cm^{-1}. The band corresponding to $\nu(N^2–H)$ present in the ligands disappeared in the spectrum of compound **7** indicating the enolization of the thioketo group followed by deprotonation [22,23]. The azomethine band found at 1603 cm^{-1} for the uncomplexed ligand is shifted to 1596 cm^{-1} upon coordination. The band at 1640 cm^{-1} is assigned to the C=N–N=C moiety, newly formed as a result of enolization of the ligand on coordination. Coordination via the thiolato sulfur is indicated by a decrease in the frequency to 1328 and 797 cm^{-1} of the thioamide band which was observed at 1360 and 872 cm^{-1} for the uncomplexed ligand. Ring breathing vibrations shift to 1406 cm^{-1} and in-plane ring deformation band to 724 cm^{-1}.

Table 5.1 IR spectral assignments of nickel(II) complexes.

Compound	$\nu(N^4–H)$ / $\nu(N^2–H)$	ν(C=N)	ν/δ(C–S)	ν(N–N)	Band III pyridine ring	py(ip)
H_2bts	3214 /3160	1603	1360, 872	1103	1441	715
[Ni(bts)]· 0.5 DMF (**7**)	3306, 3155	1596	1328, 797	1050	1406	724
H_2bmts	3164	1613	1361, 792	1103	1463	741
[Ni(Hbmts)Cl]Cl· CH_3CN (**8**)	--	1594	1310, 802	1110	1462	645

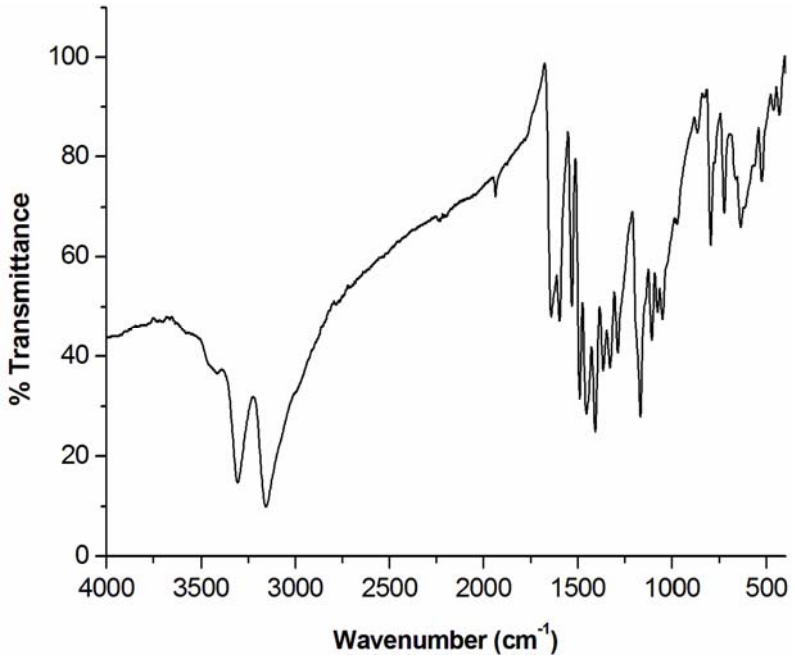

Fig. 5.1 IR spectrum of [Ni(bts)]·0.5 DMF (**7**).

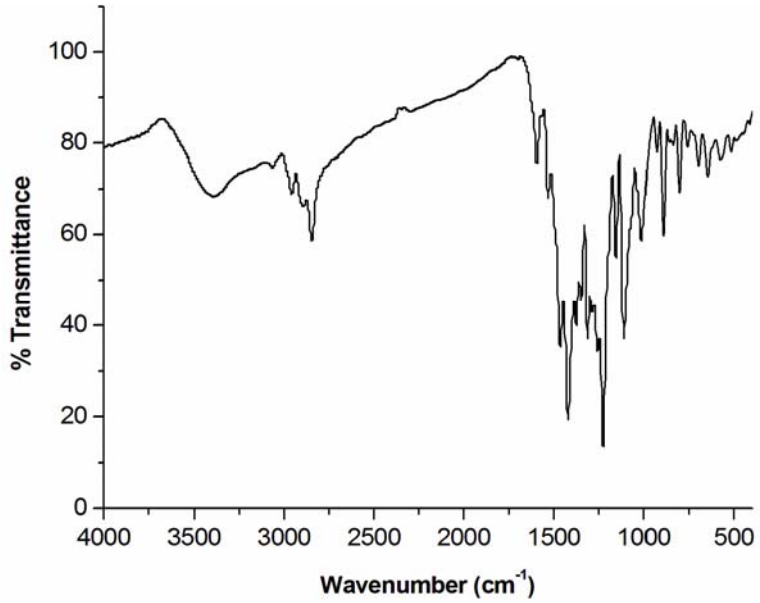

Fig. 5.2 IR spectrum of [Ni(Hbmts)Cl]Cl·CH_3CN (**8**).

In the spectrum of complex **8** (Fig. 5.2) the vibrations due to the methylene groups of the morpholine ring are observed at 2965 and 2840 cm^{-1}.

The azomethine band shifts to 1594 cm^{-1} on coordination. Coordination of the pyridine nitrogen is confirmed by the in-plane ring deformation band at 645 cm^{-1}. A broad band at 325 cm^{-1} in the far-IR spectrum shows Ni–Cl coordination [24].

5.3.2 Electronic spectra

For an octahedral nickel(II) complex, three spin allowed transitions are expected in the following wavenumber regions *viz*.

ν_1 (8000 -13000 cm^{-1})	$^3T_{2g}$ (F) ← $^3A_{2g}$
ν_2 (15000 -19000 cm^{-1})	$^3T_{1g}$(F) ← $^3A_{2g}$
ν_3 (25000 -30000 cm^{-1})	$^3T_{1g}$(P) ← $^3A_{2g}$

The higher energy band observed is usually obscured by strong charge transfer transitions. In addition two spin forbidden transitions are also usually observed. For tetrahedral nickel(II) complexes also three transitions are expected as $^3T_2$ (F) ← $^3T_1$(F), $^3A_2$ (F) ← $^3T_1$(F) and $^3T_1$ (P) ← $^3T_1$(F).

The electronic absorption spectral data of the complexes recorded in acetonitrile solution are given in Table 5.2. The spectra of the complexes **7** and **8** are shown in Fig. 5.3 with the *d-d* absorption bands in the same row. The high energy bands can be assigned to the intraligand transitions. The intraligand transitions have undergone a bathochromic shift due to the donation of a lone pair of electrons to the metal indicating the coordination of azomethine nitrogen. In the spectrum of complex **7** the broad bands appearing around 20000- 15,000 cm^{-1} can be assigned to $^3A_{2g}$ ← $^3T_{1g}$(F) and $^3A_{2g}$ ← $^3T_{1g}$(P) [25]. The charge transfer band observed at *ca*. 25000 cm^{-1} may have masked the other *d-d* transitions for compound **8**.

Table 5.2 Electronic spectral assignment of Ni(II) complexes.

Compound	UV-vis absorption bands (cm^{-1})
H_2bts	32130, 30540
[Ni(bts)]·0.5 DMF (**7**)	37690, 28530, 20970, 17750, 15470
H_2bmts	37640, 32250, 29810, 24390
[Ni(Hbmts)Cl]Cl·CH_3CN (**8**)	37100, 31730, 27590, 24100, 16760

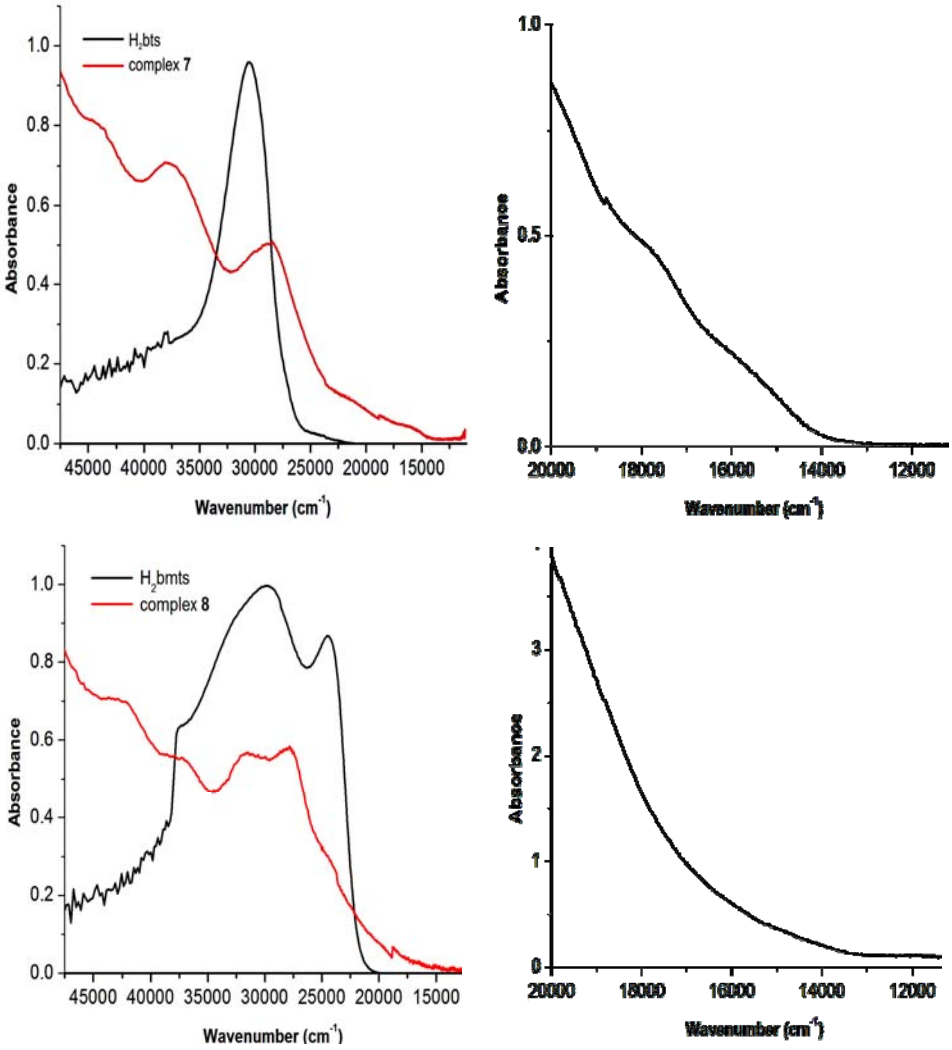

Fig. 5.3 Comparative electronic spectra of Ni(II) complexes with 20000 -12000 cm^{-1} region of the respective complex on the right.

5.3.3 ^{1}H NMR spectral studies

The ^{1}H NMR studies of the complex **7** was done. But the spectrum was too broadened such that no results could be interpreted. This supports the weakly paramagnetic nature of the metal in complex **7**.

5.4 Conclusion

This chapter deals with the synthesis and spectral characterization of two nickel complexes. One of the complexes [Ni(bts)] was found to be weakly paramagnetic suggesting a polymeric structure. IR spectral studies indicate the ligand to be pentadentate. Electronic spectrum of compound **7** revealed weak d-d transition bands for two spin allowed transitions. The elemental analysis data and spectral characterization suggest the compound **8** to be having a distorted octahedral geometry.

Reference

[1] G. Foulds, Coord. Chem. Rev. 169 (1998) 82.

[2] www.webelements.com/nickel.

[3] W.P. Schammel, L. Lawrence, D.H. Busch, Inorg. Chem. 19 (1980) 3159.

[4] M.A. Halcrow, G. Christou, Chem. Rev. 94 (1994) 2421.

[5] W. Levason, C.A. McAuliffe, Coord. Chem. Rev. 12 (1974) 151.

[6] H.J. Kruger, R.H. Holm, Inorg. Chem. 26 (1987) 3645.

[7] V.V. Pavlishchuk, S.V. Kolotilov, A.W. Addison, R.J. Butcher, E. Sinn, J. Chem. Soc., Dalton Trans. (2000) 355.

[8] R. Cammack, D.S. Patil, E.C. Hatchikian, V.M. Femande, Biochem. Biophys. Acta 98 (1987) 912.

[9] D.L. Tennent, R.D. McMillin, J. Am. Chem. Soc. 101 (1979) 2307.

[10] V. Lum, H.B. Gray, Isr. J. Chem. 21 (1981) 23.

[11] H.R. Engeseth, D.R. McMillin, E.L. Ulrich, Inorg. Chim. Acta 67 (1982) 145.

[12] N.C. Kasuga, K. Sekino, C. Koumo, N. Shimada, M. Ishikawa, K. Nomiya, J. Inorg. Biochem. 84 (2001) 55.

[13] D.X. West, G.A. Bain, R.J. Butcher, J.P. Jasinski, Y. Li, R.Y. Pozdniakiv, J. Valdes-Martinez, R.A. Toscano, S. Hernandez-Ortega, Polyhedron 15 (1996) 665.

[14] D.X. West, S.B. Padhye, P.B. Sonawane, Struct. Bond. 76 (1991) 1.

[15] D.X. West, J.S. Ives, G.A. Bain, A.E. Liberta, J. Valdes-Martinez, K.H. Ebert, S. Hernandez-Ortega, Polyhedron 16 (1997) 855.

[16] H. Beraldo, L.P. Boyd, D.X. West, Trans. Met. Chem. 23 (1998) 67.

[17] G. Paolucci, S.Stelluto, S. Sitran, D. Ajo, F. Benetollo, A. Polo, G. Bombieri, Inorg. Chim. Acta 193 (1992) 57.

[18] M.A. Ali, A.H. Mirza, R.J. Butcher, M.T.H. Tarafder, M.A. Ali, Inorg. Chim. Acta 320 (2001) 1.

[19] C.A. Brown, W. Kaminsky, K.A. Claborn, K.I. Goldberg, D.X. West, Braz. Chem. Soc. 13 (2002) 10.

[20] M. Mathew, G.J. Palenik, G.R. Clark, J. Inorg. Chem. 12 (1973) 446.

[21] C.A. Brown, D.X. West, Trans. Met. Chem. 28 (2003) 154.

[22] V. Philip, V. Suni, M.R.P. Kurup, M. Nethaji, Polyhedron 23 (2004) 1225.

[23] B.S. Garg, M.R.P. Kurup, S.K. Jain, Y.K. Bhoon, Trans. Met. Chem. 13 (1988) 309.

[24] K. Nakamoto, Infrared and Raman spectra of Inorganic and Coordination compounds, 5th ed., Wiley, New York, 1997.

[25] S.B. Padhye, G.B. Kauffman, Coord. Chem. Rev. 63 (1985) 127.

Chapter 6

Synthesis, Structures and Characterization of Copper(II) Complexes

Contents

6.1 Introduction

Copper is widely distributed in nature as sulphides, carbonates, chlorides etc [1]. It is the third most abundant transition element in biological systems [2]. Copper is required by all living systems. Though toxic, cells have a variety of mechanisms to deal with this essential trace element. Copper containing enzymes and proteins constitute an important class of biologically active compounds. Copper proteins and enzymes show various biological roles in electron transport, dioxygen transport, oxygenation, disproportionation and redox reaction [3].

Copper complexes of various thiosemicarbazones have been studied for their antitumor [4] and antimicrobial [5] activity. The coordination chemistry of copper bis(thiosemicarbazones) is now an area of interest because of their potential applications targeted as positron emission tomography tracers for non-invasive diagnostic imaging [6]. The hypoxic selectivity of these complexes has been forced to develop better imaging techniques by attaching fluorescent tags. The high resolution of fluorescence microcopy techniques offers potential advantages over radioactive detection methods [7,8]. Synthesis

of dinuclear and tetranuclear cluster helicates of bis(thiosemicarbazones) provide a new perspective on reproducible metallosupramolecular architectures with high nuclearity and programmable properties.

Copper being d^9 is found in +2 oxidation state which is the most stable and important state. This configuration makes Cu(II) subject to Jahn Teller distortion if placed in a cubic environment *ie*. regular octahedral geometry. This has found to produce a profound effect on its stereochemistry [9,10]. Five coordinate Cu(II) complexes are quite common, but relatively few of these complexes have pentadentate ligands. The stereochemistry adopted by these complexes is found to be intermediate between square pyramidal (SP) and trigonal bipyramidal (TBP).

6.2 Experimental

6.2.1 Materials

The syntheses of the proligands are discussed in Chapter 2. Solvents being pure are used as supplied. Copper acetate monohydrate and chloride dihydrate (E-merck) were used as supplied for the preparation of the complexes. Solvents used were methanol and dimethylformamide.

6.2.2 Synthesis of complexes

6.2.2.1 *Synthesis of [Cu(bts)]·H_2O (**9**)*

H_2bts (0.155 g, 0.5 mmol) was dissolved in 2 ml of DMF and diluted with 15 ml methanol. This was slowly added to a hot solution of $Cu(OAc)_2 \cdot H_2O$ (0.100 g, 0.5 mmol) in 15 ml methanol. The mixture was refluxed for 3 hours and allowed to cool. The brown complex formed was filtered, washed in methanol followed by ether and dried *in vacuo* over P_4O_{10}.

Yield 60%, Elem. Anal. found (calcd)% for $C_{11}H_{15}CuN_7OS_2$: C, 34.46 (33.97); H, 3.37 (3.89); N, 25.20 (25.21); μ (B.M.), 1.69.

6.2.2.2 *Synthesis of [$Cu_3(bmts)_2(OAc)_2$] (**10**)*

The synthesis was done using Schlenk line technique. H_2bmts (0.225 g, 0.5 mmol) was dissolved in 2 ml of DMF and diluted with 15 ml methanol. After keeping in Schlenk line a solution of $Cu(OAc)_2 \cdot H_2O$ (0.100 g, 0.5 mmol) in 15 ml methanol was injected. The mixture was refluxed for 3 hours in inert atmosphere and kept for two days. The dark green crystalline complex suitable for single crystal study formed was filtered, washed in methanol followed by ether and dried over P_4O_{10} *in vacuo*.

Yield 50%, Elem. Anal. found (calcd)% for $C_{42}H_{56}Cu_3N_{14}O_6S_4$: C, 43.34 (43.05); H, 4.56 (4.82); N, 16.67 (16.73); S, 10.05 (10.9); μ (B.M.), 0.976.

6.2.2.3 *Synthesis of [Cu(H_2bmts)]$Cl_2 \cdot 2CH_3OH$ (**11**)*

H_2bmts (0.225 g, 0.5 mmol) was dissolved in 2 ml of DMF and diluted with 15 ml methanol. This was slowly added to a hot solution of $CuCl_2 \cdot 2H_2O$ (0.085 g, 0.5 mmol) in 15 ml methanol. The mixture was refluxed for 3 hours and allowed to cool. The dark green complex formed was filtered, washed in methanol followed by ether and dried over P_4O_{10} *in vacuo*.

Yield 59%, Elem. Anal. found (calcd)% for $C_{21}H_{35}Cl_2CuN_7O_4S_2$: C, 38.23 (38.92); H, 5.17 (5.44); N, 14.89 (15.13); S, 8.20 (9.89); μ (B.M.), 1.69; Λ_M, 118 $ohm^{-1}\,cm^2\,mol^{-1}$.

6.2.2.4 *Synthesis of [Cu(bpts)] (**12**)*

H_2bpts (0.209 g, 0.5 mmol) was dissolved in 2 ml of DMF and diluted with 15 ml methanol. This was slowly added to a hot solution of $Cu(OAc)_2 \cdot H_2O$ (0.100 g, 0.5 mmol) in 15 ml methanol. The mixture was refluxed for 3 hours and allowed to cool. The brown crystalline complex formed was filtered, washed in methanol followed by ether and dried over P_4O_{10} *in vacuo*.

Yield 65%, Elem. Anal. found (calcd)% for $C_{19}H_{25}CuN_7S_2$: C, 47.64 (47.63); H, 5.7 (5.26); N, 20.44 (20.46); S, 14.28 (13.38); μ (B.M.), 1.39.

6.2.2.5 *Synthesis of [Cu(mts)]* ***(13)***

H_2mts (0.153 g, 0.5 mmol) was dissolved in 2 ml of DMF and diluted with 15 ml methanol. After keeping in Schlenk line, a solution of $Cu(OAc)_2 \cdot H_2O$ (0.100 g, 0.5 mmol) in 15 ml methanol was injected to it. The mixture was refluxed for 3 hours in inert atmosphere and allowed to cool. The brown crystals (suitable for single crystal study, yield 40%) of the complex formed were filtered, washed in methanol followed by ether and dried over P_4O_{10} *in vacuo*.

6.2.3 Physical measurements

Various physical measurements used are discussed in Chapter 1. CHNS analyses were carried out using Vario EL III CHNS analyzer at the SAIF, Kochi, India. IR spectra were recorded on a Thermo Nicolet AVATAR 370 DTGS model FT-IR Spectrophotometer with KBr pellets at the SAIF, Kochi, India. The far-IR spectra were recorded using polyethylene pellets in the 500 -100 cm^{-1} region on a nicolet Magna 550 FTIR instrument at the SAIF, Indian Institute of Technology, Mumbai. Electronic spectra in the range 200-500 nm were recorded on a Cary 5000 version 1.09 UV-VIS-NIR Spectrophotometer using solutions in DMF/DMSO at the SAIF, Kochi, India. EPR spectra were recorded in a Varian E-112 X-band EPR Spectrometer using TCNE as a standard at the SAIF, IIT, Bombay, India. The *g* factors were quoted relative to the standard marker TCNE (g = 2.00277).

6.3 Results and discussion

Equimolar ratios of the ligands and the metal acetate/chloride yielded the brown or dark green colored metal complexes. Elemental analyses data and magnetic susceptibility values of the complexes are presented along with synthesis. The elemental analyses data showed that the compounds **9** and **12**

were found to coordinate in the doubly deprotonated form. The compound **10** is suggested to be a trinuclear complex with two doubly deprotonated ligand moieties. Though single crystals suitable for X-ray diffraction studies were obtained for **10** it did not diffract. Compound **11** is found to be a chloro complex with a neutral ligand moiety. Single crystals of compound **13** could be isolated and the structure was concluded by single crystal XRD. Due to poor yield, elemental analysis and magnetic studies were not done for compound **13**.

The yellow/bright yellow ligands change to dark green/brown complexes. The ligand is found to be getting converted to the thiolato form and gets deprotonated when copper acetate is the salt taken. They are found to be soluble in solvents like dimethylformamide, dimethylsulfoxide, dichloromethane etc.

Molar conductances of the complexes measured using 10^{-3} M DMF solution showed all the complexes except **11** to be non-electrolytes [11]. The latter gave a molar conductance of 118 ohm^{-1} mol^{-1} cm^{-1} showing 2:1 electrolytic nature and hence $[Cu(H_2bmts)]Cl_2{\cdot}2CH_3OH$ was the molecular formula assigned.

The magnetic moments of the complexes are calculated from magnetic susceptibility measurements at room temperature. The values of all the complexes except compound **10** are found to be in the range of 1.69–1.76 B.M. Mononuclear Cu(II) complexes exhibit magnetic moments in this range which are close to the spin only value. The low magnetic moment of compound **10** found as 0.97 B.M. may be attributed to the presence of a strong antiferromagnetic spin-spin interaction [12]. From the elemental analyses data compound **10** was found to be a trinuclear complex and magnetic moment value supports this.

6.3.1 IR spectra

The significant bands obtained in the vibrational spectra of the four ligands and their Cu(II) complexes along with their tentative assignments are

given in Table 6.1. The ν(C=N) band of all the complexes are found to be shifted to lower wavenumber in the spectra indicating the coordination of the azomethine nitrogen to the metal. This is also supported by the shift in ν(N–N) to higher frequencies. The increase in the frequency of this band in the spectra of the complexes, due to the increase in the bond strength, again confirms the coordination via the azomethine nitrogen. Involvement of the pyridine nitrogen in coordination is indicated by the variations observed in the ring breathing vibrations and the in-plane ring deformation band of pyridine ring as noted earlier. Systematic shifts of the ν(C=S) absorption bands to lower frequencies indicate the coordination of the sulfur group.

In compound **9** (Fig. 6.1) it is difficult to observe the disappearance of $\nu(N^2–H)$ band due to the presence of bands of (N^4–H) and H_2O. The ν(C=N) band of compound **9** suffers a red shift from 1603 to 1588 cm^{-1} in the spectrum. The ring breathing vibrations and the in-plane ring deformation band of pyridine ring shift from 1441 to 1443 cm^{-1} and from 715 to 770 cm^{-1} respectively. This confirms the involvement of the pyridine nitrogen in coordination. The stretching and bending vibrations of the thioamide band observed at 1360 and 872 cm^{-1} shift to 1349 and 800 cm^{-1} respectively.

In the spectrum of the complex **10** (Fig. 6.2) the $\nu(N^2–H)$ vibration band observed in the ligand disappears. The azomethine band found at 1613 cm^{-1} for the uncomplexed ligand is shifted to 1576 cm^{-1} upon coordination. Coordination via the thiolato sulfur is indicated by a decrease in the frequency of the thioamide band from 1361 to 1355 cm^{-1}. An increase in the δ(C=S) frequency from 792 to 814 cm^{-1} may be due to the rigidity occurred due to coordination [10]. The ring breathing vibrations and in-plane ring deformation band of pyridine ring have been shifted to lower frequencies indicating coordination of pyridine nitrogen. The vibrations due to the methylene groups of the morpholine ring are observed at 2974 and 2854 cm^{-1}. The bands at

1688 and 1386 cm^{-1} correspond to the symmetric and asymmetric stretching vibrations of the acetate group, consistent with the presence of a monodentate acetate group in the complex [13].

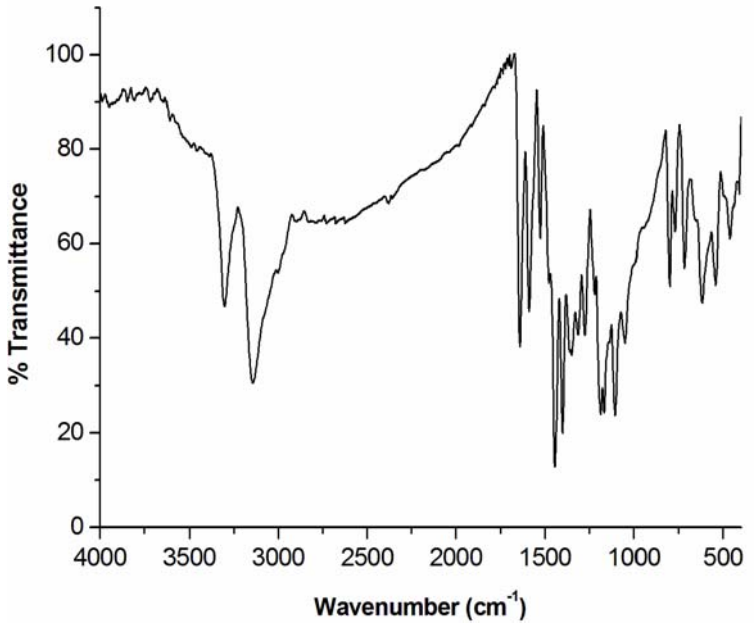

Fig. 6.1 IR spectrum of [Cu(bts)]· H_2O (**9**).

Table 6.1 IR spectral assignments (cm^{-1}) of copper complexes.

Compound	$\nu(N^4–H)$ / $\nu(N^2–H)$	ν(C=O)	ν(C=N)	ν/δ(C–S)	ν(N–N)	Band III pyridine ring	py(ip)
H_2bts·CH_3OH	3214/3160	--	1603	1360, 872	1103	1441	715
[Cu(bts)]· H_2O (**9**)	3302, 3143	--	1588	1349, 800	1049	1443	770
H_2bmts	3164	--	1613	1361, 792	1103	1463	741
$[Cu_3(bmts)_2(OAc)_2]$ (**10**)		--	1576	1355, 814		1433	645
$[Cu(H_2bmts)]\ Cl_2$·$2CH_3OH$ (**11**)	3405	--	1585	1307, 810	1111	1485	692
H_2bpts·H_2O	3370	--	1605	1360, 818	1130	1450	658
[Cu(bpts)] (**12**)	--	--	1589	1303, 804	1144	1421	630
H_2mts	3094	1691	1613	1365, 814	1110	1463	734
[Cu(mts)] (**13**)	--	1654	1589	1375, 804	1113	1491	744

In the spectrum of complex **11** (Fig. 6.3) also the $\nu(N^2–H)$ peak though obscured by the broad –OH band is found at 3071 cm^{-1}. This supports the coordination of the ligand in the neutral form. The azomethine band found at 1613 cm^{-1} for the uncomplexed ligand is shifted to 1585 cm^{-1} upon coordination. Coordination via the thione sulfur is indicated by a decrease in the frequency to 1352 and 752 cm^{-1} of the thioamide band which was observed at 1361 and 792 cm^{-1} for the uncomplexed ligand. The ring breathing vibration and in-plane ring deformation bands of pyridine ring have been shifted to lower frequencies indicating coordination of pyridine nitrogen. The appearance of a strong band at 303 cm^{-1} indicates the coordination of the chloro group. The far-IR spectrum showed ν(Cu–N) band at 423 cm^{-1} and ν(Cu–S) at 351 cm^{-1} confirming the coordination of azomethine and thione sulfur [5].

In complex **12** (Fig. 6.4), the disappearance of the peak shows the coordination of the thiolate form of the ligand after deprotonation. Shifting of the azomethine band found at 1605 cm^{-1} for the uncomplexed ligand to 1589 cm^{-1} in the complex confirms the coordination of the azomethine group. The shifting of the vibration band due to the methylene groups of the pyrrolidine ring to 2947 and 2862 cm^{-1} may be due to weakening of the ring on coordination. The ν(N–N) band shifts to 1149 cm^{-1} on coordination which is a measure of the increase in bond strength. Coordination via the thiolato sulfur is indicated by a decrease in the frequency to 1303 and 804 cm^{-1} of the thioamide band which was observed at 1360 and 818 cm^{-1} before coordination. Coordination of the pyridine nitrogen is confirmed by the lowering of ring breathing vibrations and the in-plane ring deformation band energy to 1421 and 630 cm^{-1}.

The spectrum of complex **13** (Fig. 6.5) reveals a deprotonated anionic structure for the ligand. The shifting of the absorption band due to the keto group from 1691 to 1654 cm^{-1} supports the enolisation of the keto group. This confirms the coordination of the deprotonated form of enol group. The

azomethine band shifts to 1589 cm^{-1} on coordination from 1613 cm^{-1} in the uncomplexed ligand. The stretching and bending vibrations due to the thioketo group lowers when compared with the free ligand indicating strong coordination with enolization followed by deprotonation. The variation in the ring breathing vibrations and the in-plane ring deformation band energy confirm the coordination of the pyridine nitrogen.

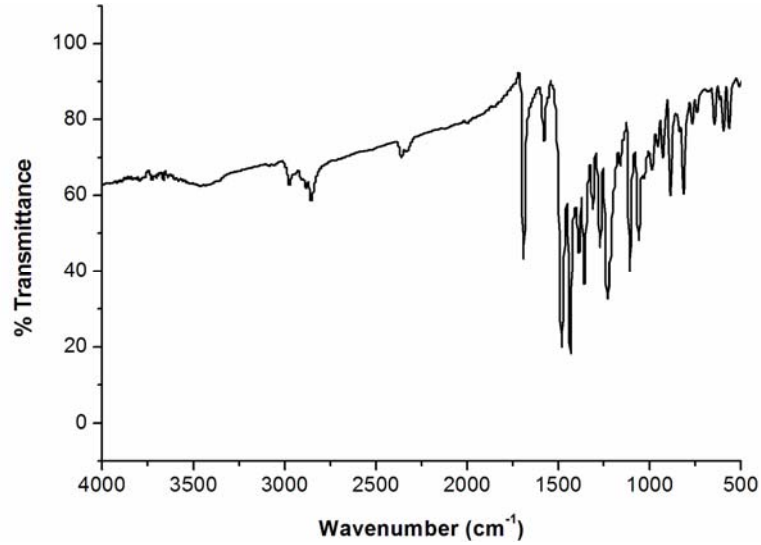

Fig. 6.2 IR spectrum of $[Cu_3(bmts)_2(OAc)_2]$ (**10**).

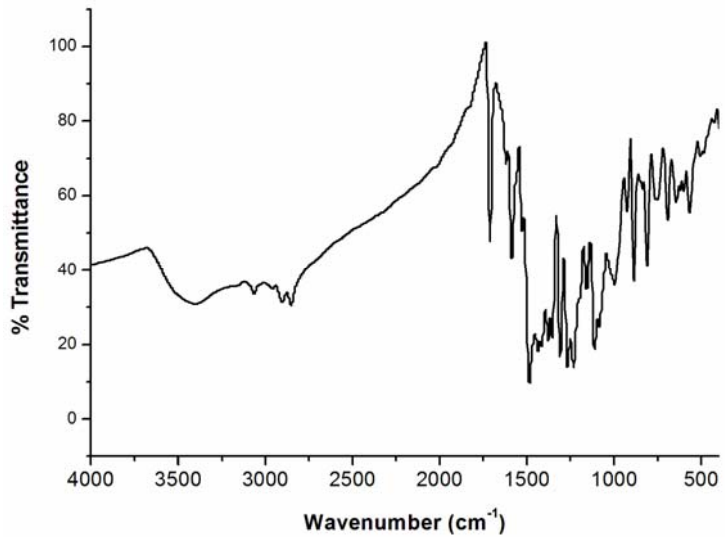

Fig. 6.3 IR spectrum of $[Cu(H_2bmts)]Cl_2{\cdot}2CH_3OH$ (**11**).

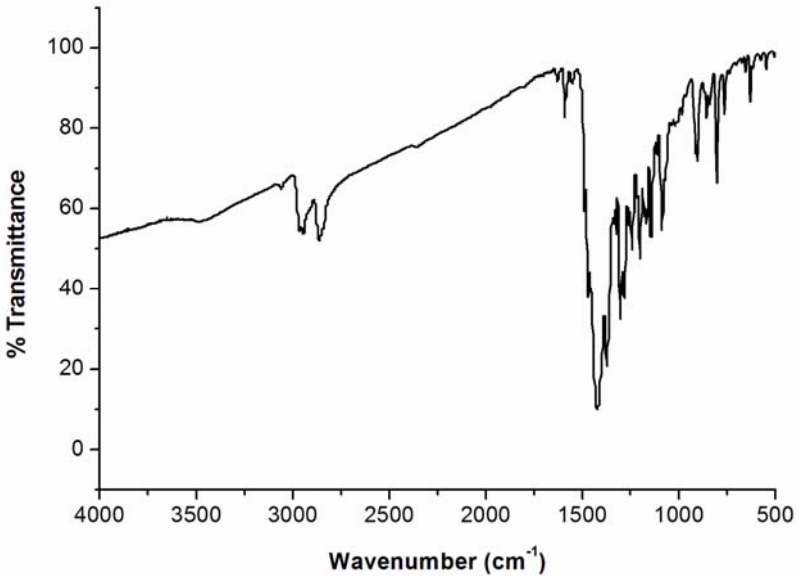

Fig.6.4 IR spectrum of [Cu(bpts)] (**12**).

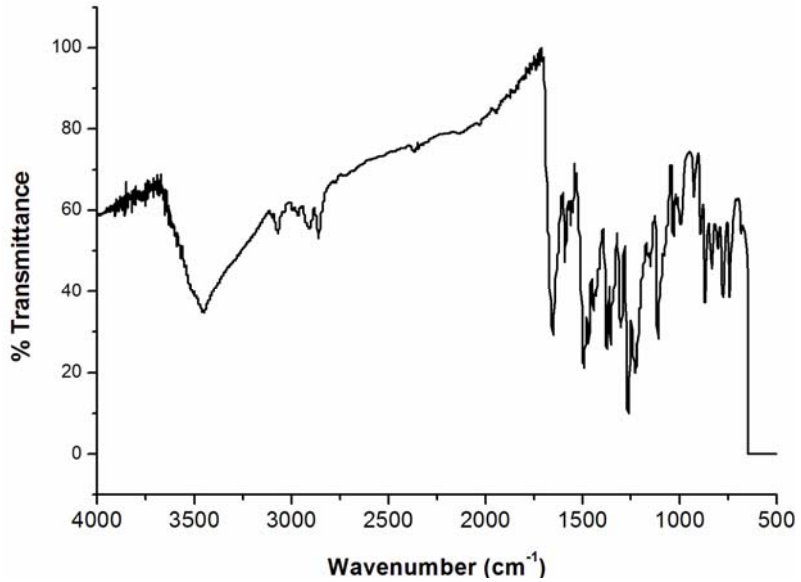

Fig. 6.5 IR spectrum of [Cu(mts)] (**13**).

6.3.2 Electronic spectra

The significant electronic spectral bands for the Cu(II) complexes in acetonitrile are depicted in Table 6.2 and the spectra in Figs. 6.6 and 6.7.

In case of copper(II) being d^9 configuration due to Jahn-Teller distortion further splitting of the $^2T_{2g}$ and ^2E_g may occur and give rise to three spin allowed transitions in the following wavenumber region viz.,

ν_1 (11760 - 18180 cm^{-1})	$^2A_{1g} \leftarrow {}^2B_{1g}$
ν_2 (15500 – 18010 cm^{-1})	$^2B_{2g} \leftarrow {}^2B_{1g}$
ν_3 (17240 – 20000 cm^{-1})	$^2E_g \leftarrow {}^2B_{1g}$

But often these transitions are not seen in practice because of overlapping of bands. Due to the very small energy difference between the *d* levels it seems difficult to resolve them into separate bands.

Table 6.2 Electronic spectral assignment of Cu(II) complexes.

Compound	UV-vis absorption bands (cm^{-1})
H_2bts	32130, 30540
[Cu(bts)]·H_2O (**9**)	31560, 23230, 16900
H_2bmts	37640, 32250, 29810, 24390
[Cu_3(bmts)$_2$(OAc)$_2$] (**10**)	31470, 27280, 16710
[Cu(H_2bmts)]Cl_2·2CH_3OH (**11**)	30920, 24100, 16570
H_2bpts	43820, 33680, 31000, 24450
[Cu(bpts)] (**12**)	30700, 16330, 12630
H_2mts	43680, 37840, 29500, 24750
[Cu(mts)] (**13**)	38000, 32440, 24180, 18090

For compounds **9, 10** and **12** charge transfer bands are found as weak shoulders whereas for **11** and **13** they are sharp bands (Fig. 6.6). Due to the easiness to reduce Cu(II) to Cu(I) many ligands give rise to LMCT transitions. Usually halogen to copper charge transfer occur at relatively low energy independent of stereochemistry. The high energy bands observed show a blue shift indicating the coordination of azomethine nitrogen [14]. Strong charge transfer band in a tetragonal field is an indication of equatorial binding of the halogen group since axial binding groups are far away [15].

Since the ground state in an octahedral field is the Jahn-Teller unstable ^2E_g, most of the complexes are in a distorted state. The lowest *g* value of a compressed octahedron is generally closer to 2.00 than in an elongated octahedron. For five coordinate copper(II) complexes there are two extreme structures, the square pyramid and trigonal bipyramid. For trigonal bipyramid complexes the spectra are found to be with peaks extending from 10500 – 14600 cm^{-1} with greater absorption intensity to lower energy region. For square pyramidal complexes it is with peak extending from 11400 – 15000 cm^{-1}, but with greater absorption intensity to higher energy region. In case of such complexes the transitions can be represented as $d_{x^2-y^2} \rightarrow d_{xz}, d_{yz}$ and $d_{x^2-y^2} \rightarrow d_{z^2}$ [3]. Compound **12** (Fig. 6.7) gave two transitions at 16330 and 12630 cm^{-1} and hence assigned a trigonal bipyramidal geometry.

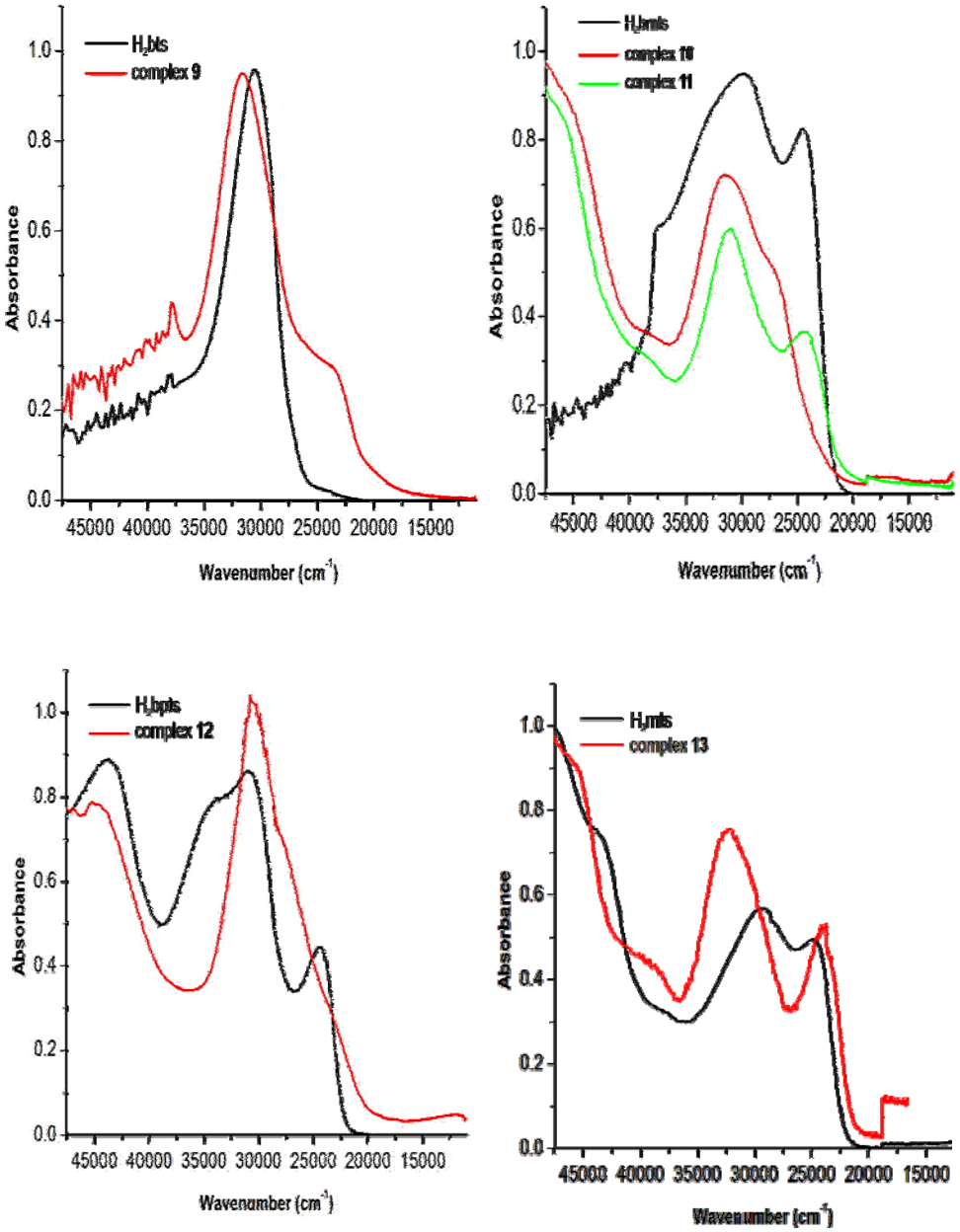

Fig. 6.6 Electronic spectra of Cu(II) complexes in the 45000- 20000 cm^{-1} region.

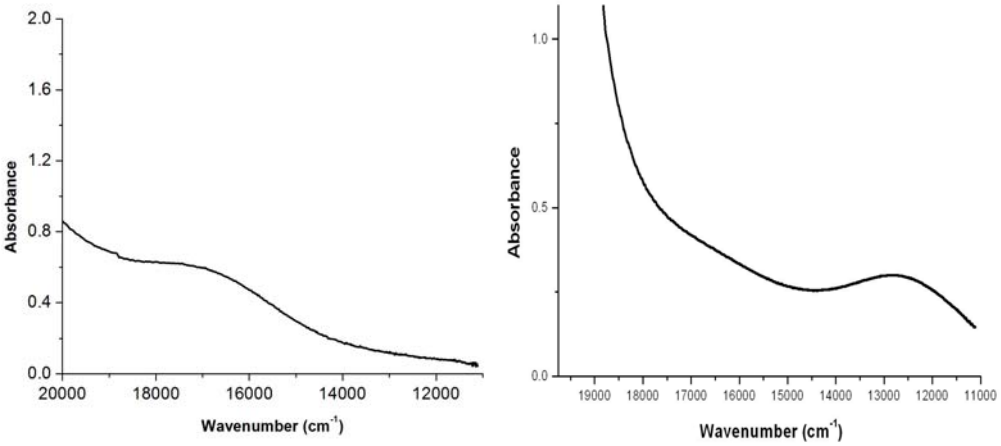

Fig. 6.7 Electronic spectra of complexes **10** (left) and **12** (right) in the 20000 -11000 cm^{-1} region.

Square planar complexes of Cu(II) are extensively studied by electronic spectra. For d^9 system $d_{x^2-y^2}$ is the ground state and three transitions are possible as detailed above. Since four *d* orbitals lie very close together, each transition cannot be distinguished by their energy and hence it is very difficult to resolve the three bands into separate components [3]. For compound **13**, a weak *d-d* transition band found at 18090 cm^{-1} indicates square planar nature of the compound.

6.3.3 EPR spectral studies

The EPR spectra of polycrystalline sample at 298 K and solution at 77 K were recorded in the X-band using 100 kHz field modulation. The *g* factors were quoted relative to the standard marker TCNE (*g* = 2.00277). The EPR spectral and bonding parameters are presented in Table 6.3. The spectra in the polycrystalline state gave much information about the coordination environment around the copper(II) ion in these complexes. The spectra of complexes **11** and **12** are simulated using EasySpin [16] and the experimental (red) and simulated (blue) best fits are included.

EPR spectra can be mainly of four types isotropic, axial, rhombic and reverse axial. An isotropic spectrum with a single *g* value shows a cubic coordination environment. Sometimes broadening of signal can also occur which is attributable to enhanced spin lattice relaxation and dipolar interaction. For axial spectrum there will be at least three fold axis of symmetry in which $g_{\|}$ is when the axis is aligned parallel to *z* axis. Signal due to $g_{\perp}$ is obtained when the axis is aligned perpendicular to *z* axis. A rhombic spectrum shows no axis of symmetry and hence three g values are obtained. In addition to these, hyperfine and superhyperfine lines can also be used to interpret characteristic features about the coordination environment. The ^{14}N superhyperfine structure though not usually clearly seen in the parallel region is very clear in the perpendicular region. Theoretically, three peaks (triplet, with line intensities 1:1:1), five peaks (quintet, with line intensities 1:2:3:2:1), seven peaks (septet, with line intensities 1:3:6:7:6:3:1) and nine peaks (nonet, with line intensities 1:4:10:16:19:16:10:4:1) can be solved for one, two, three and four equivalent nitrogens in superhyperfine multiplets [17,18] respectively. However the situation is more complicated in the experimental conditions. Unambiguous analysis of this superhyperfine multiplet is difficult, because of the number of physical contributions to this region of the spectra. Also clarity in resolution of peaks may be absent, due to poor signal-to-noise ratio.

The geometric parameter G, which is a measure of the exchange interaction between the copper centers in the polycrystalline state is calculated using the equation,

$G = g_{\|} - 2.0023 / g_{\perp} - 2.0023$ for axial spectra.

For rhombic spectra,

$G = g_3 - 2.0023 / g_{\perp} - 2.0023$ where $g_{\perp} = (g_1 + g_2) / 2$.

If G > 4.4, exchange interaction is negligible and if G < 4.4 considerable exchange interaction is indicated in the solid state [19,20].

Table 6.3 EPR spectral assignments for Cu(II) Complexes in polycrystalline state at 298 K and in DMF solution spectrum at 77 K.

	(9)	(10)	(11)	(12)	(13)
Polycrystalline (298 K)					
$g_{\|}/g_1$	2.143	2.520	3.318		2.155
$g_{\perp}/g_2, g_3,$	2.072	2.145	1.980		2.053
g_{iso}				2.083	
DMF at 77 K					
$g_{\|}/g_1$	2.159	2.154		1.948	2.162
$g_{\perp}/g_2, g_3,$	2.066	2.039		2.076, 2.197	2.044
g_{iso}			2.07		
$A_{\|}$ [a]	190				166
$A_{\perp}$ [a]	49				15
A_N [a]	13				16
G/R	2.018	3.627	59	R, 1.03	3.011
f	113				130
α^2	0.7517				0.6787
β^2	0.8604				0.9733
γ^2	1.097				0.9947
$K_{\|}$	0.6468				0.6605
$K_{\perp}$	0.8249				0.6751

[a] Expressed in units of cm^{-1} multiplied by a factor of 10^{-4}.

EPR spectra of all the complexes except [Cu(bpts)] gave an axial spectra in polycrystalline state at 298 K. Typical axial spectra shown by complexes **9** (Fig. 6.8), **10** (Fig. 6.10), **11** (Fig. 6.12) and **13** (Fig. 6.16) have well defined $g_{\|}$ and $g_{\perp}$ values. In all the above compounds $g_{\|} > g_{\perp} > 2.0023$ is consistent with a $d_{x^2-y^2}$ ground state [21]. In compounds **9**, **10** and **13** considerable exchange interaction is indicated since the G value obtained is in the range 2.0 -3.6 [14]. Cu(bpts) in polycrystalline state at 298 K gave an isotropic spectrum (Fig. 6.14) may be due to dipolar interactions and enhanced spin lattice relaxation.

The spectra in DMF at 77 K of all the complexes except **11** and **12** are found to be axial. Complexes **9** show well resolved axial anisotropy with four hyperfine splittings, which arise from the coupling of the odd electron with Cu nuclei (^{63}Cu, I = 3/2). These lines are observed in both parallel and perpendicular region.

The spectrum of complex **9** (Fig. 6.9) in DMF at 77 K gave superhyperfine lines in the parallel and perpendicular region with an average spacing of 13 x 10^{-4} cm^{-1}, which arise from the coupling of the electron spin with the nuclear spin of three nitrogen atoms. This confirms the coordination of pyridine nitrogen and two azomethine nitrogens. The $g_{\|} > g_{\perp}$ values account to the distorted square pyramidal structure in pentacoordinated complexes and rules out the possibility of a trigonal bipyramid structure for which a value $g_{\|} < g_{\perp}$ is expected.

Complex **10** has a normal axial spectrum (Fig. 6.10) consistent with a $d_{x^2-y^2}$ ground state at 298 K in polycrystalline state. Based on similar spectra for CuN_2SCl, it is suggested to have considerable axial interaction [22,23]. In $[Cu_3(bmts)_2(OAc)_2]$, two of the copper(II) centers involve the pyridyl nitrogen, the imine nitrogen and thiolato sulfur of one thiosemicarbazone moiety of H_2bmts along with an acetate group. The third copper(II) center is likely to be coordinated as CuN_2S_2 by the remaining thiosemicarbazone moiety. Since the two centers CuN_2SOAc and CuN_2S_2 are similar a spectrum for a single type of Cu(II) center is obtained. Similar complexes have been reported [22,24] to have considerable solvent interaction. A proposed structure of a similar compound reported Brown and West [22] is given in Fig. 1.7. It is interesting to see that the spectrum obtained (Fig. 6.11) in DMF at 77 K is found to be almost the same with slight shift towards the high energy region.

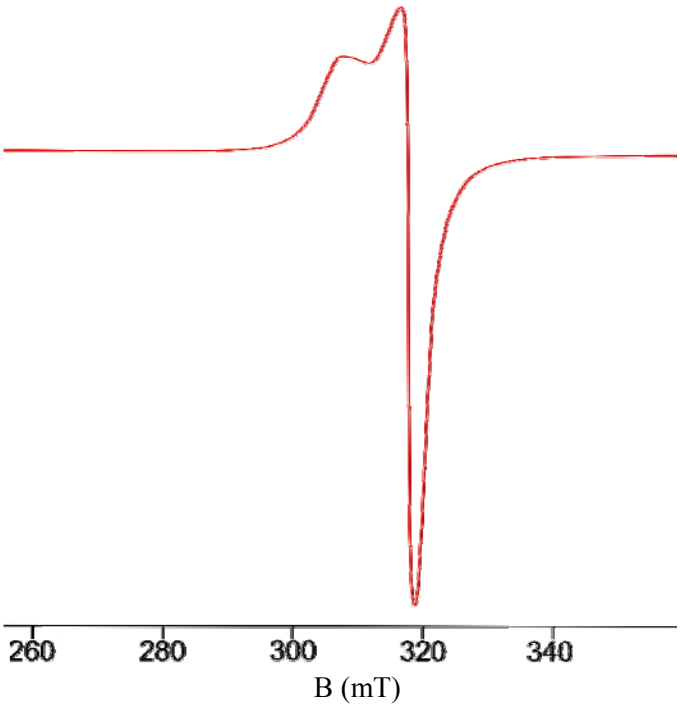

Fig 6.8 EPR spectrum of Cu(bts) (**9**) in polycrystalline state at 298 K.

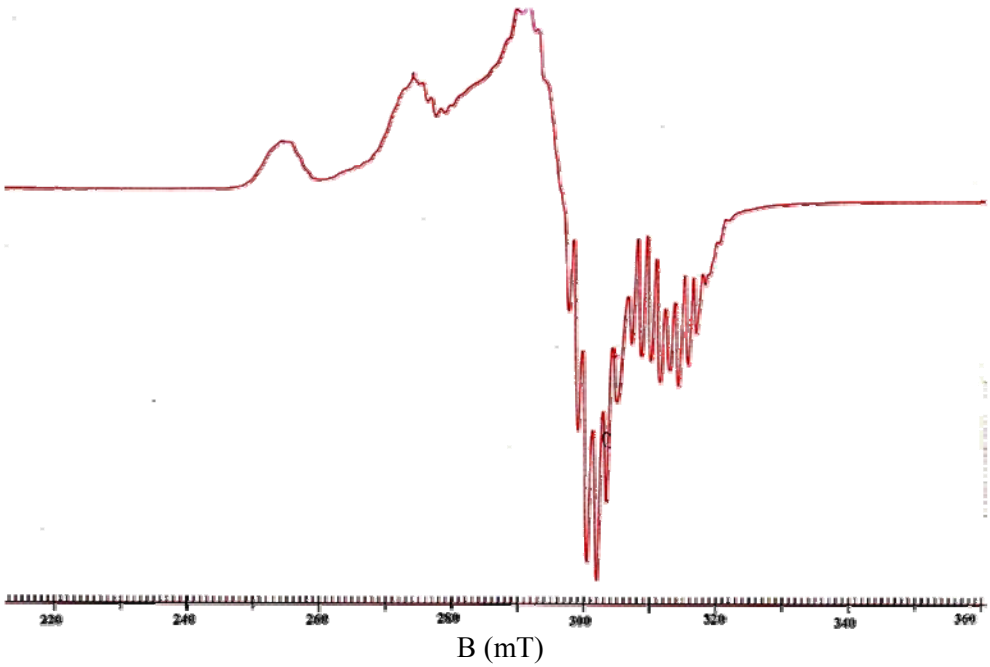

Fig 6.9 EPR spectrum of Cu(bts) (**9**) in DMF at 77 K.

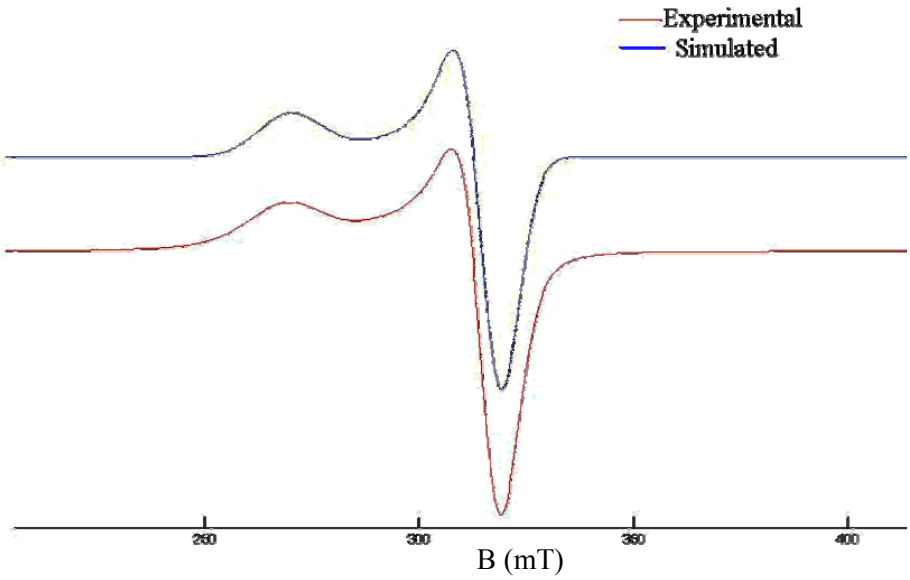

Fig 6.10 Experimental (red) and simulated best fit (blue) of EPR spectrum of $Cu_3(bmts)_2(OAc)_2$ (**10**) in polycrystalline state at 298 K.

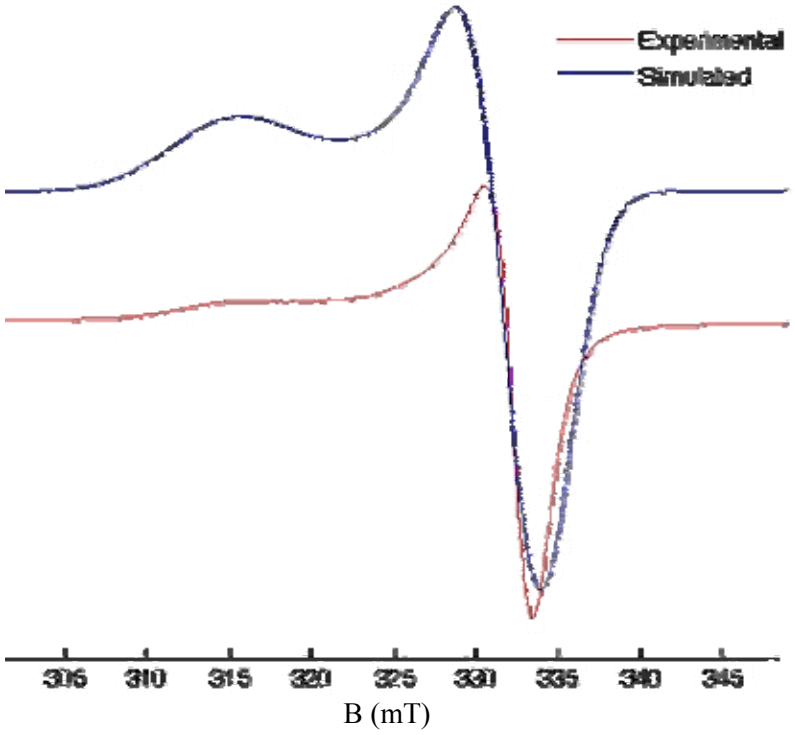

Fig. 6.11 Experimental (red) and simulated best fit (blue) of EPR spectrum of $Cu_3(bmts)_2(OAc)_2$ (**10**) in DMF at 77 K.

The spectrum (Fig. 6.12) of compound **11** was not at all informative due to the broadening which obscures the sharpness of the peaks. It revealed a $g_{\perp}$ value 1.98 less than that of free electron and $g_{\|}$ value 3.318 at low energy region on simulation at 298 K in polycrystalline state. The $g_{\|}$ value less than 2.3 indicate considerable covalent character to the M–L bond and greater than 2.3 indicates ionic character. The $g_{\|}$ values of the complex indicate considerable ionic character to the M–L bond. But the spectrum for solution in DMF at 77 K (Fig. 6.13) revealed was an isotropic one with *g* value of 2.07. This may be due to poor glass formation in frozen state.

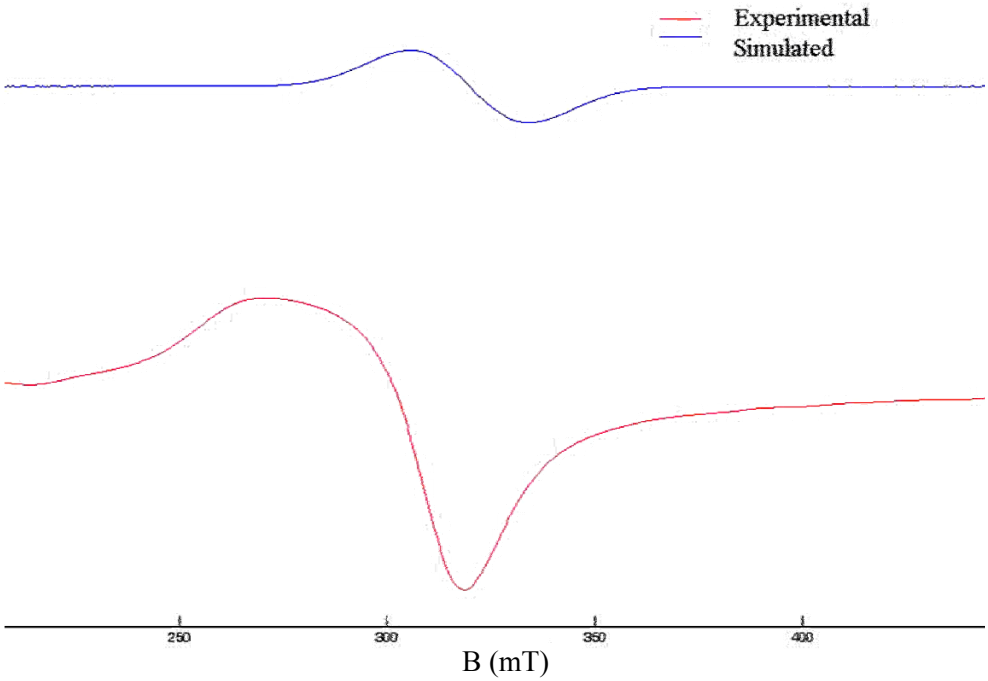

Fig 6.12 Experimental (red) and simulated best fit (blue) of EPR spectrum of $[Cu(H_2bmts)]Cl_2$ (**11**) in polycrystalline state at 298 K.

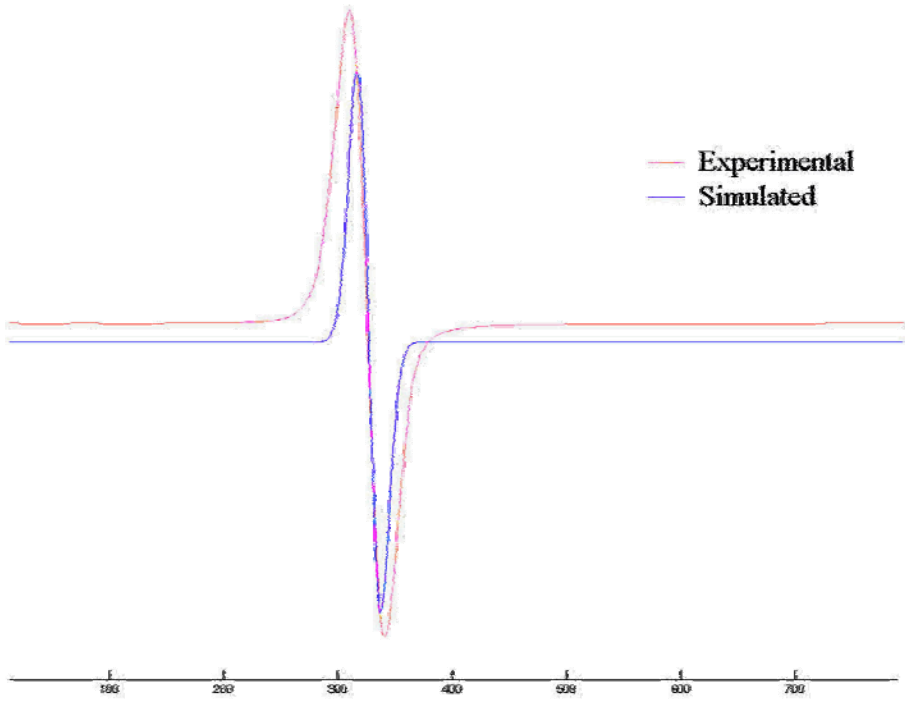

Fig. 6.13 Experimental (red) and simulated best fit (blue) of EPR spectrum of $[Cu(H_2bmts)]Cl_2$ (**11**) in DMF at 77 K.

The spectrum of compound **12** in polycrystalline state at 298 K (Fig. 6.14) was also less informative in interpreting the geometry since the broad spectrum showed isotropic features with a *g* value of 2.083. But it revealed rhombic features at 77 K for solution in DMF with three *g* values. The rhombic parameter R, $\{R = (g_2 - g_1) / (g_3 - g_2)\}$ calculated for compound **12** is found to be 1.03. R < 1 indicates $d_{x^2-y^2}$ ground state for the copper(II) ion whereas R > 1 indicates a predominant d_{z^2} ground state. When R = 1 the ground state is actually a mixture of d_{z^2} and $d_{x^2-y^2}$. It is suggested that the coordinating geometry of compound **12** is an intermediate of square pyramid and trigonal bipyramid.

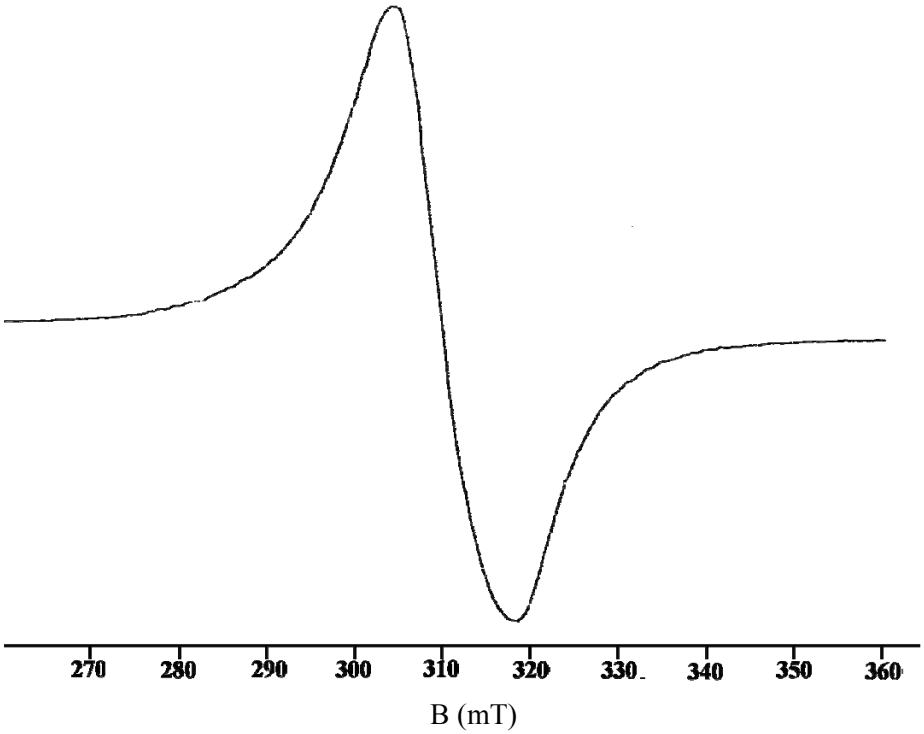

Fig 6.14 EPR spectrum of [Cu(bpts)] (**12**) in polycrystalline state at 298 K.

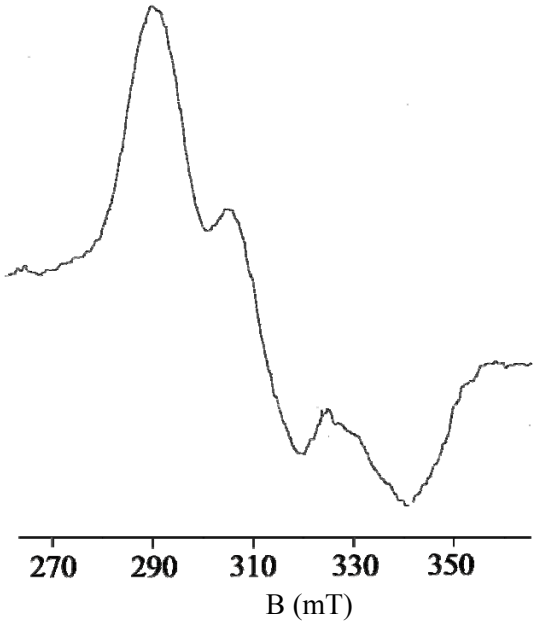

Fig. 6.15 EPR spectrum of [Cu(bpts)] (**12**) in DMF at 77 K.

The spectrum of compound **13** at 298 K in polycrystalline state (Fig. 6.16) is found to be having an axial nature. G value of 3.0 corresponds to strong exchange interaction with $d_{x^2-y^2}$ ground state. The spectrum of **13** in DMF at 77 K (Fig. 6.17) gave an axial spectrum with four hyperfine splittings in both parallel and perpendicular region with an average spacing as shown in Table 6.3. This is due to the coupling of the electron spin with the nuclear spin of ^{63}Cu (I = 3/2) with $g_{\|} > g_{\perp} > 2.0023$ consistent with a $d_{x^2-y^2}$ ground state and a square planar geometry. In addition to these, two superhyperfine lines in the perpendicular region with an average spacing of 16 x 10^{-4} cm^{-1} are also observed. This can be due to the coupling of electron spin with nuclear spin of nitrogen. This indicates the coordination of the azomethine nitrogen and pyridyl nitrogen of which the pyridyl nitrogen dominates in bonding.

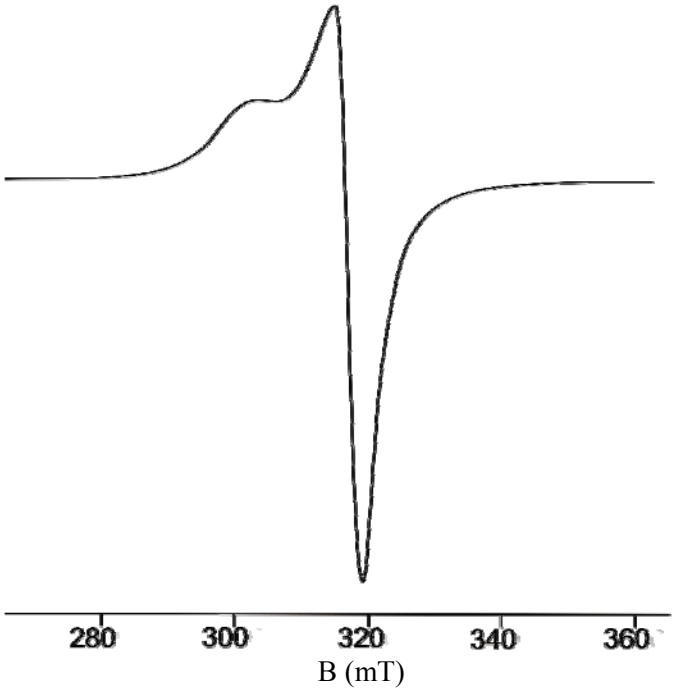

Fig 6.16 EPR spectrum of [Cu(mts)] (**13**) in polycrystalline state at 298 K.

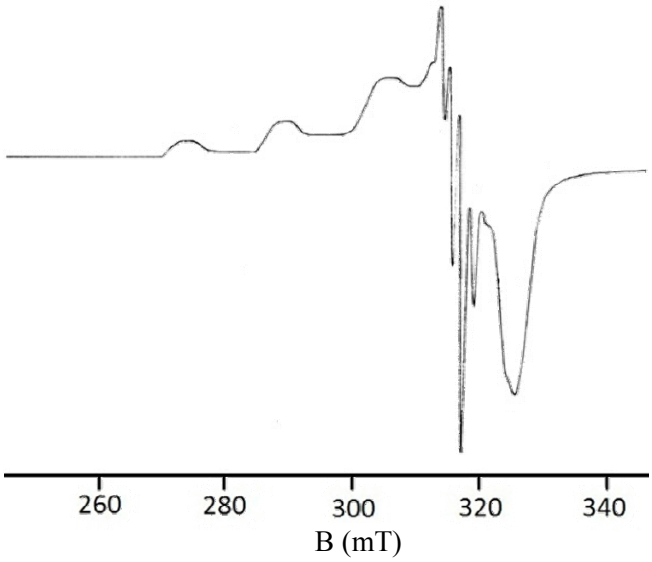

Fig. 6.17 EPR spectrum of [Cu (mts)] (**13**) in DMF at 77 K.

The EPR parameters $g_{\|}$, $g_{\perp}$, $A_{\|}$, $A_{\perp}$ and energies of *d-d* transitions were used to calculate the bonding parameters α^2, β^2 and γ^2, which may be regarded as a measure of covalency of the in-plane σ bonds, in-plane π bonds and out-of-plane π bonds, respectively [25].

The value of in-plane σ bonding parameter α^2 was estimated from the expression [19,26], $\alpha^2 = -\frac{A_{\|}}{0.036} + (g_{\|} - 2.0023) + \frac{3}{7}(g_{\perp} - 2.0023) + 0.04$

β^2 and γ^2 were calculated using the equation $K_{\|} = \alpha^2\beta^2$ and $K_{\perp} = \alpha^2\gamma^2$

The orbital reduction factors, $K_{\|}$ and $K_{\perp}$ were calculated using the following expressions [19,25],

$$K_{\|} = \frac{(g_{\|} - 2.0023)E_{d-d}}{8\lambda_0}$$

$$K_{\perp} = \frac{(g_{\perp} - 2.0023)E_{d-d}}{2\lambda_0}$$

where λ_0 is the spin orbit coupling constant for the free ion with a value of -828 cm^{-1} for Cu(II) d^9 system.

According to Hathaway [27], for pure σ bonding $K_{\|} \approx K_{\perp} \approx 0.77$, and for in-plane π bonding, $K_{\|} < K_{\perp}$; while for out-of-plane π bonding $K_{\perp} < K_{\|}$. For complexes **9** and **13** it is observed that $K_{\|} < K_{\perp}$ which indicates the presence of significant in-plane π bonding. The values of the bonding parameters α^2 and $\beta^2 < 1.0$ (value of 1.0 for 100% ionic character) indicate significant in-plane σ bonding and in-plane π bonding respectively.

6.3.4 Single crystal XRD study of complex 13

X-ray quality single crystals of the complexes **10** and **13** obtained from the reaction medium. Unfortunately complex **10** not at all diffracted. Brown plate like crystal of [Cu(mts)] having approximate dimensions 0.36 x 0.20 x 0.06 mm^3 was selected and diffraction data were collected on a Bruker Smart Apex CCD diffractometer equipped with a fine focus sealed tube, at the National Single Crystal X-ray Facility at the School of Chemistry, University of Hyderabad, Hyderabad. The unit cell parameters were determined and the data collections were performed using a graphite-monochromated Mo Kα (λ = 0.71073 Å) radiation at 298 K and data acquisition and reduction done on a Bruker SAINT software. The trial structure was obtained by direct methods with the program SHELXTL [28] and refined by full matrix least squares on F^2 using SHELXL-97 [29]. The graphical tool used was DIAMOND [30] and MERCURY [31]. All non hydrogen atoms were refined anisotropically and all hydrogen atoms were geometrically fixed at calculated positions. The summary of crystal data and structure refinement are given in Table 6.4.

Table 6.4 Crystal data and experimental parameters of compound **13.**

Empirical formula		$C_{14}H_{16}CuN_4O_2S$
Formula weight		381.93
Temperature (K)		298(2)°
Wavelength (Å)		0.71073
Crystal system		Monoclinic
Space group		$P2_1$
Unit cell dimensions		
	a (Å)	4.3089(19)
	b (Å)	30.189(13)
	c (Å)	11.840(5)
	α (°)	90.00
	β (°)	94.723(7)
	γ (°)	90.00
Volume		1534.9(11)
Z		4
Calculated density (mg m^{-3})		1.653
Absorption coefficient, μ(mm^{-1})		1.578
F(000)		784
Crystal size (mm^3)		0.36 x 0.20 x 0.06
θ range for data collection		2.19 - 24.05
Index ranges		$-4 \leq h \leq 5$, $-37 \leq k \leq 36$, $-14 \leq l \leq 14$
Reflections collected		6111
Refinement method		Full matrix on F_0^2
Data/ restraints /parameters		5874/1/417
Goodness-of-fit on F^2		1.005
Final R indices		
[I >2σ(1)]		R_1 =0.0556, wR_2 = 0.1173
R indices (all data)		R_1= 0.0749, wR_2 = 0.1258

$R_1 = \Sigma||F_o| - |F_c|| / \Sigma|F_o|$ $wR_2 = [\Sigma w(|F_o|^2 - |F_c|^2)^2 / \Sigma w(F_o^2)^2]^{½}$

6.3.5 Crystal structure of [Cu(mts)]

The molecular structure of the copper monothiosemicarbazone complex with atom numbering scheme is given in Fig. 6.18. Selected bond lengths and bond angles are represented in Table 6.5. The compound crystallized with two molecules per asymmetric unit into a monoclinic crystal system space group $P2_1$. The copper in the mononuclear complex is tetracoordinated through thiolato sulfur S1 [Cu1–S1, 2.2107(19) Å], pyridine nitrogen N1 [Cu1–N1, 1.893(5) Å], azomethine nitrogen N2 [Cu1–N2, 1.969 (5) Å] and acetyl oxygen [Cu1–O1, 1.989 (5) Å] to form a distorted square planar structure. There is a marked decrease in metal ligand bond lengths when compared with similar complexes. When the bond angles are summed N1–Cu1–N2, 79.8(2)°, N1–Cu1–O1, 81.8(2)°, N2–Cu1–S1, 85.70(15)°, and O1–Cu1–S1, 111.95(16)° it comes to 359.3. This illustrates that the complex is having a slight distortion from planarity. The large deviation for the [O1–Cu–S1] angle may be due to the bite angle extended by the chelating rings involving pyridine nitrogen and azomethine nitrogen.

The formation of chelate rings Cu1–N1–C7–C8–N2 and Cu1–N1–C3–C2–O1 with Cu1–N1 as common axis are almost planar with a dihedral angle of 3.8(3)°. The bonding distance of C9–S1, 1.753(7) Å agree with the coordinating pattern of thiosemicarbazone via the thiolate form. The cadmium complex of unsubstituted 2,6-diacetylpyridine monothiosemicarbazone is found to form a neutral distorted pentagonal bipyramid along with two chloro and an aqua ligand [32]. The almost planar C8–N2–N3–C9–S–N4 chain adopts an *E* configuration about the azomethine bond and *Z* configuration about the hydrazinic bond. The inclusion of sulfur donor atom in the coordination sphere significantly increases the steric hindrance and hence chelating ring containing sulfur is found to be twisted on Cu1–S1 which is supported by puckering analysis {Q = 0.096(4) Å, $\varphi = 203(3)^{\circ}$} [33].

The C2–O1 bond length (1.292(9) Å) is found to be considerably longer than the standard C=O bond length 1.21 Å [34] and C1–C2 bond length (1.212(9) Å) is found to be considerably shorter than C–C single bond length [35,36]. The deviation of bond angles around C2 from 120° [O1–C2–C3 114.1(6)°] is due to the bite angle extended by the chelating ring. Hence it can be inferred that the keto group is coordinated by enolization followed by deprotonation. The morpholine ring adopts a chair conformation in the structure.

Table 6.5 Selected bond lengths (Å) and bond angles (°) of [Cu(mts)] (**13**)

Bond length (Å)		**Bond angles (°)**	
Cu1–N1	1.893(5)	N1–Cu1–N2	79.8(2)
Cu1–N2	1.969(5)	N1–Cu1–O1	81.8(2)
Cu1–O1	1.989(5)	N2–Cu1–S1	85.70(15)
Cu1–S1	2.211(11)	O1–Cu1–S1	111.95(16)
S1–C9	1.753(7)	N2–Cu1–O1	161.1(2)
		N1–Cu1–S1	164.11(17)
Cu2–N5	1.925(5)	N5–Cu2–N6	79.5(2)
Cu2–N6	1.974(5)	N6–Cu2–O3	81.9(2)
Cu2–O3	1.986(5)	N6–Cu2–S2	85.33(15)
Cu2–S2	2.235(18)	O3–Cu2–S2	112.54(17)
S2–C23	1.753(6)	N6–Cu2–O3	160.9(2)
		N5–Cu2–S2	163.44(19)

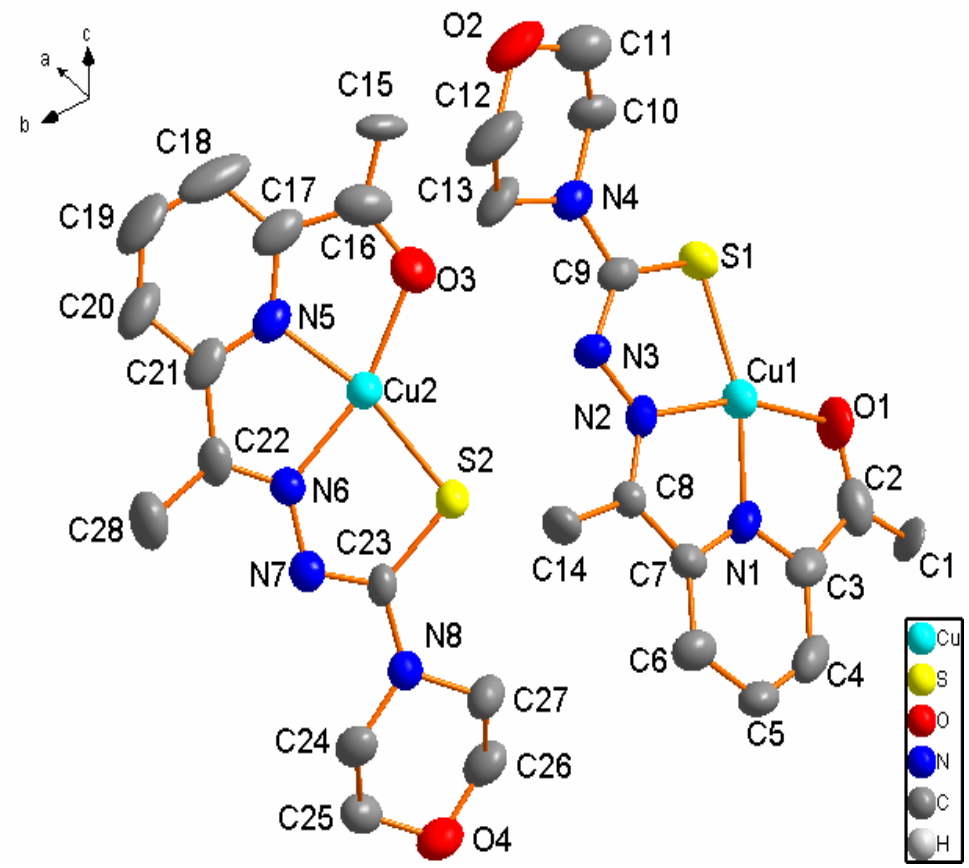

Fig. 6.18 Molecular structure of [Cu(mts)] (**13**) along with atom numbering scheme.

The packing of molecules along the *a* axis with Cu···Cu distance as 4.309 Å can be seen in Fig. 6.19. EPR spectral studies also support considerable metal-metal interaction in this complex. The packing of the molecule is stabilized by π–π, ring–metal and CH–π interactions. These interaction data are given in Table 6.6. A peculiarity observed is the involvement of the Cg(2) and Cg(6) chelate rings in interaction which are formed by the coordination of keto groups O1 and O3 after enolization. Short metal ring interaction of the chelate rings Cg(1), Cg(2), and Cg(5) with Cu1 are observed at a distance of 3.781, 3.708 and 3.566 Å respectively. Similar ring metal interactions are perceived from Cu2 also.

The centroid Cg(1) is involved in π–π interactions with Cg(3) at 3.352(3) Å and with pyridyl ring, Cg(5) of the neighboring unit at a distance of 3.738(3) Å. The X–H centroid (H··· Cg) distances are in the range of 2.79–3.00 Å and the γ angles usually have values below 10° [37]. The C14–H14A···Cg(6) distance is found as 2.96 Å. The C–H··· Cg angle 124° is still below the optimal value 180° for the strongest CH··· π interaction, which may be due to the steric constraints in the molecule. This kind of CH··· π (planar chelate ring) interaction in complex **13** can be thought as a structural evidence for the metalloaromaticity of such planar chelate rings, a classical concept reviewed by Masui [38,39]. These diverse interactions result in superimposing of molecules to give one dimensional polymeric chains which appear as huge tower like molecular architectures as seen in Fig. 6.20.

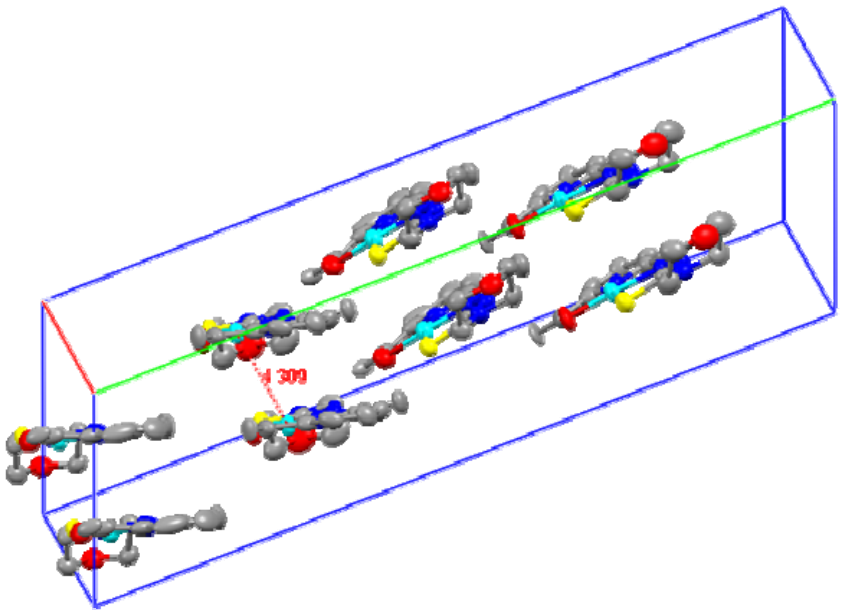

Fig. 6.19 Packing of the molecule in the unit cell with a Cu··· Cu distance of 4.309 Å in between molecules.

Table 6.6 Interaction parameters of compound (**13**)

π–π interactions			
Cg(I)···Cg(J)	Cg···Cg (Å)	α°	β°
Cg(1)···Cg(3)[a]	3.352(3)	4.0(2)	12.33
Cg(1)···Cg(5)[a]	3.738(3)	3.8(3)	24.03
Ring···Metal Interactions			
Cg(I)···Me(J)	Cg(I) ···Me(J) (Å)		β°
Cg(1)···Cu(1)[a]	3.781		33.31
Cg(2)···Cu(1)[b]	3.708		22.10
Cg(5)···Cu(1)[b]	3.566		16.00
Cg(6)···Cu(2)[a]	3.855		34.07
Cg(7)···Cu(2)[b]	3.765		23.32
Cg(10)···Cu(2)[b]	3.533		11.99
X–H···Cg interactions			
X–H(I)···Cg(J)	H···Cg (Å)	X–H···Cg (°)	X···Cg (Å)
C(14)–H(14A)···Cg(6)[a]	2.96	124	3.585(7)

D, donor; A, acceptor; Cg, centroid; α, dihedral angles between planes I and J;

β, angle between Cg(I)–Cg(J) vector and normal to plane I.

Cg(1) = Cu(1), S(1),C(10), N(3), N(2); Cg(2) = Cu(1), O(1), C(2), C(1), N(1);

Cg(3) = Cu(1), N(1), C(7), C(8), N(2); Cg(5)= N(1), C(1), C(4), C(5), C(6), C(7);

Cg(6) = Cu(2), S(2), C(24), N(7), N(6); Cg(7) = Cu(2), O(3), C(16), C(15), N(5);

Cg(10) = N(5), C(15), C(18), C(19), C(20), C(21).

Equivalent position codes:

a = 1+x, y, z; *b* = -1+x, y, z

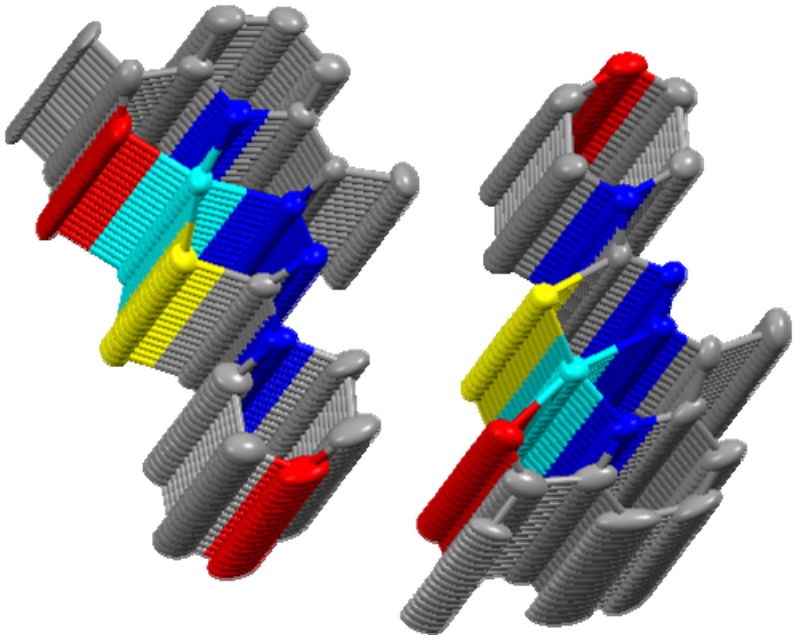

Fig. 6.20 One dimensional molecular architecture formed by metal–ring and π–π interactions.

6.4 Conclusion

Five copper complexes with chelating rings were synthesized. All the compounds except **11** were found to coordinate in the deprotonated dianionic form. Elemental analyses showed that copper acetate yielded anionic form of the ligand in complexes whereas copper chloride the neutral form. Conductivity studies revealed 2:1 electrolytic nature for compound **11**. IR and electronic spectral studies confirm pentacoordination of H_2bts, H_2bmts and H_2bpts. The monothiosemicarbazone gave tetradentate complex in which the ligand is thiolato enolic form. Spectral studies give voluminous information regarding the stereochemistry of the complexes. Normal magnetic moment values are obtained for all complexes except **10**. Compound **10** gives a sub-normal value corresponding to a trinuclear copper which is supported by elemental analyses data. All the compounds are found to be in $d_{x^2-y^2}$ ground state. Coordination of azomethine and pyridine nitrogens are confirmed by the

superhyperfine splitting obtained in the EPR spectral studies. In **9** and **13** there is considerable exchange interaction between the metal centers. Single crystal studies show [Cu(mts)] to have a distorted square planar geometry with a dianionic ligand. The packing structure showed that the crystal structure is a polymeric one dimensional chain stabilized by ring-ring and ring-metal interactions.

References

[1] F.A. Cotton, G. Wilkinson, C.A. Murillo, M. Bochmann, Advanced Inorganic Chemistry, 6th ed., Wiley, New York, 1999.

[2] C.J. Jones, d- and f- Block Chemistry, The Royal Society of Chemistry, UK, 2001.

[3] J.E. Huheey, E.A. Keiter, R.L. Keiter, O.K. Medhi, Inorganic Chemistry: Principles of Structure and Reactivity, 4th ed., Pearson Education.

[4] M. Mohan, P. Sharma, M. Kumar, N.K. Jha, Inorg. Chim. Acta 125 (1986) 9.

[5] M. Joseph, M. Kuriakose, M.R.P. Kurup, E. Suresh, A. Kishore, S.G. Bhat, Polyhedron 25 (2006) 61.

[6] P.S. Donelly, Dalton Trans. 40 (2011) 999.

[7] S. Lim, K.A. Price, S.-F. Chong, B.M. Paterson, A. Caragounis, K.J. Barnham, P. J. Crouch, J.M. Peach, J.R. Dilworth, A.R. White, P.S. Donnelly, J. Biol. Inorg. Chem. 15 (2010) 225.

[8] S. Lim, B.M. Paterson, M.T. Fodero-Tavoletti, G.J. O'Keefe, R. Cappai, K.J. Barnham, V.L. Villemagne, P.S. Donnelly, Chem. Commun. 46 (2010) 5437.

[9] J.D. Lee, Concise Inorganic Chemistry, 4th ed., Oxford University Press, 1991.

[10] L. Latheef, E. Manoj, M.R.P. Kurup, Polyhedron 26 (2007) 4107.

[11] W.J. Geary, Coord. Chem. Rev. 7 (1971) 81.

[12] M. Maji, S. Ghosh, S.K. Chattopadhyay, Trans. Met. Chem. 23 (1998) 81.

[13] B.S. Garg, M.R.P. Kurup, S.K. Jain, Y.K. Bhoon, Trans. Met. Chem. 13 (1988) 309.

[14] L. Latheef, M.R.P. Kurup, Spectrochim. Acta Part A70 (2008) 86.

[15] A.B.P. Lever, Inorganic Electronic Spectroscopy, Elsevier, Amsterdam, 1984.

[16] S. Stoll, a. Schweiger, J. Magn. Reson. 178 (2006) 42.

[17] L. Martiska, L. Husarikova, Z. Repicka, D. Valigura, M. Valko, M. Mazur, Appl. Magn. Reson. 39 (2010) 423.

[18] B.A. Goodman, J.B. Raynor, Adv. Inorg. Chem. Radiochem. 13 (1970) 135.

[19] A.H. Maki, B.R. McGarvey, J. Chem. Phys. 29 (1958) 35.

[20] B.J. Hathaway, D.E. Billing, Coord. Chem. Rev. 5 (1970) 1949.

[21] M.J. Bew, B.J. Hathaway, R.R. Faraday, J. Chem. Soc., Dalton Trans. (1970) 1229.

[22] C.A. Brown, D.X. West, Trans. Met. Chem. 28 (2003) 154.

[23] D.X. West, J.K. Swearingen, T.J. Romack, I.S. Billeh, J.P. Jasinski, Y. Li, R.J. Staples, J. Mol. Struct. 570 (2001) 129.

[24] S. Krishnan, Ph.D Thesis, Cochin University of Science and Technology (2008).

[25] D. Kivelson, R. Neiman, J. Chem. Soc., Dalton Trans. 35 (1961) 149.

[26] J.R. Wasson, C. Trap, J. Phys. Chem. 73 (1969) 3763.

[27] B.J. Hathaway, Struct. Bond., Springer Verlag, Hiedelberg 4 (1973) 60.

[28] G. M. Sheldrick, Acta Cryst. A64 (2008) 211.

[29] G.M. Sheldrick, SHELXL97, SHELXS97, University of Göttingen, Germany, 1997.

[30] K. Brandenburg, DIAMOND Version 3.1f, Crystal Impact GbR, Bonn, Germany, 2008.

[31] C.F. Macrae, P.R. Edington, P. McCabe, E. Pidcock, G.P. Shields, R. Taylor, M. Towler, J. van de Streek, J. Appl. Cryst. 39 (2006) 453.

[32] J.S. Casas, E.E. Castellano, M.S. Garcia-Tasende, A. Sanchez, J. Sordo, J. Zukerman-Schpector, Z. Anorg. Allg. Chem. 623 (1997) 825.

[33] D. Cremer, J.A. Pople, J. Amer. Chem. Soc. 97 (1975) 1354.

[34] B.N.B. Raj, M.R.P. Kurup, E. Suresh, Spectrochim. Acta Part A71 (2008) 1253.

[35] E. Manoj, M.R.P. Kurup, H.-K. Fun, S. Chantrapromma, Acta. Cryst. E61 (2005) 4110.

[36] I.L. Finar, Organic Chemistry Vol. I: The Fundamental Principles 6th Ed. Longman 1973.

[37] Y. Jiang, C. Xu, Y. Liu, J. Niclós-Gutiérrez, D. Choquesillo-Lazarte, Eur. J. Inorg. Chem. (2005) 1585.

[38] H. Masui, Cord. Chem. Rev. 957 (2001) 219.

[39] V. Philip, V. Suni, M.R.P. Kurup, M. Nethaji, Polyhedron 23 (2004) 1225.

Chapter 7

Synthesis, Structures and Spectral Characterization of Zinc(II) Complexes

Contents

7.1 Introduction

Zinc always occurring as a divalent cation zinc(II) in biological systems, is the second most abundant transition metal following iron [1]. Zinc, since having a filled *d* orbital shows few of the characteristic properties of transition metals despite their position in the *d*-block of the periodic table. Since d^{10} configuration affords no crystal field stabilization the stereochemistry of a compound depends on the size and polarizing power of the cation and the steric requirement of the ligand.

Zinc ions are well known to play diverse roles like regulators of enzyme, DNA binding and recognition (zinc finger family of proteins), structural cofactor (Cu-Zn SOD) or as a catalytic center in carbonic anhydrase in biological processes. The neurological role of zinc as a neurotransmitter and modulator has attracted much attention in recent years. Various neurological diseases such as Alzheimer's disease, Parkinson's disease, hypoxia-ischemia and epilepsy are closely related to a disorder of zinc metabolism [2]. Fluorescence method stands a method of choice for this d^{10} metal since analytical techniques like NMR or EPR cannot be used in biological systems.

Designing of zinc fluorescent probes is an innovative area for studying the diverse physiological roles especially neural "free" or weakly bonded zinc [3]. Zinc deficiency can result in alterations in iron transport, storage, and regulatory proteins, which facilitate iron accumulation in cells [4].

Bis(thiosemicarbazones) are well known by their versatile coordination capabilities and broad therapeutic activity. They are also found to be useful ligands for generating interesting supramolecular motifs [5]. Different zinc complexes of substituted and unsubstituted 2,6-diaetylpyridine bis(thiosemicarbazones) are reported to be yielding both mono and dinuclear complexes with interesting structural features [6]. In some of the binuclear zinc complexes the donor environments are found to be same or different which can be represented as {6+6}, {6+4}, {4+4} and {5+5} in the solid state [7-9]. Mixed ligand dimeric complex of zinc with {7+7} geometry also have been reported [6]. The energy differences between the different crystalline forms may be very small and this points that more studies are required about rules governing the process. Standard chemical procedures like template method [10], electrochemical technique [9] etc have been tried and may be a factor to obtain different coordination isomers of binuclear zinc complexes.

7.2 Experimental

7.2.1 Materials

The reagents used for the synthesis of the proligands are discussed in Chapter 2. Solvents being pure were used as supplied. Zinc acetate and nitrate used were Analar grade and used as supplied for the preparation of the complexes. Solvents used were methanol and dimethylformamide.

7.2.2 Synthesis of complexes

7.2.2.1 *Synthesis of $[Zn_2(bts)_2]\cdot DMF\cdot CH_3OH$ (**14**)*

Zinc acetate was used for preparing the complex. H_2bts (0.155 g, 0.5 mmol) was dissolved in 2 ml of DMF and diluted with 15 ml methanol. This

was slowly added to a hot solution of $Zn(OAc)_2$ (0.107 g, 0.5 mmol) in 15 ml methanol. The mixture was refluxed for 3 hours and allowed to cool. The yellow complex formed with 70% yield was filtered, washed in methanol, followed by ether and dried *in vacuo* over P_4O_{10}. The crystals obtained were found to be suitable for single crystal X-ray diffraction studies.

7.2.2.2 *Synthesis of [Zn(bmts)]·H_2O (**15**)*

Zinc acetate (0.107 g, 0.5 mmol) was dissolved in 15 ml methanol and heated. H_2bmts (0.225 g, 0.5 mmol) was dissolved in 2 ml of DMF and diluted with 15 ml methanol. This was slowly added to a hot solution of $Zn(OAc)_2$. The mixture was refluxed for 3 hours and allowed to cool. The yellow complex formed was filtered, washed in methanol followed by ether and dried over P_4O_{10} *in vacuo*.

Yield 75%, Elem. Anal. found (calcd)% for $C_{19}H_{27}N_7O_3S_2Zn$: C, 43.12 (42.98); H, 4.67 (5.13); N, 17.78 (18.46); S, 12.16 (12.08).

7.2.2.3 *Synthesis of [Zn_2(bpts)$_2$] (**16**)*

Zinc nitrate (0.149 g, 0.5 mmol) was dissolved in 15 ml methanol and slowly heated. H_2bpts (0.209 g, 0.5 mmol) was dissolved in 2 ml of DMF and diluted with 15 ml methanol. This was slowly added to the above mixture. The mixture was refluxed for 3 hours and allowed to cool. The yellow crystalline complex formed was filtered, washed in methanol followed by ether and dried over P_4O_{10} *in vacuo*. The crystals obtained were found to be suitable for single crystal X-ray studies.

Yield 63%, Elem. Anal. found (calcd)% for $C_{19}H_{25}N_7S_2Zn$: C, 46.98 (47.44); H, 5.11 (5.24); N, 20.44 (20.38); S, 13.68 (13.33).

7.2.2.4 *Synthesis of [Zn(bpts)]·H_2O (**17**)*

Zinc acetate was used for preparing the complex. H_2bpts (0.209 g, 0.5 mmol) was dissolved in 2 ml of DMF and diluted with 15 ml methanol.

This was slowly added to a hot solution of $Zn(OAc)_2$ (0.107 g, 0.5 mmol) dissolved in 15 ml methanol. The mixture was refluxed for 3 hours and allowed to cool. The dark yellow complex formed was filtered, washed in methanol followed by ether and dried over P_4O_{10} *in vacuo*.

Yield 73%, Elem. Anal. found (calcd)% for $C_{19}H_{27}N_7OS_2Zn$: C, 45.78 (45.73); H, 4.78 (5.45); N, 20.05 (19.65); S, 13.16 (12.85).

7.2.2.5 *Synthesis of* $[Zn(Hmts)_2]\cdot H_2O$ (***18***)

Zinc acetate was used for preparing the complex. H_2mts (0.153 g, 0.5 mmol) was dissolved in 2 ml of DMF and diluted with 15 ml methanol. This was slowly added to a hot solution of $Zn(OAc)_2$ (0.107 g, 0.5 mmol) dissolved in 15 ml methanol. The mixture was refluxed for 3 hours and allowed to cool. The yellow complex formed was filtered, washed in methanol followed by ether and dried over P_4O_{10} *in vacuo*.

Yield 70%, Elem. Anal. found (calcd)% for $C_{28}H_{38}N_8O_6S_2Zn$: C, 47.69 (47.22); H, 5.54 (5.38); N, 15.97 (15.73); S, 9.17 (9.18).

7.2.3 Physical measurements

Various characterization techniques used are discussed in Chapter 1.

7.3 Results and discussion

Equimolar ratios of the ligands and the metal salts yielded the yellow colored metal complexes. Many related ligands have been found to form complexes containing both protonated and deprotonated forms of the ligands [1,10]. All the compounds were found to coordinate in the deprotonated form irrespective of the salt used. For compound **16** though zinc nitrate was the salt used a compound very similar in elemental analyses data to compound **17** was obtained**.**

In the solid state though the ligand is in the thioketo form, in solution and in presence of zinc(II) ion it is quickly converted to the thiol form and get deprotonated. For the compounds **14** and **16** two crystals of the complexes were obtained. Compound **14** contains uncoordinated methanol and DMF molecules. The elemental analysis data is not given with synthesis since it is found to be disagreeing with theoretical data.

All the complexes are expected to be diamagnetic due to the d^{10} configuration of the metal ion.

7.3.1 IR spectra

The significant bands obtained in the vibrational spectra of the four ligands and their Zn(II) complexes along with their tentative assignments are given in Table 7.1. The bands corresponding to ν(N–H) present in the ligands disappeared in the spectra of all the compounds indicating the enolization of the thioketo group followed by deprotonation. The shifting of the ν(C=N) band to lower and ν(N–N) to higher wavenumbers in the spectra indicate the coordination of the azomethine nitrogen to the metal. Involvement of the pyridine nitrogen in coordination is indicated by the variations observed in the ring breathing vibrations of pyridine ring and the in-plane ring deformation band of pyridine [11].

In the spectrum of the complex **14** (Fig. 7.1), $\nu(N^4–H)$ vibrations are observed at 3068 cm^{-1}. The azomethine band found at 1603 cm^{-1} for the uncomplexed ligand is shifted to 1576 cm^{-1} upon coordination. The band at 1621 cm^{-1} is assigned to the -C=N–N=C- moiety, newly formed as a result of deprotonation of the ligand for coordination. The increase in the absorption band due to the ν(N–N) stretching vibration indicates the increase in the bond strength due to the increase in double bond character. Coordination via the thiolato sulfur is indicated by a decrease in the frequency to 1351 and 783 cm^{-1}

of the thioamide band which was observed at 1360 and 872 cm^{-1} for the uncomplexed ligand. Ring breathing vibrations shift to 1384 cm^{-1} and in-plane ring deformation band to 751 cm^{-1}.

The spectrum of complex **15** (Fig. 7.2) reveals a broad band with low intensity around 3440 cm^{-1}. This can be due to the presence of non-hydrogen bonded lattice water content in the sample. The vibrations due to the methylene groups of the morpholine ring are observed at 2965 and 2840 cm^{-1}. The azomethine band shifts to 1591 cm^{-1} on coordination. Coordination of the pyridine nitrogen is confirmed by the in-plane ring deformation band at 803 cm^{-1}.

The spectrum of complex **16** (Fig. 7.3) shows a lowering of the frequency of the azomethine band to 1589 cm^{-1} confirming the coordination of the N_{azo} to zinc. The vibrations due to the methylene groups of the pyrrolidine ring are observed at 2966 and 2865 cm^{-1}.

Table 7.1 IR spectral assignments (cm^{-1}) of zinc complexes.

Compound	$\nu(N^4–H)$ / $\nu(N^2–H)$	ν(C=O)	ν(C=N)	ν/δ(C–S)	ν(N–N)	Band III pyridine ring	py(ip)
H_2bts	3214/3160	--	1603	1360, 872	1103	1441	715
[Zn_2(bts)$_2$] (**14**)	3391/3068	--	1576	1351, 783	1110	1384	751
H_2bmts	3164	--	1613	1361, 792	1103	1463	741
[Zn(bmts)]· H_2O (**15**)	--	--	1591	1350, 803	1111	1464	643
H_2bpts	3370	--	1605	1360, 818	1130	1450	658
[Zn_2(bpts)$_2$] (**16**)	--	--	1589	1369, 804	1174	1418	631
[Zn(bpts)]·H_2O (**17**)	--	--	1589	1369, 806	1164	1419	631
H_2mts	3094	1691	1613	1365, 814	1110	1463	734
[Zn(Hmts)$_2$]· 2H_2O (**18**)	--	1693	1577	1352, 879	1112	1469	765

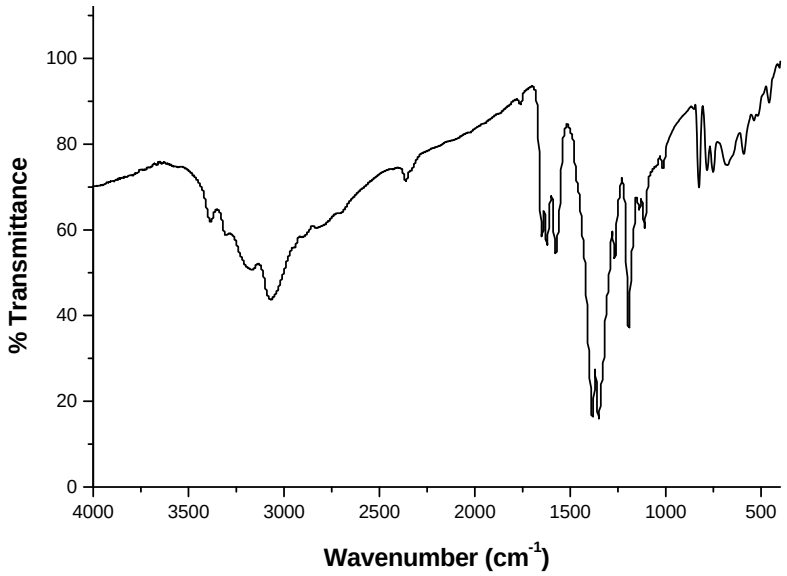

Fig. 7.1 IR spectrum of $[Zn_2(bts_2)]$ (**14**).

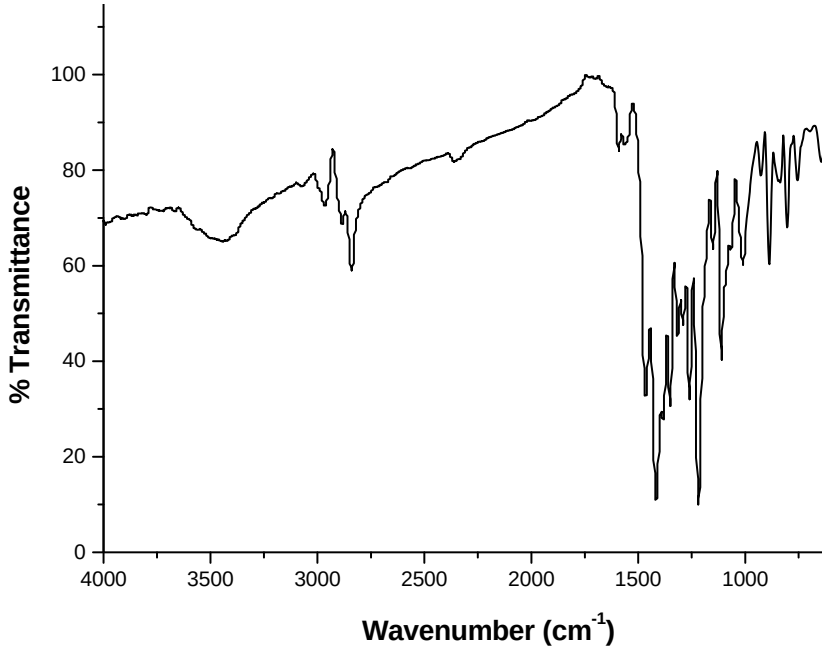

Fig. 7.2 IR spectrum of [Zn(bmts)] (**15**).

The ν(N–N) band shifts to 1164 cm^{-1} on coordination which is a measure of the increase in bond strength. Coordination of the pyridine nitrogen is confirmed by the in-plane ring deformation band at 626 cm^{-1}.

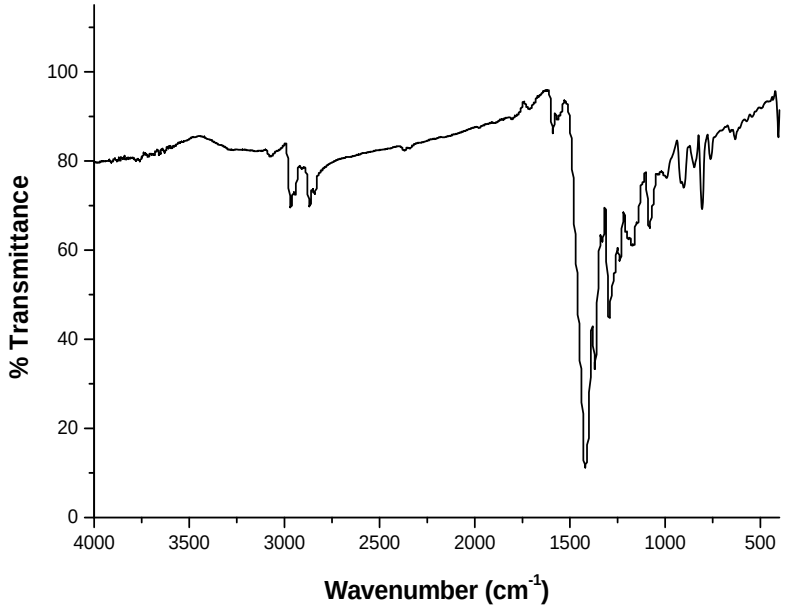

Fig. 7.3 IR spectrum of $[Zn_2(bpts)_2]$ (**16**).

The spectrum (Fig. 7.4) of complex **17** is found to be almost same as that of the above. The observable difference is the low intensity band at 3440 cm^{-1} which may be due to the water content present as revealed by the elemental analysis.

In the spectrum of complex **18** (Fig. 7.4) a low intensity broad band at 3440 cm^{-1} may be due to the presence of lattice water. The vibrations due to the methylene groups of the morpholine ring are observed at 2956 and 2851 cm^{-1}. The band due to keto group of the compound undergoes a blue shift indicating the coordination. The azomethine band shifts to 1577 cm^{-1} on coordination from 1613 cm^{-1} in the uncomplexed ligand. The stretching and bending vibrations due to the thioketo group lowers when compared with the free ligand indicating strong coordination with enolization followed by

deprotonation. Coordination of the pyridine nitrogen is confirmed by the in-plane ring deformation band at 744 cm^{-1}.

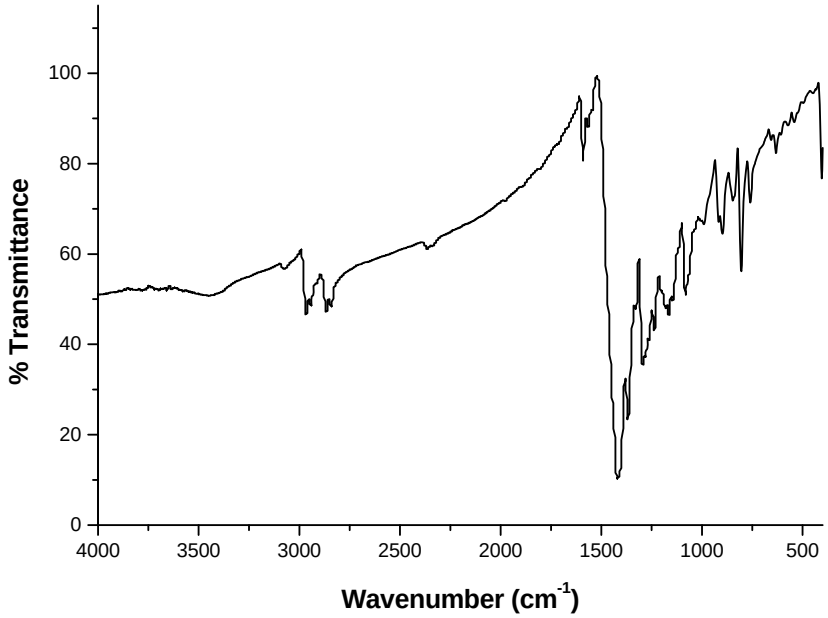

Fig. 7.4 IR spectrum of Zn[bpts] (**17**).

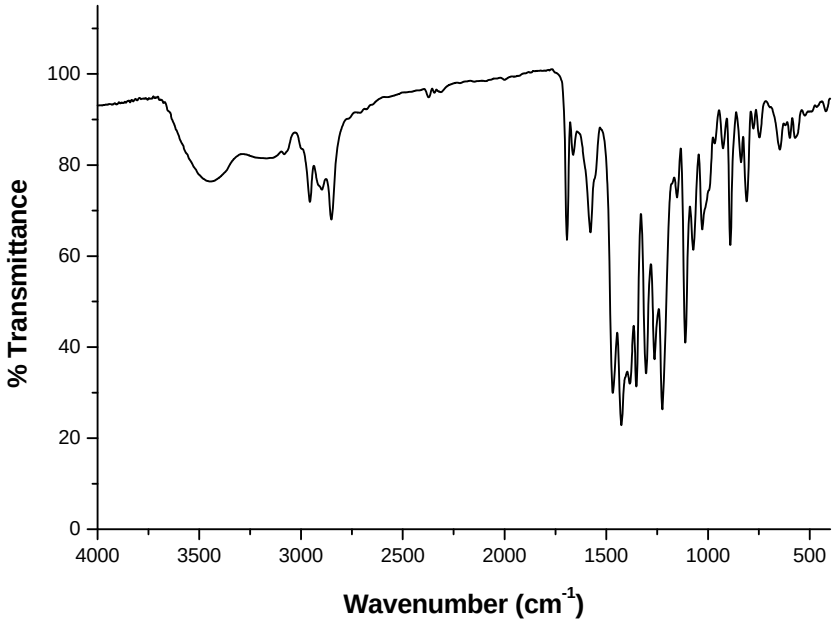

Fig. 7.5 IR spectrum of $[Zn(Hmts)_2]$ (**18**).

7.3.2 Electronic spectra

For zinc(II) complexes no *d-d* transitions are expected since zinc is with a d^{10} configuration and no vacant *d* orbitals are there. All the zinc complexes synthesized are found to be yellow in color. This color arises due to charge transfer transitions. The significant spectral assignments for various intra-ligand and charge transfer transitions are listed in Table 7.2. The intraligand transitions have undergone a bathochromic shift due to the donation of a lone pair of electrons to the metal indicating the coordination of azomethine nitrogen. It can also be due to the >C=S bond being weakened and the conjugation system getting enhanced on complexation[12,13]. In addition to these transitions a new charge transfer band is also observed about 24000 cm^{-1}. The moderately intense broad bands can be assigned Zn(II)→S metal to ligand charge transfer transition (MLCT). The electronic spectra of the complexes are presented in Fig. 7.6.

Table 7.2 Electronic spectral data of Zn(II) complexes.

Compound	UV-vis absorption bands (cm^{-1})
H_2bts	32130, 30540
$[Zn_2(bts)_2]$ (**14**)	39150, 32340, 25750
H_2bmts	37640, 32250, 29810, 24390
[Zn(bmts)]· H_2O (**15**)	29220, 24990
H_2bpts	43820, 33680, 31000, 24450
$[Zn_2(bpts)_2]$ (**16**)	29460, 24750
[Zn(bpts)] (**17**)	36500, 32330, 28740, 23620
Hmts	43680, 37840, 29500, 24750
$[Zn(Hmts)_2]\cdot H_2O$ (**18**)	33070, 26760

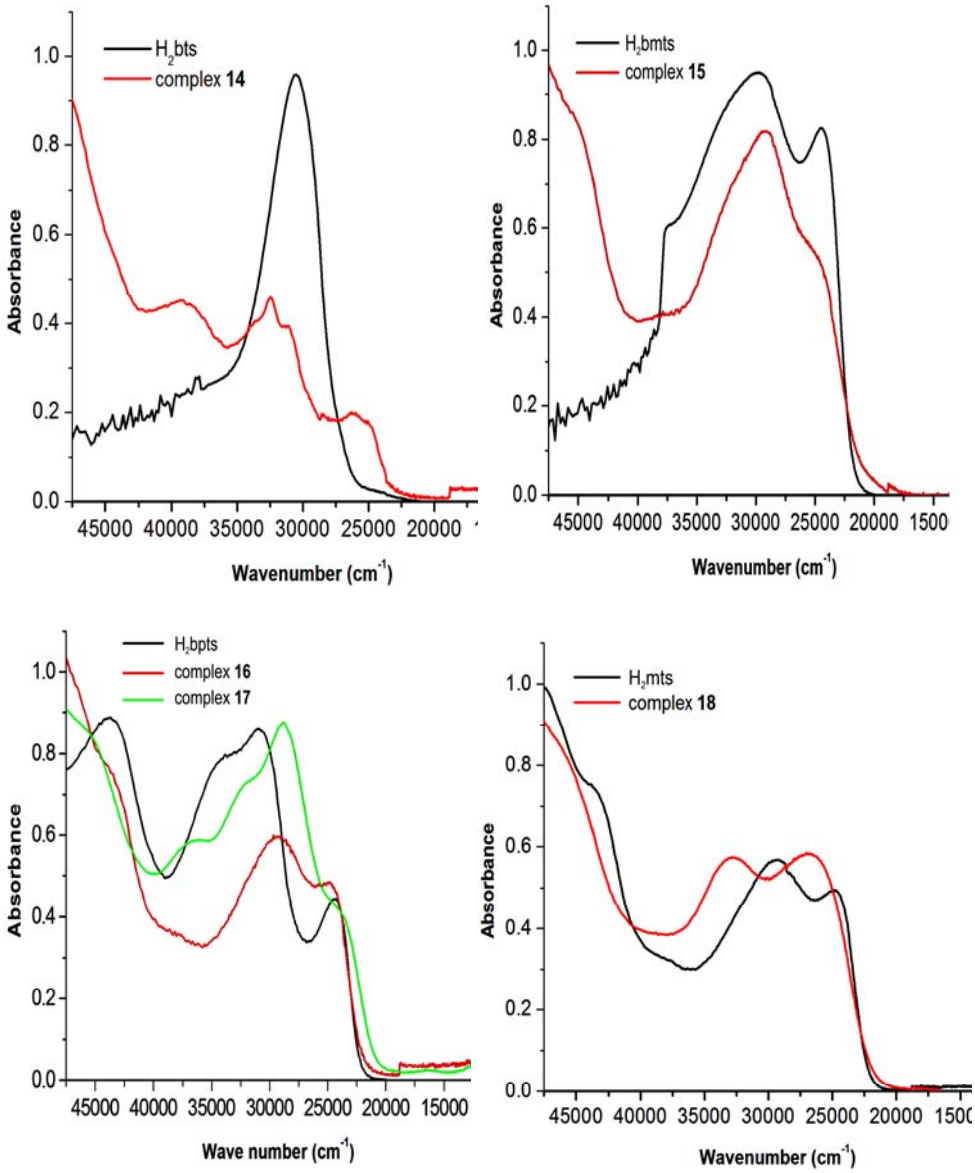

Fig. 7.6 Electronic spectra of Zn(II) complexes along with ligands.

7.3.3 ^{1}H NMR spectral studies

Proton Magnetic Resonance Spectroscopy is a powerful tool for the spectral studies of diamagnetic complexes like that of zinc. ^{1}H NMR assignments of the ligands and the Zn(II) complexes are presented in Table 7.3. Assignment of terminal NH and internal NH for complexes of H_2bts are given

in separate columns as NH^{term} and NH^{int}. The ^1H NMR spectra of some of the complexes along with the proton numbering scheme adopted for identifying corresponding protons are given in Figs 7.7-7.9. The singlet which integrate as a single hydrogen present in the spectra of the ligands around 8 and 15 ppm disappear in the spectra of the complexes because of deprotonation on complex formation. This provides an evidence for the coordination of thiolato sulfur of both arms.

Table 7.3 ^1H NMR assignments of Zn(II) complexes with ligands.

Compound	Aliphatic protons	Aromatic protons	NH^{term}	NH^{int}
H_2bts	2.43	7.78-8.42	10.32	8.15
$Zn_2(bts)_2$ (**14**)	2.43	7.55-8.59	10.57	--
H_2bmts	2.66	7.62-7.96		
[Zn(bmts)] (**15**)	2.4	7.66-7.97		--
H_2bpts	2.55	7.45-7.96		8.68, 15.2
[Zn(bpts)] (**17**)	2.33	7.52-7.88		--
H_2mts	2.65, 2.93	7.68-8.06		15.2
[Zn(Hmts)$_2$] (**18**)	2.2, 2.4	7.02-8.06		--

In compound **14**, N2 and N6 protons which appeared at 10.32 ppm in the ligand disappeared indicating enolisation followed by deprotonation. The protons at terminal nitrogens N1 and N7 are more shielded and a signal at 6.68 ppm indicate free rotation around C–NH_2 bond. This behaviour is consistent with a decrease in the C–N bond order in the complex when the thiol form is adopted [14]. The aliphatic protons are found to be shielded when compared with that of the ligand. Of the pyridine protons C5/7 protons are found to be shielded whereas C6 proton is deshielded. This is in accordance with the trend observed for pyridine protons under nitrogen protonation and this behavior are similar to that reported earlier [15].

In compound **15** (Fig.7.7), N2/6 proton signals disappear confirming the coordination of thiolato group after deprotonation. The multiplet found for the pyridine protons are very much differentiated to a doublet and triplet for C9/11 and C10 protons respectively. The shielding of aliphatic protons may be due to the coordination of azomethine nitrogens. The peaks for the morpholine ring protons are more shielded, the multiplet nature changed to doublets and closer each other (3.57 and 3.67 ppm when compared with 3.76 to 4.18 ppm). This indicates on complexation the two arms of the ligands are almost magnetically equivalent [16].

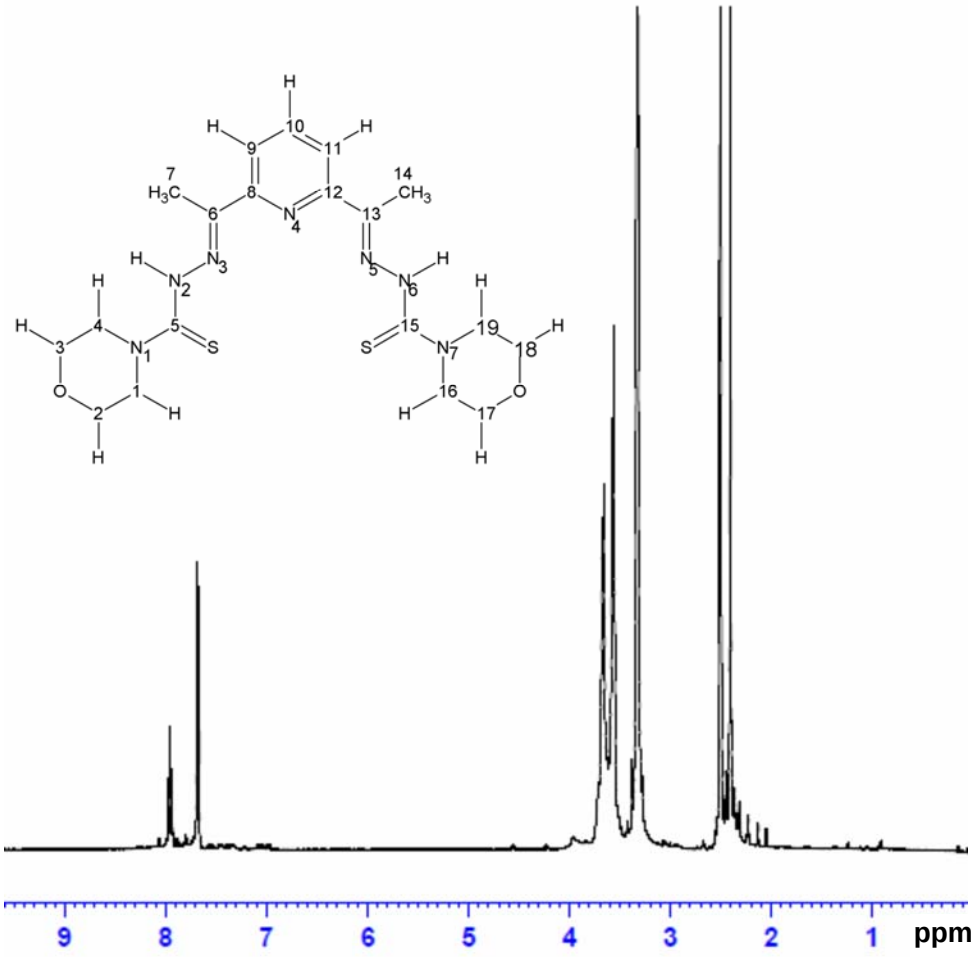

Fig 7.7 ^{1}H NMR spectrum of [Zn(bmts)] (**15**) along with numbering of H_2bmts.

In compound **17** (Fig. 7.8) the singlet which integrates as single hydrogen present in the spectrum of the ligand around 8.68 and 15.2 ppm disappear in the spectrum of the complex because of its loss on complex formation. This provides an evidence for the coordination of thiolato sulfur after enolization followed by deprotonation. The pyrrolidine ring protons found at 3.95 and 1.98 ppm in H_2bpts are deshielded to 2.7 and 1.8 ppm indicating the weakening of the pyrrolidine ring on coordination of the thioamide group. Similar to compound **15** the aromatic protons region contains a doublet and triplet only. The pyridine ring protons are found to be shielded for C9/11 protons and deshielded for the C10 and this confirms the coordination of pyridine nitrogen.

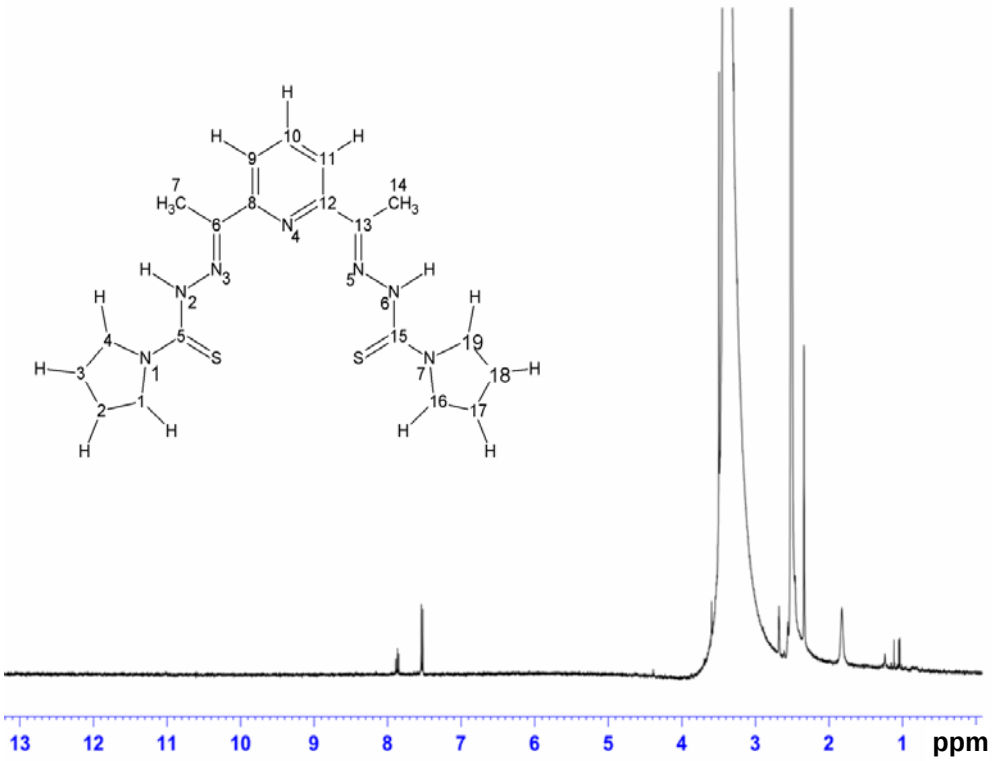

Fig. 7.8 NMR spectrum of [Zn(bpts)] (**17**) along with numbering of H_2bpts.

In compound **18** (Fig. 7.9) the signal obtained at 15.2 ppm disappeared as a consequence of the deprotonation of the ligand. Pyridyl ring protons are found as a broader multiplet. The broadening of protons signal makes the assignment difficult. The singlet due to protons on C14 which is close to the keto group is shielded which shows the involvement of the keto group in the coordination sphere. This is supported by the IR spectrum also. The formation of multiplets and broadening may be due to the presence of two ligand units coordinated to the same zinc center.

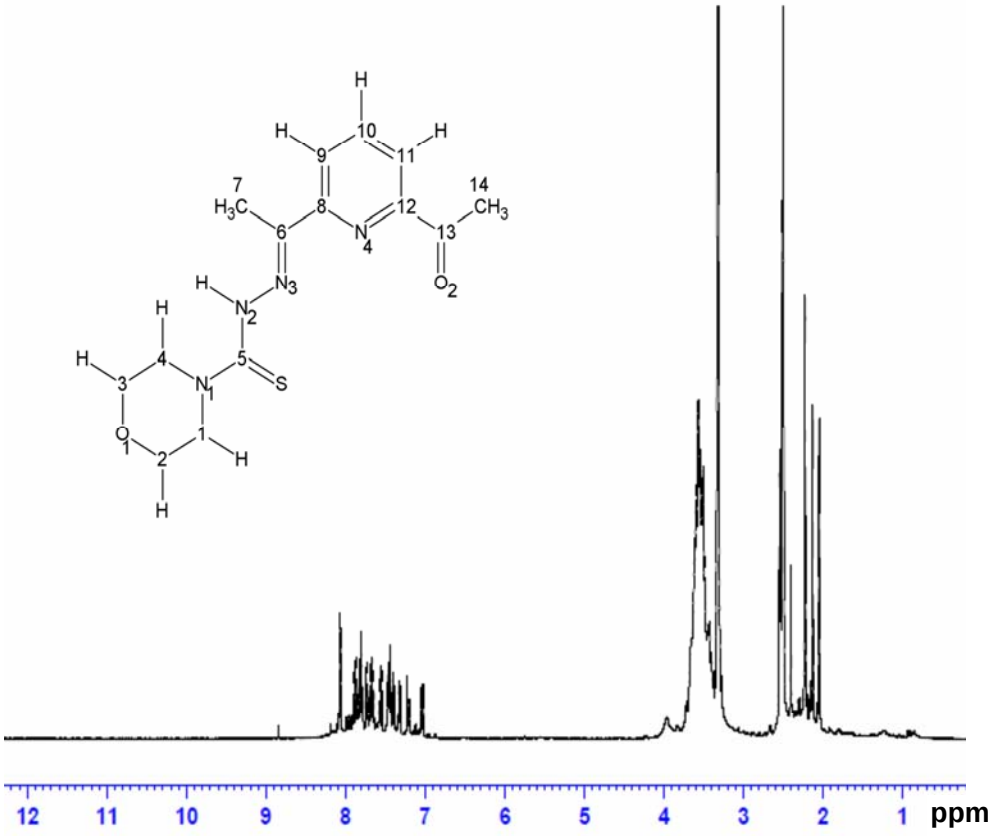

Fig 7.9 NMR spectrum of $[Zn(Hmts)_2]$ (**18**) along with the numbering of H_2mts.

7.3.4 Single crystal XRD study

X ray quality single crystals of the complexes **14** and **16** were obtained from its medium of synthesis. The crystallographic data and structure refinement parameters for the compounds **14** and **16** are given in Table 7.4.

Pale yellow thin plate like crystal of the compound **14** having approximate dimensions of 0.34 x 0.26 x 0.22 mm^3 was selected. The unit cell parameters were determined and the data collections were performed on a CrysAlis CCD diffractometer with graphite-monochromated Mo Kα (λ = 0.71073 Å) radiation at the National Single Crystal X-ray Facility, IIT Bombay, Mumbai, India. The program CrysAlis RED was used for data reduction and cell refinement. The structure was solved by direct methods using SHELX-97 [17] which revealed the position of all non-hydrogen atoms and refined to convergence by full-matrix least-squares refinement on F^2 using SHELXL-97 [18]. The hydrogen atoms were geometrically fixed at calculated positions. The graphic tools used were DIAMOND [19] and MERCURY [20].

Yellow plate like crystal of the compound **16** having approximate dimensions of 0.32 x 0.11 x 0.04 mm^3 was selected. X-ray diffraction measurements were carried out on a Bruker Smart Apex CCD diffractometer equipped with fine focused sealed tube at the Analytical Sciences Division, Central Salt & Marine Chemicals Research Institute, Gujarat. All non-hydrogen atoms except C3 in the asymmetric unit were refined anisotropically and all hydrogen atoms were geometrically fixed at calculated positions. Refinement of the C3 atom led to non-positive definite thermal parameters. Since it exhibited unsatisfactory anisotropic temperature factors, even with the use of (ISOR) restraints, it was refined isotropically. The crystal data, experimental and refinement parameters are presented in Table 7.4.

Table 7.4 Crystal data and experimental parameters of compound **14** and compound **16.**

	14	**16**
Empirical formula	$C_{26}H_{37}N_{15}O_2S_4Zn_2$	$C_{38}H_{50}N_{14}S_4Zn_2$
Formula weight (M)	850.69	961.97
Temperature (T) K	150(2) °	293(2)
Wavelength (Mo Kα) (Å)	0.71073	0.71073
Crystal system	Monoclinic	Monoclinic
Space group	$P2_1/c$	$C2/c$
Unit cell dimensions		
a (Å)	13.7475(5)	18.975(12)
b (Å)	14.4933(5)	18.328(15)
c (Å)	18.7720(6)	14.612(12)
α (°)	90.00	90.00
β (°)	107.821(4)	124.11(4)
γ (°)	90.00	90.00
Volume V (Å)	3560.8(2)	4207(6)
Z	4	4
Calculated density (ρ) (Mg m^{-3})	1.587	1.459
Absorption coefficient, μ (mm^{-1})	1.632	1.378
F(000)	1752	1830
Crystal size (mm^3)	0.34 x 0.26 x 0.22	0.32 x 0.11 x 0.04
θ range for data collection	3.03 – 25.00	1.71 – 25.00
Index ranges	$-16 \le h \le 16$, $-17 \le k \le 16$, $-22 \le l \le 22$	$-19 \le h \le 22$, $-21 \le k \le 21$ $-17 \le l \le 8$
Reflections collected	32715	10430
Refinement method	Full matrix on F_0^2	Full matrix on F_0^2
Data/ restraints /parameters	6253/0/485	3687/0/259
Goodness-of-fit on F^2	1.051	1.185
Final *R* indices		
[I >2σ(1)]	R_1= 0.0507 wR_2 = 0.0935	R_1= 0.0903 wR_2 = 0.1955
R indices (all data)	R_1 =0.0821 wR_2 = 0.1077	R_1=0.1215, wR_2 = 0.2172

$R_1 = \Sigma||F_o| - |F_c|| / \Sigma|F_o|$ $wR_2 = [\Sigma w(|F_o|^2 - |F_c|^2)^2 / \Sigma w(F_o^2)^2]^{½}$

7.3.5 Crystal structure of $[Zn_2(bts)_2]\cdot DMF\cdot CH_3OH$ (14)

The molecular structure of the compound **14** along with the atom numbering scheme is given in Fig. 7.10. The crystallographic information data are given in Table 7.4. whereas the selected bond lengths and bond angles are summarized in Table 7.5.

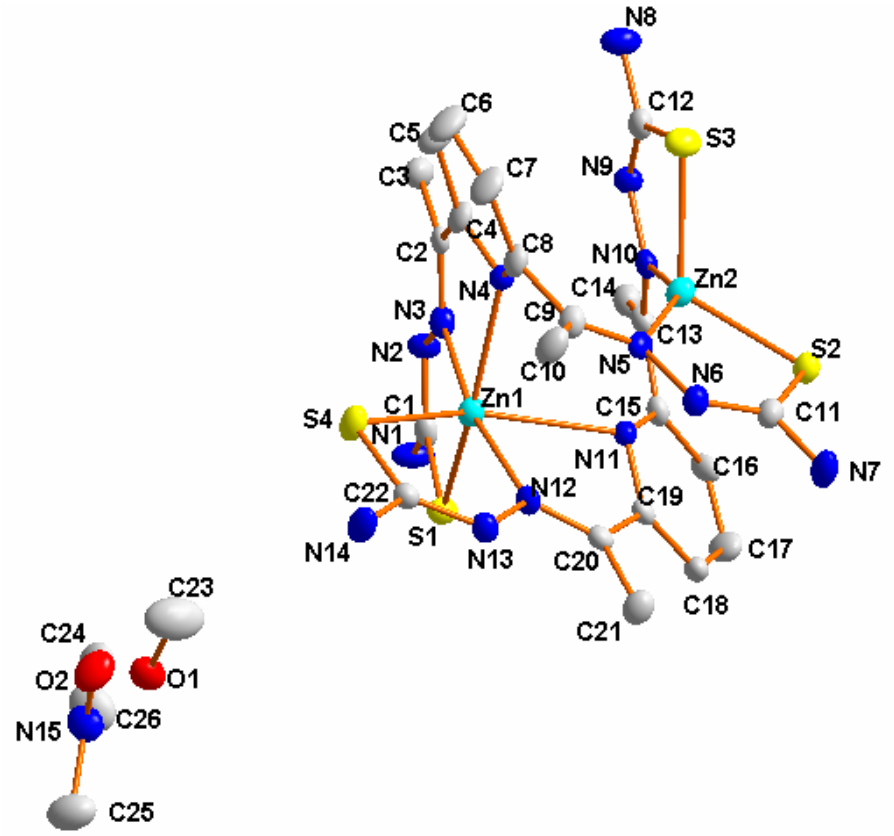

Fig. 7.10 Molecular structure of $[Zn_2(bts)_2]\cdot DMF\cdot CH_3OH$ (**14**) Hydrogen atoms are omitted for clarity.

The molecule crystallizes with a DMF and methanol from the solvent medium. The unit cell of the crystal is monoclinic with space group symmetry $P2_1/c$. The asymmetric unit is binuclear with two zinc centers. Zn1, one of the zinc atoms is coordinated to four nitrogen and two sulfur in a distorted octahedral and the other, Zn2 is coordinated to two nitrogens and two sulfur in

a distorted tetrahedral geometry. From Table 7.5 it can be seen that most of the angles deviate considerably from the ideal 90, 180 and 109.28° considerably.

Table 7.5 Selected bond lengths (Å) and bond angles (°) of $[Zn_2(bts)_2]$ (**14**)

Bond lengths (Å)		**Bond angles (°)**	
Zn1–N12	2.075(3)	N12–Zn1–N3	166.85(14)
Zn1–N3	2.088(3)	S4–Zn1–N11	154.48(8)
Zn1–N4	2.327(4)	N4–Zn1–S4	88.49(9)
Zn1–S4	2.387(12)	S4–Zn1–S1	106.43(5)
Zn1–S1	2.4137(13)	S1–Zn1–N11	83.12(9)
Zn1–N11	2.526(3)	N4–Zn1–N11	92.08(12)
S1–C5	1.735(4)	C1–S1–Zn1	94.55(17)
S2–C13	1.746(4)	C11–S2–Zn2	93.70(15)
Zn2–N10	2.063(3)	N10–Zn2–S3	84.05(11)
Zn2–N5	2.078(3)	N10–Zn2–N5	145.56(14)
Zn2–S2	2.3137(12)	N10–Zn2–S2	118.08(10)
Zn2–S3	2.3384(14)	N5–Zn2–S2	85.29(10)
		N5–Zn2–S3	107.87(11)
		S2–Zn2–S3	118.30(5)

Of the six pentachelating systems formed altogether, four rings are at the octahedral center and two at the tetrahedral center. At the octahedral center two ring systems lie along the equatorial plane whereas the other two lie along the axial plane. At the tetrahedral center the two ring systems lie almost tetrahedral to each other.

On going through Table 7.5 it can be seen that the four nitrogens coordinated to octahedral Zn1 are two pyridine nitrogens (N_{py}) and two azomethine nitrogens (N_{azo}). Two Zn–N_{py} bonds {Zn1–N4, 2.327(4) Å; Zn1–N11, 2.526(3) Å} are found to be considerably longer than the two Zn– N_{azo} bonds {Zn1–N12, 2.075(3) Å; Zn1–N3 2.088(3) Å}. The very long

Zn2–N_{py} separations {2.815(6) and 2.663(7) Å} and the relative positions of the pyridine rings in space rule out the possibility for a bridging to Zn2. The Zn1 Zn2 separation is found to be 3.786 Å. The two N_{py} subtend an angle of 92.08(12) Å at Zn1.

A similar compound of **14** reported by Binu and Cohen crystallized with methanol and water molecules into a triclinic space group *P*1. Though instead of zinc acetate, zinc chloride was used the coordination geometry was the same. The coordinating bonds are found to be slightly shorter for the present compound along with slight variation in bond angles. This shows that irrespective of the methods used, formation of {6+4} zinc complex produced a possible generalization about the synthesis and structure of the zinc complexes of H_2bts [8]. Later Pedrido [7] and Labisbel [9] also synthesized similar compounds.

The C1–S1 and C11–S2 bond distances (1.735(4) and 1.746(4) Å) showed that both ligands in the dimer are coordinated in their deprotonated thiolate forms. While coordinating in the deprotonated iminothiolate form, an intermediate bond distance {N2–C1 1.327(6) Å, N6–C11 1.325(6) Å}; {N2–N3 1.373(5) Å, N5–N6 1.387(5) Å}; {N3–C2 1.303(6) Å, N5–C9 1.292(6) Å} is found for both arms of the ligand. This is due to the negative charge generated upon loss of the proton from the thiol sulfur atom, being delocalized in the –C=N–N=C– skeleton. Similar observations have been made for 2,6-diacetylpyridine bis(thiosemicrabazone) systems of zinc [21,8].

Though classical hydrogen bonds are not found in the lattice N1H is having weak interactions with methanol oxygen and N13 of neighboring molecule. The interactions with distances are shown in Fig. 7.11. Weak ring interactions and CH···π interactions are also found to be involved in maintaining the molecular architecture. The interaction parameters are presented in Table 7.6.

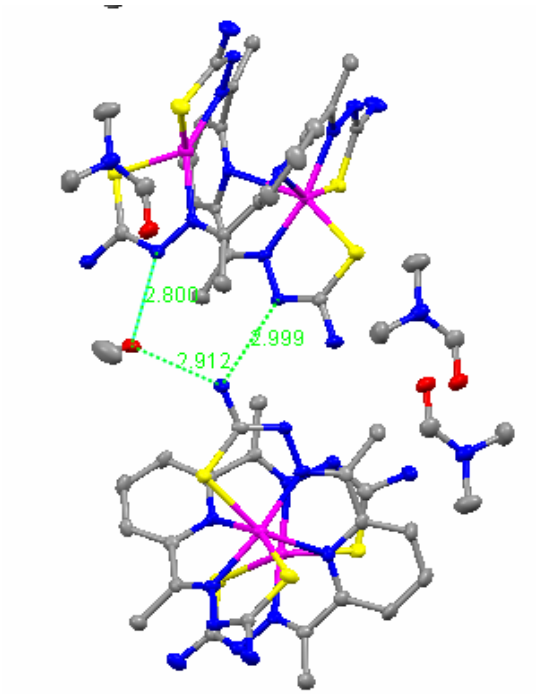

Fig. 7.11 Packing diagram of $[Zn_2(bts)_2]\cdot DMF\cdot CH_3OH$ (**14**) hydrogen bonding interactions.

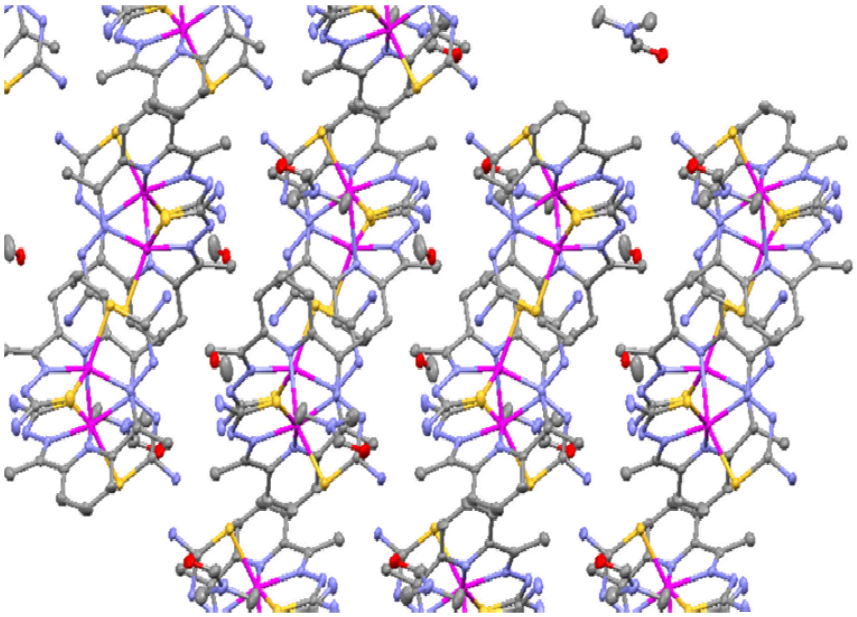

Fig. 7.12 Packing diagram of $[Zn_2(bts)_2]\cdot DMF\cdot CH_3OH$ (**14**) along b axis.

Table 7.6 Interaction parameters of compound (**14**).

H-bonding interactions				
D–H···A	**D–H (Å)**	**H···A (Å)**	**D···A (Å)**	**D–H···A (°)**
N1–H···O222[a]	0.80	2.15	2.912	157
N1–H···.N13[b]	0.95	2.07	2.998	166
N7–H···S1[c]	0.83	2.57	3.3674	162
O222– H11···N6 [d]	0.96	2.12	2.7998	164

π–π interactions			
Cg(I)···Cg(J)	**Cg–Cg (Å)**	**α°**	**β°**
Cg(1)···Cg(6)[e]	4.7729(22)	4.70	50.51
Cg(1)···Cg(8) [e]	3.9032(24)	44.81	28.76
Cg(2)···Cg(5)[e]	4.5327(21)	2.54	48.84
Cg(2)···Cg(7)[e]	4.2292(25)	58.03	38.45
Cg(5)···Cg(8)[e]	3.8737(23)	34.89	28.23
Cg(5)···Cg(8)[f]	4.6577(24)	28.72	29.59
Cg(6)···Cg(7)[e]	3.4772(24)	21.07	18.46

X–H···Cg (π-ring) Interactions			
X–H(I)···Cg(J)	**H···Cg (Å)**	**X–H···Cg (°)**	**X···Cg (Å)**
C(6)–H(6)···Cg(1)	2.64	173	3.566

D, donor; A, acceptor; Cg, centroid; α, dihedral angles between planes I and J;
β, angle between Cg(I)–Cg(J) vector and normal to plane I.
Cg1 = Zn1,S1,C1,N2,N3; Cg2 = Zn1,S4,C22,N13,N12;
Cg5 = Zn2,S2,C11,N6,N5; Cg6= Zn2,S3,C12,N9,N10;
Cg7 = N4, C4, C5, C6, C7, C8; Cg8 = N11, C15, C16, C17, C18, C19;
Equivalent position codes:
a = 1-x, - ½+y, ½-z; b = x, ½- y, -½+z;
c =1- x, ½+ y, ½-z; d = 1-x, 1-y, 1-z
e = x, y, z; f = 1-x, -1/2+y, 3/2-z

7.3.6 Crystal structure of $[Zn_2(bpts)_2]$ (16)

The molecular structure of the compound **16** along with the atom numbering scheme is given in Fig. 7.13. The crystallographic information data are given in Table 7.4 and the selected bond lengths and bond angles are summarized in Table 7.7. The unit cell of the crystal is monoclinic space group *C*2/c. With four molecules in the unit cell there is only half of

$[Zn_2(bpts)_2]$ in the asymmetric unit with the other half related by a crystallographic inversion center. The molecule is binuclear in which each of the two zinc center adopt a five coordinating geometry with an N_3S_2 donor environment. The thiolato S and the N_{azo} of one limb and N_{py} of one ligand coordinate to a Zn(II) ion whereas the coordination sphere is completed by the thiolate S and azomethine N of the other limb from the second ligand with the coordinating distances as given. {Zn1–S1, 2.3449; Zn1–S2a, 2.4058; Zn1–N3, 2.0822; Zn1–N4a, 2.0806; Zn1–N7a, 2.4645 Å}. It shows the symmetrical intertwining of the two ligand strands at an angle of 62.321(23)° perpendicular to the helical axis (Zn···Zn distance = 3.8362(21) Å). Both pyridine rings lie at an angle of 33.969(27) Å to each other. A >C–S bond length of 1.73 and 1.719 Å show that both ligands in the dimer are coordinated in their deprotonated thiolate forms.

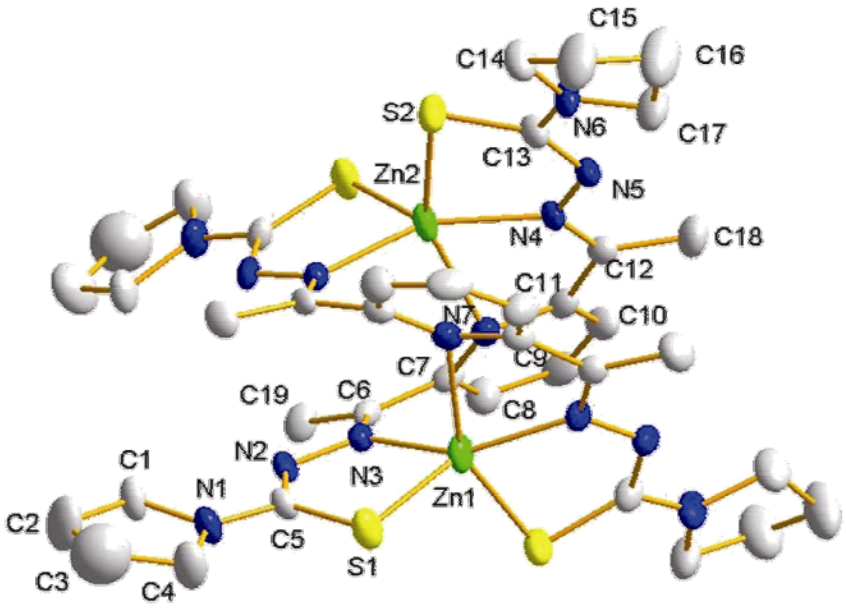

Fig. 7.13 The molecular structure of $[Zn_2(bpts)_2]$ (**16**). Hydrogen atoms are omitted for clarity.

The negative charge generated upon the loss of the proton from the thiol sulfur atom is delocalized in the –C=N–N=C– system as shown by the

intermediate bond distances {C5–N2 1.337, C14–N5 1.327 Å}; {N2–N3 1.373, N4–N5 1.391 Å}; {C6–N3 1.289, C12–N4 1.285 Å} for both arms of the ligand similar to compound **14**.

Table 7.7 Selected bond lengths (Å) and bond angles (°) of $[Zn_2(bpts)_2]$ (**16**).

Bond lengths (Å)		Bond angles (°)	
Zn(1)–N(4)a	2.083(6)	N(3)–Zn(1) –S(1)	84.67(18)
Zn(1)–N(3)	2.083(6)	N(3)–Zn(1)–S(2)a	97.84(18)
Zn(1)–S(1)	2.345(3)	S(2)a–Zn(1)–N(4)a	81.97(18)
Zn(1)–S(2)a	2.406(3)	N(4)a–Zn(1) –N(7)a	71.5(2)
Zn(1)–N(7)a	2.465(7)	N(3) –Zn(1) –N(7)a	102.5(2)
S(1)–C(5)	1.732(7)	N(4)a–Zn(1) –N(3)	147.7(2)
S(2)–C(13)	1.718(8)	S(2)a–Zn(1)–N(7)a	153.25(16)

The stereochemistry adopted by each zinc(II) ion in the $Zn_2(SNNNS)_2$ dimer is intermediate between a square pyramidal and trigonal bipyramidal geometry. Thus taking S2 and N10 as axial donor atoms S2–Zn1–N10 is subtending an angle of 153.24(15)° at the zinc center which is much smaller than the theoretical value of 180°. The angles between the three equatorial donors range from 84.74 to 147.61° showing a marked difference from the ideal value of 120°.

The trigonality index, τ is calculated using Addison's formula [22]

$\tau = [(\beta - \alpha) / 60] \times 100$

where α and β are the largest and second largest angles subtended at each Zn(II) center. The value of τ is found to be 10% which supports the fact that the stereochemistry adopted by each zinc ion is best described as distorted square pyramid (SPY). This is evident by considering the plane containing S2a, N4a, N7a and N3 with bond angles {S2a–Zn1–N4a, 81.97(18)°; N4a–Zn1–N7a, 71.5(2)° ;

N7a–Zn1–N3, 102.5(2)°; N3–Zn1–S2a 97.84(18)°} deviating from 90°. Zn1 is slightly displaced from the plane towards the pyramidal S1 at a distance of 0.325 Å which is evident from the bond angles {N3–Zn1–N4, 147.7(2)° and S2–Zn1–N7, 153.25(16)°}. The deviation from an ideal value may be attributed to the restricted bite angle of the ligand.

The dihedral angles between the chelating rings Cg1 {Zn1–S1–C5–N2–N3} and Cg2 {Zn1–S2a–C13a–N5a–N4a} with Cg3 {Zn1–N4a–C12a–C11a–N7a} are found to be considerably large. At each pentadentate Zn(II) center Cg1 and Cg2 formed from different arms of the two ligand moieties are at an angle of 9.50° to each other. The third ring Cg3 formed by fusing with Cg2 is at an angle of ≈ 78.89° with the other two. Due to the long armed ligand stretching on both sides a double helicate structure of the zinc complex is formed as given in Fig. 7.14.

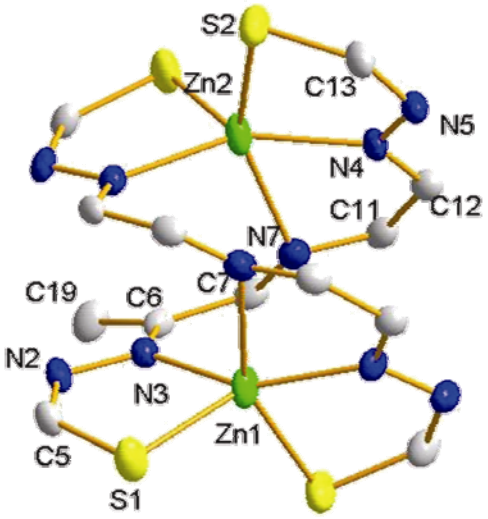

Fig. 7.14 Double helicate structure of $[Zn_2(bpts)_2]$ (**16**) with coordination sphere.

Large voids (Fig. 7.15) created by the helical structure can be seen on viewing through *b* axis. This deviation from coplanarity does not make any hindrance to the delocalization of electrons, and the stability of the complex is sustained. Ring puckering analysis shows that the five membered chelating ring

Cg1 is puckered and adopt an envelope conformation with S1 forming the flap of the envelope {Q = 0.104(6) Å., φ= 30(4) °} [23]. The remaining chelating rings are also puckered, some adopting a twisted and others envelope conformations.

The unit cell viewed along the *b* axis (Fig. 7.15) and *c* axis (Fig. 7.16) with four molecules arranged in unit cell volume produces attractive molecular architectures. Neither hydrogen bonding nor solvent interactions are found in the packing of molecules. Weak Cg···Cg interactions found in between Cg1···Cg1, Cg1···Cg8 and Cg8···Cg8 are reported in Table 7.8, which reinforce crystal structure cohesion in the packing. An intramolecular CH···π interaction between C19H19 and the pyrrolidine ring also contributes to packing.

Zn(II) complexes of 2,6-diacetylpyridine bis(N^4-dimethylthiosemicarbazone) [10] and S-benzyldithiocarbazate derivative of 2,6-diacetylpyridine bis (thiosemicarbazone) [21] are reported to have a {5+5} coordination geometry. On comparing the Zn···Zn distance lowest (3.692 Å) is for the dimethyl derivative. The dimethyl derivative showed a helical structure similar to compound **16** whereas the dithiocarbazate derivative formed has a cage like structure.

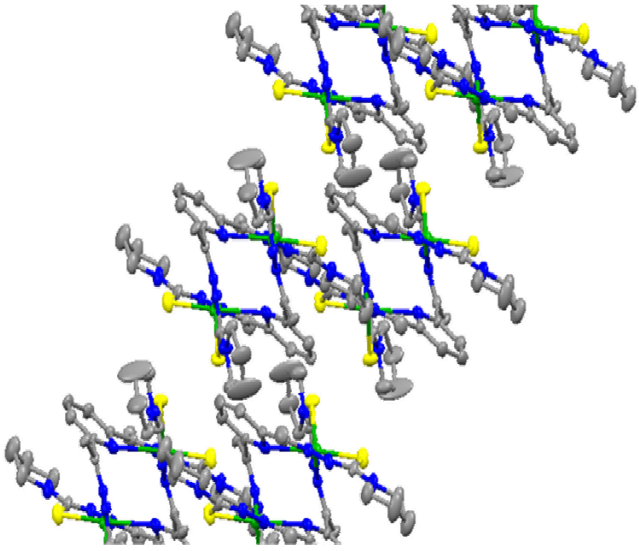

Fig. 7.15 Packing structure of $[Zn_2(bpts)_2]$ (**16**) along *b* axis.

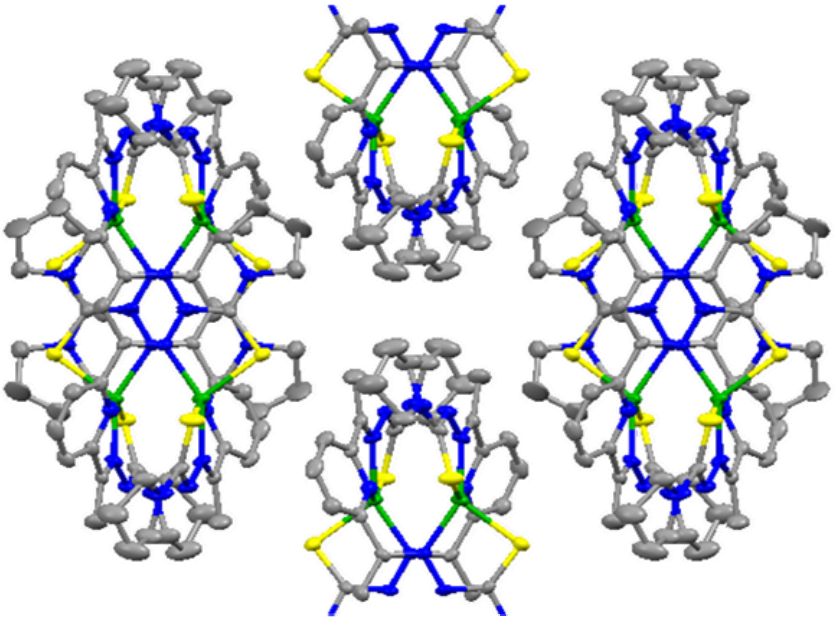

Fig. 7.16 Packing structure of $[Zn_2(bpts)_2]$ (**16**) along *c* axis.

Table 7.8 Interaction parameters for $[Zn_2(bts)_2]$ (**14**)

Cg(I)–Cg(J) interactions			
Cg(I)···Cg(J)	**Cg–Cg (Å)**	**α (°)**	**β (°)**
Cg(1)···Cg(1)[a]	4.067(6)	5	43.23
Cg(1)···Cg(8)[a]	4.337(5)	52.1(4)	37.05
Cg(8)···Cg(8) [b]	4.404(7)	0	42.38

X-H...Cg (π-ring) Interactions			
X–H(I)···CgJ	**H···Cg (Å)**	**X–H···Cg (°)**	**X···Cg (Å)**
C19–H19···Cg5[a]	2.850	166	3.788(11)

D, donor; A, acceptor; Cg, centroid; α, dihedral angles between planes I and J;
β, angle between Cg(I)–Cg(J) vector and normal to plane I.

Cg1 = Zn1, S1, C5, N2, N3; Cg5 = N1, C1, C2, C3, C4;

Cg8 = N7, C7, C8, C9, C10, C11.

Equivalent position codes: a = 1-x,y,1/2-z; b = 3/2-x,1/2-y,1-z.

7.4 Conclusion

Five Zn(II) complexes were synthesized and characterized by spectroscopic techniques and single crystal XRD. Elemental analyses showed the dianionic nature of bis(thiosemicarbazones) and monoanionic nature of H_2mts in $Zn(Hmts)_2$. IR and NMR spectral studies showed that ligands are more stabilized on complexation. Single crystal studies of compounds **14** and **16** and showed that they exist in {6+4} and {5+5} geometry. The centrosymmetric $[Zn_2(bpts)_2]$ showed a double helicate structure. Compound **14** is stabilized by H-bonding and ring-ring interactions including solvent molecules whereas compound **16** is stabilized by weak ring interactions alone. They exhibit beautiful molecular architectures. There is possibility for compounds **15** and **17** in dimeric form, but cannot be confirmed since attempts to separate single crystals fail. An octahedral coordination is proposed for compound **18**.

References

[1] P. Jiang, Z. Guo, Coord. Chem. Rev. 248 (2004) 205.

[2] P.S. Donnelly, A. Caragounis, T. Du, K.M. Laughton, I. Volitakis, R.A. Cherny, R.A. Sharples, A.F. Hill, Q.-X. Li, C.L. Masters, K.J. Barnham, A.R. White, J. Biol. Chem. 283 (2008) 4568.

[3] E.P. Huang, Proc. Natl. Acad. Sci. U.S.A. 94 (1997) 13386.

[4] B.J. Niles, M.S. Clegg, L.A. Hanna, S.S. Chou, T.Y. Momma, H. Hong, C.L. Keen, J. Biol. Chem. 283 (2008) 5168.

[5] M.R. Bermejo, A.M. González-Noya, R.M. Pedrido, M.J. Romero, M. Vázquez, Angew. Chem. Int. Ed. 44 (2005) 4182.

[6] A.I. Matesanz, I. Cuadrado, C. Pastor, P. Souza, Z. Anorg. Allg. Chem. 631(2005) 780.

[7] R. Pedrido, M.R. Bermejo, M.J. Romero, M. Vázquez, A.M. González-Noya, M. Maneiro, M.J. Rodríguez, M.I. Fernández, Dalton Trans. (2005) 572.

[8] A. Bino, N. Cohen, Inorg. Chim. Acta 210 (1993) 11.

[9] E. Labisbel, A. Castineiras, C.A. Brown, D.X. West, Z. Naturforsch. 56 (2001) 229.

[10] R. Pedrido, M.R. Bermejo, M.J. Romero, A.M. González-Noya, M. Maneiro, M.I. Fernández, Inorg. Chem. Commun. 8 (2005) 1036.

[11] K. Nakamoto, Infrared and Raman spectra of Inorganic and Coordination compounds, 5th ed., Wiley, New York, 1997.

[12] V. Philip, V. Suni, M. Nethaji, M.R.P. Kurup, Polyhedron 25 (2006) 1931.

[13] I.-X. Li, H.-.Tang, Yi-Zhi Li, M. Wang, L.-F. Wang, C.-G. Xia, J. Inorg. Biochem 78 (2000) 167.

[14] M.C. Rodrìguez-Arguelles, M.B. Ferrari, F. Bisceglie, C. Pelizzi, G. Pelosi, S. Pinelli, M. Sassi, J. Inorg. Biochem. 98 (2004) 313.

[15] J.S. Casas, A. Castifieiras, A. Sanchez, J. Sordo, A. VazquezLopez, M.C. Ro driguez-Argiielles, U. Russo, Inorg. Chim. Acta 221 (1994) 61.

[16] N.C. Kasuga, K. Sekino, M. Ishikawa, A. Honda, M. Yokoyama, S. Nakano, N. Shimada, C. Koumo, K. Nomiya, J. Inorg. Biochem. 96 (2003) 298.

[17] G.M. Sheldrick, Acta Cryst. A46 *(*1990*)* 467.

[18] G.M. Sheldrick, SHELXL97, SHELXS97, University of Göttingen, Germany, 1997.

[19] K. Brandenburg, DIAMOND Version 3.1f, Crystal Impact GbR, Bonn, Germany, 2008.

[20] C.F. Macrae, P.R. Edington, P. McCabe, E. Pidcock, G.P. Shields, R. Taylor, M. Towler, J. van de Streek, J. Appl. Cryst. 39 (2006) 453.

[21] M.A. Ali, A.H. Mirza, C.W. Voo, A.L. Tan, P.V. Bernhardt, Polyhedron 22 (2003) 3433.

[22] A.W. Addison, T. Rao, J. Reedjik, J.V. Rijn, G. Verschoor, J. Chem. Soc., Dalton Trans. (1984) 1349.

[23] D. Cremer, J.A. Pople, J. Amer. Chem. Soc. 97 (1975) 1354.

…..ꕥ…..

Chapter 8

Synthesis and Characterization of Cd(II) Complexes

Contents

8.1 Introduction

Cadmium, a d^{10} element belonging to the second row transition series holds its name from the latin word *cadmia*, the ancient name for calamine. The element, being a byproduct of zinc mining, fossil fuel, combustion and atmospheric transport is a toxic metal and a potent carcinogen [1-3]. It is increasingly important as an environmental hazard to both humans and wildlife. It exemplifies the double edged nature of many toxic substances. On one hand it acts as a mitogen, inhibit apoptosis it causes tissue damage in the kidney causing cell death. On the other hand, stimulates cell proliferation and promote cancer in a number of tissues [4].

Though thought as toxic to organisms it behaves exactly like a nutrient in the sea. It is depleted to very low concentrations as a result of biological uptake at the surface and remineralized at depth. It is an important micronutrient for marine phytoplankton. Certain diatoms possess a Cd-carbonic anhydrase enzyme, which is involved in the acquisition of inorganic carbon for photosynthesis [5].

The chemical similarity of zinc(II) and cadmium(II) suggests that the latter may displace the former from a critical site in zinc(II) enzymes [6]. Cadmium is a

catalytic inhibitor of DNA Topoisomerase II, a nuclear enzyme [7]. The mobilization and immobilization of cadmium in the environment have been shown to depend on the complexation of chelating nitrogen donors [8]. Complexes of Cd(II) with different molecular architectures with the same trimesate ligands showing strong fluorescence have been reported [9].

Optical properties of thiosemicarbazone complexes have not been studied much. Quenching of fluorescence of a ligand by transition metal ions during complexation is usually observed. Enhancement of fluorescence through complexation attracts much interest since it opens up the opportunity for the photochemical applications of these complexes. The enhanced fluorescence can be due to simple binding of ligand to d^{10} metal ion or an increased rigidity in the structure of the complexes [10,11].

8.2 Experimental

8.2.1 Materials

The details regarding the synthesis of the proligands are discussed in Chapter 2. Solvents being pure were used as supplied. Cadmium acetate dihydrate (E-merck) and bromide tetrahydrate (Aldrich) were used as supplied for the preparation of the complexes. Solvents used were methanol and dimethylformamide.

8.2.2 Synthesis of complexes

8.2.2.1 *Synthesis of [Cd(bts)]* ***(19)***

Cadmium acetate was the salt employed for preparing the complex. H_2bts (0.155 g, 0.5 mmol) was dissolved in 2 ml of DMF and diluted with 15 ml methanol. This was slowly added to a hot solution of $Cd(OAc)_2{\cdot}2H_2O$ (0.133 g, 0.5 mmol) in 15 ml methanol. The mixture was refluxed for 3 hours and allowed to cool. The yellow complex formed was filtered, washed in methanol followed by ether and dried *in vacuo* over P_4O_{10}.

Yield, 75%; Elem. Anal. Found (calcd)% for $C_{11}H_{13}CdN_7S_2$: C, 31.39 (31.47); H, 3.26 (3.12); N, 23.19 (23.36).

8.2.2.2 *Synthesis of [Cd(H_2bmts)Br_2] (**20**)*

Cadmium bromide was used for preparing the complex. H_2bmts (0.225 g, 0.5 mmol) was dissolved in 2 ml of DMF and diluted with 15 ml methanol. This was slowly added to a hot solution of $CdBr_2 \cdot 4H_2O$ (0.136 g, 0.5 mmol) in 15 ml methanol. The mixture was refluxed for 3 hours and allowed to cool. The yellow complex formed was filtered, washed in methanol followed by ether and dried over P_4O_{10} *in vacuo*.

Yield, 70%; Elem. Anal. Found (calcd)% for $C_{19}H_{27}Br_2CdN_7O_2S_2$: C, 31.35 (31.62); H, 3.79 (3.77); N, 13.72 (13.58).

8.2.2.3 *Synthesis of [Cd(bmts)]·H_2O (**21**)*

H_2bmts (0.225 g, 0.5 mmol) was dissolved in 2 ml of DMF and diluted with 15 ml methanol. This was slowly added to a hot solution of $Cd(OAc)_2 \cdot 2H_2O$ (0.133 g, 0.5 mmol) in 15 ml methanol. The mixture was refluxed for 3 hours and allowed to cool. The yellow complex formed was filtered, washed in methanol followed by ether and dried over P_4O_{10} *in vacuo*.

Yield, 65%; Elem. Anal. Found (calcd)% for $C_{19}H_{27}CdN_7O_3S_2$: C, 38.99 (39.48); H, 4.42 (4.71); N, 11.72 (11.10).

8.2.2.4 *Synthesis of [Cd(H_2bpts) Br_2]·2.5 H_2O (**22**)*

H_2bpts (0.209 g, 0.5 mmol) was dissolved in 2 ml of DMF and diluted with 15 ml methanol. This was slowly added to a hot solution of $CdBr_2 \cdot 4H_2O$ (0.136 g, 0.5 mmol) in 15 ml methanol. The mixture was refluxed for 3 hours and allowed to cool. The yellow crystalline complex formed was filtered, washed in methanol followed by ether and dried over P_4O_{10} *in vacuo*.

Yield, 73%; Elem. Anal. Found (calcd)% for $C_{19}H_{32}Br_2Cd\ N_7O_{2.5}S_2$: C, 30.67 (31.05); H, 4.37 (4.39); N, 13.09 (13.34); S, 8.71 (8.73).

8.2.2.5 *Synthesis of [Cd(bpts)]* ***(23)***

H_2bpts (0.209 g, 0.5 mmol) was dissolved in 2 ml of DMF and diluted with 15 ml methanol. This was slowly added to a hot solution of $Cd(OAc)_2 \cdot 2H_2O$ (0.133 g, 0.5 mmol) in 15 ml methanol. The mixture was refluxed for 3 hours and allowed to cool. The yellow complex formed was filtered, washed in methanol followed by ether and dried over P_4O_{10} *in vacuo*.

Yield, 72%; Elem. Anal. Found (calcd)% for $C_{19}H_{25}CdN_7S_2$: C, 31.96 (31.51); H, 3.25 (3.97); N, 10.73 (10.50); S, 5.91 (6.01).

8.2.2.6 *Synthesis of [Cd(Hmts)Br]·2H_2O* ***(24)***

Cadmium bromide was used for preparing the complex. H_2mts (0.153 g, 0.5 mmol) was dissolved in 15 ml dichloromethane. This was slowly added to a hot solution of $CdBr_2 \cdot 4H_2O$ (0.136 g, 0.5 mmol) in 15 ml methanol. The mixture was refluxed for 3 hours and allowed to cool. The yellow complex formed was filtered, washed in methanol followed by ether and dried over P_4O_{10} *in vacuo*.

Yield, 75%; Elem. Anal. Found (calcd) % for $C_{14}H_{21}BrCdN_4O_4S$: C, 43.53 (43.22); H, 3.86 (4.77); N, 18.64 (18.57); S, 12.95 (12.15).

8.2.3 Physical measurements

Various physical measurements used are discussed in Chapter 1.

8.3 Results and discussion

Equimolar ratios of the ligands and the metal salts yielded the yellow colored metal complexes. The many related ligands have been found to form complexes containing both protonated and deprotonated forms of the ligands [12]. Ali et al. have reported that despite repeated attempts, isolation of single crystals of cadmium complexes suitable for X-ray diffraction studies was not fruitful. It has been reported that due to the low solubility in most polar and non

polar solvents a monomeric five coordinate geometry is unlikely for similar complexes. And because of the tendency of cadmium ion to form six coordinate complexes a dimeric structure similar to Zn complexes have been proposed [13]. However the crystal structures of pentagonal-bipyramidal complexes of Cd(II) with neutral and anionic N_3S_2 thiosemicarbazones have been reported [14,15]. Compounds **20** and **22** are found to coordinate in the neutral form where cadmium bromide was taken as salt. In the case of all other compounds cadmium acetate was the salt used and resulted in dianionic thiolate form**.** Colors and elemental analyses data of the complexes are presented along with synthesis. All the complexes are diamagnetic due to the d^{10} configuration of the metal ion. They have been found to be fairly soluble in DMF and dichloromethane and conductivity studies show their non-electrolytic nature.

8.3.1 IR spectra

The significant bands obtained in the vibrational spectra of the four ligands and their Cd(II) complexes along with their tentative assignments are given in Table 8.1. The bands corresponding to ν(N–H) present in the ligands disappeared in the spectra of all the compounds except **20** and **22** indicating the enolization of the thioketo group followed by deprotonation. The ν(C=N) band of thiosemicarbazones are found to be shifted to lower wavenumbers in the spectra of all the complexes indicating the coordination of the azomethine nitrogen to the metal. This is also supported by the shift in ν(N–N) to higher frequencies. Coordination via the thiolato sulfur is indicated by a variation in the frequency of the thioamide band [16]. Involvement of the pyridine nitrogen in coordination is indicated by the variations observed in the ring breathing vibrations of pyridine ring and the in-plane ring deformation band of pyridine.

In the spectrum of the complex **19** (Fig. 8.1), $\nu(N^4\text{-H})$ vibrations are observed at 3273 cm^{-1} whereas the band due to $\nu(N^2\text{–H})$ almost disappears. The band due to azomethine group found at 1603 cm^{-1} for the uncomplexed

ligand is shifted to 1583 cm^{-1} in the complex. A weak band at 1611 cm^{-1} is assigned to the –C=N–N=C– moiety, newly formed as a result of deprotonation of the ligand for coordination. Coordination via the thiolato sulfur is indicated by a decrease in the frequency to 1313 and 803 cm^{-1} of the thioamide band which was observed at 1360 and 872 cm^{-1} for the uncomplexed ligand. Coordination of pyridine nitrogen is confirmed by the variations in the ring breathing vibrations and in-plane ring deformation band of pyridine.

In the spectrum of complex **20** (Fig. 8.2), the vibrations due to the methylene groups of the morpholine ring are shifted to low energy region. The azomethine band also shows a red shift to 1583 cm^{-1} on coordination. Coordination of the pyridine nitrogen is confirmed by the in-plane ring deformation band at 643 cm^{-1}.

In the spectrum of the complex **21** (Fig. 8.3), a low intensity band around 3436 cm^{-1} may be due to the coordinated water. The $\nu(N^2–H)$ vibration band observed in the ligand disappears. The azomethine band found at 1613 cm^{-1} for the uncomplexed ligand is shifted to 1548 cm^{-1} upon coordination. Coordination via the thiolato sulfur is indicated by a decrease in the frequency of the thioamide band from 1361 to 1302 cm^{-1}. An increase in the δ(C=S) frequency from 792 to 814 cm^{-1} may be due to the rigidity occurred due to coordination [12]. The ring breathing vibrations and in-plane ring deformation band of pyridine ring have been shifted to lower frequencies indicating coordination of pyridine nitrogen. The vibrations due to the methylene groups of the morpholine ring are observed at 2974 and 2854 cm^{-1}.

Table 8.1 IR spectral assignments (cm^{-1}) of cadmium complexes.

Compound	$\nu(N^4-H)$ / $\nu(N^2-H)$	ν(C=O)	ν(C=N)	ν/δ(C–S)	ν(N–N)	Band III pyridine ring	py(ip)
H_2bts	3214/3160	--	1603	1360, 872	1103	1441	715
[Cd(bts)] **(19)**	3273, 3159	--	1583	1313, 803	1023	1402	725
H_2bmts	3164	--	1613	1361, 792	1103	1463	741
[Cd(H_2bmts)Br_2] (**20**)	2956	--	1583	1350, 796	1110	1464	643
[Cd(bmts)]· H_2O (**21**)	--	--	1548	1302, 803	1111	1464	648
H_2bpts	3370	--	1605	1360, 818	1130	1450	658
Cd(H_2bpts)Br_2] (**22**)	3164	--	1615	1373, 801	1135	1440	631
[Cd(bpts)] (**23**)	--	--	1585	1323, 798	1150	1397	626
H_2mts	3094	1691	1613	1365, 814	1110	1463	734
[Cd(Hmts)Br]·$2H_2O$ **(24)**	--	1688	1588	1351, 810	1108	1474	736

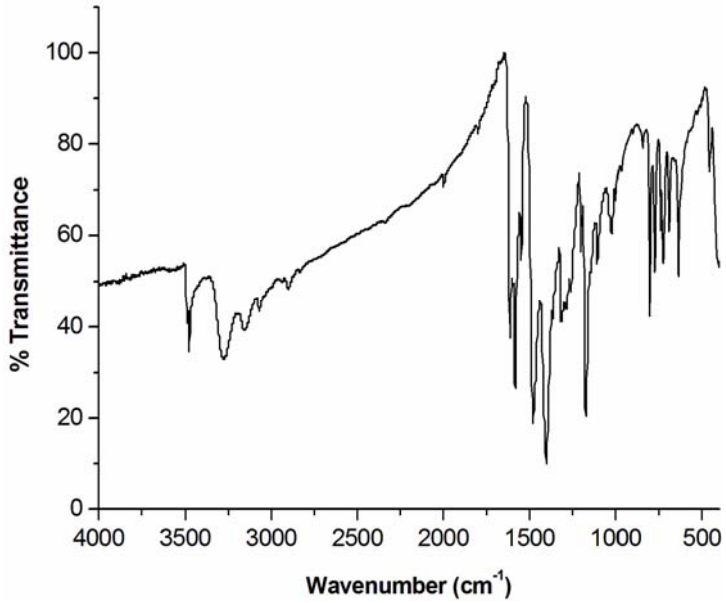

Fig. 8.1 IR spectrum of [Cd(bts)] (**19**).

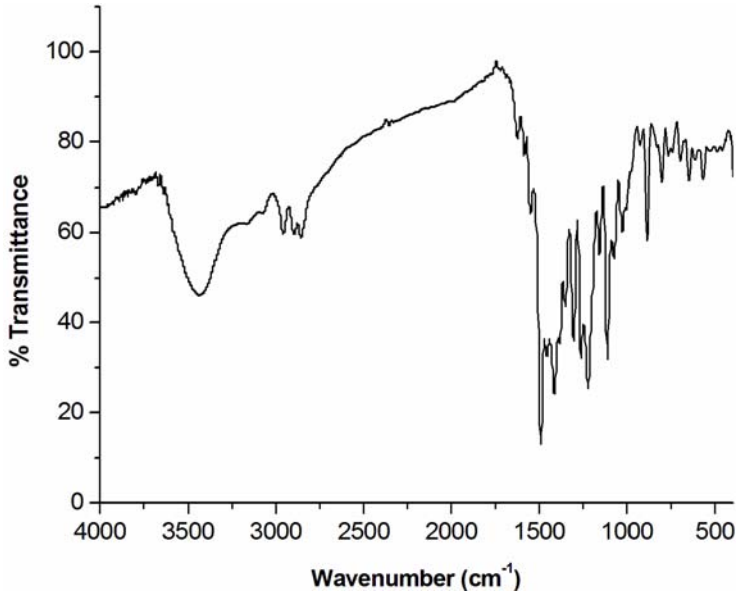

Fig. 8.2 IR spectrum of $[Cd(H_2bmts)Br_2]$ (20).

The spectrum of complex **22** (Fig. 8.4), a low intensity band observed at 3164 cm^{-1} can be due to $\nu(N^2–H)$ vibration. The azomethine band at 1605 cm^{-1} on coordination suffers a blue shift. The ν(N–N) band shifts to 1135 cm^{-1}. Coordination of the pyridine nitrogen is confirmed by the variations of the ring breathing vibrations and in-plane ring deformation band. The far-IR spectrum of the compound **22** shows bands at 397 and 279 cm^{-1} which correspond to ν(Cd–N) ν(Cd–S) respectively. The band observed at 248 cm^{-1} assigned as ν(Cd–Br) is a strong evidence for the coordination of bromo group to cadmium centre.

The spectrum of complex **23** (Fig. 8.3), shows a lowering of the frequency of the azomethine band to 1585 cm^{-1} confirming the coordination of the azomethine nitrogen to cadmium center. The vibrations due to the methylene groups of the pyrrolidine ring are observed at 2966 and 2865 cm^{-1}. The ν(N–N) band shifts to 1150 cm^{-1} on coordination which is a measure of the increase in bond strength. Coordination of the pyridine nitrogen is confirmed by the in-plane ring deformation band at 626 cm^{-1}.

The spectrum of complex **24** (Fig. 8.6), reveals a broad band with low intensity around 3440 cm^{-1} due to the presence of lattice water. The vibrations due to the methylene groups of the morpholine ring are observed at 2952 and 2851 cm^{-1}. The band due to the keto group of the ligand observed at 1691 cm^{-1} is shifted to 1688 cm^{-1} in the complex. Hence the coordination of the keto form of the ligand is suggested. The azomethine band shifts to 1588 cm^{-1} on coordination from 1613 cm^{-1} in the uncomplexed ligand [17]. The stretching and bending vibrations due to the thioketo group lowers when compared with the free ligand indicating strong coordination with enolization followed by deprotonation. The absorption band at 1548 cm^{-1} is due to the newly formed –C=N–N=C– bond. Coordination of the pyridine nitrogen is confirmed by the shift observed in the ring breathing vibrations of the pyridine ring.

The far-IR spectra of the compounds **20** and **24** taken gave peaks at 397, 280 and 250 cm^{-1} which correspond to ν(Cd–N), ν(Cd–S) and ν(Cd–Br) respectively. Sharp peaks were obtained for compound **24** indicating strog coordination.

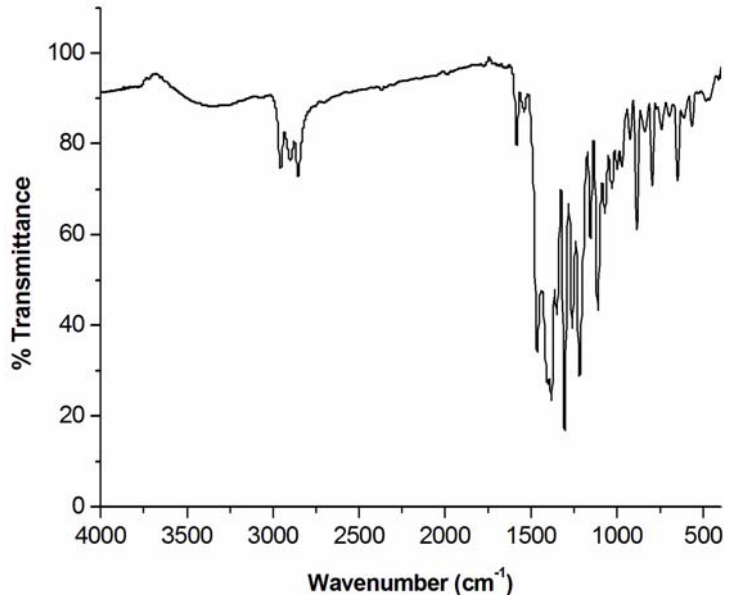

Fig. 8.3 IR spectrum of [Cd(bmts)]·H_2O (**21**).

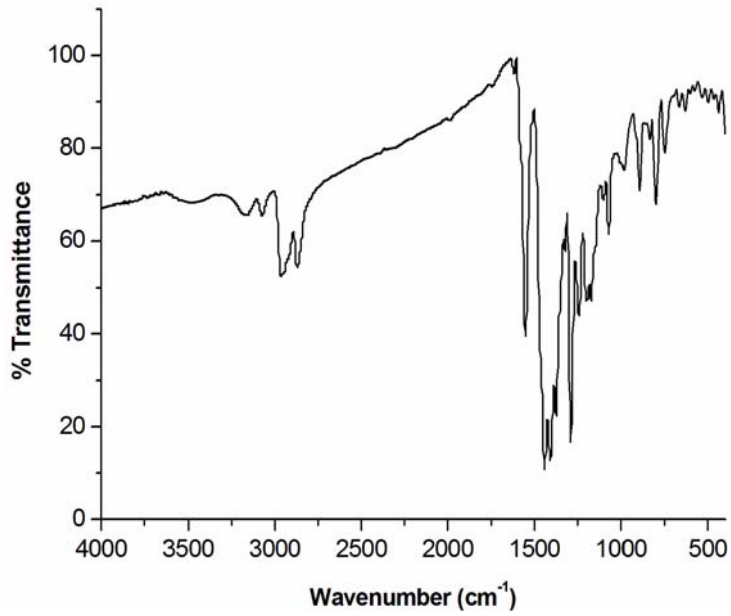

Fig. 8.4 IR spectrum of [Cd(H_2bpts) Br_2]·2.5 H_2O (**22**).

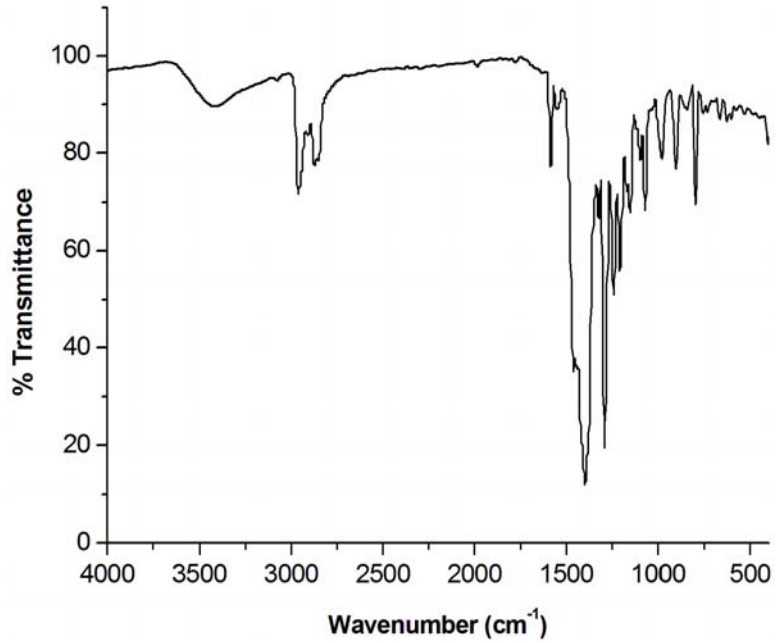

Fig. 8.5 IR spectrum of [Cd(bpts)] (**23**).

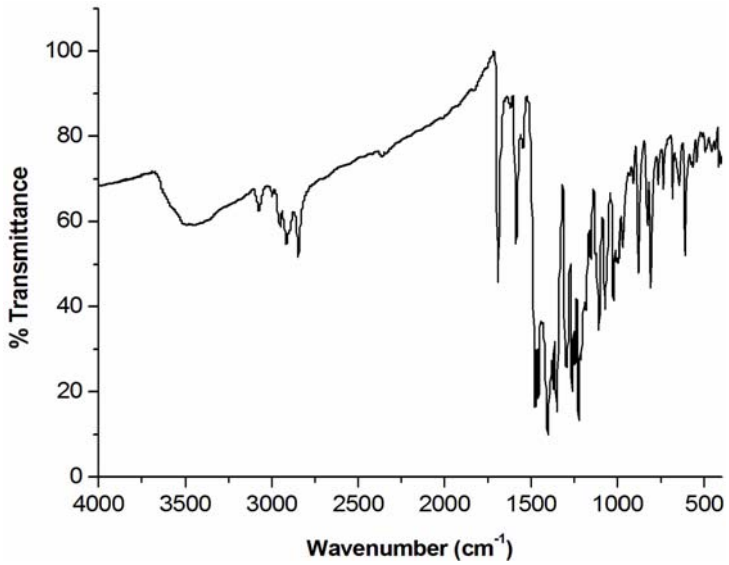

Fig. 8.6 IR spectrum of [Cd(Hmts)Br]·2H_2O (**24**).

8.3.2 Electronic spectra

For cadmium(II) complexes no d-d transitions are expected since it is with d^{10} configuration and no vacant d orbitals are there. All the cadmium complexes synthesized are colored yellow. This color arises due to charge transfer transitions. Spectral assignments for various intraligand and charge transfer transitions are listed in Table 8.2. and the spectra in Fig. 8.7.

Table 8.2 Electronic spectral data of cadmium complexes

Compound	UV-vis absorption bands (cm^{-1})
H_2bts	32130, 30540
[Cd(bts)] (**19**)	32220, 28810, 23210
H_2bmts	37640, 32250, 29810, 24390
[Cd(H_2bmts)Br_2] (**20**)	28570, 23210
[Cd(bmts)]·H_2O (**21**)	29620, 22470
H_2bpts	43820, 33680, 31000, 24450
[Cd(H_2bpts) Br_2]·2.5 H_2O (**22**)	26810 , 23230, 20620
[Cd(bpts)] (**23**)	34360 , 29610, 22750
H_2mts	43680, 37840, 29500, 24750
[Cd(Hmts)Br]·2H_2O (**24**)	30440, 26290, 23940

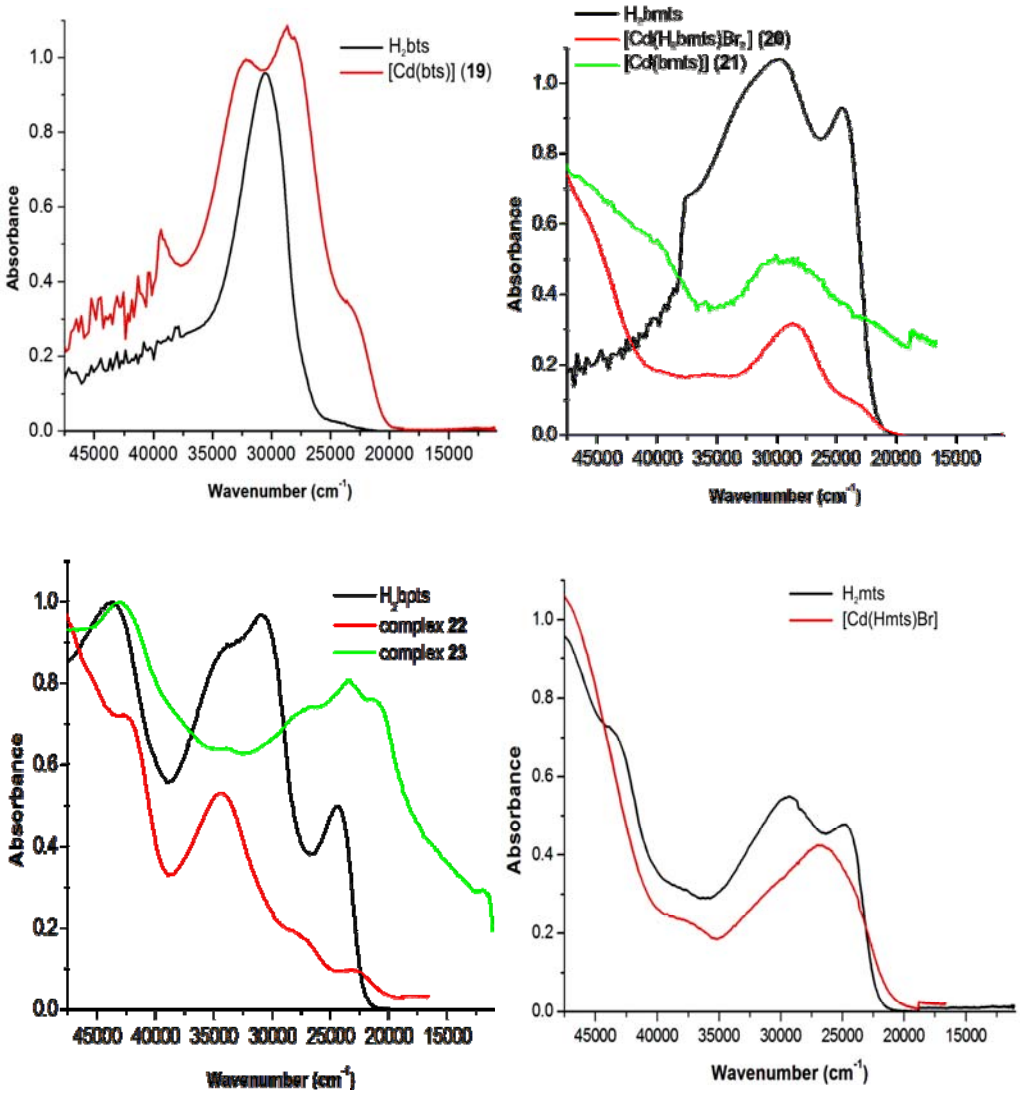

Fig. 8.7 Electronic spectra of Cd(II) complexes (color) along with ligands (black).

The spectra are represented by comparing the corresponding ligand (black) and complexes (red and green). The intraligand transitions have undergone a bathochromic shift indicating the coordination of azomethine nitrogen [18-20]. It can be also due to the weakening of >C=S bond and enhancement of the conjugation system on complexation [21,22]. In addition to these transitions a new charge transfer band is also observed about 24000

cm^{-1}. The moderately intense broad band can be assigned Cd(II) → S metal to ligand charge transfer transition (MLCT).

8.3.5 ^{1}H NMR spectral studies

The ^{1}H NMR assignments of the Cd(II) complexes are placed in Table 8.3 along with ligands. The spectra of some of the complexes along with the proton numbering scheme adopted for identifying corresponding protons are given in Figs 8.8-8.11.

Table 8.3 NMR spectral assignments of Cd (II) complexes

Compound	Aliphatic protons	Aromatic protons	NH^{term}	NH^{int}
H2bts	2.43	7.78-8.42	8.15	10.32
[Cd(bts)] (**19**)	2.38	7.68-8.3	6.68	--
H_2bmts	2.66	7.62-7.96	--	8.58, 15.4
[Cd(H_2bmts)Br_2] (**20**)	2.4	7.9-8.2	--	11.6, 11.68
H_2bpts	2.55	7.45-7.96	--	8.68, 15.2
[Cd(bpts)] (**23**)	1.3	7.9-7.75	--	--
H_2mts	2.65	7.68-8.06	--	15.2
[Cd(Hmts)Br]·2H_2O (**24**)	2.4	7.9-8.2	--	--

In compound **19** (Fig. 8.8), N2 and N6 protons which appeared at 10.32 ppm in the ligand disappeared indicating enolisation followed by deprotonation. The protons at terminal nitrogens N1 and N7 are more shielded and a signal at 6.68 ppm indicate free rotation around C–NH_2 bond. This behavior is consistent with a decrease in the C–N bond order in the complex when the thiol form is adopted [23]. The aliphatic and aromatic protons are found to be shielded when compared with that of the ligand.

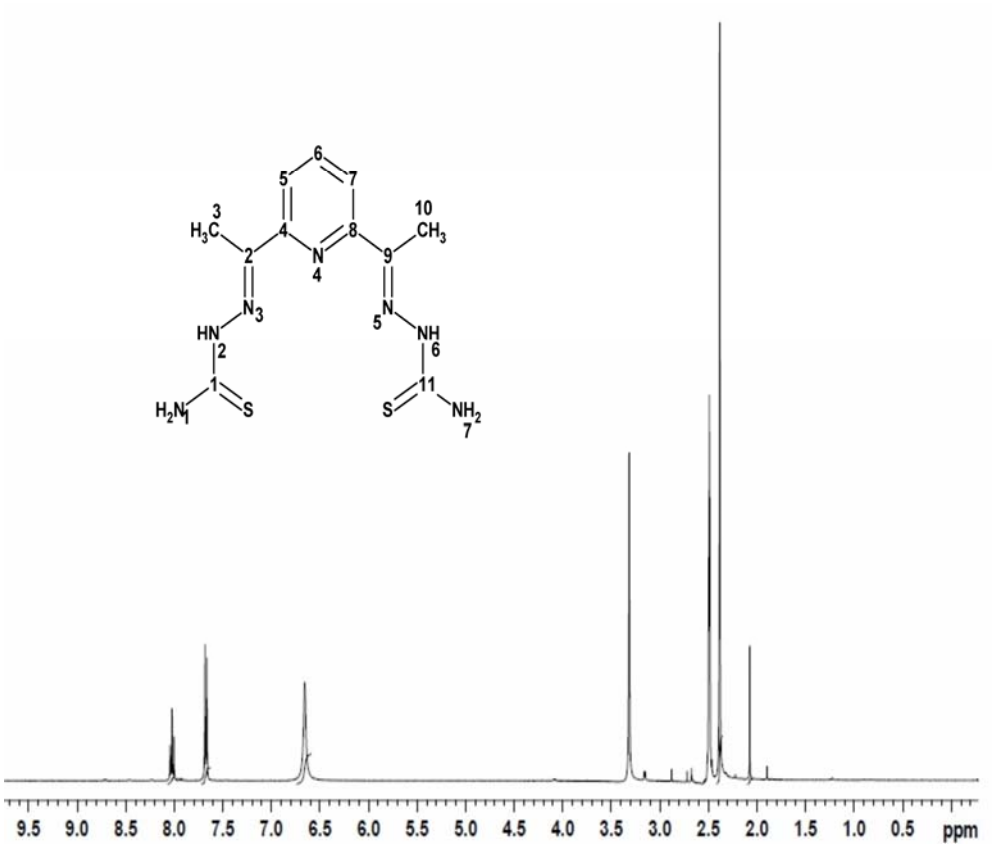

Fig.8.8 ^{1}H NMR spectrum of [Cd(bts)] (**19**) along with numbering of H_2bts.

In compound **20** (Fig. 8.9.), the aromatic protons are found to be slightly deshielded when compared to the ligand whereas the aliphatic protons are shielded. The NH protons average from 8.58 and 15.4 ppm and merge into a single signal at 11.6 ppm. This indicates on complexation the two arms of the ligands acquire a magnetically equivalent nature. The coordination of the ligand in neutral form can be concluded from the NH signal.

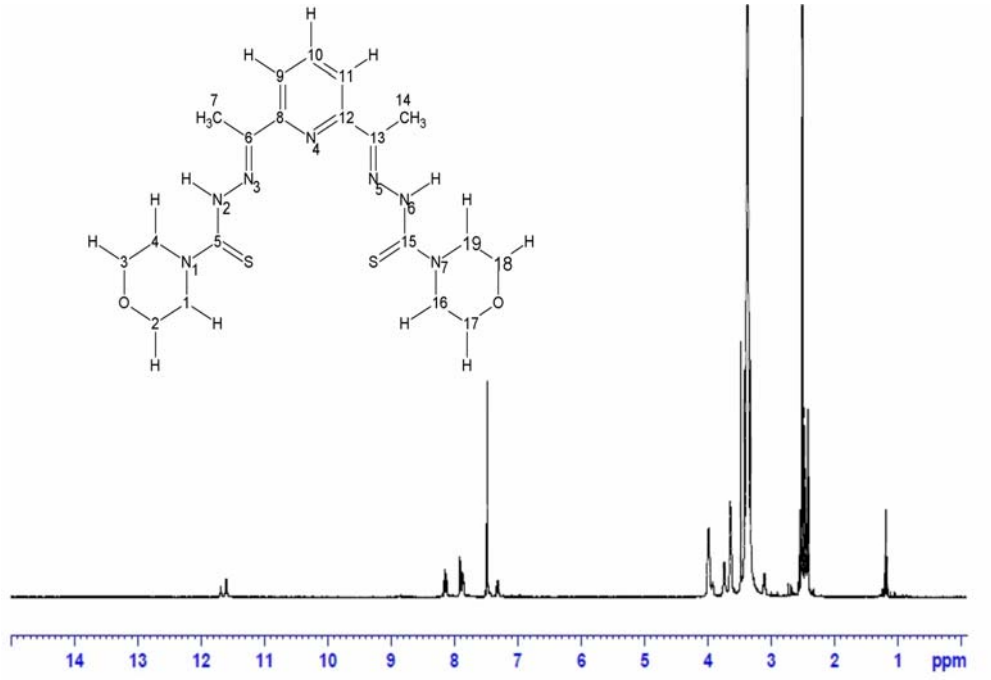

Fig. 8.9 ^{1}H NMR spectrum of [Cd(H_2bmts)Br_2] (**20**) along with numbering of H_2bmts.

In compound **23** (Fig.8.10), the singlet which integrate as a single hydrogen present in the spectrum of the ligand around 8.68 and 15.2 ppm disappear in the spectra of the complexes because of their loss on complex formation. This provides an evidence for the coordination of thiolate sulfur after enolization followed by deprotonation. The pyrrolidine ring protons found at 3.95 and 1.98 ppm in H_2bpts are deshielded to 4.2 and 2.2 ppm indicating the weakening of the pyrrolidine ring on coordination of the thioamide group.

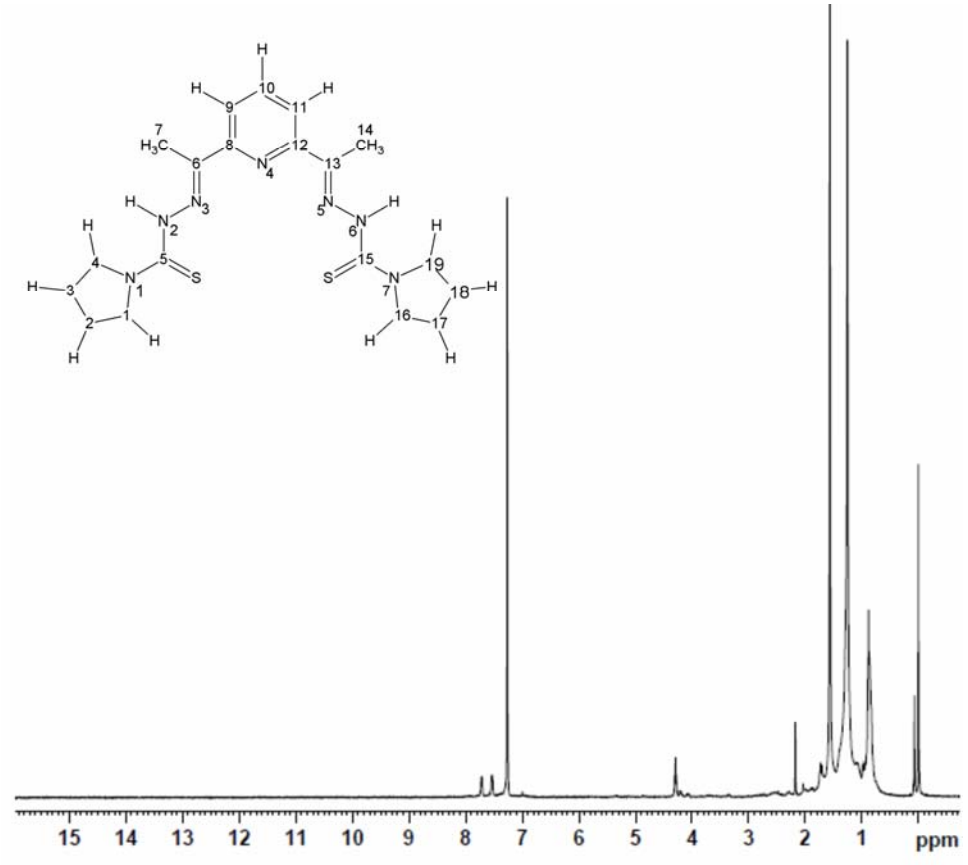

Fig. 8.10 ^{1}H NMR spectrum of [Cd(bpts)] (**23**) along with numbering of H_2bpts.

In compound **24** (Fig. 8.11), the signal obtained at 15.2 ppm disappeared supporting evidence for deprotonation followed by enolization. The aromatic protons found as two doublets and a triplet indicates the magnetically nonequivalent nature of two meta protons. The more deshielded meta proton is nearer to keto group [17]. The protons of the morpholine ring are deshielded slightly. The singlet due to protons on C14 which are close to the keto group is slightly shielded hence the involvement of the keto group in the coordination sphere.

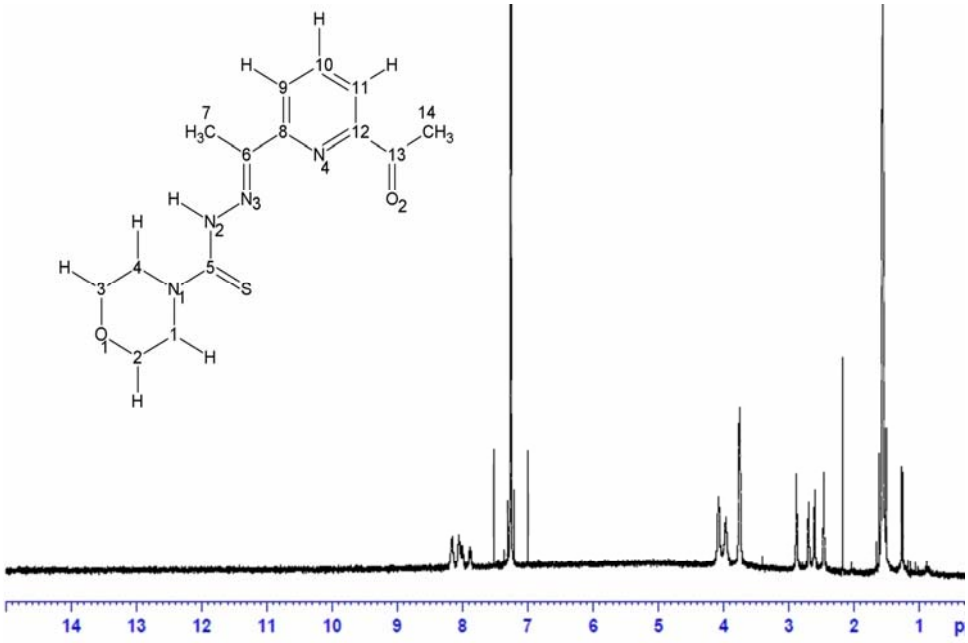

Fig. 8.11 ^{1}H NMR spectrum of $[Cd(Hmts)Br]\cdot 2H_2O$ (**24**) along with numbering of H_2mts.

8.4.1 Fluorescence studies of complex 23

Fluorescence studies are conducted with a Cary Eclipse fluorescence spectrophotometer with scan software 1.1(132) at the International School of Photonics, Cochin University of Science and Technology, Kerala. All the measurements were made at room temperature with 10 nm for both entrance and exit slit. The solvents selected are dimethylformamide and dichloromethane. Both excitation and emission spectra for the proligand and cadmium complex are measured. The concentration studies are done after preparing 0.0625 mmol, 0.125 mmol, 0.25 mmol, 0.5 mmol, 0.7 mmol and 1 mmol solutions in DMF. Emission spectra at various excitation wavelengths from 230-385 nm were measured.

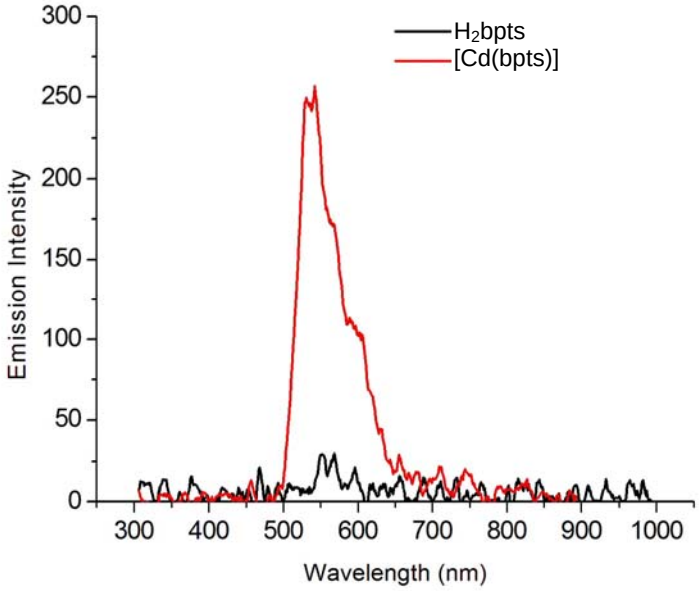

Fig. 8.12 Fluorescence spectra of the ligand and the Cd(II) complex.

Cd(II) complex exhibits yellow fluorescence which can be readily observed by the naked eye. Fluorescence spectra of the ligand and the Cd(II) complex are shown in Fig. 8.12. There is a significant increase in fluorescence intensity for the complex when compared with the ligand at an excitation wavelength of 275 nm. The emission wavelength of the ligand observed at 552 nm undergoes a slight blue shift to 541 nm for the complex. The fluorescence intensity is about nineteen times of that of the ligand. Since cadmium acetate is colorless and has no fluorescence, the observed fluorescence is attributed to the coordinated ligand. Also the fluorescence intensity of the ligand is dramatically enhanced, which clearly shows complexation has occurred. The intensity of the spectra when compared with DCM and DMF as the solvents, a solvent quenching effect is found with dichloromethane. The emission spectra at various concentrations and various excitation energies have been studied and graphical plots are shown below.

8.4.1.1 Emission spectra at varying excitation energies

The emission spectra plotted for 0.0625, 0.125, 0.250 and 0.5 millimolar concentration of [Cd(bpts)] at various excitation wavelengths are shown in Fig. 8.13.

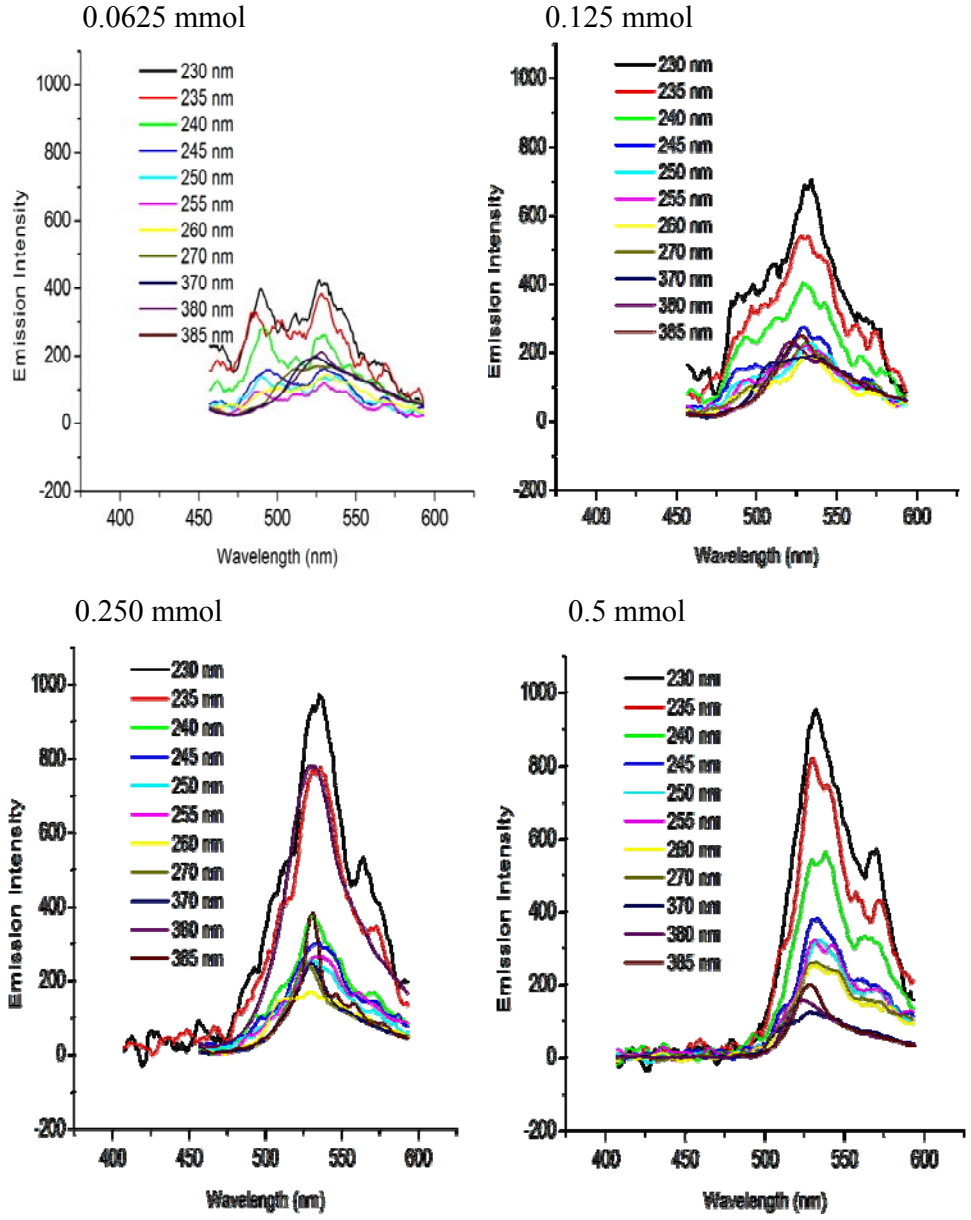

Fig 8.13 Emission spectra of [Cd(bpts)] complex at various excitation wavelengths for 0.0625, 0.125, 0.25 and 0.5 mmol solutions.

It was observed that 0.0625 mmol solution when excited at 230 nm two medium intensity peaks were observed at 490 and 527 nm. Increase in excitation wavelength resulted in decrease in intensity of these two peaks and beyond 270 nm a new peak emerges at 530 nm. Beyond 370 nm only that peak is observed. From the graph it can be concluded that a maximum emission is found when the excitation energy is 270 nm at all concentrations.

8.4.1.2 Emission spectra at different concentrations

The emission spectra of [Cd(bpts)] plotted at excitation wavelengths of 230 and 250 nm are shown in Fig. 8.14. It can be seen that there is an increase in intensity of fluorescence with concentration upto 0.5 mmol, which decreases further indicating a concentration quenching. With increase in concentration the peak at 490 nm disappears and for 0.5 mmol and 0.25 mmol reappears at 570 nm region. Hence fluorescence emission is absorbed with increase in concentration and is reemitted at longer wavelength region. This results in an energy transfer between shorter wavelength region and longer wavelength region.

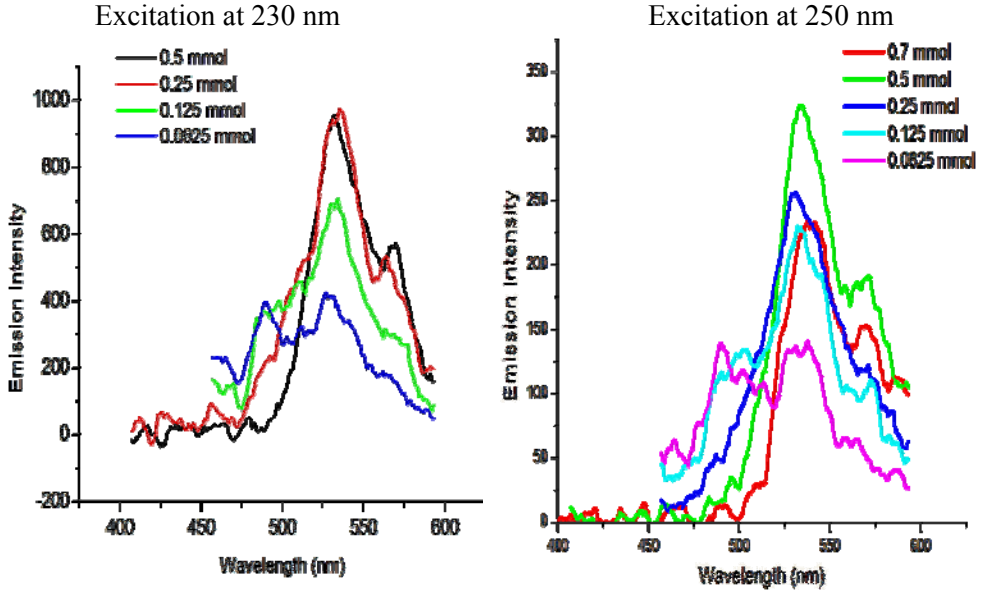

Fig. 8.14 Emission spectra of [Cd(bpts)] complex at various concentrations for excitation wavelength 230 and 250 nm.

The absorption and emission spectra of [Cd(bpts)] are given in Fig. 8.15. From the spectra it can be seen that there is an appreciable Stoke's shift which is the difference between absorption and emission wavelength maxima observed. The enhanced fluorescence emission of the complex can be attributed to the chelation of H_2bpts to the Cd(II) that effectively increases the rigidity of the ligand and reduces the loss of energy via radiationless thermal vibrations [24]. This emission mechanism has been suggested for dipyridylamine and 8-hydroxyquinoline complexes [25].

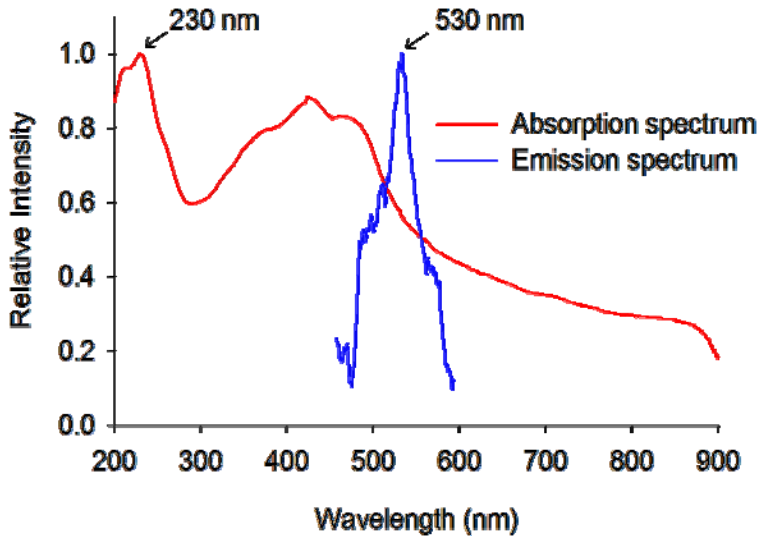

Fig. 8.15 Absorbance and emission spectra of [Cd(bpts)].

8.5 Conclusion

This chapter deals with synthesis and spectral characterization of six Cd(II) complexes. Four of them were found to contain dianionic ligands for which cadmium acetate was used for the synthesis. The remaining two were found to contain neutral ligands where cadmium bromide was used for synthesis. One of the cadmium complex was found to show fluorescence to the naked eye for which the concentration quenching and solvent quenching were studied.

References

[1] R.N. Singhal, M. Jain. Bull. Environ. Contam. Toxicol. 58 (1997) 456.

[2] M.A. Romero-Molina, M.D. Gutirrez-Valuro, R.Lopez-Garzon, J.M. Salas-Peregrin, M.I. Arriortua, F.J. Zufiiga, Inorg. Chim. Acta 136 (1987) 87.

[3] G. Atassi, P. Dumont, J.C. Harteel, Eur. J. Cancer 15 (1979) 451.

[4] D.M. Templeton, Y. Liu, Chem.-Biol. Interact. 188 (2010) 267.

[5] T.W. Lane, M.A. Saito, G.N. George, I.J. Pickering, R.C. Prince, F.M.M. Morel, Nature 435 (2005) 42.

[6] M.N. Hughes, The Inorganic Chemistry of Biological Processes, Wiley, NewYork, 1981.

[7] X. Wu, J. C. Yalowich, B.B. Hassinoff, J. Inorg. Biochem. 105 (2011) 833.

[8] A. Majumder, G.M. Rosair, A. Mallick, N. Chattopadhyay, S. Mitra, Polyhedron 25 (2006) 1753.

[9] J-C. Dai, X-T. Wu, Z-Y. Fu, C-P. Cui, S-M. Hu, W-X. Du, L-M. Wu, H-H. Zhang, R-Q. Sun, Inorg. Chem. 41 (2002) 1391.

[10] D. Rendell, Fluorescence and Phosphorescence, Wiley, New York, 1987.

[11] T. Ohno, S. Kato, Bull. Chem. Soc. Jpn. 47 (1974) 1901.

[12] M. Mohan, A. Agarwal, N.K. Jha, J. Inorg. Biochem. 34 (1988) 41.

[13] M.A. Ali, A.H. Mirza, C.W. Voo, A.L. Tan, P.V. Bernhardt, Polyhedron 22 (2003) 3433.

[14] M.A. Ali, A.H. Mirza, W.B. Ejau, P.V. Bernhardt, Polyhedron 25 (2006) 3337.

[15] M.A. Ali, A.H. Mirza, J.D. Chartres, P.V. Bernhardt, Polyhedron 30 (2011) 299.

[16] L. Latheef, E. Manoj, M.R.P. Kurup, Polyhedron 26 (2007) 4107.

[17] J.S. Casas, E.E. Castellano, M.S. Garcia-Tasende, A. Sanchez, J. Sordo, J. Zukerman-Schpector, Z. Anorg. Allg. Chem. 623 (1997) 825.

[18] A. Bino, N. Cohen, Inorg. Chim. Acta 210 (1993) 11.

[19] W.J. Geary, Coord. Chem. Rev. 7 (1971) 81.

[20] R.P. John, A. Sreekanth, M.R.P. Kurup, H.-K. Fun, Polyhedron 24 (2005) 601.

[21] V. Philip, V. Suni, M. Nethaji, M.R.P. Kurup, Polyhedron 25 (2006) 1931.

[22] I.-X. Li, H.-.Tang, Yi-Zhi Li, M. Wang, L.-F. Wang, C.-G. Xia, J. Inorg. Biochem. 78 (2000) 167.

[23] M.C. Rodriguez-Arguelles, M.B. Ferrari, F. Bisceglie, C. Pelizzi, G. Pelosi, S. Pinelli, M. Sassi, J. Inorg. Biochem. 98 (2004) 313.

[24] H. Zhu, M. Strobele, Z. Yu, Z. Wang, H-J. Meyer, X. You, Inorg. Chem. Commun. 4 (2001) 577.

[25] H. Yersin, A. Vogler (Eds.), Photochemistry and Photophysics of Coordination Compounds, Springer, Berlin, 1987.

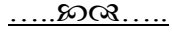

Summary and Conclusions

The coordination chemistry of transition metals with pentadentate bis(thiosemicarbazones) has been getting considerable attention due to their biological activity, formation of systems capable of mimicking several metalloenzymes and their applications in analytical chemistry. Bis(thiosemicarbazones) are offered a prime position because they can form neutral, singly and doubly deprotonated chelating agents yielding both mono- and binuclear complexes with interesting structural features. Recently many bis(thiosemicarbazones) show fluorescent nature which make them useful as chemosensors or biosensors.

In the present work, the chelating behaviour of thiosemicarbazones of a heterocyclic diketone, 2,6-diacetylpyridine is studied, with the aim of investigating the influence coordination exerts on their conformation and/or configuration, in connection with the nature of the metal and of the counter ion. The various possibilities like unsubstitution, ring incorporation at terminal nitrogen and condensation of one of the ketone group alone have been tried for ligand selection. Mainly first row transition metals like manganese, iron, nickel, copper, zinc and cadmium are studied. Metals like cobalt also were studied but could not result in fruitful isolation of the compound due to solubility problems. Different spectroscopic and characterization techniques have been utilized to reveal the nature of the metal and the ligands in coordinated metal complex.

The work presented in this thesis is divided into eight chapters:

Chapter 1 describes a brief introduction on thiosemicarbazones, their transition metal complexes, historical aspects, present scenario and objectives

of the present study. Different characterization techniques used for the study are also briefly explained.

Chapter 2 deals with syntheses, structure and characterization of the proligands used for the study. Four ligands were selected and following acronyms were given.

1) 2,6-diacetylpyridine bis(thiosemicarbazone) [H_2bts]
2) 2,6-diacetylpyridine bis(3-morpholinothiosemicarbazone) [H_2bmts]
3) 2,6-diacetylpyridine bis(3-pyrroldinothiosemicarbazone) [H_2bpts]
4) 2,6-diacetylpyridine mono(3-morpholinothiosemicarbazone) [H_2mts]

The first three proligands are supposed to be pentadentate with an N_3S_2 coordinating environment whereas H_2mts is supposed to be tridentate (NNS) or tetradentate (ONNS). All of them were characterized by ^{1}H NMR, ^{13}C NMR, IR and electronic spectral studies. The studies show that both arms of the bileptic ligand are not symmetric or equivalent. Due to the two thione groups present during complexation they can form neutral, monoanionic or dianionic complexes. NMR studies show that ring incorporated ligands exist in the bifurcated form also along with *E* form in chloroform solution. CV study of H_2mts gave an irreversible oxidation peak.

Chapter 3 gives an overview of the four Mn(II) compounds synthesized and characterized by various spectroscopic techniques such as IR, electronic spectral studies, CV and EPR. The elemental analyses show that the ligands coordinate in monoanionic as well as dianionic forms. The magnetic susceptibility measurements showed the paramagnetic nature of manganese in the complexes. The IR spectral studies revealed that the azomethine, thioamide and pyridine bands are shifted from that of the ligands which indicates the coordination of that group to the metal centre. In the electronic

spectral studies, the *d-d* transitions are found to be very weak and obscured by charge transfer transitions. The EPR studies depict the high spin state of manganese with five transitions and the lines due to nuclear hyperfine interactions with ^{55}Mn nucleus which come to thirty peaks altogether. CV studies gave an irreversible reduction peak for compound (**4**).

Chapter 4 deals with the synthesis and characterization of two Fe(III) compounds. Elemental analyses suggest the ligand coordination to be in neutral form in **5** whereas the other anionic form. Conductivity studies revealed 1:1 electrolytic nature of compound **5**. Single crystals of $Fe(Hmts)Cl_2$ were isolated but did not diffract. The IR and electronic spectral studies confirm the coordination of the ligands. Far IR spectra confirmed coordination of the coligand. Though EPR spectrum of compound **6** showed two transitions at 298 K, the low energy region shifted to high energy region at 77 K. CV studies gave an irreversible reduction peak for compound **6.**

Chapter 5 describes the synthesis and characterization of two nickel complexes. Elemental analyses show one of the compounds to be anionic and other neutral. One of the complexes [Ni(bts)] was found to be weakly paramagnetic suggesting a polymeric structure. IR spectral studies indicate the ligand to be pentadentate. Electronic spectrum of compound **7** revealed weak d-d transition bands for two spin allowed transitions. The elemental analysis data and spectral characterization suggest the compound **8** to be having a distorted octahedral geometry with a 1:1 electrolytic nature.

Chapter 6 includes the synthesis and spectral characterization of five copper(II) complexes. Five copper complexes with chelating rings were synthesized. All the compounds except **11** were found to coordinate in the deprotonated dianionic form. Elemental analyses showed that complexes synthesized from copper acetate yielded anionic form of the ligand whereas

copper chloride the neutral form. The molar conductivity measurements revealed 2:1 electrolytic nature of compound **11**. IR and electronic spectral studies confirm first three ligands to be pentadentate and H_2mts tetradentate. Normal magnetic moment values are obtained for all complexes except **10**. Compound **10** gives a sub-normal value corresponding to a trinuclear copper complex which is supported by elemental analyses data. Copper in all the compounds are found to be in $d_{x^2-y^2}$ ground state. Coordination of azomethine and pyridine nitrogens are confirmed by the superhyperfine splitting obtained in the EPR spectral studies. In **9** and **13** there is considerable exchange interaction between the metal centers. The single crystal X-ray studies show H_2mts to be diprotic and tetradentate with [Cu(mts)] having a distorted square planar structure. The one dimensional packing structure showed the molecular architecture stabilized by π-π CH-π and metal-π interactions.

Chapter 7 delineates the syntheses and characterization by spectroscopic techniques and single crystal XRD. Elemental analyses showed the dianionic nature of bis(thiosemicarbazones) and monoanionic nature of H_2mts in $Zn(Hmts)_2$. IR and NMR spectral studies showed that ligands are more stabilized on complexation. Single crystal studies of compounds **14** and **16** and showed that they exist in {6+4} and {5+5} geometry. Compound **14** is stabilized by π-π and H-bonding interactions including solvent molecules whereas compound **16** is stabilized by weak π-π and C–H-π interactions alone. The centrosymmetric $[Zn_2(bpts)_2]$ showed a double helicate structure. They exhibit beautiful molecular architectures. Possibility for compounds **15** and **17** in dimeric form cannot be confirmed since attempts to separate single crystals fail. An octahedral geometry with the zinc center coordinated in an N_4S_2 manner by two ligand moieties is proposed for compound **18.**

Chapter 8 deals with synthesis and spectral characterization of six Cd(II) complexes. Four of them were found to contain dianionic ligands for which cadmium acetate was used for the synthesis. The remaining two were found to contain neutral ligands where cadmium bromide was used for synthesis. All of them were non-electrolytes with moderate solubility in common solvents. The IR and electronic spectra confirmed pentadentate nature of H_2bts, H_2bmts and H_2bpts and tetradentate nature for H_2mts. NMR spectral studies supported the findings. One of the cadmium complex was found to show fluorescence to the naked eye for which the concentration quenching and solvent quenching were studied. The fluorescent nature of H_2bpts was very much enhanced on complexation. The enhanced fluorescence emission of the complex can be attributed to the chelation of H_2bpts to the Cd(II) that effectively increases the rigidity of the ligand and reduces the loss of energy via radiationless thermal vibrations.

In conclusion pentadentate ligands showed an N_3S_2 coordinating environment with the complexes having an octahedral or trigonal bipyramidal geometry. H_2mts was found to be tridentate or tetradentate in complexes. Zinc and manganese complexes were proposed to be having meridional nature. Many complexes with novel properties were synthesized and characterized, but further application oriented studies are to be done to utilize these applications.

…..ஜ۞ஜ…..